1-1-1993

Residual Strength of Damaged and Deteriorated Offshore Structures: Volume 1; Residual Strength of Damaged and Deteriorated Tubular Members in Offshore Structures

Alexis Ostapenko

B. A. Wood

A. Chowdhury

M. F. Hebor

ADVANCED TECHNOLOGY FOR
LARGE STRUCTURAL SYSTEMS

Lehigh University

Residual Strength of Damaged and Deteriorated Offshore Structures

Volume One

RESIDUAL STRENGTH OF DAMAGED AND DETERIORATED TUBULAR MEMBERS IN OFFSHORE STRUCTURES

By
A. Ostapenko
B. A. Wood
A. Chowdhury
M.F. Hebor

Research Sponsored by

American Iron and Steel Institute (AISI)
Chevron Oil Field Research Company
Exxon Production Research Company
Marine Technology Support Unit (MaTSU, U.K.)
Minerals Management Service (MMS/DOI)
Mobil Research and Development Corporation
Shell Oil Company
Texaco, Inc.

ATLSS Report No. 93-03

January 1993
[Distribution restricted until January 1994]

ATLSS Engineering Research Center
Lehigh University
117 ATLSS Dr., Imbt Laboratories
Bethlehem, PA 18015-4729
(215) 758-3525

An NSF Sponsored Engineering Research Center

TABLE OF CONTENTS

ABSTRACT

Ultimate capacity and the post-ultimate residual strength of axially-loaded damaged (dented and/or bent) and deteriorated (corroded) tubular members were studied by conducting tests on eleven salvaged, seven fabricated and two small-scale manufactured column specimens.

The nominal (specified minimum) yield stress of the specimens was either 36 or 50 ksi. The salvaged and fabricated specimens had lengths ranging from 22 to 35.4 feet and mid-thickness diameters ranging from 10.4 to 24.5 inches. The specimens had diameter-to-thickness ratios ranging from 28 to 95.

All fabricated and small-scale manufactured specimens and four salvaged specimens were dented at mid-length with the dent depth varying from 5 % to 15 % of the diameter. Of these specimens, two were tested with fixed-ends, two with end eccentricity and nine with pinned ends. Comparison of the tests on the salvaged seamless specimens and the fabricated cold-rolled and welded specimens indicated that residual stresses apparently had little effect on the ultimate strength and the post-ultimate behavior of dented tubular columns.

The seven remaining salvaged specimens were tested without denting, and of these, three were corroded, one was badly bent, and three were straight and had no corrosion and thus served as indicators of the original pre-damage strength.

Several methods were used to analyze the tested specimens. Comparison with test results indicated that the analytical methods could relatively accurately predict the ultimate strength for dented and undented columns, but were conservative in estimating their post-ultimate behavior. These methods were also suitable for uniformly corroded specimens. However, the behavior of the two specimens with localized corrosion which failed by local buckling could not be predicted by these methods. A limited study was made of an approach for evaluating the effect of localized (patch) corrosion on local buckling and reduction of member strength.

1. INTRODUCTION

The problems of damaged and deteriorated (corroded) tubular members in offshore platforms have been recognized for many years. Damage and corrosion reduce both the axial capacity and the post-ultimate behavior (residual strength) of tubular members. The reduction of strength of these members must be known in order to properly evaluate the overall safety of existing and future platforms.

Several researchers have studied the residual strength of damaged tubular members. C.S. Smith considered the effect of local dents on 16 quarter-scale specimens.[14] Rashed [12] tested 21 dented specimens, and Ueda [19] tested 21 additional small-scale specimens. Taby developed a computer program DENTA based on a simplified physical model which was adjusted on the basis of data from 109 small-scale tests. [18] Ellinas used the results from the published data to formulate a lower bound solution for the ultimate strength of damaged columns.[6] Padula and Ostapenko conducted tests on two short dented specimens with large (D_m/t)[1] and developed an approximate method for predicting the load-shortening behavior of dented columns. [9 and 10]

The small-scale specimens in the above work were made from drawn tubing, ERW pipe, or cold-rolled plate. In essentially all cases, the specimens were annealed to remove residual stresses before they were dented and tested. Smith conducted large-scale tests on two columns from a retired offshore platform in 1981 and concluded that the companion small-scale tests approximately duplicated the behavior of the large-scale specimens.[15] However, the results indicated that the small-scale tests underestimated the ultimate load by as much as 15 percent and the post-ultimate strength by as much as 30 percent.[15] More than two tests are needed to verify that small-scale experiments could adequately predict the load-response of large-scale fabricated tubes such as those used in offshore structures.

In the fabrication process of tubular members, a flat steel plate is cold-rolled into cans and the cans are butt-welded to form a column. Cold-rolling and welding introduce residual stresses. When a column with residual stresses is compressed, the areas of compressive residual stress yield first. The analytical understanding of the behavior of a dented fabricated tubular column is further complicated by factors such as strain hardening, local plastification of the cross section, and growth of the dent. By testing dented cold-rolled fabricated specimens, the effects of fabrication on the ultimate

[1] D_m is the mid-thickness diameter (OD-t). All references to diameter (Dm or D) will mean the mid-thickness measurements. The outside diameter will be explicitly called 'OD' and the inside diameter 'ID'.

strength behavior of dented members can be explored.

Table 1-1 lists the column specimens tested in the current research program. Photo 1-1 gives views of these specimens in the same order. There are seven (7) newly fabricated, eleven (11) salvaged, and two (2) small-scale manufactured column specimens. The nominal yield stress of the specimen material was either 36 ksi or 50 ksi. The fabricated and salvaged specimens had lengths ranging from 22 to 35.4 feet, and mid-thickness diameters ranging from 10.4 to 24.5 inches. The specimens had diameter-to-thickness ratios from 28 to 95.

The fabricated column specimens were given number and letter designations to identify them. For all of them, the first letter was P. The specimens were divided into four (4) groups based on the (D_m/t) ratio of the column. Letters 'P' and 'F' in the third position were used to designate pinned or fixed ends (Groups 1 and 2), and, letters 'A' and 'B' designated different dent depths (Group 3). All of the fabricated specimens were dented at mid-length.

The eleven (11) salvaged specimens were divided into four groups depending on the column slenderness (L/r) and the diameter-to-thickness ratio (D_m/t). In each group, the specimens were given a letter designation to specify the testing conditions. Letter 'B' (e.g. Specimen B3) indicated that the specimen was bent and the number specified that it was a member of group 3. Letter 'C' (e.g. Specimen C2) indicated that the column was corroded. Letter 'D' (e.g. Specimen D3) indicated that the column was to be dented before the axial test. Letter 'E' (e.g. Specimen E3) specified that the column was to be dented and tested with a 25% end eccentricity. Letter 'S' (e.g. Specimen S3) indicated that the column was straight, had no corrosion, and served as a bench mark for evaluating the reduction of strength due to damage or corrosion.

A description of the project work is detailed in the following chapters. Chapters 2 through 6 describe the preparatory work conducted before the long-column specimens were tested. This work included the following: the layout and preparation of the specimens for testing (Chapter 2), the measurement of initial geometry (Chapter 3), the determination of material properties (Chapters 4 and 5) and the denting procedure (Chapter 6).

Chapters 7 through 9 describe the procedures and results from the long-column tests. Chapter 7 describes the tests of damaged columns using cylindrical bearing fixtures, Chapter 8 describes the tests on damaged columns with fixed-ends, and Chapter 9 describes the tests on the straight corroded and uncorroded columns. Chapter 10 compares the test results of the specimens within each group of specimens, and the application of the finite element program ADINA to analyze the test specimens

is outlined in Chapter 11. Chapter 12 compares the test results with several analytical methods. A study of the end eccentricity as determined analytically from the test data is described in Chapter 13. A study of the effect of corrosion on the behavior of tubular columns is given in Chapter 14.

2. LAYOUT OF SPECIMENS

2.1 Salvaged Specimens

The salvaged specimens were shipped covered with barnacles, some also had K-joints welded on, and two had Monel sheet coverings still attached. In the course of the initial preparation of the test specimens the following had to be done:

- The dried barnacles and layers of rust (up to one-half inch thick) were remove with hammer and chisel.
- The K-joints were cut off using a torch and ground down.
- The Monel coverings were cut with a torch and removed.

2.1.1 LAYOUT FOR STUB COLUMNS AND TENSILE COUPONS

The salvaged columns were laid out to ensure that appropriate lengths for the long columns, tensile coupons, and stub columns were cut. Most of the salvaged tubes were too short to include stub columns, but Specimens E1, S2, E3, and C4B had sufficient lengths.

Specimens E1 and E3 had sufficient lengths for stub columns, but they also had transverse welds located near the mid-length where the dent was to be made. In laying out the cuts for these specimens, the transverse weld was placed as far as possible from the mid-length of the long column. The reason for this was that the presence of the weld metal and of the two different materials near the dented portion of the column could have lead to confusing test results. Thus, it was highly desirable to locate this discontinuity of material as far from the dented portion of the column as possible. The second objective was to take the stub column from the same tube portion in which the dent would be made. However, this caused the transverse weld to be located too close to the dent. Thus, in order to keep the location of the transverse weld away from the dented portion at mid-length, the stub column was not taken from the same tube portion in which the dent was made.(Fig. 2-1) Hardness tests indicated that the materials of the two joined portions were similar. Tensile coupon results for Specimen E1 confirmed that the two joined portions had similar yield strengths, and therefore, the behavior of the stub column was representative for the dented portion.

The long columns, stub columns, and tensile coupons were all laid out and marked to identify which end came from where in the origional tube.(Fig. 2-1) Each side of a saw cut had an 'A' and a 'B' side. The stub column and long column therefore had 'A' and 'B' ends. These designations were maintained throughout the layout, surveying, and testing procedures.

2.1.2 DETERMINATION OF REFERENCE LINES

The longitudinal reference lines for the salvaged columns were established with respect to the longitudinal line of maximum out-of-straightness of the specimen. A carpenter level and square were used to determine the 'top' of the specimen for both ends of the specimen and for the mid-length portion.(Fig 2-2) After the survey, made by using a survey level and a rod with a 1/64th-inch division scale attached, the specimen was rolled a fraction of an inch and three new 'top' points were marked and surveyed. This procedure was repeated until the maximum out-of-straightness was found.

The line of the maximum convex out-of-straightness was labeled the '180 degree' line and the maximum concave out-of-straightness was labeled the '0 degree' line. The '90 degree' and '270 degree' lines were determined by going clockwise around the column at the 'A' end of the specimen.(Fig. 2-3) Since all the columns had single-curvature out-of-straightness, the 90 degree and 270 degree reference lines had no measurable out-of-straightness. To make sure that the maximum line of out-of-straightness was located, these reference lines were checked before the lines were center-punched.

Once the four reference lines were established, the specimen was rotated so that the 180 degree line was the 'top' line. A carpenter chalk line was used to produce a continuous line through the two 'top' end points and the 'top' center point of the specimen, then a steel measuring tape was pulled tight and clamped next to the line at both ends of the column. The 'A' end of the column was taken as the origin, and two-foot intervals were marked off using a center-punch. The specimens that were to be dented had a closer spacing of points near the mid-length, as well as, additional reference lines at 45, 135 , 225, and 315 degrees, so that the shape of the dented portion could be measured more accurately after the denting process.

2.2 Fabricated Specimens

2.2.1 LAYOUT FOR LONG COLUMNS, STUB COLUMNS AND TENSILE COUPONS

Each of the fabricated specimens consisted of five 'cans'. The cans were cold-rolled from flat plate and manually butt welded together to form the specimen. The central cans of the fixed-ended and pin-ended specimens, the end cans of the fixed specimens, the stub column, and the longitudinal and transverse tensile coupons were all taken from the same steel plate. This was done to ensure that all the critical

portions of the specimens in a particular group (P1-, P2- , and P3-) had the same material properties.(Fig. 2-4) The remaining cans for the specimens came from plates that had similar hardness and the same thickness as the plate in the critical sections.

The labeling scheme for the cans of the fabricated specimens followed a preset pattern. For example, the can label P1P3-1 for Specimen P1P means the following: P1P is the specimen designation; '3' gives the location of the can in the specimen with can '1' at the 'A' end and can '5' at the 'B' end; the number after the hyphen identifies the plate from which the can was made. Thus, it was clear where each can came from and how it was placed in the specimen.(Fig. 2-5)

The longitudinal seam welds on the five cans were rotated by 90 degrees form each other, as is commonly done in the fabrication of offshore structures.(Fig. 2-5)

2.2.2 DETERMINATION OF REFERENCE LINES

As for the salvaged specimens, four longitudinal reference lines were established on the surface of the fabricated specimens. The location of the '180 degree' reference line was set to coincide with the seam weld in the central can. The dent location was on the '0 degree' reference line, directly opposite the longitudinal weld in the central can.

The procedure for chalking and center-punching the fabricated specimens was the same as for the salvaged specimens. The center-punched points were measured from the 'A' end of the specimen which was the bottom of the specimen during testing. Since the end plates were already welded to the ends of the specimen, when leveled, they served to define the 0, 90, 180, and 270 degree reference lines. The 45, 135, 225, and 315 degree lines were made 'top' by using a carpenter level and square.

2.3 End Plates for Long-Column Specimens

2.3.1 END PLATES FOR SALVAGED SPECIMENS

The dented salvaged specimens and the bent specimen had Type 1 fabricated end plates welded to them once their reference lines were established. (Fig. 2-6) Specimens E1 and E3 had Type 1 end plates welded with intentional offsets.(Fig. 7-5) The straight salvaged specimens were tested with spherical bearings and had 3-inch thick end plates tack-welded to their ends.(Fig. 2-7)

2.3.2 END PLATES FOR FABRICATED SPECIMENS

End plates for the fabricated specimens were welded at the fabrication plant. The pin-ended specimens with diameters under 24 inches had Type 1 end plates. (Fig. 2-6) The 24.5-inch diameter specimens had Type 2 square end plates. The fixed-ended specimens used Type 3 end plates which were thicker than the other end plates, and they were welded with a three-inch lip on the side to be used for clamping the specimen down.

3. INITIAL MEASUREMENT OF GEOMETRIC PROPERTIES

3.1 Thickness Measurements

3.1.1 MEASUREMENT OF THICKNESS WITH A MICROMETER

A 0.001-inch micrometer was used to measure the thickness at the ends for all the salvaged specimens. The non-corroded specimens varied in thickness around the circumference of the ends by as much as 0.06 inches (Tables 3-1 to 3-9). Thus, readings were taken every two-inches around the circumference, going clockwise with respect to the 'A' end. (Fig. 2-3) These end thickness readings were later used to calibrate the Ultrasonic Thickness Measurement equipment. This equipment was used to measure the thickness of certain interior sections of the salvaged specimens. A micrometer was also used to field inspect the steel plates used for the fabricated specimens.

3.1.2 MEASUREMENT OF THICKNESS WITH ULTRASONIC EQUIPMENT

Ultrasonic thickness measurements were conducted using an Epoch Model 2002 Unit[1] with an accuracy of ± 0.001 inch. Mainly, the Ultrasonic thickness measurements were made to determine the thickness at points away from the ends of the specimen where a micrometer could not be used.

Ultrasonic thickness measurements were made to check the uniformity of thickness for the salvaged specimens in the interior sections of the specimen. Since the ends of the salvaged specimens varied in thickness around the circumference, it was important to check the variation of thickness of the interior sections. For the heavily corroded salvaged specimens, the thickness was also measured in the areas of corrosion and in the critical areas where local buckles developed during the axial tests.

After the axial tests, a two-inch by two-inch grid was used to measure the thickness variation of the buckled sections of the corroded specimens.(Tables 3-10 to 3-13) (Such thickness maps will be later used to establish local buckling criteria for the corroded specimens.)

The limitation of the ultrasonic thickness measurements was that they had to be taken on a surface which was flat and free of rust. The corroded specimens were cleaned of rust, but the surface in many areas was heavily pitted and irregular. Since the thinner points were located in deep and narrow pits, which the ultrasonic thickness transducer could not fit into, the measured average thickness is actually an upper bound of the actual average thickness.

[1]Epoch Model 2002 Ultrasonic Thickness Gage by Parametrics

3.1.3 MEASUREMENT OF THE AVERAGE THICKNESS BY WEIGHING

Since it was very difficult to accurately determine the average thickness of the corroded specimens using a micrometer or the ultrasonic thickness equipment, the salvaged Specimens C1, C2, C4B and S1 were also weighed to determine the average thickness. With a steel density of 490 lb/ft^3, the weight of the specimen indicated the volume of material, which was then used to compute the average thickness. Since these specimens were corroded only on the outside surface, and the inside surface had no or only slight surface corrosion, the inside diameter was used as a known quantity.

With the inside diameter, weight, and length diameter known, the average thickness was calculated using the following equation:

$$t = \frac{D_i}{2}\left[\sqrt{1 + \frac{4\ \text{Weight}}{\pi D_i^2 L\ \gamma}} - 1\right] \tag{3.1}$$

where D_i is the inside diameter, L is the length of the tube, $\gamma = g\rho$ is the unit weight of the material with g being the gravity acceleration and ρ the unit density.

Using the commonly recommended unit weight of steel γ=gρ=490 lbs/ft^3, the inside diameter D_i in inches, the length L in feet and Weight in pounds, Eq. 3.1 becomes Eq. 3.2.

$$t_{ave} = \frac{1}{2}\left[\sqrt{D_i^2 + 0.37418\frac{\text{Weight}}{L}} - D_i^2\right] \tag{3.2}$$

The average thickness values are listed and compared against the end thickness measrements in Table 3-14.

The weight of the specimens was determined from the following procedure. A U-shaped aluminum load cell with an accuracy of ± 2 pounds and a capacity of 2000 pounds was used for the weighing procedure. As shown in Fig. 3-1, the specimen was placed into a sling and lifted at the center using a fork lift. The load cell was between the sling and the fork lift. A "zero" voltage reading was taken with the specimen on the ground and another voltage reading was taken after the specimen was lifted and stabilized. The procedure was repeated more than 12 times, with a maximum voltage variation of less than 2.6 percent. The load cell calibration curve was used to convert the voltage reading to the weight of the specimen.

3.1.4 LOCAL THICKNESS PROFILE BY SCRIBING

A scribing technique was developed to obtain detailed thickness measurements in the areas of heavy corrosion. At a given corroded cross section, a piece of steel with a sharp point and a pencil were held in a vertical position and dragged over the pitted

surface of the corroded specimen. The pencil scribed the profile onto a sheet of paper.(Fig. 3-2) Multiple ultrasonic measurements were taken at the flat points along the scribed path. After smoothening the penciled line, a best-fit curve was passed through the points of known thickness. This curve produced a cross-sectional representation of the thickness variation in the relevant portions of a corroded specimen.(Fig. 3-3) This procedure was carried out at several cross sections and a thickness map was prepared.

3.2 Initial Out-of-Straightness

A survey level and 1/64th-inch scale were used to measure the initial out-of-straightness of all specimens. To ease the task of rotating the specimens, they were placed on two sets of steel rollers. The 0, 90, 180 and 270-degree reference lines were each placed in the 'top' position and the center-punched points were surveyed. The survey level was set up at one end of the specimen, and the scale was attached to a wooden rod with a nail in the bottom. The nail in the rod was positioned in the center punch points along the specimen and the scale was read using the survey level.

Out-of-straightness of a specimen was determined by measuring the reference line of maximum sagging curvature; that is, the zero (0) degree line, as well as, the 180 degree reference line which was directly opposite.(Fig. 2-3) Measurements of the lines drawn on the surface at 45, 90, 135, 225, 270, and 315 degree lines around the perimeter were taken as well. This was done to clearly identify the initial tube profile in order to compare it with the survey profiles after denting and after the axial tests.

4. MATERIAL PROPERTIES

4.1 Hardness Measurements

Hardness tests were conducted with a Riehle portable hardness tester[1], as shown in Photo 4-1. The Rockwell B hardness scale was used for all the tests since it was suitable for the measurement of the 36-ksi material as well as the 50-ksi material.

The salvaged specimens were hardness tested to make initial estimates of their ultimate and yield stresses.(Tables 4-1 and 4-2) The specimens that had transverse welds located near mid-length were hardness tested at each end to verify that the two welded portions had similar yield stresses. Specimens D1, E1, C2, E3, C4A and C4B had transverse welds, and after hardness measurements, it was found that the yield stresses of the two pieces were very similar for all the specimens except C4A. Specimen C4A had an estimated F_u= 69 ksi at end 'A' and F_u= 54 ksi at end 'B'. (Table 4-2) In addition to the different materials, there was heavy corrosion and many bracket attachments near the transverse weld at mid-length. Therefore, this specimen was not included in the testing program since the results for the axial test would have been ambiguous.

The plates for the fabricated specimens were hardness tested after delivery at the fabrication plant, but before the cold-rolling to insure that the plates had the intended yield stresses. (Table 4-3)[2] The tensile coupons for the salvaged and fabricated specimens were also hardness tested to study the correlation between the hardness readings and the tensile properties of the materials used.(Section 4.3)

4.2 Tensile Coupons

The tensile properties of the fabricated and salvaged columns were determined by conducting tensile coupon tests. The coupons for the salvaged specimens were machined from the cut-off ends of the specimens.(Fig. 2-1) The coupons for the fabricated specimen were cut in two directions from the flat plate before cold-rolling. These coupons were taken in the direction of rolling of the plate in the steel plant and also in the direction of the column 'can' axis (which is transverse to the plate). (Fig. 2-4) The coupons taken in the direction of the column 'can' axis (labeled -T) had higher yield stresses, but the maximum difference was only 3.6 percent. The tensile

[1]Riehle Model PHT-2 Portable Hardness Tester, AMETEK Inc., East Moline, Illinois

[2]In fact, the plates that were initially shipped were tested, and it was determined that the material order had been mixed up. Instead of three 50-ksi and one 36-ksi plates, one 50-ksi and three 36-ksi plates were delivered. This potentially grave error was averted because hardness testing exposed the mistake.

properties for the coupons taken in the direction of the columns 'can' axis were used as the material properties of the column specimens.(Table 4-4) The tensile coupon stresses (longitudinal and transverse) of each column were averaged to be used in comparison to the Rockwell hardness test predictions. This was done because the hardness test is dependent on the yield stress in both directions of the plate. These averaged stresses were labeled as $[F_y(t)_{ave}]$ and $[F_u(t)_{ave}]$ for the yield and ultimate stresses respectively. (See Section 4-3)

The coupons were fabricated according to ASTM standards using a 2-inch gage length and a 0.5-inch gage width.[4] (Fig. 4-1) The coupons were tested in a 120-kip Tinius-Olsen universal testing machine[3] with controlled displacement. A 2-inch extensometer was used to measure the strain in the gage portion and a 0.001-inch dial gage to measure the head displacement.

The coupons were pre-loaded to one-third of F_y to insure that the gaging equipment was recording properly and then unloaded to a near-zero load. At each load increment in the elastic range, the machine was stopped to measure the static load and the head motion. After the coupon yielded, the F_{yd} (dynamic yield) was read and the head motion was stopped to allow the load to stabilize to F_{ys} (static yield). Multiple load/stop steps were required to properly define the static yield portion of the stress/strain curve.(Fig. 4-2) The coupons were loaded to failure, noting the dynamic and static loads at ultimate. The final width, thickness, and elongation were measured after fracture to establish the total elongation and the reduction of the cross-sectional area. The measured values of the dynamic and static yield and ultimate stresses, as well as, the total elongation and the reduction of the cross-sectional area are listed in Tables 4-5 and 4-6.

4.3 Correlation of Hardness Measurements with Tensile Coupon Tests

After the hardness measurement data and tensile coupon results were compiled, the ultimate stress $[F_u(h)]$ was estimated from the hardness readings. The estimated yield stress $[F_y(h)]$, the ultimate tensile stress $[F_u(t)_{ave}]$, and the tensile yield stress $[F_y(t)_{ave}]$ of the tensile coupons were compared. $[F_y(t)_{ave}]$ and $[F_u(t)_{ave}]$ are the average of the yield stresses and the average of the ultimate stresses, respectively, from the tensile coupons parallel to the direction of rolling and those transverse to the direction of rolling.

[3]Tinius-Olsen Machine Co., Willow Grove, PA

4.3.1 INITIAL OBSERVATIONS

The estimates of the ultimate stress [$F_u(h)$] were based on Table 4-7, a chart of Rockwell B hardness readings and ultimate stresses taken from the manual for the hardness tester.[13] These values were multiplied by 0.70 to compute [$F_y(h)$], the estimated yield stress. The 0.70 value was based on previous experience and it agreed with the tensile coupon results from specimen E1. However, the results from the E3 tensile coupons indicated that the value should be 0.60. This discrepancy pointed out that material variability might affect the accuracy of this procedure.

4.3.2 DIFFICULTIES IN EVALUATION OF HARDNESS READINGS

Three unknown factors affected the accuracy of the $F_y(h)$ estimation. The first factor was the repeatability of the hardness measurements. It was difficult to achieve consistent hardness readings for the salvaged specimens because their surface was curved, pitted and rough. (Tables 4-1 and 4-2) The hardness readings taken from the tensile coupons were much more consistent, yet repeatability was still somewhat dependent on the technique of the person conducting the hardness tests. Practice was required to develop a technique which produced consistent reliable hardness measurements.

The second factor which caused difficulties was the uncertainty of the ratio of $[F_y(t)_{ave}] / [F_u(t)_{ave}]$. The ratio of $[F_y(t)_{ave}] / [F_u(t)_{ave}]$ for the tensile coupons ranged from 0.59 to 0.86 (Table 4-8), this indicated that there was a large variability of chemical composition for the different steels tested. The result was that the accuracy of the estimated yield stress was difficult to gage before the tensile coupons were tested. (Fig. 4-3)

The third factor which caused difficulties was the accuracy of the ultimate stress estimation table (Table 4-7) that converted the hardness readings to [$F_u(h)$] [13]. The data for Table 4-7 came from the manual for the hardness tester and was a convenient tool, but the estimated ultimate tensile stresses were high for all the steels tested. For some specimens, the difference was as high as 1.25 $F_u(t)_{ave}$.(Fig. 4-4)

4.3.3 COMPARISON

Although there were many factors contributing to the error in the yield stress determination from hardness readings, the errors often canceled themselves out, giving an excellent estimate of the yield stress. The coupons for the fabricated columns were flat, unpitted, with a thin coating of mill scale. For the four different thicknesses, the variation between the tensile coupon ultimate [$F_u(t)_{ave}$] and the estimated ultimate

from hardness value $[F_u(h)]$ was small except for plate P4. The 0.70 $[F_u(h)]$ estimated yield stress was remarkably close to $[F_y(t)_{ave}]$ for all the fabricated specimens. (Table 4-8)

There were mixed results in using the $0.7[F_u(h)]$ estimate for the salvaged specimens. For the Series 1 specimens and Specimen C4B, the $0.7[F_u(h)]$ estimate was close only because the estimated $[F_u(h)]$ was $1.26[F_u(t)_{ave}]$ and the $[F_y(t)_{ave}] / [F_u(t)_{ave}]$ ratio was small. The hardness readings for the Series 2 and Series 3 specimens estimated $[F_u(t)_{ave}]$ accurately. However, the ratio of $[F_y(t)_{ave}] / [F_u(t)_{ave}]$ was large, and caused the $0.7[F_u(h)]$ estimate to be too high.(Table 4-8)

4.3.4 CONCLUSIONS AND RECOMMENDATIONS

The Rockwell hardness measurements and the static yield stresses from the tensile coupons are shown in Fig. 4-5. In Fig. 4-3, there appears to be a functional relationship for estimating the yield stress as the band of points forms almost a straight line. The points for the fabricated specimens are quite consistent. On the other hand, the salvaged specimens with 41-ksi material had a greater variability of hardness.

In Fig. 4-3, a straight line approximation of the band gives the following formula for estimating the stress $[F_y(h)]$ based on the hardness readings by using $[F_u(h)]$ from Table 4-7.

$$F_y(h) = \frac{0.330467}{\frac{1}{F_u(h)} - 0.006347} \tag{4.1}$$

The standard deviation for this plot is 12%. Further study is needed to understand the range of variables and to reduce the variability of the hardness readings.

One suggestion was to use the Brinell hardness test instead of the Rockwell B hardness test, since Brinell hardness test uses a 1/8th-inch diameter ball-bearing, instead of a 1/16th-inch ball-bearing. It was felt the larger diameter ball-bearing might give a better representation of the material properties through the thickness.

5. STUB-COLUMN TESTS

5.1 Stub-Column Layout and Test Setup

Stub-column tests were conducted to determine the compressive properties of the tube wall material and to estimate the intensity of longitudinal residual stresses in the section. The guidelines of the Structural Stability Research Council (SSRC) Technical Note B-3 were followed for these tests.[17] Each Series of the fabricated specimens had a stub-column rolled from the plate used in the critical section(s) of the long columns.(Fig. 2-4) The stub-columns for the salvaged specimens were cut from one of the tubes in each Series.(Fig. 2-1)

5.1.1 STUB-COLUMNS FOR FABRICATED SPECIMENS

The stub-columns were cold-rolled and welded, following the same procedure for cold-rolling as for the cans of the long specimens. A square steel end plate was welded to each end of the stub-column.

A typical setup for testing stub-columns is shown in Fig. 5-1 and in Photo 5-1. A thin layer of Hydrostone[1] grout was used to minimize the effects of warping in the end plates and to compensate for any misalignment of the machine head. In the setup procedure, a layer of wet Hydrostone mix was spread on the testing pedestal protected by a plastic sheet. Four 1/16-inch wooden strips were taped to the bottom of the stub-column to ensure that there would be no metal to metal contact, and the specimen was lowered and centered. The specimen was slightly twisted back and forth until the Hydrostone was fully spread and the weight of the stub-column was resting fully on the wooden wedges. The top was prepared by attaching a plastic sheet to the machine head, and lowering the head until a thin gap was left between the machine head and the highest point of the top end plate. The gap in one corner of the specimen was gaged with a wooden wedge, then the machine head was raised. Hydrostone was placed on top of the end plate, and the head quickly lowered to the same corner gap checked with the wooden wedge. The Hydrostone was allowed to set for an hour before testing in order to develop strength. Meanwhile, the instrumentation was installed.

5.1.2 STUB-COLUMNS FOR SALVAGED SPECIMENS

The stub-columns for salvaged specimens were saw-cut to the required lengths. Three types of end conditions were used: stub-columns E1-SC and E3-SC were tested with square end plates welded to both ends, stub-column S2-SC had an end plate welded to only one end, and C4B-SC had no end plates.

[1]Hydrostone Gypsum Cement, United States Gypsum, Chicago, Illinois

Stub-columns E1-SC and E3-SC, which had end plates at both ends, had the same test setup as the fabricated stub-columns.(Fig. 5-1 and Photo 5-1) After E1-SC and E3-SC were tested, it was determined that the saw cut ends were flat enough to not require welded end plates. The setup of stub-columns S2-SC and C4B-SC was changed to take advantage of this.

Stub column S2-SC was placed into the testing machine with the cut end on a hardened steel plate, with aluminum foil placed between the column and the hardened plate. (Fig. 5-2) The aluminum foil was used to eliminate the effects of burrs and marks from the saw cutting process. The Hydrostone was placed on the top welded end plate, and the machine head, with plastic taped to it, was lowered onto the Hydrostone, as was done with the fabricated stub-columns.

Stub column C4B-SC was placed into the machine with the 'A' end on a hardened steel plate, with aluminum foil placed between the saw cut end and the hardened plate. (Fig. 5-3) Aluminum foil was placed over the top end of the specimen and a hardened steel plate on top of it. Wet Hydrostone was placed on top of the hardened steel plate and the machine head lowered as done previously for the fabricated stub-columns.

5.1.3 STUB-COLUMNS FOR SMALL-SCALE MANUFACTURED SPECIMENS

Stub-columns P1S-SC and P2S-SC, the small-scale manufactured specimens, were saw-cut to the required lengths. Both specimens were tested without end plates, as shown in Fig. 5-3. The specimens were placed in the machine on a hardened steel plate, with aluminum foil between the saw cut end and the plate. A second hardened plate was placed on top of each specimen, again separated by aluminum foil. Wet Hydrostone was placed on top of the plate and the machine head lowered as done previously for the large-scale fabricated stub-columns.

During shipment, the tube for specimen P1S was accidentally dented slightly. The tube was to be cut so as to have this dent positioned on a scrap portion. However, due to a misinterpretation of the lay-out for the cuts, a wrong cut was made and the dent was positioned on the stub-column section of the tube. There was not enough tubing left to cut another stub-column, and trying to cut out the dented section of P1S-SC would have produced a stub-column of insufficient length.

It was then decided to repair the dent so that it would not cause the stub-column to fail there, thereby giving inaccurate test results. This repair was accomplished by applying a steel patch of approximately half the tube thickness over the dent. The patch used for this repair is shown in Fig. 5-21 and Photo 5-3. The patch was cut to extend at least one inch past the visible dent-affected area of the tube in all directions,

then it was pre-formed to fit the outside surface of the tube. The surface of the dent was cleaned and coated with Epoxy cement. The patch was then placed over the dent, and three steel hose clamps were tightened around the patch. The straps were tightened starting at the center and working out to the edges of the patch in order to squeeze Epoxy out at all edges of the patch. This assured proper attachment of the patch to the tube. The Epoxy was then allowed to harden for 24 hours before testing the stub-column.

5.1.4 INSTRUMENTATION

All of the large-scale stub-column tests were conducted in the Baldwin 5-million pound universal testing machine[2], and the small-scale tests in the 120 kip Tinius-Olsen testing machine. The testing procedure as described in the SSRC Technical Bulletin B-3 was followed.[17] The instrumentation arrangement is shown in Fig. 5-4 and Photos 5-1 and 5-2. Four 0.0001-inch dial gages labeled G1 to G4 were attached to the 1/2-inch diameter studs located in the central gage length of the stub-column to measure the axial strains. The gage lengths used were as follows:

All large-scale specimens → Gage Length = 10 in.
P1S-SC → Gage Length = 7 in.
P2S-SC → Gage Length = 8 in.

Note that overall shorter gage lengths were used for P1S-SC and P2S-SC due to their smaller size. Also, the 7-inch gage length was used for P1S-SC because the patch mentioned earlier did not allow enough space for properly positioning the 8-inch gage length.

Steel studs were welded to the specimens to support all instrumentation. However, specimen P1S-SC had a thin wall thickness; too thin for welding the studs. In this case, the studs were cut from a dense plastic polymer, and then Epoxied to the column surface. A wire was also strung through a hole in each stud as a precaution to keep a stud from falling off should the Epoxied connection fail. All instrumentation was then secured to these plastic studs.

Overall axial deformation of large-scale stub-columns was measured as follows. A 0.0001-inch dial gage labeled L1 was connected to the studs at the bottom of the specimen, and then tied with a wire to a stud at the top end in order to measure the overall axial shortening. A 0.001-inch dial gage labeled L2 was used to measure the head motion of the machine. An LVDT labeled L1A was also used for some of the stub-columns in addition to the dial gage.

The arrangement for small-scale stub-columns (P1S-SC and P2S-SC) was similar

[2]Baldwin-Lima-Hamilton Corp., Philadelphia, PA

to the above, except that no LVDTs were used. All measurements were take with dial gages.

5.2 General Test Procedure and Observations

The stub-columns had a linear load-deformation response until the onset of yielding. The average stress at first yielding indicated the level of the longitudinal compressive residual stresses. For the salvaged specimens, which were seamless tubes with low residual stresses, the response was linear almost until the level of overall yielding. The fabricated specimens first yielded at about 70 percent of the overall yield stress or somewhat higher. This meant that the level of compressive residual stresses was 30 percent of the overall yield stress or less. After the entire section yielded, the yield plateau measured the overall compressive yield stress.

The testing procedure for the stub-columns had several phases. The initial phase was to load the stub-column in small load increments to insure that the dial gages in the central gage portion of the specimen were behaving uniformly. After five load steps, larger load steps were used until the load-deformation response for the specimen became non-linear which was indicated by larger displacement increments of the dial gages for a given load step. The load increment was reduced at this point to better define the load-deformation response, and these load steps were continued until either the specimen could not maintain the load or axial shortening was excessive. Then, increments of head motion were used to continue the test until a local buckle formed and the load steeply dropped. Then, the specimen was unloaded in several steps.

In most cases, the local buckle formed a distinctive ring bulge near the top or bottom end. Typical ring bulges are shown in Photos 5-1 and 5-4.

5.3 Description of Individual Stub-Column Tests

5.3.1 STUB-COLUMN P1-SC

The fabricated stub-column P1-SC (L=48 inches) was loaded in increments to a load of 375 kips (30.6 ksi) when the strain increments in the central gage portion began to increase indicating the initiation of yielding due to compressive residual stresses. The specimen was loaded for three more increments, after which dial gage G4 stopped moving and dial gage G3 had large strain increments. (Fig. 5-5) The explanation for these irregular readings at the time of the test was the formation of a bulge above the G4 dial gage location. Further testing of the specimen was controlled by head motion increments.

The specimen attained a static yield load of 468 kips (38.3 ksi) which lasted five compression increments. (Fig. 5-6) The stub-column load began to increase after this point and reached a static ultimate load of 516 kips (42.1 ksi). Then, the strain increments in dial gage G2 began to decrease. A substantial local buckle developed in the longitudinal weld near the top of the specimen, and the specimen lost load after this point. The ring bulge at the top of the specimen grew to 6 inches in length before the stub-column was unloaded in five steps. In summary, the proportional limit at initial yielding was 76 percent of the yield stress. (F_y=40.2 ksi.)

5.3.2 STUB-COLUMN P1S-SC

The small-scale stub-column P1S-SC (L=20.0 inches) was loaded in increments to a load of 23.3 kips (31.37 ksi) when the strain increments in the central gage portion began to increase indicating the initiation of yielding due to compressive residual stresses. One more load increment was completed. Then, the G2 and G4 strain readings began to decrease, and G1 and G3 had very high positive strain increments. These gage readings corresponded to a bulge forming at the opposite sides of the column below gages G2 and G4. Further testing of the specimen was controlled by head motion increments. Waves could be seen along the full length of the column during this period. In the next load increment, G1 and G3 also started giving negative strain increment readings. These readings corresponded to a fully developed ring bulge at the bottom of the stub-column.(Fig. 5-5a)

The specimen attained a static yield load of 28.1 kips (37.84 ksi) after which the column immediately started losing load (Fig. 5-6a), and the bulge began to grow very rapidly. The column was unloaded in three steps.

In summary, the yield stress and ultimate stress are the same because the column started losing load immediately after reaching the yield load. The proportional limit at initial yielding was 31.37 ksi; that is 83 percent of F_y=37.84 ksi.

The patch applied to the column, as described earlier in Section 5.1.3, performed well during the stub-column test. In the early stages of the test, the patched area took most of the strains in the tube. But, as the load increased, the strain distribution around the circumference of the tube evened out as if the patch were not present.

5.3.3 STUB-COLUMN P2-SC

The fabricated stub-column P2-SC (L=54 inches) was loaded in small steps to a load of 800 kips (39.9 ksi) when the strain increments in the central gage portion began to increase indicating the initiation of yielding due to compressive residual stresses. The specimen was loaded two more increments, and then the strain increments began to

grow rapidly. (Fig. 5-7) Further testing was controlled by head motion increments.

The specimen attained a static yield load of 1128 kips (56.3 ksi) which lasted for five more compression increments.(Fig. 5-8) Waves in the side of the column appeared along the full length during this period. Then the load began to increase and reached a static ultimate load of 1145 kips (57.2 ksi). After this, the load dropped, and the waves in the column wall concentrated in a ring bulge at the bottom of the specimen. The specimen was compressed three more increments, and the local buckle was allowed to grow further, then the stub-column was unloaded in six steps. In summary, the proportional limit at initial yielding was 70.8 percent of the yield stress. (F_y=56.3 ksi)

5.3.4 STUB-COLUMN P2S-SC

The small-scale stub-column P2S-SC (L=29.625 inches) was loaded in increments to a load of 63.7 kips. (31.93 ksi) The strain increments in the central gage portion began to increase, indicating the initiation of yielding due to compressive residual stresses. The specimen was loaded one more increment, before the strain increments began to rapidly increase. (Fig. 5-7a) Further testing was controlled by head motion increments.

The specimen attained a static yield load of 80.9 kips (40.55 ksi) which lasted for several more compression increments.(Fig. 5-8a) Waves in the side of the column appeared along the full length during this period. Then the load began to increase and reached a static ultimate load of 88.7 kips (44.56 ksi). After this, the load dropped and the waves concentrated in a ring bulge at the top of the specimen. The specimen was compressed four more increments, and the local buckle was allowed to grow further before the stub-column was finally unloaded in two steps. In summary, the proportional limit at initial yielding was at a load of 63.7 kips; that is, 78.7 percent of the yield stress. (F_y=40.55 ksi)

5.3.5 STUB-COLUMN P3-SC

The fabricated stub-column P3-SC (L=75 inches) was loaded in increments to a load of 1000 kips (40.5 ksi). Then the strain increments in the central gage portion began to increase much faster, indicating the initiation of yielding due to compressive residual stresses. The specimen attained a static yield load of 1379 kips (55.8 ksi), after which, further testing was controlled by head motion increments. (Fig. 5-9)

The specimen reached an ultimate load of 1385 kips (56 ksi) (Fig. 5-10). This load was sustained for three more increments before the load dropped and a noticeable bulge developed at the bottom of the specimen. The stub-column was compressed a total of 0.872-inches and stabilized at a load of 680 kips (27.5 ksi) before the

longitudinal weld popped at the bottom of the then 6-inch-long bulge. The specimen was unloaded in four steps. In summary, the proportional limit at initial yielding was 79.4 percent of the yield stress. (F_y=51 ksi)

5.3.6 STUB-COLUMN P4-SC

While the fabricated stub-column P4-SC (L=60 inches) was placed into the testing machine, the wooden wedge that was used to measure the gap got caught between the machine head and the top plate of the stub-column above the location of dial gage G4. There was concern that the wedge might lead to a stress concentration at that corner of the specimen.

After the Hydrostone set, the stub-column was loaded in 25-kip increments. The dial gages in the middle gage portion indicated that the strain increments at dial gage G4 were higher than at the other three gages. (Fig. 5-11) When the specimen was loaded to 175 kips (15 ksi) the strain increments around the circumference became uniform. The 25-kip load increments were continued until the specimen reached a static load of 558 kips (48.1ksi). Then, a bulge above dial gage G4 was observed. The specimen quickly lost load with additional axial compression.(Fig. 5-12) After a total axial shortening of 0.283 inches, the specimen was unloaded in three steps.

It was not fully clear whether the bulge above dial gage G4 was due to the wooden wedge accidentally left above that location or due to the high D_m/t ratio of the specimen (D_m/t = 95.18).

5.3.7 STUB-COLUMN E1-SC

In addition to the regular instruments described in Section 5.1.4, the salvaged stub-column E1-SC (L=42 inches) had sensors attached to its surface to monitor acoustic emissions during the test. Stub-column E1-SC was loaded in equal load increments to a load of 487 kips (39.8 ksi). During the last load step, the acoustic sensing equipment began 'crackling' and the strains in the specimen began to increase, indicating the initiation of local yielding. The specimen reached a dynamic load of 629 kips (51.5 ksi) and stabilized at a load of 607 kips (49.7 ksi).(Fig. 5-13) Further testing was controlled by displacement increments of the machine head.

The specimen had a static yield load of 612 kips (50 ksi) which remained unchanged for six increments before the load began to climb due to strain hardening.(Fig. 5-14) The specimen reached a static ultimate load of 727 kips (59.5 ksi) before a ring bulge developed at the bottom of the specimen and the load dropped off. Then, the specimen was unloaded in six steps. In summary, the stub-column behavior indicated that longitudinal residual stresses were very small.

5.3.8 STUB-COLUMN S2-SC

The salvaged stub-column S2-SC (L=42 inches) had acoustic sensors attached to its surface to monitor the acoustic emissions during the test. Stub-column S2-SC had one end plate welded at the top, and aluminum foil placed at the bottom under the saw cut end.(Section 5.1.2) The specimen was loaded in 80 kip increments and the strain increments were uniform up to a load of 750 kips (39.5 ksi).(Fig. 5-15) Further testing was controlled by displacement increments of the machine head.

The specimen had a static yield load of 758 kips (40 ksi) which stayed constant for five additional displacement increments.(Fig. 5-16) During this stage, yielding was accompanied by wide-spread flaking of rust from the specimen surface and also 'crackling' of the acoustic sensing equipment. The load then increased, and a small bulge formed near the bottom of the specimen. After four additional deformation increments, a bulge also began to develop at the top of the specimen near the end plate. The specimen reached a static ultimate load of 1025 kips (54 ksi) just before a large buckle formed in the corroded area at the bottom of the specimen between dial gages G1 and G4. Then, the specimen was unloaded in five load steps. Judging by the behavior, there were no longitudinal residual stresses in the specimen.

5.3.9 STUB-COLUMN E3-SC

The salvaged stub-column E3-SC (L=42 inches) was initially loaded in increments of 80 kips, and the strain around the cross section was uniform except for at dial gage G3. It was determined after several more load steps that the dial gage was not tracking properly, so it was replaced with another 0.0001-inch dial gage. After the specimen reached a load of 480 kips (25.7 ksi), the stub-column was unloaded by 20 kips to confirm the linearity of unloading. Then it was reloaded by one increment of 100 kips. The stub-column was loaded in increments until a dynamic load of 782 kips (41.3 ksi) was reached and the column stabilized at a load of 749 kips (39.6 ksi).(Fig. 5-17) After this point, the specimen was loaded two more increments, but the gages in the central gage length of the column and the head motion gage continued to move. It turned out that the new machine operator had left the valve on and was trying to maintain the load instead of stopping the machine head.

The specimen had a long yield plateau at the load of 763 kips (40.7 ksi). Then, the load increased gradually with additional axial compression, and a bulge began to form at the top of the specimen. The load continued to increase with axial compression until it reached a static ultimate load of 1088 kips (55.9 ksi). Shortly after this point, a bulge formed at the bottom of the column, and the load dropped off. Five additional

compression increments were made before the specimen was unloaded in several steps.(Fig. 5-18)

5.3.10 STUB-COLUMN C4B-SC

Stub-column C4B-SC (L=36 inches) had no end plates and was tested with aluminum foil at both ends.(Section 5.1.2) The walls of the specimen were heavily corroded, and after several 50-kip load increments, the pattern of strain readings in the midsection became erratic. This was apparently due to the effects of localized corrosion. The specimen was loaded to 300 kips, when it was decided to unload the section to check the linearity of the strains. The specimen was reloaded in 50-kip increments, but the pattern of strains remained erratic. Loading was continued until a static yield load of 542 kips (39.3 ksi) was recorded.(Fig. 5-19) The load increased with axial shortening and attained a static ultimate load of 586 kips (42.5 ksi) before the member gradually lost load.(Fig. 5-20) During this process, several large, irregular buckles formed over the whole surface of the specimen (See Photo 5-6). The specimen was compressed several more increments to enlarge the size of the buckles before it was unloaded.

6. DENTING OF TEST SPECIMENS

6.1 Initial Small-Scale Tests

Tests were conducted on several small-diameter tubes to get an idea of how the specimens with low (D_m/t)[1] would behave when dented. The concern was that the indenter would squash the specimens into an oval shape instead of forming a sharp V-shaped dent. As shown if Fig. 6-1, three different methods of supporting the specimens were tested to determine the most suitable setup: an H-beam filled with sand, a 90-degree angle, and a flat surface. The tests were conducted in a testing machine or, as simply as in a hand-screw vise as shown in Photo 6-1.

The small-scale tubular specimens had $t = 0.065$ inches, $D_m = 1.75$ inches $(D_m/t = 27)$, and an average hardness of 80 (approximate $F_y = 54$ ksi). Since Specimens E1 and E3 had similar properties, the behavior of the small-scale specimens was expected to be similar to that of the large-scale specimens. The results indicated that the specimen formed a sharp V-shape dent with a minimum amount of squashing regardless of the type of support, although the flat surface induced a slightly larger amount of end uplift. Since denting the specimen on a flat surface was the simplest method, the specimens were dented in this manner.

A series of five dents, approximately equal to $0.15\,D_m$, were made in the small-scale specimens to estimate the amount of elastic return for specimens E1 and E3. It was determined that the small-scale specimen had an elastic return of approximately 14.5 percent of the loaded dent depth. This meant that if the small-scale specimen was loaded with a dent depth of 0.275 inches, it had a dent depth of 0.235 inches after the load was removed. This relationship was used for the denting of Specimens E1 and E3.

6.2 Denting of Specimens in 800-kip Machine

6.2.1 SETUP AND INSTRUMENTATION

Salvaged specimens E1 and E3 were dented with a dent of $0.15\,D_m$ using the 800-kip machine[2].(See Photos 6-2 and 6-3.) Four 0.001-inch dial gages were used to measure the specimen response to mid-length load application. As shown in Fig. 6-2, two dial gages located at the ends measured the end uplift, one dial gage measured the side expansion of the specimen (the 'squash' displacement), and the fourth dial gage measured the machine head displacement (dent depth). The indenter used for the experiment had a 1.0-inch radius, a height of six inches, and a length of 12 inches.

[1] D_m is the mid-thickness diameter

[2] Riehle Testing Machine Corp., 1905

The specimens were placed into the 800-kip machine with the mid-length of the specimen centered under the machine head. After rotating the specimen to position the zero reference line on 'top', it was held in place with wooden wedges. The indenter was placed on top of the specimen at mid-length and the machine head lowered until it pressed against the indenter, thus keeping the indenter from falling off the specimen.

6.2.2 DENTING OF SPECIMENS E1 AND E3

6.2.2.1 Specimen E1

Specimen E1 (D_m= 10.38 inches) was designed to have a $0.15\,D_m$ (1.56-in.) dent depth. The peak denting load was 75.3 kips at an indentation depth of 1.9 inches. The specimen was unloaded to 5 kips and the remaining indentation depth of 1.46 inches. (Fig. 6-3) After the machine head was raised, the specimen was surveyed and the measured dent depth was 1.41 inches ($0.136\,D_m$). This was accepted to be close enough to the intended $0.15\,D_m$ dent depth. The measured length of the observable dent was 4.75 feet.(Fig. 7-39)

6.2.2.2 Specimen E3

Specimen E3 (D_m= 13.59 inches) was designed to have a $0.15D_m$ (2.03-inch) dent depth. The peak denting load was 89.1 kips at an indentation depth of 2.42 inches. The specimen was unloaded to 5 kips and the remaining indentation depth of 2.04 inches.(Fig. 6-4) After the machine head was raised, the specimen was surveyed and the measured dent depth was 1.87 inches ($0.138D_m$). This was accepted to be close enough to the intended $0.15\,D_m$ dent depth. The measured length of the observable dent was 6.5 feet.(Fig. 7-45)

6.3 Denting with Hydraulic Jack

6.3.1 SETUP AND INSTRUMENTATION

Since many of the fabricated specimens were longer than 28 feet, the denting procedure could not be conducted in the 800-kip machine, and the test setup was changed. The specimens were dented with a hydraulic jack applying the load in the horizontal direction, as shown in Photo 6-4. The specimens were laid on their side with the zero reference line facing the indenter. A large, 10-foot long box beam served as a back support. To insure continuous contact between the box beam and the specimen, Hydrostone grout was poured into the small gap between the specimen and the box beam.(Photo 6-5) The space between the beam and specimen at the bottom was

stuffed with foam and paper over the length of three diameters to prevent the grout from leaking through the gap. The grout was poured and allowed to set for an hour before starting the denting process was started.

The instrumentation for the denting procedure consisted of four 0.001-inch dial gages, a 1/64th-inch division scale, a transit and a load cell.(Fig. 6-5 and Photo 6-6) One horizontal dial gage was located at each end of the specimen to measure the end displacements. However, they were removed when it was discovered that the friction of the end plates on the floor was causing unequal motion of the two ends. One 'squash' and one dent dial gages were located at the dent. The 1/64th-inch scale was attached to the indenter, and the transit was located at one end of the specimen to measure the horizontal motion of the hydraulic jack head. The load cell attached to the hydraulic jack measured the indentation load. The indenter was the same 1.0-inch radius and 12-inch length indenter that was used for Specimens E1 and E3 in the 800-kip machine.

Since neither the small-scale tests described in Section 6.1 nor the earlier theoretical work [11] were sufficiently adequate to predict the amount of elastic recovery, many load and unload cycles were required to produce the desired final dent depth. The reason for this was the non-linear behavior of the load-response curve for tube denting and the changing slope of the elastic return.

The specimens were loaded to a dent equal to the desired dent depth and then unloaded to determine the slope of the elastic return. The slope of the loading curve and the slope of the elastic return were used to estimate the peak load and indentation depth to produce the desired final unloaded dent depth. Since the slope of the unloading curve changed with the increased indentation depths and the loading curve became flatter, small indentation increments were used to produce the correct final dent depth.(Fig. 6-9) However, once the load-response curve for a specimen of a certain (D_m/t) and yield stress was established, the denting of the companion specimen was easier.

6.3.2 DESCRIPTION OF DENTING OF INDIVIDUAL SPECIMENS

6.3.2.1 Specimens P1P and P1F

Specimens P1P and P1F (D_m= 15.0 in.) were designed to have a $0.05\,D_m$ (0.75-inch) dent depth. Specimen P1P was loaded and unloaded three times to produce the desired dent depth. The peak indentation load was 20.8 kips at an indentation depth of 1.29 inches. The indentation depth at almost zero load was 0.75 inches. (Fig. 6-6) Specimen P1F was loaded and unloaded three times. The peak indentation load was 20.3 kips at an indentation depth of 1.34 inches. The indentation depth at almost zero load was 0.79 inches. (Fig. 6-6) Thus, the elastic return was approximately 0.55 inches for both specimens.

The survey results show that Specimen P1P had a dent depth of 0.71 inches and Specimen P1F had a dent depth of 0.74 inches, which were very close to the desired dent depth of 0.75 inches. The small deviation between the survey results and the test was due to the small non-zero load and because a 1/64th-inch scale was used to survey the specimens. The measured length of the observable dented zone was 2.6 feet. (Figs. 7-27 and 8-6)

6.3.2.2 Specimen P1PS

Specimen P1PS (D_m= 3.94 inches) was designed to have a $0.05\,D_m$ (0.197 inch) dent depth. Specimen P1PS was loaded and unloaded four times to produce the desired dent depth. The peak indentation load was 1.085 kips at an indentation depth of 0.301 inches. The indentation depth at almost zero load was 0.190 inches. (Fig. 6-6a) Thus, the elastic return was approximately 0.111 inches.

The survey results showed that Specimen P1PS had a dent depth of 0.200 inches, which was very close to the desired dent depth of 0.197 inches. The small deviation between the survey results and the test was due to the small non-zero load and because a 1/64th-inch scale was used to survey the specimen. The measured length of the observable dented zone was 10.5 inches.(Fig. 9-25)

6.3.2.3 Specimen P2P and P2F

Specimens P2P and P2F (D_m= 17.0 inches) were designed to have a $0.096\,D_m$ (1.63-inch) dent depth. Due to misinterpretation of instructions, P2P was dented with a $0.14\,D_m$ (2.36-inch) dent depth. In order to keep Specimens P2P and P2F the same except for the end conditions, Specimen P2F was dented with the same dent depth. The load-response curves for the denting of P2P and P2F were almost identical. The peak load for both specimens was 80 kips at an indentation depth of 3.25 inches. The dent depth at near zero load was 2.36 inches for Specimen P2P and 2.33 inches for Specimen P2F.(Fig. 6-7) The profile survey and diameter measurements indicated a slightly different dent depth values of 2.37 inches for Specimen P2P and 2.31 inches for Specimen P2F. (Figs. 7-30 and 8-8) The elastic return for both specimens was 0.89 inches. The measured length of the observable dented zone was 5.0 feet.

6.3.2.4 Specimen P2PS

Specimen P2PS (D_m= 5.382 inches) was designed to have a $0.096\,D_m$ (0.517 inch) dent depth. However, the corresponding large-scale specimen, P2P, was dented with a $0.14D_m$ (2.36-inch) dent depth. In order to keep Specimens P2P and P2PS scaled correctly, specimen P2PS was dented with the same dent depth percentage

($0.14D_m$=0.753 inches). Specimen P2PS was loaded and unloaded three times to produce the desired dent depth. The peak load for the specimen was 6.88 kips at an indentation depth of 0.990 inches. The dent depth at near zero load was 0.774 inches.(Fig. 6-7a) The profile survey and diameter measurements indicated a slightly different dent depth values of 0.740 inches. (Figs. 9-31) The elastic return for the specimen was 0.216 inches. The measured length of the observable dented zone was 2.15 feet.

6.3.2.5 Specimens P3PA and P3PB

Specimens P3PA and P3PB (D_m= 24.5 inches) were designed to have a $0.048\,D_m$ (1.18-inch) and $0.15D_m$ (3.67-inch) dent depths, respectively. Since the 12-inch long indenter used for the other specimens may not have been long enough to span the dented section, a two foot long rocker bearing with an edge radius of 1.0 inch was used.

Specimen P3PA was loaded and unloaded three times to attain the desired dent depth. The peak load was 37 kips at an indentation depth of 2.5 inches and a near zero load indentation depth of 1.26 inches. Specimen P3PB was loaded and unloaded four times before the desired dent depth was produced. The peak load was 62.5 kips at an indentation depth of 5.45 inches and a near zero load indentation depth of 3.64 inches. The load-response curves for the two specimens closely matched, as can be seen in Fig. 6-8. The elastic return was 1.24 inches for P3PA and 1.81 inches for P3PB. The measured length of the observable dented region was 10.0 feet for P3PA and 15.0 feet for P3PB.(Figs. 7-31 and 7-33)

6.3.2.6 Specimen P4P

Specimen P4P (D_m= 18.75 inches) was designed to have a $0.115\,D_m$ (2.16-inch) dent depth. It was the first specimen to be dented using the hydraulic jack and the rigid box beam. The specimen was placed directly against the box beam without grout. It was dented 2.089 inches when it was noticed that the longitudinal weld, which was directly opposite the indenter, was not in contact with the box beam, but only the transverse welds at the ends of the central can were in contact.

The specimen was removed and surveyed to establish the current dent depth and out-of-straightness. Then, the specimen was placed against the box beam and grouted with Hydrostone to insure that there would be a continuous bearing against the back support. (This procedure was then used for all subsequent specimens dented with the horizontal jack.)

Since the first denting procedure formed a 0.62-inch dent depth, an additional 1.54-inch dent depth was required to produce the design dent depth. The peak load was

27.35 kips at a total indentation depth of 2.72 inches.(Fig.6-9) The final dent depth was 2.58 inches which was somewhat higher than the design 2.16-inch dent depth. The measured length of the observable dent was 11.0 feet. (Fig.7-35)

6.3.2.7 Specimen D1

The salvaged Specimen D1 (D_m= 10.36 inches) was designed to have a $0.15\,D_m$ (1.56-inch) dent depth. The specimen was loaded using the expected load response curve from Specimen E1. The peak load of Specimen D1 was 52.9 kips at an indentation depth of 2.07 inches.(Fig. 6-3) The final dent depth was 1.60 inches and the measured length of the observable dent was 5.0 feet. (Fig. 7-37)

6.3.2.8 Specimen D3

The salvaged Specimen D3 (D_m= 13.55 inches) was designed to have a $0.15\,D_m$ (2.03-inch) dent depth. The specimen was loaded following the expected load response curve from Specimen E3. The peak load of Specimen D3 was 88.8 kips at an indentation depth of 2.7-inches.(Fig. 6-4) The final dent depth was 2.12 inches and the measured length of the observable dent was 6.5 feet. (Fig. 7-43)

6.4 Pre-Test Surface Profiles

The longitudinal surface profiles were made after denting to check the accuracy of the dent depth measurements. The dent depth results from the denting procedure were slightly higher than the surveyed results due to the small non-zero load at which the final dent depth reading was made. This small load was required to insure that the indenter was still in contact with the specimen surface, but it also caused a small indentation. It should also be noted here that the surveys were conducted with a 1/64-inch division scale, so that a deviation of 0.02 inches in the dent depth is not unreasonable.

The survey results indicated that for a few specimens the side opposite the dent was deformed in the process of denting. The extent was over the Hydrostone supported length, and this meant that the three-diameter length of support was not sufficient for some of the specimens especially those with larger D_m/t ratio.

7. LONG-COLUMN TESTS USING CYLINDRICAL BEARING FIXTURES

7.1 Instrumentation

The instrumentation for testing the long columns using cylindrical bearing fixtures consisted of strain gages, rotation gages, LVDT's (linear voltage displacement transducers), and 0.001-inch dial gages. A consistent labeling scheme, with adaptations to individual specimens was used. Fundamentally, the four longitudinal reference lines at 0, 90, 180 and 270 degrees around the circumference and the distance from the bottom of the specimen (designated by 'Levels') uniquely identified the position of the gages. The arrangement of instrumentation is shown in Fig. 7-1 and Photos 7-1 and 1-1B(a).

7.1.1 ARRANGEMENT OF GAGES

The initial column setup for Specimens E1, B3, and E3 used two different labeling schemes: one for the strain gages and one for the LVDT's. The strain gages were arrayed around the specimen at the four longitudinal reference lines and at five 'Levels'. The strain gage locations at a given Level were labeled Lines 1, 2, 3, and 4 corresponding to the 0, 90, 180, and 270 degree longitudinal reference lines. The Levels of the strain gages were determined by dividing the specimen into 'sixths' as shown in Fig. 7-1. Level 0 (zero) was located at the 'A' end (bottom) and Level 6 (six) was located at the 'B' end (top) of the specimen. An example of a strain gage location is SG23. The 'SG' stands for strain gage, the '2' for the second strain gage 'Level' and the '3' for that the gage was on Line 3 (180-degree Reference Line)

Five LVDT 'Levels' were used in testing Specimens E1, B3 and E3. The LVDT's were located at the quarter points and at the ends of the specimen. Level 0 was at the bottom and Level 4 at the top. An example of an LVDT location is L21. This means that the LVDT was located at the mid-length (second quarter) on Line 1 (0-degree Reference Line). The label for LVDT L23 meant that it was located on the same Level as L21, but on Line 3 (180-degree Reference Line), that is, directly opposite the dent.

To provide a more complete displacement profile of the specimens, seven, rather than five, LVDT Levels were used for the dented specimens tested after Specimens E1, B3 and E3.(Fig. 7-2) The Levels were located at the sixth points along the length of the specimen and at the ends. Level 0 was at the bottom and Level 6 at the top of the specimen. An example of an LVDT label is LVDT L33 which means the location at the

mid-length (the third sixth) and on Line 3 (180-degree Reference Line).

7.1.2 GAGE INSTALLATION

The LVDT's were connected to long aluminum rods which were attached to the specimen wall by Epoxied wooden blocks. The rods were free to rotate as the attached points displaced vertically, but only the horizontal motion of the specimen was transmitted to the LVDT. The LVDT in the dent was attached to a hardened screw driven into a small pre-drilled hole in the dent, rather than to an Epoxied wooden block. This was necessary since the Epoxy would break off due to the extensive yielding in the dented portion. (This actually occurred during the test of Specimen E1.)

Dial gages were used in addition to LVDT's at several critical points to ensure the accuracy of the results and to have a back-up system in case of an electrical failure. For example, dial 'D33' was located at mid-length on Line 3 (180 Reference Line), opposite the dent. This was used to verify the accuracy of the readings from LVDT 'L33'. Dial gages D01 and DH0 were at the bottom of the specimen to verify L03. Dial gage D01 measured the lateral motion at the strain gages of Level 0, and DH0 measured the horizontal motion of the end fixture. Dial gage DV1 (with an extension wire) was used to measure the machine head motion. These arrangements are shown in Fig. 7-3 for Specimens E1, B3, and E3 and in Fig. 7-4 for the other dented specimens.

Axial shortening was measured by LVDT LV1 with an extension wire under tension. The gage was attached to the bottom fixture by a special arrangement which allowed the LVDT to remain vertical independent of the rotation of the end fixture. The top end of the wire was tied to a bolt in the top fixture. This measurement was considered to be the axial shortening of the specimen. Dial gage DV1 was attached to the machine base and the end of the extension wire was tied to the machine head. The results for these two measurements differed slightly due to the squashing of gaps in the fixtures under high loads. (For example, see Fig. 7-10 for Specimen P3PA.)

Rotation gages were used to record rotations at key locations along the specimen. The first pin-ended specimens E1, B3 and E3 had rotation gages 7.5 inches from the ends.(Fig. 7-3) For the subsequent specimens, four rotation gages were available. One was attached to each end fixture and one just above and below the dented portion.(Fig. 7-4) This gave a better representation of the sharp deflection discontinuity in the dented portion during testing.

Except for the end rotation gages, all electronic sensors (strain gages and LVDT's) were read and recorded using a MEGADAC data acquisition unit[1]. The dial

gages and the end rotation gages were read and recorded manually.

7.2 General Test Setup

The pin-ended damaged specimens were tested with cylindrical end fixtures, as shown in Photos 7-1 and 7-2. The design of the fixtures allowed for rotation in one plane, with only rolling friction of a cylindrical surface on a flat plate at the ends. Eccentricity in the direction perpendicular to the plane of rolling was eliminated by placing Hydrostone between the fixture and the end plate of the specimen during installation and, in a few cases when eccentricity developed later, by adjusting the fixtures.

The installation procedure was as follows. One cylindrical end fixture was attached to the machine head. The specimen was rolled into the machine while in the upright vertical position and bolted to the top cylindrical end fixture. Next, the specimen was lifted two feet by the machine head and the bottom fixture was positioned under the specimen. Then, the specimen was lowered onto the bottom fixture. After the specimen was positioned, the two end plate hold-down bolts were loosened and the specimen was lifted about two inches. Wood strips were taped to the bottom of the end plate. Hydrostone was placed on the end fixture, and the specimen lowered onto the grout until it sat on the wood strip which eliminated any metal-to-metal contact. The grouting of the top end fixture was similar except a wooden wedge was used to measure the gap at the top, as the top cylindrical end fixture and machine head were lowered onto the Hydrostone-covered top end plate.

The final step was to connect all the wires, brackets, LVDT's, strain gages, and dial gages and check that all were functioning properly before starting the test.

7.3 General Testing Procedure

The loading of the specimens was divided into two ranges: the pre-ultimate range and the post-ultimate range. In the pre-ultimate range, readings were taken after each load increment and again a few minutes later after the load had stabilized. The first few load increments were small to accommodate the initial adjustments of the end fixtures. Then the load steps were increased and later reduced as the anticipated ultimate load was approached. At all steps, the mid-length lateral displacement and axial shortening were plotted against the load to estimate the approach of the ultimate load. The peak load was recorded as the dynamic ultimate load, and the static ultimate

[1]MEGADAC Data Acquisition Unit, OPTIM Corp., Germantown, Maryland

load was read after the load had stabilized at approximately the same axial deformation.

In the post-ultimate range, the specimens were compressed by axial shortening displacement increments. Readings were taken after each displacement increment and again a few minutes after the load had stabilized. This procedure was discontinued at an axial shortening of about two-and-half to four times the axial shortening at the ultimate load. Then, the specimen was unloaded in several steps.

7.4 Description of Axial Tests on Individual Specimens

The description of the axial tests is given in the order of the listing of the specimens in Table 1-1 and not necessarily in the order of actual testing. The pre-test and post-test views of the individual specimens are shown in Photos 1-1A through 1-1E.

7.4.1 SPECIMEN P1P

During the initial loading of Specimen P1P, the lateral displacements and the strain gage readings showed that, due to the small dent size and the negative initial out-of-straightness (result of fabrication), the specimen was bending to produce tension on the dent side. This led to a lateral motion which was opposite to the intended direction. Additional load increments up to $0.53P_y$ (275 kips) confirmed that the specimen would first yield in compression on the side opposite the dent. The test was stopped and the specimen unloaded.

It was determined that a small positive end eccentricity of 0.75 inches would ensure that the specimen would fail at mid-length on the dent side.(Fig. 7-5) The holes in the end plates were slotted by using a cutting torch to provide for such an eccentricity and the specimen was reset and re-grouted at both ends.

The specimen was reloaded in 20-kip increments and the readings confirmed that the lateral motion of the specimen was in the direction that would cause higher compressive stress on the dent side. The dynamic ultimate load was $0.627\,P_y$ (328 kips) and the static ultimate load was $0.611P_y$ (320 kips).(Fig. 7-6) After the ultimate load, the specimen quickly lost its strength with additional axial displacement. After 12 axial compression increments, the total axial shortening was 1.94 times the axial shortening at the ultimate load, and the load was $0.29\,P_y$ (152 kips). The specimen was unloaded in four steps. (Photos 1-1A (a) and (b))

7.4.2 SPECIMEN P2P

Specimen P2P was initially loaded in 50-kip increments. but, after a load of $0.35\,P_y$ (400 kips), 20-kip increments were used because the mid-length lateral displacement indicated that the ultimate load was being approached. The dynamic ultimate load was $0.46\,P_y$ (530 kips) and the static ultimate load $0.45\,P_y$ (516 kips). After the ultimate load, the specimen gradually lost its strength with additional axial shortening.(Fig. 7-8) After 16 axial compression increments, the total axial displacement was 3.1 times the axial displacement at the ultimate load, and the load was $0.21P_y$ (242 kips). The specimen was unloaded in three steps. (Photo 1-1B (a).)

7.4.3 SPECIMEN P3PA

Specimen P3PA was initially loaded in 50-kip increments, but, after a load of $0.58\,P_y$ (850 kips), 25-kip increments were used because the mid-length lateral displacement indicated that the ultimate load was being approached. The dynamic ultimate load was $0.648\,P_y$ (950 kips) and the specimen quickly lost its strength and stabilized to a load of $0.56\,P_y$ (825 kips).(Fig. 7-10) The specimen had a sharp loss of strength with increasing axial displacement. After a total axial displacement of 2.5 times the axial shortening at the ultimate load, the load was $0.22\,P_y$ (316 kips). The specimen was unloaded in two steps. (Photo 1-1C (a).)

7.4.4 SPECIMEN P3PB

Specimen P3PB was initially loaded in 50-kip increments, but, after a load of $0.375\,P_y$ (550 kips), 25-kip increments were used because the mid-length lateral displacement indicated that the ultimate load was being approached. The dynamic ultimate load was $0.43\,P_y$ (630 kips) and the static ultimate load $0.423\,P_y$ (620 kips). (Fig. 7-12) The specimen had a gradual reduction in strength with increasing axial displacement, and, after a total axial displacement of 3.4 times the axial shortening at ultimate load, the load was $0.22\,P_y$ (318 kips). The specimen was unloaded in five increments. (Photo 1-1C (b).)

7.4.5 SPECIMEN P4P

Specimen P4P was loaded in 10-kip increments to a load of $0.05\,P_y$ (30 kips). Then the load increment was increased to 20-kips and a dynamic ultimate load of $0.45\,P_y$ (289 kips) and a static ultimate load of $0.44\,P_y$ (283 kips) were reached. (Fig. 7-14) The specimen had a gradual loss of strength with increasing axial displacement, and, after a total axial displacement of 4.1 times the axial shortening at

the ultimate load, the load was $0.15\,P_y$ (96 kips). The specimen was unloaded in four increments. (Photos 1-1C (c) and (d).)

7.4.6 SPECIMEN D1

Specimen D1 was initially loaded in 20-kip increments. However, after three increments, it was observed that strain increments in strain gages SG02 and SG04 were not equal. Since there should be no eccentricity in the direction transverse to the plane of bending, the load was reduced to 20 to 30 kips and adjustments made to the bottom fixture. The specimen was reloaded and the strain gages checked again. Two additional adjustments were required to bring the strain gages into agreement.

The specimen was reloaded to $0.24\,P_y$ (150 kips) during this adjustment procedure. After the final adjustment was made, the specimen was loaded from 30 kips to $0.24\,P_y$ (150 kips) in one load step. One additional load increment of 30 kips was made before the specimen failed at a dynamic load of $0.304\,P_y$ (193 kips) and then stabilized to a load of $0.296\,P_y$ (188 kips).(Fig. 7-16) The specimen displayed a gradual loss of strength with increased axial displacement. After a total axial displacement of 2.7 times the axial shortening at the ultimate load, the load was $0.11P_y$ (71 kips). At this point the specimen cracked at mid-length on the side opposite the dent.

The crack was found to be in an area that had significant reduction of wall thickness due to corrosion on the inside of the specimen. Ultrasonic thickness measurements indicated that the thickness in this area was 0.21 inches, that is 58 percent of the average thickness of the specimen.(Photo 7-3 shows the crack.) After cracking, the specimen was unloaded. (Photo 1-1C (f).)

7.4.7 SPECIMEN E1

Specimen E1 was the first dented specimen tested in this program, and it provided important insight into the behavior of the dented columns and many firsts for the testing procedure. A $0.25\,D$ (2.6-inch) end eccentricity with respect to the center of gravity at the end was intended for the specimen. A misinterpretation of the end eccentricity versus the total effective eccentricity at the dent (OOS + e) resulted in the actual geometric end eccentricity of 0.9 inches instead of the intended 2.6 inches.(Fig. 7-5)

At mid-length, an additional strain gage was installed on the 315-degree reference line between SG33 and SG34. During the test, the wooden block Epoxied in the dent for LVDT L21 spalled off, and the dent deflection readings taken later were measured with calipers. A screw attachment was used at this location for all subsequent tests.

The specimen was loaded in 20-kip increments until it reached $0.247\,P_y$ (160 kips) when the testing machine indicated an overload in the low range (of the machine). The specimen was unloaded to 20 kips and a valve was adjusted to correct the problem. The specimen was reloaded to $0.247\,P_y$ (160 kips) and then loaded three more increments before the specimen reached a dynamic ultimate load of $0.366\,P_y$ (237 kips) and stabilized to a load of $0.358\,P_y$ (232 kips).(Fig. 7-18) The acoustic sensors confirmed the onset of yielding in the specimen. The specimen had a gradual loss of strength with increased axial displacement. After a total axial shortening of three times the axial shortening at ultimate load, the load was $0.190\,P_y$ (125 kips). The specimen was unloaded in four steps. (Photos 1-1D (a) and (b).)

7.4.8 SPECIMEN B3

Specimen B3 was not dented to have a V-shaped dent as the others; it was already damaged when it was delivered by an out-of-straightness of 3.75 inches and a 0.75-inch ovalization extending over three diameters in the mid-length area. Location of the strain gages and LVDT's in this specimen was different than for the pin-ended dented specimens. The strain gages were located 2 inches from each end, at the bottom quarter, at the mid-length, and at the top sixth point of the specimen.(Fig. 7-20) The LVDT's were attached at the quarter points except for L21 which was located 12 inches above the mid-length. A 0.001-inch dial gage was used at L03 to replace a damaged LVDT.

Specimen B3 was loaded in 25-kip increments to a dynamic ultimate load of $0.516\,P_y$ (392 kips), which stabilized to a static ultimate load of $0.504\,P_y$ (383 kips). (Fig. 7-21) The spalling of rust from the surface and increased acoustic emissions during the last load step indicated that failure was imminent. The specimen lost its strength gradually, and, after a total axial shortening of 3.6 times the axial shortening at the ultimate load, the load was $0.340\,P_y$ (258 kips). The specimen was unloaded in five load steps. (Photos 1-1E (a) and (b).)

7.4.9 SPECIMEN D3

Specimen D3 was loaded in 20-kip increments until, at a load of $0.12\,P_y$ (100 kips), it was observed that the strain increments for strain gages SG02 and SG04 at the bottom end of the specimen were not equal. Since there should not be any eccentricity in the direction transverse to the plane of bending, the specimen was unloaded to 50 kips and the bottom fixture was adjusted. The specimen was reloaded

to $0.12\,P_y$ (100 kips), and the adjustment proved to be effective.

The specimen was loaded in 25-kip increments to a dynamic ultimate load of $0.549\,P_y$ (456 kips) and a static ultimate load of $0.542\,P_y$ (450 kips). (Fig. 7-23) A steep loss of strength then followed as the specimen was compressed. After the specimen was compressed to a total of 2.5 times the axial shortening at the ultimate load, the load stabilized to $0.24\,P_y$ (202 kips). The specimen was unloaded in four steps. (Photo 1-1E (c).)

7.4.10 SPECIMEN E3

Specimen E3 was designed to have a geometric end eccentricity of $0.25\,D$ (3.4 inches). A misinterpretation of the end eccentricity versus the total effective eccentricity at the dent (OOS + e) resulted in an actual geometric end eccentricity of 2.2 inches instead of 3.4-inches. (Fig. 7-5)

The LVDT arrangement was successful except that LVDT L03 had to be replaced by a 0.001-inch dial gage due to a malfunction. (Fig. 7-3).

Specimen E3 was loaded in 25-kip increments to a dynamic ultimate load of $0.444\,P_y$ (337 kips), and it stabilized to a static ultimate load of $0.431\,P_y$ (327 kips). (Fig. 7-25) The acoustic sensors indicated increased activity during the last load steps before the ultimate load. The remainder of the barnacles and rust also began to flake off near the ultimate load. The specimen sustained the ultimate load for three compression increments before the load gradually dropped. After a total axial displacement of 3.5 times the axial shortening at the ultimate load, the load was $0.23\,P_y$ (173 kips). The specimen was unloaded in six steps. (Photo 1-1E (d).)

8. TEST ON LONG COLUMNS WITH FIXED ENDS

8.1 Instrumentation

The instrumentation for the tests on long columns with fixed ends consisted of strain gages, LVDT's , 0.001-inch dial gages and rotation gages. The labeling schemes for theses tests included the 'Level' concept from the pin-ended specimens and the longitudinal reference lines at 0, 90, 180, and 270 degrees labeled as Lines 1, 2, 3 and 4 respectively.

The arrangement of instrumentation is shown in Fig. 8-1 and Photos 8-1, 8-2, and 1-1B (c).

Four longitudinal strain gages were placed at each of the seven Levels along the specimen. These included one Level of strain gages $1.5\,D_m$ above the mid-length and one Level $1.5\,D_m$ below the mid-length of the specimen. The LVDT's were at seven Levels. The three lower LVDT's (L03, L13, and L23), were at the strain gage Levels, and the upper LVDT's (L63 and L53) were placed symmetrically to L03 and L13, respectively. LVDT L43 was at the upper quarter point which was expected to be near the inflection point.

The rotation gages were attached to the specimen two diameters above and below the mid-length of the specimen and 8 inches away from the ends.

Lateral displacement dial gages were attached opposite the dent at the mid-length, at the Level of strain gages $1.5\,D_m$ above the dent, and at the D01 position. LVDT LV1 (with a tensioned extension wire) measured the axial shortening, and dial gage DV1 (with an extension wire) measured the head motion.

8.2 Test Setup

In order to develop moments at the ends of the specimen, the fixed-ended damaged specimens were tested with their ends bolt clamped to the machine head and a large plate. The arrangement at the bottom is shown in Photos 8-1 and 8-2.

The procedure for the setup followed the steps described next. The specimen was rolled into the machine in the upright vertical position, centered and clamped to the machine head. Then, the specimen and a large (6-foot by 4-foot, 2-inch thick) bottom plate were lifted off the rollers and then lowered to rest on the machine base. The specimen was unclamped from the large bottom plate and lifted two inches so that the large plate could be centered with respect to the machine base. Wooden strips were taped to the specimen end plate to eliminate metal-to-metal contact, and Hydrostone grout poured on top of the large plate. The specimen was lowered onto the grout,

aligned on the plate, and secured. Later, after the grout set, the end plate of the specimen was bolt clamped to the large plate. The grouting of the top involved pouring grout onto a plastic sheet and placing the sheet on top of the specimen. The machine head was lowered and a wooden wedge was used to measure the size of the gap between the top of the specimen and the machine head. The specimen was bolt clamped to the machine head after the grout had set for an hour.

The final step was to connect all the wires, brackets, LVDT's, gages, and dials and check that all were functioning properly before starting the test.

8.3 Description of Individual Tests and Test Results

8.3.1 SPECIMEN P1F

Specimen P1F was very straight with a $0.05\,D_m$ (0.74-inch) dent at the mid-length. Due to this small imperfection, it was not clear if the specimen would fail at the mid-length or at the ends. Thus, prior to the test, the specimen was white washed at the mid-length (dent area) and at the lower end in order to observe the yield patterns at these locations.

The specimen was loaded in 25-kip increments until it reached a dynamic ultimate load of $0.813\,P_y$ (425.5 kips). During the last load step, the white wash at the mid-length showed yield lines, and the strain gages also indicated that the specimen had yielded there. The specimen stabilized to a static ultimate load of $0.794\,P_y$ (415.5 kips).(Fig. 8-2) During the next compression increment, the white wash at the bottom end showed yield lines on the side opposite the dent. This indicated that the dented segment yielded just before the ends yielded.

The specimen gradually lost its strength with additional axial compression. After a total axial displacement of 2.8 times the axial shortening at the ultimate load, the specimen gave off a loud sound. It was suspected that the weld at the top cracked at this point in the test. However, there was no loss of strength, so the test was continued. After a total axial displacement of four times the axial shortening at the ultimate load, the load was $0.35\,P_y$ (183 kips). The specimen was unloaded in two steps. (Photo 1-1A (c))

8.3.2 SPECIMEN P2F

Specimen P2F had an out-of-straightness of 0.94 inches and a $0.136\,D_m$ (2.37-inch) dent depth. Due to the size of the dent and the out-of-straightness, it was expected that initial yielding would occur at the mid-length.

The specimen was loaded in 25-kip increments until it reached a dynamic ultimate load of $0.682\,P_y$ (782 kips). During the last load step the strain gages also indicated that the specimen had yielded there.

The specimen stabilized to a static ultimate load of $0.67\,P_y$ (768 kips). (Fig. 8-4) The specimen gradually lost its strength with additional axial displacement. After most of the mill scale and rust had flaked-off the lower end, a bulge developed on the side opposite the dent. After a total axial displacement of 3.2 times the axial shortening at the ultimate load, the load was $0.375\,P_y$ (430 kips). At this point, the bottom weld fractured on the tension side. The specimen was unloaded in one step. (Photos 1-1B (b) and (c))

8.4 Post-Test Surface Profiles

The profiles of the specimens were measured using the survey level and a 1/64th-inch division scale. The line of center-punched points was positioned on 'top' and the out-of-straightness was measured at each point. As shown in Fig. 8-7 for Specimen P1F and Fig. 8-9 for Specimen P2F, the post-test profiles were plotted with the pre-test profiles to illustrate the growth of the dent depth.

9. STRAIGHT SPECIMEN TESTS USING SPHERICAL BEARING FIXTURES

9.1 Instrumentation

Spherical bearing end fixtures were used for the tests on straight, corroded and uncorroded specimens since the direction of lateral deformation was not known in advance. Spherical bearings were also used for the small-scale specimens, mainly for the convenience of testing in the 800 kip machine. The instrumentation was designed accordingly to measure lateral displacement in any direction.

9.1.1 LARGE-SCALE SPECIMENS

As for the other tests, the instrumentation for the tests with spherical fixtures included strain gages, LVDT's, 0.001-inch dial gages, and rotation gages. Five Levels of strain gages and LVDT's were attached at the quarter points and at a distance of one diameter from the ends. The strain gages were on the four longitudinal reference lines at 0, 90, 180 and 270 degrees labeled Lines 1, 2, 3 and 4. Pairs of LVDT's were positioned perpendicular to each other at each level to define the lateral displacement of the specimens in two different component directions.(Fig. 9-1)

As shown in Fig. 9-1, dial gages D2E and D2W (with extension wires) were attached to the specimen by screws drilled into the specimen at the mid-length, opposite LVDT's L2W and L2E.(Letters E and W stand for east and west respectively, to designate the orientation.) The axial shortening of the specimen was measured using vertical LVDT's LVE and LVW with extension wires. These vertical LVDT's were attached to bolts welded to the specimen five inches from the bottom on Lines 2 and 4, and the wires were tied to the bolts welded five inches from the top. Also, dial gage DV1 was placed on the machine base, and its extension wire was tied to the machine head to measure the head displacement. (Fig. 9-2)

Two top rotation gages were attached to the bolts welded five inches from the top of the specimen, as shown in Photo 9-1. The rotation gages on Lines 1 and 2 were labeled 'North' and 'West' respectively.

The other two available rotation gages were of a different type and were not used in these tests because out-of-plane tilting distorted their readings. Instead, long lever arms with dial gages or LVDT's were used at the bottom end. (Fig. 9-3, Photo 9-2)

Unfortunately, the dial gage rotation readings were not very reliable because the 0.001-inch dial gages used were not sensitive enough to detect the rotation developing before the ultimate load. On the other hand, when the specimen did fail and during the

post-ultimate range, the amount of end rotation quickly exceeded the stroke of the one-inch dial gages.

9.1.2 SMALL-SCALE SPECIMENS P1PS AND P2PS

The test set-up for the small-scale specimens was essentially the same as for the large-scale specimens. The strain gages were positioned the same as for the large-scale specimens. However, LVDTs were used only on the side of the tube opposite the dent and were perpendicular to the dent. The one exception was at Level 3 (mid-length), where LVDTs L3W and L3E were placed at 45-degree angles to the dent, and dial gages D31 and D33 were used perpendicular to the dent on both sides of the tube. (Fig. 9.2a and Photo 1-1B(d)) Dial gage DH0 measured the lateral displacement at the bottom bearing, and dial DH1 was a check for LVDT 03, to monitor the accuracy of the LVDT measurements.(Fig. 9-2a) Rotation gages were used at the top and bottom, and were positioned as close to the ends as physically possible. Two LVDTs, LVW and LVE, were secured to the bottom of the tube longitudinally on their respective west and east sides (Fig. 9-2a). These LVDTs measured the axial shortening of the tube by means of a wire extended to the top of the specimen, while dial gage DV1 measured the machine head displacement. All attachments to the tubes were accomplished by means of Epoxy cement.

9.2 General Test Setup

9.2.1 LARGE-SCALE SPECIMENS

A 2.5-million pound capacity spherical bearing was attached to the machine head of the testing machine and a 1.5-million pound capacity spherical bearing was placed on the machine base, as shown in Photos 9-1 and 9-2. The specimens were spot welded to a pair of machined three-inch thick end plates which were then placed on the bearings. Each end plate had four steel lugs welded to it to keep the bearing in the center of the end plate. Wooden wedges were driven between the bearing and the lugs to allow for finer adjustments and to hold the bearing in position. (Wedging, as shown in Fig.2-7, was used in order to avoid welding the bearings to the end plates.)

The installation of the specimen into the machine followed a predetermined procedure. Each specimen was rolled into the testing machine in an upright, vertical position and then lifted by the machine head using the lifting lugs welded near the top to the specimen. The specimen was centered and lowered onto the bottom spherical fixture, aligned, and the wooden wedges were driven into the gaps between the bearing and the four steel lugs. The specimen was held in the vertical position using angle cross

braces bolted to the top end plate. The machine head and the top spherical fixture were lowered and wedged into place once the specimen was properly centered. Grouting was not necessary for these tests because all the contact surfaces were machined and the spherical fixtures were self adjusting.

The final step was to connect all the wires, brackets, LVDT's, gages and dials, and to check that all were functioning properly before starting the test.

9.2.2 SMALL-SCALE SPECIMENS

The small-scale specimens were tested in the 800-kip machine. Specimen P2PS was tested first, and the same set-up as described for the large-scale specimens was used. (Fig. 2-7 and Photo 1-1B(d)) However, during testing it appeared that the slight deformation of the end plates induced erratic strains in the gages, particularly at the ends. At the time, these erratic strains were attributed to the thin wall thickness of the tube. Taking this into account, Specimen P1PS was tested without end plates. The tube was centered on the spherical bearings, then Epoxy was used to secure the tube in place. Grout was not used because all contact surfaces were machined. After the specimens were secured in the machine, the instrumentation was installed and checked.

9.3 General Testing Procedure

The testing procedure for the specimens was divided into the pre-ultimate and post-ultimate ranges. The pre-ultimate range was controlled by load increments and the post-ultimate range by displacement increments.

The extent of the post-ultimate range was limited either by the 5-degree rotation capacity of the top spherical bearing or by the stroke of the horizontal LVDT's in the upper portion of the specimen. (Whereas the lower dial gages and LVDT's could be reset, the upper gages in the large scale specimens were not accessible.)

9.4 Description of Individual Tests

9.4.1 SPECIMEN C1

Specimen C1 had considerable corrosion, including a hole, near the 'B' end. In order to facilitate observation of this area, the specimen was tested with the 'B' end at the bottom.

The specimen was loaded in 15-kip increments to a dynamic ultimate load of $0.443\,P_y$ (183 kips). During the last load step, flakes of rust were spalling off the sides.

The load stabilized to a static ultimate load of $0.428\,P_y$ (177 kips). An almost complete ring bulge developed two feet above 'Level' 1 strain gages. Surprisingly, no signs of local buckling appeared in the area of the hole. The specimen maintained the load for three more displacement increments, before it rapidly lost its strength. (Fig. 9-4) The specimen stabilized to a load of $0.283\,P_y$ (117 kips) and the test was stopped at this point so that the pattern of the buckled section would not be too distorted. The specimen was unloaded in three steps. Photo 1-1C(e) shows an overall view of the specimen.

The thickness of the buckled area was measured using ultrasonic equipment in a 2-inch by 2-inch grid. The thickness of the section with the hole was also mapped and scribed.(See Photos 9-3 and 9-4.) The results for these two areas are shown in Tables 3-10 and 3-11, respectively. Each thickness reading is approximately in the center of a square between the grid lines. It is clear from these results that the buckled area had a more extensive reduction of thickness than the area with the hole. (A more detailed discussion on this is in Chapter 14.)

9.4.2 SPECIMEN S1

Specimen S1 was essentially straight and had little surface corrosion. It was intended to be a comparison specimen for the dented Specimens D1 and E1 and the corroded Specimen C1. Specimen S1 was loaded in 25-kip increments to a dynamic ultimate load of $0.738\,P_y$ (469 kips), which stabilized to a static ultimate load of $0.722P_y$ (459 kips).(Fig. 9-6) The specimen was compressed a small increment and again reached a dynamic load of $0.738\,P_y$ (469 kips) but quickly lost its strength and deflected a total of 4.0 inches at the mid-length. (Fig. 9-7) At this point, the static load was $0.418P_y$ (266 kips). After resetting many of the LVDT's and dial gages, the specimen was compressed two more times. At a static load of $0.395\,P_y$ (251 kips), there was excessive rotation in the top bearing. The specimen was unloaded in two steps. (Photo 1-1D (c))

9.4.3 SPECIMEN C2

The corroded specimen C2 was loaded in 25-kip increments. At the load of $0.743\,P_y$ (500 kips), the strain gages indicated that yielding had occurred at Level 4, and a bulge was noticed between strain gages SG42 and SG43. The loading was then continued. A dynamic load of $0.806\,P_y$ (542 kips) was reached, and it stabilized to a static load of $0.788\,P_y$ (530 kips). Axial shortening at this point was increasing rapidly with small increases of load. Increments of displacement were made after this point. After seven increments, the specimen reached the dynamic ultimate load of $0.862\,P_y$

(576 kips), which stabilized to a static ultimate load of $0.826\,P_y$ (556 kips).(Fig. 9-8) After this point, lateral deflection increased rapidly with additional axial compression. (Fig. 9-9) At a load of $0.758\,P_y$ (510 kips), the lateral deflection readings, rotation readings, and strain readings indicated that a portion near the top end was developing a sharp dent-like buckle between strain gages SG42 and SG43. The test was continued until it had to be stopped because of the excessive rotation in the top spherical bearing. The specimen was unloaded in two steps. (Photo 1-1D (d))

The buckled portion of the specimen was surveyed and the thickness was mapped in a 2-inch by 2-inch grid.(Table 3-12 and Photo 9-5) Thickness measurements showed that the reduction of thickness due to corrosion was concentrated in the area where the buckling occurred. This thickness reduction is what led to the sharp dent-like kink that formed in this area.

9.4.4 SPECIMEN S2

Specimen S2 was essentially straight and had little surface corrosion. It was intended to be a comparison specimen for the corroded specimen C2. Specimen S2 was loaded in 25-kip increments to a dynamic ultimate load of $1.022P_y$ (794 kips) which stabilized to a static ultimate load of $0.986P_y$ (766 kips). The specimen maintained this load for five displacement increments. After the last increment, the load stabilized to a lower load of $0.94P_y$ (730 kips).(Fig. 9-10) After the next displacement increment, the load stabilized to $0.747P_y$ (580 kips), and a lateral displacement of two inches was recorded at the mid-length.(Fig. 9-11) The LVDT's and dial gages were reset and another displacement increment was made. The load stabilized to $0.61P_y$ (474 kips) with a 4.75-inch mid-length lateral displacement. At this point, the axial shortening was 0.81 inches and several of the gages were at the end of their stroke. The specimen was unloaded in two steps. (Photo 1-1D (e))

9.4.5 SPECIMEN S3

Specimen S3 was essentially straight and had little surface corrosion. It was intended to be a comparison specimen for the dented Specimens D3, E3 and the bent Specimen B3.

Specimen S3 was loaded in 25-kip increments to a dynamic load of $0.885\,P_y$ (675 kips), which stabilized to a static load of $0.88\,P_y$ (672 kips). Then, a displacement increment was attempted. However, after the load reached a dynamic ultimate load of $0.904\,P_y$ (690 kips), the specimen lost stiffness, deflected 2.4 inches at the mid-length and stabilized to a load of $0.577\,P_y$ (440 kips). (Fig. 9-13) After this point, the specimen gradually lost its strength with increased axial shortening. The test was stopped at a

load of $0.498\,P_y$ (380 kips) when most of the LVDT's were at the end of their stroke. The specimen was unloaded in three steps. (Photo 1-1E (e))

9.4.6 SPECIMEN C4B

Specimen C4B was loaded in 25-kip increments to a dynamic ultimate load of $0.836\,P_y$ (494 kips) which stabilized to a static ultimate load of $0.813\,P_y$ (480 kips). After two displacement increments, the load stabilized to a static load of $0.8\,P_y$ (472 kips). During the next increment, the load quickly dropped and stabilized to $0.708\,P_y$ (418 kips).(Fig. 9-14) At this point, a local buckle was noticed 2.7 inches above the mid-length. The specimen gradually lost load with additional axial deformation. After several displacement increments the load stabilized to $0.527\,P_y$ (311 kips). Since there was an excessive rotation in the top bearing, the specimen was unloaded in three steps. (Photo 1-1E (f))

The final out-of-straightness of the specimen was measured, and a 2-inch by 2-inch thickness map was made for the buckled area.(Table 3-13)

9.4.7 SPECIMEN P1PS

Specimen P1PS was intended to be a small-scale comparison specimen for the dented specimen P1P. Specimen P1PS was loaded in 2-kip increments for three steps, then the load steps were reduced to 1 kip due to the erratic dial gage readings. The Specimen was loaded to a dynamic ultimate load of $0.867\,P_y$ (24.8 kips) which stabilized to a static ultimate load of $0.815\,P_y$ (23.3 kips). In the next load increment, the specimen immediately started losing its strength.(Figs. 9-22 and 9-23) Then, the specimen was loaded to a dynamic load of $0.832\,P_y$ (23.8 kips); however, before dial gage readings could be taken the specimen suddenly failed and stabilized at a load of $0.140P_y$ (4.00 kips). The axial shortening was 0.54 inches, and a lateral displacement of 2.9 inches was recorded at the mid-length. At the time, this failure was attributed to the small dent size and the high degree of straightness of the specimen. A plot tracking the movement of the centroid of the tube at mid-length (Fig. 9-24) shows how erratically the tube was deflecting laterally until the dent took over and caused failure to the south. (Photos 1-1A (d) and (e))

Final out-of-straightness surveys of the specimen show an out-of-straightness of 2.8 inches on the 180 degree side. (Fig. 9-25 to 9-27)

9.4.8 SPECIMEN P2PS

Specimen P2PS was intended to be a small-scale comparison specimen for the dented specimen P2P. Specimen P2PS was loaded in 5-kip increments to a dynamic ultimate load of $0.555\,P_y$ (46.6 kips), which stabilized to a static ultimate load of $0.517\,P_y$ (43.4 kips).(Fig. 9-28) The specimen was compressed by a small increment, and a very small loss of strength was recorded. During the following displacement increments, the specimen lost its strength more quickly and deflected laterally a total of 4.0 inches at the mid-length. (Fig. 9-30) At this point, the static load was $0.204\,P_y$ (17.1 kips). The specimen was unloaded in four steps. (Photo 1-1B (d))

Final out-of-straightness measurements were taken are they are shown in Figs. 9-31 to 9-33.

10. COMPARISON OF SPECIMEN BEHAVIOR AND STRENGTH

10.1 Specimens P1P and P1F

Specimens P1P and P1F were tested to determine the effects of end restraint on the ultimate load and on the post-ultimate behavior of specimens with small dent depths. P1P, a pin-ended specimen, and P1F, a fixed-ended specimen, were designed to have the same $0.05\,D_m$ dent. The actual dent was $0.047\,D_m$ for the two specimens and the measured out-of-straightness for the pinned specimen was $(-)0.3$ inches and 0.37 inches for the fixed specimen.(Table 10-1)

During testing, the pre-ultimate axial stiffness of the pin-ended and the fixed-ended specimens was very similar. The ultimate load for the pin-ended specimen was $0.611P_y$ (301 kips) and $0.794\,P_y$ (415.5 kips) for the fixed-ended specimen. Thus, the fixed-ended specimen had 1.26 the ultimate load of the pin-ended specimen.(Fig. 10-1)

The post-ultimate behavior of the two specimens was quite different. The pin-ended specimen carried $0.31P_y$ (152 kips) after a total axial displacement of 1.94 times the axial shortening at the ultimate load, that is a decrease of 49.5%. The fixed-ended specimen carried $0.57\,P_y$ (298 kips) after the same relative displacement, thus, a decrease of only 28.3%.

10.2 Specimens P2P and P2F

Specimens P2P and P2F were tested to determine the effect of end restraints on the ultimate load and post-ultimate behavior of specimens with a larger dent. Specimen P2P, a pin-ended specimen, and P2F, a fixed-ended specimen, were dented with identical $0.14\,D_m$ (2.33-inch) depth dents. The measured out-of-straightness for the pinned specimen was 0.66 inches, and 0.94 inches for the fixed specimen. (Table 10-2)

During testing, the pre-ultimate axial stiffness for the two specimens was very similar. The ultimate load for the pin-ended specimen was $0.45\,P_y$ (516 kips), and $0.617\,P_y$ (762 kips) for the fixed-ended specimen. Thus, the fixed-ended specimen had 1.48 the ultimate load of the pin-ended specimen.(Fig. 10-2)

The post-ultimate behavior of the two specimens was not as dramatically different as for the specimens with a smaller dent (Specimens P1P and P1F). The pin-ended specimen carried $0.21\,P_y$ (242 kips) after a total axial shortening of 3.1 times the axial shortening at the ultimate load, a decrease of 53.1%. The fixed specimen carried $0.389\,P_y$ (442 kips) after the same relative displacement-- a decrease of 42% . The slopes in the post-ultimate range were relatively similar for the two specimens.

10.3 Specimens P1P, P1PS and IAI

Specimens P1P and P1PS were tested to compare the results of small scale tests with large scale tests to see how well the small-scale results predict the large-scale results. The results were also compared with the small-scale Specimen IAI by Taby to see how well the new small-scale test correlated with the previous small-scale results.[12] Figure 10-7 shows a non-dimensionalized comparison of the three specimens. The pre-ultimate behavior of P1PS shows a parallel, but longer elastic range than either Specimen P1P or IAI. Specimen P1PS also shows a higher ultimate than the other two. The ultimate load for Specimen P1PS was $0.814P_y$; $0.611\,P_y$ for Specimen P1P; and $0.666P_y$ for Specimen IAI. Thus, Specimen P1PS carried 1.33 the non-dimensionalized ultimate load of Specimen P1P and Specimen IAI carried 1.09 the ultimate load of Specimen P1P.

The post-ultimate behavior of Specimen P1PS appears to be quite different than that of P1P and IAI, however, because of the sudden failure of Specimen P1PS, only one post-ultimate point could be recorded. This does not provide enough data to make a reliable comparison. Table 10-9 gives a comparison between these small- and large-scale specimens. Another comparison was provided by Specimens P2P and P2PS as disscussed next.

10.4 Specimens P2P, P2PS and PIA

Specimens P2P and P2PS were tested to compare the results of small-scale tests with large-scale tests for the same non-dimensionalized parameters. The small-scale Specimen PIA by Smith was also included.[??] Figure 10-8 shows a non-dimensionalized comparison of these three specimens. The pre-ultimate stiffness of the three specimens was very similar. The ultimate load for Specimen P2PS was $0.517\,P_y$; $0.450\,P_y$ for Specimen P2P; and $0.635\,P_y$ for Specimen PIA. Thus, Specimen P2PS carried 1.15 the non-dimensionalized ultimate load of Specimen P2P, and Specimen PIA 1.41 of Specimen P2P.

The post-ultimate behavior of the three specimens was not dramatically different. The post-ultimate curves are similar for all three specimens. Specimen P2PS had a strength decrease of 32% when the strain was double the strain at the ultimate load, Specimen P2P 33%, and Specimen PIA 45%. Table 10-9 gives a comparison of these small- and large-scale specimens.

10.5 Specimens P3PA and P3PB

Specimens P3PA and P3PB were tested to evaluate the effects of different dent depths on specimens with a high (D_m/t). Specimen P3PA was dented $0.051\,D_m$, and Specimen P3PB $0.148\,D_m$. The out-of-straightness for P3PA was 0.3 inches and for P3PB, 0.98 inches. The ultimate load for Specimen P3PA was $0.648\,P_y$ (950 kips), and $0.423\,P_y$ (610 kips) for Specimen P3PB.(Table 10-3)

The post-ultimate behavior of the two specimens was quite different.(Fig. 10-3) Specimen P3PA had a sharp loss of strength after the ultimate load and leveled off after significant axial displacement. Specimen P3PB had a more gradual loss of strength after the ultimate load. This behavior may be attributed to a significantly larger initial out-of-straightness of this specimen than of Specimen P3PA. Specimen P3PA carried $0.3\,P_y$ (432 kips) after a total axial displacement of 2.0 times the axial shortening at the ultimate load-- a decrease in strength of 54.5%. Specimen P3PB carried $0.3\,P_y$ (430 kips) after the same relative displacement-- a decrease of 29.5%.

10.6 Salvaged Specimens of Series 1

The four salvaged specimens of Series 1: C1, D1, E1 and S1, each had a $D_m/t = 27.5$, $L/r = 80$ and $F_y = 50$ ksi. The purpose of the tests was to evaluate the effects of a dent, a dent and an end eccentricity, and corrosion on a specimen. Specimens D1 and E1 were intended to have the same dent depth of $0.15\,D_m$, and Specimen S1 was not damaged. (Table 10-5) The ultimate load for Specimen D1 was less than the ultimate load for Specimen E1 due to the corrosion of the cross section near mid-length, and the consequent fracture. But, the post-ultimate slopes of D1 and E1 were similar.(Fig. 10-4) The test of Specimen C1 showed that the ultimate load was greatly reduced by the local buckling of the wall weakened by corrosion. Specimen S1 indicated by its higher strength how damage and corrosion significantly reduce the ultimate capacity of tubular members.

10.7 Salvaged Specimens of Series 2

Specimens C2 and S2 were tested to measure the effects of corrosion on a specimen with a low L/r ratio. The two specimens had the following parameters: $D_m/t = 30.5$, $L/r = 60$, and F_y approxtmately 40 ksi.(Table 10-6)

The effect of corrosion on Specimen C2 reduced its capacity by 27 percent.(Table 10-6 and Fig. 10-5)

10.8 Salvaged Specimens of Series 3

Specimens B3, D3, E3 and S3 were tested to compare the effects of out-of-straightness, a dent, and a dent and an end eccentricity. The four specimens had the following parameters: D_m/t= 30.5, L/r= 70 and F_y approximately 40 ksi. (Table 10-7)

As expected, Specimen E3, which was dented and had an end eccentricity, had the lowest ultimate load. (Fig. 10-6) The bent Specimen B3 and the dented Specimen D3 had similar ultimate loads. The straight specimen S3 indicated that damage significantly reduced the capacity of the specimens.

11. FINITE ELEMENT ANALYSIS OF TEST SPECIMENS

11.1. General

Nonlinear finite element models of the specimens were developed and the commercially available finite element analysis program 'ADINA' was used to analyze the behavior of the test specimens.[1] This program is capable of considering geometric and material nonlinearity and large-deformation behavior and provides advanced element types and sophisticated control mechanisms allowing customization of the analysis process. These capabilities were essential in developing the finite element models required for this study.

The program was run on the following platforms:

a. CDC-CYBER 180 under NOS-VE operating system .
b. SUN workstations (SPARC-Station I & II) under UNIX operating system.

The results of the analysis are presented and discussed in Chapter 12 (Comparison of Tests with Analytical Methods).

11.2. Description of Finite Element Models

Two different finite element models were used: one for pin-ended specimens (specimens tested with cylindrical or spherical end fixtures) and the other for fixed-ended specimens which were prevented from rotation at the ends.

11.2.1 F.E. MODEL for PIN – ENDED SPECIMENS

A typical finite element model developed for modeling pin-ended specimens is shown in Fig. 11.1. This model has 274 nodes and 1162 degrees-of-freedom (DOF). Most of the nonlinear behavior in these specimens is localized in and near the dent area at mid-length. Thus, higher-order isoparametric shell elements (drawn as surface elements in Fig. 11.1) are used for modeling this area. The rest of the column (in pin-ended columns) behaves linearly and can be modeled using beam-column elements (drawn as line elements in Fig. 11.1) . The finite element model used here is based on the models developed by Padula and Ostapenko.[10] The scheme of generating the geometry of the damaged specimen is taken from that work also.

The transition between the beam-column elements and shell elements is modeled by enforcing the 'plane section remains plane' requirement at this point. This is necessary since the beam elements model the member along the center line of the tubular specimen while the shell elements model the specimen on the surface. The transition is implemented by providing constraints so that the rotation and

displacement of the end of the beam element at the center line defines the rotations and displacements of the shell elements at the surface.

In order to reduce the size of the problem and computational effort, advantage is taken of the symmetry with respect to the mid-span and the plane of bending, and, as shown in Fig. 11.1, only a quarter of the member is modeled. The symmetry is implemented by requiring that the displacement and rotation along the planes of symmetry be prevented.

The material was assumed to be bi-linear with the strain-hardening modulus equal to 1/2500 of the elastic modulus. The following values were used for all specimens:

Modulus of Elasticity,	E = 29,500 ksi
Poisson's ratio,	ν = 0.3
Strain-Hardening Modulus,	E_{SH} = 15 ksi

The yield stress for each specimen was taken as listed in Table 11.1.

11.2.2 F.E. MODEL for FIXED – ENDED SPECIMENS

The fixed-ended specimens were entirely modeled with 16-node isoparametric shell elements, with all the nodes located on the middle surface (mid-thickness). Figure 11.1 shows a finite element model for a typical fixed-ended specimen (Specimen P2F). This model has 365 nodes, 72 shell elements and 2979 global degrees-of-freedom (DOF). As for pin-ended specimens, symmetry with respect to the mid-length and the plane of bending is used, and thus, only a quarter of the structure is modeled.

In a fixed-ended specimen, nonlinearity is expected at the central dented portion (due to damage) of the member and also at the fixed ends. Thus, to model this nonlinear behavior, it was necessary to use shell elements in both these areas. Since shell elements were needed at the dent (mid-length) and at the ends, it was decided to model the whole member with shell elements, rather than introduce beam elements (and transition constraints) in the portion expected to remain elastic, as was done for the pin-ended specimens. To model the fixed-end condition, all the shell nodes at the end were allowed only the axial displacement degree-of-freedom (DOF). Kinematic constraints were introduced for applying the end displacement and measuring the axial load. The end displacement was applied (and the axial load measured) at the node located at the center of the end cross-section. The shell nodes were constrained to displace axially the same amount as this central node. The applied axial load was measured from the equilibrium of the central node.

Geometry in the dented part of the model was generated by using the same

process as for pin-ended specimens. Sections 11.6 and 11.7 explain how the out-of-straightness and dented shape of the member were modeled. The bi-linear elasto-plastic material model used for the pin-ended specimens was also used for the fixed-end model, except that a strain-hardening modulus of 60 ksi was used since the ultimate strength measurements from the tensile coupon tests indicated that this was a more realistic estimate of strain hardening.

11.3. Solution Process

A static nonlinear model was used. The solution process mimics the test procedure. Since the post-ultimate behavior is of interest, a displacement-controlled analysis approach is used. At each step, a small displacement increment is made, and then, iterations of the load are performed until equilibrium is achieved. The Newton-Raphson iteration approach is used and the stiffness matrix is reformed at each iteration. Figures 11.2 and 11.3 show the deformations in the model for a typical specimen at two different stages – soon after reaching the ultimate load and far into the post-ultimate range. The solution traces the load-displacement path of the specimen. This process is carried to the ultimate load and two to three times the displacement at the ultimate load. Figure 11.6 shows a typical load-deformation relationship obtained in the analysis of Specimen D3. Each point in the curve indicates the load-deformation combination to which the program converged after a displacement increment.

The axial load is applied to the end node of the member. (See Fig. 11.1) This process works well for the cases where there is no applied end eccentricity. However, in many of the tests there is some end eccentricity that has to be accounted for in the finite element model. In these cases, the end eccentricity is modeled by introducing a moment in the plane of deflection of the member along with the axial load at the same node. The moment is specified to be equal to the end-eccentricity multiplied by the axial load at each load step. The solution process applies the appropriate displacement increment at each load step, and satisfies equilibrium while imposing this relationship between the load and the moment.

11.4. Shell Elements

For pin-ended specimens, shell elements were used to model the dented portion of the specimen (approximately two to three diameters from the mid-length point) and three to four diameters of the undamaged portion beyond the dented part. This extension provided a smooth transition to the beam elements which modeled the rest of the specimen. As shown in Fig. 11.4, a comparatively fine mesh was used in the dented

region near the mid-length, and a coarser mesh in the areas farther away.

For the fixed-end models, shell elements modeled the entire member. Similarly to the pin-ended models the dented portion of the specimen had a fine mesh while the rest of the specimen was modeled with coarser mesh.

Primarily, sixteen-node, isoparametric shell elements were used in these models (some isoparametric shell elements used as transition elements had fewer number of nodes). All the nodes were placed at mid-surface of the shell. The degree-of-freedom corresponding to the rotation perpendicular to the surface of the shell was fixed for all these nodes, except where the shell elements met at an angle greater than 15° or at the boundaries of the model. This was necessary since no rotational stiffness contribution is made by these shell elements in the direction perpendicular to the shell surface. A reduced order of integration of $3 \times 3 \times 3$ was used for all the shell elements in order to improve the stiffness performance. The bi-linear material model provided for partial, as well as, full plastification in the shell elements. The characteristics of the shell elements were similar in both the pin-ended and the fixed-ended models. Figure 11.5 illustrates the initial and final, overall and cross-sectional deformations in the dented portion of a typical pin-ended specimen.

11.5. Beam Elements

Beam elements were used only in the pin-ended specimens. Elastic beam-column elements of tubular shape (this shape is supported by ADINA) were used to model most of the length of the member. The tubular shape is defined by the inner and outer diameters as well as by the length of the element. Since only one-half of the section needs to be modeled, the thickness of the specimen is halved while the mid-thickness diameter was kept unchanged.

11.6. Modeling of Initial Out-of-Straightness

The out-of-straightness is defined as the deviation of the centroid of a cross section from the straight line joining the centroids at ends of the member. For the finite element models in this study, the out-of-straightness was assumed to have a sinusoidal profile.

$$\delta(x) = \Delta \cos\left(\frac{\pi x}{L}\right) \tag{11.1}$$

where

Δ is the out-of-straightness at mid-length taken from the survey data.

x is measured from the mid-length point of member.

11.7. Modeling of Dented Shape

The geometry of the dented area of the specimen is complicated. This shape was generated by imposing the condition that the perimeter of the specimen was the same before and after the denting process. A generic dented shape is taken and by numerically imposing this constraint, the shape is scaled to produce the dented geometry at a section.

The extent of the dent (ℓ_d) was taken from the survey data of the dented specimens, usually three to four diameters on each side of the dent. A parabolic variation of the dent depth was used to define the dent depth $d_x(x)$ at other locations in this zone.

$$d_x(x) = d\left(1 - \frac{2x}{\ell_d}\right)^2 \tag{11.2}$$

where

x is the coordinate measured from the dent.

d is the dent depth at mid-length.

ℓ_d is the length of the dented portion.

Subsequently, in each of the sections within ℓ_d, the dented shape of the cross section was computed from the calculated dent depth d_x. Detailed explanation of generating the geometry of damaged tubular members is given by Padula and Ostapenko. [10]

12. COMPARISON OF TESTS AND ANALYTICAL METHODS

12.1 Analytical Methods

Two groups of analytical methods were compared with the test results: (a) Computer programs for obtaining the ultimate loads and load-shortening relationships, and (b) "Manual" methods for computing only the ultimate loads.

The principal features of these methods are briefly discussed next and credit is given to the organizations which performed the analysis.

12.1.1 COMPUTER PROGRAMS

The load-shortening behavior of all test specimens in the pre- and post-ultimate ranges was analyzed by using at least three of the following computer programs:

1) **DENTA** [18] – Analysis performed by Chevron Oil Research Company.

DENTA is a commercially available computer program based on a simplified physical model solved by using numerical approximations. Response of the dented segment in the post-ultimate range was adjusted to empirically fit experimental results from small-scale tests.

2) **BCDENT** [21] – Analysis performed by EXXON Production Research Co.

BCDENT is a proprietary computer program of EXXON Production Research Company. The method involves numerical integration using the projector-corrector approach (Newmark Method) with the moment-curvature response of the dented segment taken to be according to previously derived formulas.

3) **ADINA** (Designated as FE in text) [1] – Analysis performed by project staff.

ADINA is a commercially available finite element program capable of considering material and geometrical non-linearity.

4) **WBK** [7] – Analysis performed by project staff.

WBK is a computer program developed by Woobum Kim under supervision by A. Ostapenko. Similarly to BCDENT, the method involves numerical integration using the projector-corrector approach (Newmark Method). However, the moment-curvature response of the dented segment is defined by a relationship based on an array of constants which were obtained from a multivariable regression analysis of a data base generated by using a finite element program (ADINA).

12.1.2 "MANUAL" METHODS

Three methods for computing ultimate loads are suitable for manual operation, although in practice, they normally would be programmed. Two of these "manual" methods, Ellinas and Loh, can be used for computing the ultimate load of dented compression members.[1] The third method, AISC/API, is applicable only to columns without dents and is listed to provide an illustration of the loss in strength caused by dent or corrosion damage. All computational work with these methods was performed by the project staff.

1) **Ellinas** [6]
   This method is based on elastic beam-column analysis with the first-yield criterion for the ultimate load.

2) **Loh** [22]
   The method represents an interaction formula (procedure) for the ultimate strength of damaged and undamaged tubular members.

3) **AISC/API** [20,3]
   This method provides the strength of **undamaged** columns according to prevalent design specifications. Thus, the values obtained serve for comparing with undented columns, that is, they indicate the loss of the column strength due to the dent or corrosion damage. The "Allowable Stress Design" formulation was used since it is common to both specifications, and the factor of safety was set to 1.0 in computing the ultimate loads.

12.2 Comparison of Analytical Methods with Tests

12.2.1 GENERAL

The computed and test curves of the nondimensionalized load versus axial shortening relationships are shown for each specimen individually in Figs. 12-1 to 12-27. The axial load is nondimensionalized with respect to the yield load ($P_y=F_yA$), and the shortening is given in inches. Where appropriate and in order not to overcrowd the curves, the plots for a particular specimen are given in two figures on the same page.

The nondimensionalized ultimate loads for the tests and the analytical methods are listed in Table 12-1 for the computer programs and Table 12-2 for the manual methods. Each table gives two groups of nondimensionalized ultimate loads. In the first (left) group, the test and analytical loads are nondimensionalized with respect to the yield load, and, in the second (right) group, the analytical loads are nondimensionalized with respect to the test loads.

Three sets of averages (Ave.) and standard deviations (Std.Dev.) are shown for

[1]The simplified method by W. Kim for computing the ultimate strength of end-restrained dented columns is not discussed here.[7]

the second group (P_u/P_{test}) in the bottom portion of each table.

The first set is for all specimens except the corroded Specimens C1 and C2 which failed by local buckling of corroded patches and could not be properly analyzed by the methods used. (These specimens are discussed in Chapter 14.) The values listed in the tables for these specimens were computed by using average thicknesses. Also, since some methods could not be used to analyze all the specimens, the averages for these methods are based on smaller numbers of test results. Specifically, the WBK method did not include specimens without dents, and the Ellinas method did not include fixed-ended specimens.

The second set gives the averages and standard deviations only for the specimens which were dented. These include the nine (9) specimens of the P-series and Specimens D1, E1, D3 and E3 (a total of 13). Since the Ellinas method is not applicable to fixed-ended specimens, Specimens P1F and P2F are not included in the averages for this method.

The third set of averages is only for the specimens fabricated by cold-rolling and welding. These are the P-series specimens except for Specimens P1PS and P2PS which were small-scale manufactured ERW, rather than fabricated specimens. The purpose of these averages was to indicate the accuracy of the respective methods with respect to typically fabricated members in offshore platforms.

In the discussion of individual methods given below in Sections 12.2.2 and 12.2.3, reference to the locally-buckled corroded specimens C1 and C2 is omitted or minimized for the sake of brevity since none of the analytical methods used are properly applicable to these specimens.

12.2.2 COMPARISON OF COMPUTER PROGRAMS WITH TESTS

12.2.2.1 DENTA

As can be seen in Table 12-1 and in the figures (for most of the specimens, the top figure on each page), DENTA predicted the ultimate load for all the specimens (18, excluding C1 and C2) within a range of 0.725 to 1.233 times the experimental load, with an average prediction of 0.963 and the standard deviation of 0.121. The prediction for the dented specimens (13 total) falls within the same range of 0.725 to 1.233 of the test loads with the average of 0.941 and Std.Dev.=0.127. DENTA predicted the ultimate load for the fabricated specimens within the range of 0.914 to 1.075 (Ave.=0.977 and Std.Dev.=0.067). Apparently, residual stresses in the fabricated specimens had little effect on the accuracy of DENTA.

The nondimensionalized load versus axial shortening plots in Figs. 12-1 to 12-27 show that there are some significant differences between the DENTA predictions and the experimental curves. The DENTA predictions for small-scale specimens and the specimens tested with end eccentricity (P1PS, P2PS; P1P, E1, E2) deviated considerably from the test curves. In the post-ultimate range, the DENTA predictions were conservative for all the dented specimens except Specimen P2F. The DENTA prediction for the post-ultimate behavior curve of the straight specimen S2 was considerably below the experimental curve.

Whereas the patch corroded Specimens C1 and C2 could not be properly analyzed because they buckled locally before the strength based on the average thickness was reached, the uniformly corroded specimen C4B gave very good correlation of 1.09.

12.2.2.2 BCDENT

The load-shortening predictions for BCDENT and the test curves are shown in Figs. 12-1 to 12-27 and the nondimensionalized ultimate loads are listed in Table 12-1. The table shows that the prediction for all specimens (without C1 and C2) was from 0.733 to 1.418 with Ave.=0.936 and Std.Dev.=0.152. For the dented specimens, the range is the same but the average is 0.927 with Std.Dev.=0.170. The predictions for the fabricated specimens varied from 0.733 to 1.056 with Ave.=0.904 and Std.Dev.=0.109.

The axial shortening versus nondimensionalized load plots show that there are some significant differences between the BCDENT predictions and the experimental curves. As with the other methods, the BCDENT predictions for specimens tested with end eccentricity were noticeably different from the test curves. The BCDENT predictions were also drastically different for the fixed-end specimens. In the post-ultimate range, the BCDENT predictions were conservative for all the dented specimens except Specimen P1P. The predictions for the post-ultimate behavior of the straight Specimen S2 differed greatly from the experimental curve although the ultimate load was reasonably close (0.974).

12.2.2.3 ADINA [Labeled FE in the plots]

The load-shortening predictions for ADINA[1] and the test curves are shown in Figs. 12-2 to 12-27 and the nondimensionalized ultimate loads in Table 12-1.

The computed ultimate loads nondimensionalized with respect to the test loads for all specimens (excluding C1 and C2) varied from 0.802 to 1.176 with Ave.=0.954 and Std.Dev.=0.098. For the dented specimens, the range was the same, with Ave.=0.969 and Std.Dev.=0.095.

Apparently, residual stresses in the fabricated specimens had little effect on the accuracy of ADINA. It predicted the ultimate load within a range of 0.802 to 1.034 with an average prediction of 0.966 and Std.Dev.=0.080 which is even better than for all specimens.

The axial shortening versus nondimensionalized load plots show that there are some significant differences between some of the ADINA predictions and the experimental curves. In the post-ultimate range, the ADINA predictions were conservative for all the dented specimens, and the predictions for the post-ultimate behavior of the straight specimen S2 differed considerably from the experimental curve.

12.2.2.4 WBK

Since the WBK program is, at present, applicable only to specimens with dents, only the thirteen dented specimens were analyzed.

The load-shortening curves according to the WBK method and tests are shown in Figs. 12-2 to 12-26 (in most cases, the bottom figure on a page). The computed ultimate loads nondimensionalized with respect to the test loads are listed in Table 12-1. The range of the nondimensionalized ultimate loads for all analyzed specimens (dented) was from 0.942 to 1.202 with the average (Ave.) of 1.015 and the standard deviation (Std.Dev.) of 0.105. (These values are listed in Table 12-1 for the sets of all and dented specimens.) Considering only the seven fabricated specimens, the range was from 0.942 to 1.139 with the average of 1.020 and the standard deviation of 0.063. It is of note that the averages for the WBK programs are slightly above 1.0 by about 2% whereas the averages for the other computer programs (DENTA, BCDENT and ADINA/FE) are less than 1.0 by approximately 4-9%.

The load-shortening curves in Figs. 12-2 to 12-26 show that the WBK method tended to be in general agreement with the finite element (FE) curves and provided somewhat conservative (lower) loads in the post-ultimate range, but less conservative than the DENTA and the BCDENT methods.

12.2.3 COMPARISON OF MANUAL METHODS WITH TESTS

The nondimensionalized computed and test loads are listed in Table 12-2 together with the averages and standard deviations. Particular observations for each method are discussed next.

12.2.3.1 Ellinas

The Ellinas method is limited to the analysis of pin-ended members, and, thus, the fixed-ended specimens P1F and P2F are not included. The locally buckled corroded specimens C1 and C2 are also omitted from averaging.

The range of ultimate loads nondimensionalized with respect to the test loads for all specimens was from 0.567 to 1.061 with Ave.=0.834 and Std.Dev.=0.136. For the dented specimens, the method gives a range of 0.567 to 1.061 with Ave.=0.790 and Std.Dev.=0.131. Considering only the fabricated specimens, the range is 0.740 to 0.830 with Ave.=0.790 and Std.Dev.=0.035.

12.2.3.2 Loh

The Loh method is applicable to all types of specimens of this program except to the patch-corroded Specimens C1 and C2 which were analyzed assuming a constant average thickness. As can be seen in Table 12-2, the range of the nondimensionalized axial loads (P_u/P_{test}) for the remaining eighteen specimens was 0.672 to 1.016, and the average and standard deviation were 0.838 and 0.093, respectively. The dented specimens (13) had the same range of 0.672 to 1.056 with Ave.=0.844 and Std.Dev.=0.094. The seven fabricated specimens had a range of 0.672 to 0.981 with Ave.=0.835 and Std.Dev.=0.101.

12.2.3.3 AISC/API

Here, the simplest ASD (Allowable Stress Design) approach of the AISC/API method was used to analyze the specimens as pin-ended undamaged columns. (Average thickness was used for the patch-corroded specimens C1 and C2.) It should thus be expected that, except for the straight columns S1, S2 and S3, the (P_u/P_{test}) ratios for all other specimens should be greater than 1.0. And they are except for specimen P1PS (0.957). The straight Specimens S1, S2 and S3 have the ratios of 0.965, 0.883 and 0.914, respectively.

12.3 Comparison of Analytical Methods with Each Other

The following are some general observations made from comparisons of the analytical methods with each other and with the test results:

1) With a few exceptions, **analytical predictions of the ultimate loads** are conservative, that is, the computed loads are below the test loads. The computer programs

(Table 12-1) are somewhat less conservative and more consistent, having an accuracy within approximately 10%, than the manual methods (Table 12-2, Ellinas and Loh) which have an accuracy within approximately 20%. Only the WBK program tends to give slightly higher predictions than the test results, but by less than 2%.

These observations do not include the specimens with patch corrosion, C1 and C2, which failed by local buckling. Specimen D1, although included, shows a higher predicted load by all the methods used (from 1.016-Loh to 1.418-BCDENT). The reason for this systematic deviation is not yet clear. The small-scale specimens, P1PS and P2PS, were included in this appraisal, but, as a group, they gave lower predicted values than other specimens, dented or undented.

2) The **load-shortening response** provided by the computer programs used (DENTA, BCDENT, FE, WBK) has, on the average, a reasonably conservative degree of accuracy (maybe, too conservative for engineering purposes). The WBK program tends to give a slightly better correlation with test results. However, at present, the program is limited only to dented members and is not fully developed for practical application. Then, with the finite element program FE/ADINA being the most labor intensive although most accurate, programs DENTA and BCDENT currently remain as the logical choices for obtaining the load-shortening response of dented and undented members for engineering applications.

Improvement of the prediction of load-shortening behavior is expected from the finite element methods, such as ADINA, by including the effects of strain hardening and strain reversal.

13. STUDY OF END ECCENTRICITY

13.1 Need for Computation of End Eccentricity

13.1.1 INTRODUCTION

One of the difficulties in experimental work on columns is to provide the end conditions assumed in analysis: pinned, fixed, elastically restrained or the application of the axial load with a prescribed eccentricity. All mechanical end fixtures used for this purpose have a certain degree of imperfections due to friction, misalignment or other unpredictable causes. Thus, it is highly desirable to be able to check to what extent the actual end conditions in the test simulate the intended conditions.

It may appear that strain gage readings at the end of the test column should provide the needed information. However, these readings have been found to be not reliable because of the irregular strain disturbances leading to non-planar strain distribution. These are caused by local imperfections, flexibility of the end fixtures, local constraining effect of the fixtures, imperfections in contact surfaces, etc.

This chapter describes a procedure for analyzing the actual end conditions from the readings of all relevant test data acquisition units on the specimens: strain, dial and rotation gages, and LVDT's. The procedure is based on the recognition that the deformation behavior can be functionally approximated from the test readings, and the end conditions can then be deduced from this approximation.

Of particular interest in this project was a verification that the end fixtures provided the desired concentric or eccentric line of load application at the specimen end and how this eccentricity may be affected by the load level.

To accurately estimate the end eccentricity using measured data, a "curve-fitting" type procedure is employed. However, this approach is complicated by the fact that different types of quantities such as deflection, strain and rotation are measured by different types of instruments (LVDTs, strain gages or rotation gages). These instruments have different accuracies of measurement. To combine the data from these instruments in a calculation procedure, some provisions must be made to account for the differences in accuracy.

The geometrical properties, e.g., thickness, diameter, out-of-straightness , and material properties such as modulus of elasticity, are needed for use in the end eccentricity calculation procedure. Inaccuracies in these properties produce a systematic error. Thus, some correction mechanisms must be included in the calculation procedure to reduce the effect of inaccuracies of geometrical properties.

13.1.2 REDUCTION OF ACTUAL READINGS

Values read from the gages during testing cannot be directly used in computation. The data reduction process applies some simple operations to adjust these values so that they can be used. Data reduction mainly consists of zero adjustment. The zero adjustment process makes sure that any measured quantity starts from a zero reading when the load is zero. Based on linear extrapolation of the values of the measured quantity in the elastic range, a zero adjustment value is subtracted (or added) to the measured quantity in each load step.

Data reduction also checks and corrects for other situations where the value that was read may have been changed by some problems with the measuring or recording process. Sometimes, dial gages or other measuring devices need to be reset because the measured quantity goes out of range. Sensitive measuring devices, e.g., LVDT's , strain and rotation gages, sometimes have sudden shifts in the readings due to accidental movement or other effects. The process of data reduction corrects these values by compensating for the estimated value of the shift caused by resetting of the gage or by accidental effects.

13.1.3 ALTERNATE APPROACHES FOR FINDING END ECCENTRICITY

A number of different approaches were investigated for finding the end eccentricity. Initially, only the curvature readings from the end strain gages, after applying some correction to these readings to account for the out-of-plane distribution of the strain, were tried. However, it soon became apparent that the strain gage readings at the ends had too much variation and the end eccentricity to be computed was too small for this approach to work.

Next, an equilibrium approach was attempted. By calculating the absolute position of the load vector at different levels and then fitting a straight line through these positions, the end eccentricity could be computed. This approach, too, proved to be unreliable.

Finally, a regression approach was adopted which did a least squares fit of the measured data and used extrapolation of the fitted function to find the end eccentricity. Different schemes in this approach were tried using different sets of functions, dimensionalized and nondimensionalized fitting, etc. The finally selected set of functions and the nondimensionalized approach provided the best fit to the measured data and were used for the computations.

13.2 Procedure for Calculation of End Eccentricity

13.2.1 GENERAL

Calculation of the end eccentricity during column tests using the cylindrical end bearings utilizes a large number of measurements from different gages. To find the best possible estimate of the end eccentricity, a scheme of using measured data was developed. This scheme is based on regression analysis which takes advantage of an elastic beam-column curve for the portion of column near the end. Since the tested columns were damaged at mid-length, most of the column remained elastic during the test. Thus, it can be expected that the member follows an elastic curve from the end to near mid-length, and can be described by the fourth-order differential equation for beam-column behavior.

The regression scheme fits the data from the bottom half of the column to find the end eccentricity. Different types of input data (strain, displacement and rotation) and their inaccuracies must be properly reconciled before the regression analysis can be applied. So a process of nondimensionalization is applied to measurements of different quantities so that they can be compared. Weights for the measurements are developed based on the linearity of measurements in the elastic range for a particular device and correlation with other measurements.

13.2.2 MATHEMATICAL FORMULATION

The approximation function for the elastic portion of the specimen is assumed to be the solution of the fourth-order differential equation for an elastic beam-column.

$$\frac{d^4y}{dx^4} + \frac{P}{EI}\frac{d^2y}{dx^2} = 0 \tag{13.1}$$

The following substitution variables are used to nondimensionalize this equation for a tubular member:

$$\xi = \frac{x}{L} \qquad \text{and} \qquad \eta = \frac{y}{\left(\frac{D_m}{2}\right)} \tag{13.2}$$

where D_m is the mid-thickness diameter and L is the total length of the member. Then, the differential equation becomes

$$\frac{d^4\eta}{d\xi^4} + \frac{PL^2}{EI}\frac{d^2\eta}{d\xi^2} = 0 \tag{13.3}$$

with the general solution,

$$\eta = C_1 + C_2\xi + C_3\sin(\alpha\xi) + C_4\cos(\alpha\xi) \tag{13.4}$$

where $\alpha = \sqrt{\frac{PL^2}{EI}}$ and C_1, C_2, C_3 and C_4 are integration constants.

The experimental readings are reduced to the measured values of η or the derivatives of η with respect to ξ. This is done by nondimensionalizing the measured values of deflection, rotation or curvature, where the curvature is computed from the strain readings in a particular cross section. Then, for measured lateral deflection y at location ξ (with known value of α) approximated by η , the resultant expressions in terms of the yet unknown constants C_i are the following:

$$\begin{bmatrix} 1 & \xi & \sin(\alpha\xi) & \cos(\alpha\xi) \end{bmatrix} \begin{Bmatrix} C_1 \\ C_2 \\ C_3 \\ C_4 \end{Bmatrix} = \eta \approx \left[\frac{y}{\left(\frac{D_m}{2}\right)} \right] \tag{13.5}$$

$$\mathbf{b_i} \qquad \mathbf{C} = \bar{\mathbf{f}}_i \approx \mathbf{f}_i$$

Similarly, for a measured value of rotation y',

$$\begin{bmatrix} 0 & 1 & \alpha\cos(\alpha\xi) & -\alpha\sin(\alpha\xi) \end{bmatrix} \mathbf{C} = \eta' \approx \left[\frac{y' L}{\left(\frac{D_m}{2}\right)} \right] \tag{13.6}$$

$$\mathbf{b_j} \qquad \mathbf{C} = \bar{\mathbf{f}}_j \approx \mathbf{f}_j$$

Also, for measured values of curvature y",

$$\begin{bmatrix} 0 & 0 & -\alpha^2\sin(\alpha\xi) & -\alpha^2\cos(\alpha\xi) \end{bmatrix} \mathbf{C} = \eta'' \approx \left[\frac{y'' L^2}{\left(\frac{D_m}{2}\right)} \right] \tag{13.7}$$

$$\mathbf{b_k} \qquad \mathbf{C} = \bar{\mathbf{f}}_k \approx \mathbf{f}_k$$

Combination of these equations for all the measured values of y, y' and y" gives a set of approximations where B and F are known and C 's are unknown.

$$\begin{bmatrix} b_{11} & b_{12} & b_{13} & b_{14} \\ b_{21} & b_{22} & . & b_{24} \\ b_{21} & . & . & . \\ . & . & . & . \\ . & . & . & . \\ b_{n1} & b_{n2} & . & b_{n4} \end{bmatrix} \begin{Bmatrix} C_1 \\ C_2 \\ C_3 \\ C_4 \end{Bmatrix} = \begin{Bmatrix} \bar{f}_1 \\ \bar{f}_2 \\ \bar{f}_3 \\ . \\ . \\ \bar{f}_n \end{Bmatrix} \approx \begin{Bmatrix} f_1 \\ f_2 \\ f_3 \\ . \\ . \\ f_n \end{Bmatrix} \tag{13.8}$$

$$\mathbf{B} \qquad \mathbf{C} = \bar{\mathbf{F}} \approx \mathbf{F}$$

Minimization of the squared error between $\bar{\mathbf{F}}$ and F by least squares (regression)

analysis gives a solution for C. Inclusion of the weights associated with each measurement through a diagonal weight matrix W results in the best fit solution for C.

$$\mathbf{C} = [\mathbf{B}^T\mathbf{W}\mathbf{B}]^{-1}\mathbf{B}^T\mathbf{W}\mathbf{F} \tag{13.9}$$

This set of values for C is then used to substitute in the general solution to find the curvature at the bottom, y" at x = 0. The end eccentricity e_o, is then computed by relating this end curvature to the end moment.

$$y''(0) = [0 \;\; 0 \;\; 0 \;\; -\alpha^2]\,\mathbf{C}\,\frac{D/2}{L^2} \tag{13.10}$$

$$e_o = \frac{EI\,y''_{(\xi=0)}}{P} \tag{13.11}$$

13.2.3 WEIGHTS

The weights used in the regression procedure are based on the following considerations: the closeness to linearity of readings from a gage in the elastic range among different load steps and the degree of correlation of readings among different gages at a given load step.

13.2.3.1 Weights for Deflections and Rotations

The measuring devices, such as LVDTs, rotation gages, etc., are given a weight based on the closeness to linearity of their measurements. This weight has a maximum value of 1 and is found by applying linear regression approximation in an appropriate range and taking the goodness-of-fit value. This weight is used in cases where the values of y or y' are directly measured. This weight is then applied to a particular reading of deflection (y) or rotation (y').

13.2.3.2 Weights for Curvature

In case of curvature (y"), the value of the weight is found from fitting a plane through four strain gage readings at a particular level. Linearity of readings in the elastic range for each of the four strain gages is considered and a weight for each of the strain gages is calculated. These weights are used to find the weight for curvature. Also, the accuracy of the plane fit to the four readings is considered in computing the weight for curvature as shown by Eq. 13.12. The maximum possible value of the weight is again 1.0.

$$\text{Wt. for Curvature} = \left[1 - \frac{\text{Std. Dev. in Plane fit}}{\frac{1}{4}\sum \text{Strains}}\right] \frac{\sum \text{Strain Gage Wts}}{4} \quad (13.12)$$

13.2.4 MEASUREMENT OF MODULUS OF ELASTICITY

Since the eccentricity computation requires the value of the modulus of elasticity E, it is important that E be accurately known. However, E varies somewhat from specimen to specimen. To account for this variation, the modulus of elasticity for each specimen must be determined from the test data. Also, some inaccuracies in the measurement of thickness and diameter can be compensated by adjusting the value of the modulus of elasticity.

The process used for this measurement is as follows. In the elastic range, the applied load measured by the testing machine should be equal to the average strain measured at any section multiplied by the area A, and the modulus of elasticity E. The ratio of the applied load and the load measured by the four strain gages at a section are calculated using Eq. 13.13 and an estimated value of the modulus of elasticity (e.g., 29500 ksi). These ratios are calculated for different sections with strain gages, as the applied load is changed.

$$\frac{P_{measured}}{E_{estimated} A \frac{1}{4}\sum \text{Strains}} \approx 1.0 \quad (13.13)$$

Ideally, this ratio should be equal to unity. But typically the ratios are clustered around a value which is slightly different from unity. Then, the modulus of elasticity can be adjusted to bring the average to unity. This adjusted value of the modulus of elasticity is then taken as the measured value for the purpose of further calculations.

13.2.5 SAMPLE CALCULATIONS

In the following, the procedure for computing the end eccentricity is illustrated by using the data for specimen P2P which was intended to have concentric loading, that is, zero eccentricity $e_o = 0.0$.

13.2.5.1 Initial Data

The measured geometrical and material data for Specimen P2P were as follows:

Diameter	D_m	= 17.03 in.
Thickness	t	= 0.375 in.
Length	L	= 418.2 in.
Out-of-Straightness	Δ	= 0.66 in.
Yield Stress	F_y	= 57.25 ksi
Adjusted Modulus of Elasticity	E	= 31100 ksi

A sample of the instrumentation readings at the static load P = 395.594 kips ($0.344\,P_y$) is listed in Table 13-1.

13.2.5.2 Calculation of Curvature and Weights

The curvature values are calculated from the strain gage readings at each level. Typical strain gage arrangements used in the long column tests are shown in Fig. 7-1. The four strain gages at a level are placed on the circular section at 90° intervals. The numbering is sequential and counter-clockwise looking down, starting at $y = +D_m/2$ (the dent side): ϵ_1, ϵ_2, ϵ_3, ϵ_4. The curvature y" is found by fitting a plane through the strain readings.

$$y'' = \frac{\epsilon_1 - \epsilon_3}{D_m + t} \tag{13.14}$$

The standard deviation from the plane becomes

$$\text{Std.Dev.} = \tfrac{1}{4}\left[\epsilon_1 - \epsilon_2 + \epsilon_3 - \epsilon_4\right] \tag{13.15}$$

The weight for the curvature is found by using Eq.13.12.

For the data of specimen P2P (See Table 13.1), at a load of 395.59 kips, these formulas result in the following values:

$$y''(13.25) = \frac{-625.354 + 540.280}{17.03 + 0.375} = -4.8879 \ \ [\text{in./in.} \times 10^{-6}]$$

$$\text{St.Dev} = \left|\frac{-625.354 + 668.554 - 540.280 + 700.312}{4}\right| = 50.808 \ [\text{in./in.} \times 10^{-6}]$$

$$\text{Weight} = \left(1 - \frac{50.808}{\left|\frac{-625.354 - 668.554 - 540.280 - 700.3121}{4}\right|}\right) \times$$

$$\times \left(\frac{0.99916 + 0.99999 + 0.99933 + 0.99977}{4}\right) = 0.919411$$

Similarly, by applying this procedure to Levels 1 and 2 (x = 69.7 in. and x = 139.4 in.), the curvatures and weights are calculated.

$y''(69.7) = -17.8652 \ \ [\text{in./in.} \times 10^{-6}]$ Weight = 0.985482

$y''(139.4) = -26.5459 \ \ [\text{in./in.} * 10^{-6}]$ Weight = 0.976854

13.2.5.3 Non-dimensionalization of Measured Data and Computation of C's

Utilizing the equations developed in Sect. 13.2.2 (Eqs. 13.5 to 13.7), the data for Specimen P2P is then nondimensionalized and used to set up the equations $\mathbf{b}\,\mathbf{C} \approx \mathbf{f}$. First, some of the parameters needed at this stage are computed using the data given in Subsect. 13.2.5.1.

$$\alpha = \sqrt{\frac{P\,L^2}{E\,I}} = \sqrt{\frac{395.594\,(418.2)^2}{31100\,(727.336)}} = 1.74885$$

$$R = \frac{D}{2} = \frac{17.03}{2} = 8.515$$

The location of strain gages at level 0 is

$$\xi = \frac{x}{L} = \frac{13.25}{418.2} = 0.03168$$

Then, the equation for curvature at level 0 is from Eq. 13.7

$$\left[\,0 \quad 0 \quad -\,a^2 \sin(\alpha\xi) \quad -\,a^2 \cos(\alpha\xi)\right] \mathbf{C} \;\approx\; \left[\frac{y''\,L^2}{(D/2)}\right]$$

Substitution of the numerical values and the evaluation of $\mathbf{b}$ and $\mathbf{f}$ results in the equation for curvature for level 0 to be

$$\left[0 \quad 0 \quad -1.7492 \sin(1.749 \times 0.0317) \quad -1.7492 \cos(1.749 \times 0.0317)\right] \mathbf{C} \;\approx\; \left[\frac{-4.8879 \times 10^{-6} \times 418.2^2}{8.515}\right]$$

$$[0 \quad 0 \quad -0.1694 \quad -3.0543]\,\mathbf{C} \;\approx\; [-0.10039]$$

Similar procedure for all measured values of y, y' and y" and an assembly into the form of Eq. 13.8 results in the following matrix equation:

$$\begin{bmatrix} 0 & 1 & 1.749 & 0 \\ 1 & 0 & 0 & 1 \\ 0 & 0 & -0.169 & -3.054 \\ 1 & 0.167 & 0.289 & 0.958 \\ 0 & 0 & -0.882 & -2.930 \\ 1 & 0.335 & 0.553 & 0.834 \\ 0 & 0 & -1.689 & -2.547 \end{bmatrix} \begin{Bmatrix} C_1 \\ C_2 \\ C_3 \\ C_4 \end{Bmatrix} \approx \begin{Bmatrix} 0.423, \\ 0.005, \\ -0.100, \\ 0.076, \\ -0.367, \\ 0.142, \\ -0.545 \end{Bmatrix} \tag{13.16}$$

$$\mathbf{B} \qquad \mathbf{C} \approx \mathbf{F}$$

The corresponding weights are computed to be

$$\mathbf{W} = \begin{bmatrix} 0.9925 & 0 & 0 & 0 & 0 & 0 & 0 \\ 0 & 0.9935 & 0 & 0 & 0 & 0 & 0 \\ 0 & 0 & 0.9194 & 0 & 0 & 0 & 0 \\ 0 & 0 & 0 & 0.9904 & 0 & 0 & 0 \\ 0 & 0 & 0 & 0 & 0.9855 & 0 & 0 \\ 0 & 0 & 0 & 0 & 0 & 0.9932 & 0 \\ 0 & 0 & 0 & 0 & 0 & 0 & 0.9769 \end{bmatrix} \tag{13.17}$$

W is a square (7×7) diagonal matrix with the weights on the principal diagonal.

Now the unknown constants **C** can be computed from Eq. 13.9.

$$\mathbf{C} = \begin{Bmatrix} -0.0159 \\ -0.0927 \\ 0.2959 \\ 0.0241 \end{Bmatrix} \tag{13.18}$$

13.2.5.4 End Eccentricity

With the constants known, the end eccentricity is calculated by first finding the curvature of the beam-column at the bottom end, x = 0.

$$y''(0) = [0 \quad 0 \quad 0 \quad -\alpha^2]\, C \left[\frac{D/2}{L^2}\right] \tag{13.19}$$

$$\text{that is,} \qquad y''(0) = -\alpha^2 C_4 \left[\frac{D/2}{L^2}\right]$$

Substituting the numerical values,

$$y''(0) = -1.749^2 (0.0241)\left[\frac{8.515}{418.2^2}\right] = -3.5957 \times 10^{-6}$$

The end eccentricity is computed by relating the curvature at the end to the end moment and the axial load,

$$e_o = -\frac{EI\, y''(0)}{P} \tag{13.20}$$

$$e_o = -\frac{31100(727.336)(-3.5957) \times 10^{-6}}{395.594} = -0.2056 \text{ in.} \tag{13.21}$$

Thus, the computed end eccentricity is $e_o = -0.2056$ in. rather than the intended geometric zero eccentricity. This deviation can be readily accepted as negligible since it represents only 1.2% of the diameter.

13.3 Application to Cylindrical Bearings

13.3.1 COMPUTED END ECCENTRICITIES

Based on the procedure outlined in Section 13.2, the end eccentricities of all specimens tested using the cylindrical bearings were evaluated. The computed end eccentricities are presented in Figs. 13-1 to 13-10. In these figures, the end eccentricity at different load steps is plotted against the load. The heavier curve shows the pre-ultimate loading range, and the thin curve the post ultimate range. The computed end eccentricities are fairly constant in the loading range. However, there is some minor variation in the end eccentricity in the post-ultimate region. The end eccentricity for a particular specimen is computed by averaging the calculated end eccentricities over the load steps in the elastic loading range of the curve. These values are presented in Table 13-2.

13.3.2 COMPARISON WITH DESIGN VALUES

Table 13-2 provides a comparison of the design and the computed values of end eccentricity for pin-ended specimens using cylindrical bearings. The computed values of the end eccentricity are within -0.4 to +0.5 inches of the intended design values. This

is only about -4% to +5% of the diameter of the specimens.

Considering the size of the specimens tested and the tolerances in fabrication, testing and, also of the computation process, these values are considered to be quite acceptable. These results indicate that the cylindrical bearings were able to provide the pin-ended condition that was required for these tests. Thus, the use of these bearings eliminated any need for adjusting the value of the length of the member based on the inflection points since the rotation took place at the ends of the member itself.

13.4 Application to Spherical Bearings

13.4.1 APPROXIMATION OF PLANAR RESPONSE

Even though the spherical end bearings allowed specimens to flex in any direction, most specimens were found to deflect in one plane. Thus, to find the end eccentricity for spherical bearings, the procedures used for cylindrical bearings can be used (Section 13.2). However, to apply this procedure, deflections, rotations and curvatures measured for specimens tested with spherical bearings had to be transformed to the plane in which a particular specimen deflected.

In every section where deflection or rotation needed to be measured, the gages were placed in directions perpendicular to each other. Four strain gages were placed at each section where curvature was measured. These gages were directly used to measure curvature in two perpendicular directions. By applying coordinate transformations the measured quantity could be found in any direction. The procedure for weight calculation for curvature remained unchanged. For deflections, the following formula was used to find the weight from the weights of measurements from the LVDT's placed in the south-east and south-west directions (W_E , W_W) at that level. Here, θ is the angle to the plane of deflection measured counter-clockwise from the weld line (0-line).

$$W_\theta = W_E \cos^2\left(\frac{\pi}{4} - \theta\right) + W_W \sin^2\left(\frac{\pi}{4} - \theta\right) \tag{13.22}$$

For rotations Eq. 13.23 is used where W_N and W_W are the weights of the rotation measurements on the north and west faces. Angle θ is the same as for Eq. 13.22.

$$W_\theta = W_N \cos^2\theta + W_W \sin^2\theta \tag{13.23}$$

Once the deflection (y), rotation (y') or curvature (y") are found for the plane of deflection of the specimen, they can be nondimensionalized and used in the regression analysis procedure developed for the specimens with cylindrical bearings.

13.4.2 COMPUTED END ECCENTRICITIES FOR SPHERICAL BEARINGS

The computed end eccentricities for pin-ended specimens with spherical end bearings are plotted in Figs. 13-11 to 13-16. Since many of these specimens were able to sustain a high load level before failure, some of them had initiation of yielding in the bottom half of the member at loads close to the ultimate load. As strain gages cannot effectively measure strains beyond yielding, the curvature measurements at that level had to be suspended. The eccentricity computations in the post-ultimate range in some of these specimens were stopped because of the yielding.

Table 13-3 presents the computed end eccentricities averaged over the elastic region of loading. None of the specimens tested with spherical bearings had any design eccentricity. The computed eccentricity in these specimens varied within -0.27 to +0.35 inches. This variation is about -3% to +3% of the specimen diameters. This variation is quite small and can be attributed to the variations within the accuracy of erection, geometrical measurements, gage data, and end eccentricity computations. Thus, the conclusion is that the spherical end bearings provided an adequate simulation of the intended pin-ended conditions.

13.5 Conclusions and Recommendations

The procedure used for computing the actual end eccentricity is based on a logical interpretation of the specimen behavior, and it gave consistent accuracy in the loading (elastic) range. It confirmed that the intended end eccentricity was duplicated with an average deviation of 1.39% (max 4.83%) of the diameter for both the cylindrical and spherical bearings.

It may be recommended that the computed values of end eccentricity be used in an accurate analysis of the specimen behavior (computer methods) rather than the design values. Since in a few cases, in the pre-ultimate range and frequently in the post-ultimate range, the computed eccentricity indicated illogical irregularities, a more thorough study of the method and of the potential causes of irregularities is desirable.

14. EFFECT OF DETERIORATION (CORROSION)

14.1 Introduction

Deterioration of offshore platforms by corrosion leads primarily to a reduction of the wall thickness in the component members. This can be a uniform corrosion resulting in a thinner wall of relatively constant thickness or a localized corrosion in which the thickness is reduced only over small portions of the wall surface. In extreme cases, local corrosion may extend completely through the thickness to produce holes. These two basic types of corrosion tend to limit the strength of structural members by different modes of failure.

Overall corrosion leads to a uniform reduction of the wall thickness over the full length of a member which then fails as a column. (Local pitting and "marine-borer like" cavities or even small holes have relatively little effect on the overall behavior or strength of columns.)

Patch corrosion, that is, corrosion only over local portions of the tube surface, limits the member strength by local buckling or an earlier yielding in the areas affected by corrosion. Early yielding may lead to subsequent local buckling in the plastic range.

Three corroded column specimens were tested. One, Specimen C4B, had uniform corrosion and two, Specimens C1 and C2, had local (patch) corrosion.

This chapter discusses the test observations on these specimens (Section 14.2), comparison with available analytical methods (Section 14.3), and an approximate approach for assessing the effect of corrosion on member strength (Section 14.4). Emphasis is put on the specimens with patch corrosion (Specimens C1 and C2).

14.2 Tests on Corroded Specimens

14.2.1 GENERAL

The three corroded column specimens are Specimens C1, C2 and C4B. Their general geometrical and material properties are listed in Table 1.1. The effective average thickness of these specimens was determined by weighing and thickness measurements at the ends, as described in Article 3.1.3 and listed in Table 1.1,. Using

this thickness, column analysis was performed the results of which are listed in Table 12-1. The ultimate test load of Specimen C4B gave excellent correlation with the loads computed from the FE (finite element), Ellinas, and Loh methods (within 3 to 7%). (The AISC method was somewhat optimistic, resulting in a 21% higher load.) In contrast, the specimens with local corrosion, Specimens C1 and C2, showed much lower experimental ultimate loads than computed on the basis of constant average thickness. They failed prematurely due to local buckling or overstraining in the heavily corroded patches.

14.2.2 SPECIMEN C4B (Overall Corrosion)

The corroded Specimen C4B had uniform reduction of thickness and its ultimate load was governed by overall column buckling, as shown in Photo 1-1E(f). As described in Section 9.4.6 and shown in Fig. 9-14, the specimen exhibited a load vs. axial shortening curve typical for column behavior in the pre- and post-ultimate ranges. Only after some yielding in the post-ultimate range did local buckles develop at a slightly lower load. Then, the load dropped drastically as shown in the load vs. axial shortening plot in Fig. 9-14. Circumferential variation of the thickness at the local buckles (shown in Fig. 14-1) shows, that although the minimum thickness was only 0.12 in., it more than tripled to 0.38 in. within only two(2) inches on either side. Thus, the area of reduced thickness was not enough to invite local buckling until considerable straining occurred in the plastic range.

As can be seen in Photo C4B.??? (stub-column after test), locally, the wall surface was very irregular. However, as noted in Art. 14.2.1 above, the "smearing" (averaging) effect on the thickness was such that the use of the average thickness in column strength formulas resulted in a very good correlation between the experimental and theoretical ultimate loads. (Table 12.1)

14.2.3 SPECIMENS C1 AND C2 (Patch Corrosion)

Approximate maps of the unfolded surfaces of Specimens C1 and C2 are shown in Figs. 14-2 and 14-3, respectively. The areas are marked for light, moderate and heavy corrosion as estimated by visual inspection and UT (ultrasound technology) readings. The blank areas have no or very insignificant surface corrosion. The location of local buckles that developed in the tests is indicated, and other potentially sensitive locations for local buckling under higher loads are labeled A, B, C and D (C1 only).

The effect of patch corrosion on the strength of a member has the following aspects:

1) **Local increase in stress.** Compared to stresses at other locations along the member, the stress at the patch corrosion is increased not only due to the reduction of the cross-sectional area, but also due to the stress amplification. This amplification is caused by the shift of the effective centroid of the cross section and the consequent eccentricity of the axial load which is assumed to be applied at the geometric center of the inside diameter. The resultant locally increased stress may lead to yielding or local buckling under a lower load than required to cause failure elsewhere in the member.

2) **Local buckling.** Local buckling occurs when the reduction of the thickness is over an area sufficient to develop a buckle under the amplified stress. Local buckling may also develop after yielding and additional straining.

An illustration of the importance of having sufficient area of reduced thickness is provided by the observations made in testing Specimen C1. Although the specimen had a hole through the wall at one location (see Fig. 14-2) (and failure was expected by local buckling around this hole), the ultimate load was controlled by local buckling at another location where the combination of a larger area of reduced thickness and the stress amplification caused local buckling at a lower applied load.

A more detailed discussion of the individual Specimens C1 and C2 is given below.

SPECIMEN C1

General test observations of Specimen C1 are given in Art. 9.4.1. The overall view of the Specimen in Photo 1-1C(e) and the unfolded surface in Fig. 14-2 indicate the location and extent of corrosion patches. The tube segment with the hole, where local buckling was initially expected to occur, is shown in Photo 14-??c1hole. Photo 14-??C1buk shows the portion of the specimen where local buckling actually took place. It should be noted that in this view, taken after completion of the test, the buckles are significantly enlarged due to the deformations after initial buckling. Variation of the wall thickness in these two areas with close-ups at the hole and at the point with the minimum thickness (where buckling initiated) is shown in the isometric views of Figs. 14-4 and 14-5. All of these illustrate how non-uniform the thickness of the tube wall becomes due to patch corrosion.

Variation of the thickness along a line around the circumference in the area of local buckling is shown in Fig. 14-7. This plot was used to determine the effect of corrosion. The cross section modified by the reduction of the thickness was analyzed to compute its effective properties: area (A_e), moment of inertia (I_e), and the distance from the centroid to the center of the original circle (e).

Redistribution of the stresses in the cross section resulted in an increase of the stresses in the areas where the wall was the thinnest. Figure 14-9 shows the resultant stress distribution.

SPECIMEN C2

The axial test on Specimen C2 is described in Art. 9.4.3. The specimen had several patches of corrosion as can be seen in Photo 1-1D(d) and Fig. 14-3. Local buckles developed in the area near the bottom in the figure. (In the test, that end was at the top.) The buckles, with very short wave length and irregular pattern, are typical of buckling in the plastic range. They are of the same type as can be seen on stub-column C2-SC (Photo 14.5??C2SC) which was made from the same salvaged tube as test column C2. The buckles in the center portion of the stub-column are essentially identical to the buckles in the critical portion of Specimen C2. The very irregular shape of the buckle waves is again typical for the pitted pattern of the corroded surface of most of the corroded tubes of this program.

A contour map of the thickness variation in the vicinity of the local buckles is shown in Fig. 14-6 together with the isometric views of the portions where the thickness was the smallest. The variation of the thickness in the full cross section passing through the point with minimum thickness is shown in Fig. 14-8. The cross-sectional properties at this section, A_e, I_e and the shift of the centroid e were used in the analysis of local buckling, which is discussed later.

An analysis of the cross section under ultimate load indicates that local buckling took place under additional straining after the yield stress level was reached.

14.3 Comparison with Local Buckling Formulas

14.3.1 LOCAL BUCKLING FORMULAS

Both specimens with patch corrosion damage, Specimens C1 and C2, failed by local buckling. It is thus appropriate to compare the stresses in the reduced section at the failure load with local buckling stresses from engineering formulas. Although the formulas listed below were originally developed for local buckling of tubular members with constant wall thickness and subjected to concentric load, they are also acceptable for loads with small eccentricity. Here, the formulas have been modified to uniform format and notation from the formats in the source references.

API (American Petroleum Institute, RP2A) [3]

$$F_{cr} = \left(1.64 - 0.23 \sqrt[4]{\frac{D_o}{t}}\right) F_y \qquad \text{for } \frac{D_o}{t} \geq 60 \tag{14.1}$$

DNV (Det Norske Veritas) [5,8][1]

$$F_{cr} = \left[1 - \frac{1}{3}\left(\frac{1.5 + 0.001(D_o/t)}{\alpha}\right)^2\right] F_y \tag{14.2}$$

AISI (American Iron and Steel Institute) [2,15]

$$F_{cr} = (0.667 + 0.037\,\alpha) F_y \qquad \text{for } F_{cr} \leq F_y \tag{14.3}$$

SSRC (Structural Stability Research Council) [15]

$$F_{cr} = (0.61 + 0.043\,\alpha) F_y \qquad \text{for } 2.57 \leq \alpha < 9.5 \tag{14.4}$$

AO (A.Ostapenko) [8,15]

$$F_{cr} = 38\,\xi - 480\,\xi^2 + 2020\,\xi^3 \qquad \text{for } \xi < 0.07 \tag{14.5a}$$

$$F_{cr} = F_y \qquad \text{for } \xi \geq 0.07 \tag{14.5b}$$

where

D_o is the outside diameter

$D_m = D$ is the mid-thickness diameter

$$\alpha = \frac{1}{(D_o/t)} \frac{E}{F_y} \qquad \text{and} \qquad \xi = \frac{1}{(D_m/t)} \sqrt[3]{\frac{E}{F_y}} \tag{14.6}$$

Note that the API (Eq. 14.1) and DNV (Eq. 14.2) methods are commonly used in designing offshore structures.

Application of all these formulas to Specimens C1 and C2 is shown in Table 14.1. Listed are the pertinent formulas and the local buckling stresses computed for the respective values of t_{min} and diameters and non-dimensionalized with respect to the yield stress.

14.3.2 COMPARISON WITH TEST RESULTS

In the analysis of test results, the load to cause local buckling ($P_{\ell b}$) was assumed to be the load at which the load-deflection curve started to significantly deviate from the

[1]This DNV formula represents a simplification of a rather complex semi-graphical procedure of the DNV specification.[5,8]

straight line in Figs. 9.4 and 9.8. For Specimens C1 and C2, the API formula (Eq. 14.1) and the local buckling load $P_{\ell b}$ taken to be the last static load measured prior to the ultimate load were used.

The following formula for computing the equivalent wall thickness was derived by equating the local buckling stress from Eq. 14.1 to the local buckling stress from the test:

$$t_{eq} = \left(\frac{0.23}{1.64 - \frac{F_{\ell b}}{F_y}} \right)^4 D_o \qquad (14.7)$$

where

t_{eq} is the equivalent wall thickness.

$F_{\ell b}$ is the local buckling stress from the test.

$$F_{\ell b} = \frac{P_{\ell b}}{A_e} k \qquad (14.8)$$

k is the stress amplification factor, that is, the ratio of the maximum and average stresses in the cross section from Eq. 14-16 formulated below in Section 14.4.

Using the data for Specimen C1 based on the measured thickness values and the local buckling load $P_{\ell b}$, the equivalent thickness for local buckling is computed from Eq. 14.7

For $A_e = 5.71\,\text{in.}^2$, $D_o = 10.336\,\text{in.}$, k=1.246, $P_{\ell b} = 175$ kips, $F_y = 40.89$ ksi

$$t_{eq} = 0.116 \text{ in.}$$

This is larger than the minimum thickness $t_{min} = 0.10$ in. and can be considered to be the average thickness over an area sufficient to invite local buckling at the stress level corresponding to the local buckling load. The extent around the circumference in Fig. 14-7 at the point of minimum thickness to give an average thickness of t_{eq} is approximately equal to 1 to 1.4 radians, that is, 1 to 1.4 radii. However, the averaging should include the width of the buckles along the specimen. Figure 14-5 shows the rectangular area with dimensions of 1 radius circumferentially and $\frac{1}{4}$ radius longitudinally centered over the buckle. The resultant average thickness was $t_{ave} = 0.121$ in. which is very close to $t_{eq} = 0.116$ in.

Similar computations for Specimen C2 led to the conclusion that not only did the stress in the weakened area reach the yield stress level, but that most of the cross section was plastified by the time the ultimate load was attained. Local buckling took place at the yield stress level after considerable straining in the plastic range. In fact, only a small portion of the cross section remained elastic at the ultimate load.

14.4 Engineering Estimate of Local Buckling

14.4.1 APPROXIMATE ANALYSIS OF CORRODED CROSS SECTIONS

Irregular variation of the thickness shown in Figs. 14-7 and 14-8 for the two tested specimens further complicates the formulation of a method for quantifying the effect of corrosion on local buckling and strength of corroded members.

An approximate evaluation of the stress amplification due to the eccentricity of the effective centroid caused by the one-sided local reduction of the wall thickness is discussed next.

It is assumed that the thickness varies gradually from a minimum t_{min} on one side to a maximum t_{max} on the opposite side of the circumference. Also, the outside and inside surfaces are assumed to form perfect circles with the centers offset by distance s as shown in Fig. 14-11. The center of the inside circle is used as the reference point since the inside surface had insignificant corrosion compared to the outside surface and thus better retained its circularity.

$$s = \frac{t_{max} - t_{min}}{2} \tag{14.9}$$

The effective area of the resultant cross section A_e is given by the following equation:

$$A_e = \frac{\pi}{4}\left(D_o^2 - D_i^2\right) \tag{14.10}$$

where

D_i is the inside diameter.

D_o is the outside diameter.

$$D_o = D_i + (t_{max} + t_{min}) \tag{14.11}$$

The distance from the center of the inside circle to the centroid of the cross section is given by

$$e = \frac{D_o^2}{D_o^2 - D_i^2}\, s \tag{14.12}$$

Then, the effective moment of inertia I_e can be computed from

$$I_e = \frac{\pi}{4}\left\{\left(\frac{D_o^4}{16} + D_o^2(e\text{-}s)^2\right) - \left(\frac{D_i^4}{16} + D_i^2 e^2\right)\right\} \tag{14.13}$$

and the distance from the effective centroid to the mid-thickness at the thinner side from

$$c = e + \tfrac{1}{2}(D_i - t_{min}) \tag{14.14}$$

Then, the ratio of the maximum stress in the cross section to the average stress, the ***stress amplification factor***, is

$$k = 1 + \frac{A_e e c}{I_e} \tag{14.15}$$

An additional increase in the stress at the location of reduced thickness is produced by the out-of-straightness of the column at this location, δ. (As shown in Fig. 14-11, the minimum wall thickness t_{min} is conservatively assumed to be on the inside of the initial out-of-straightness curvature.) Then, with δ, the amplification factor becomes

$$k = 1 + \frac{A_e (e + \delta) c}{I_e} \tag{14.16}$$

Variation of the thickness around the circumference for this approximated cross section is given by the following formula:

$$t(\phi) = \sqrt{\left(\frac{D_o}{2}\right)^2 - s^2 \sin^2\phi} \; - \left(\frac{D_i}{2} - s\cos\phi\right) \tag{14.17}$$

where, as shown in Fig. 14-11, the argument is angle ϕ, measured counter-clockwise from the positive x-axis and starting at the point of maximum thickness. The origin is set at the center of the inside circle.

Figure 14-7 shows the thickness variation from Eq. 14.17 for Specimen C1 together with the thickness values based on the UT measurements. The unfolded circumference is plotted with the origin at the point of maximum thickness so that the minimum thickness is displayed at the middle point of the plot where the two t_{min} values are exactly equal. The two curves follow similar general patterns. Since the measured thickness tends to be higher than the approximated thickness, it is expected that the cross-sectional properties would also differ for the two thickness patterns.

Figure 14-9 shows the variation of the stresses around the circumference for the two cases, each non-dimensionalized with respect to the stress at the centroid (P/A_e). As it would be expected from the thickness distributions, the maximum stress in the approximated section is higher than in the actual (by approximately 20%). The resultant stress amplification factors for the approximated (Eq. 14.16) and measured thickness variations are

Approximated t: $k_{C1a} = 1.513$

Measured t: $k_{C1m} = 1.245$

Obviously, the difference between the two values is very dependent on the actual variation of the thickness, and thus, for some other tube or location along the tube, the

approximated cross section may give higher or lower stresses.

14.4.2 PRELIMINARY PROCEDURE FOR CHECKING LOCAL BUCKLING

Although more data on the actual thickness variations are needed to arrive at a more statistically valid formulation, the observations made in the previous section with respect to the ***equivalent thickness*** t_{eq} can be summarized into the following preliminary procedure for checking corroded tubes for local buckling.

1) Consider the area with the greatest amount of corrosion and evaluate (or estimate) the average thickness t_{ave} over a rectangular area extending one radius (1 R) around the circumference and one-third radius ($\frac{1}{4}$R) in the longitudinal direction of the member.

2) Compute the local buckling stress F_{cr} for the corresponding $\left(\frac{D}{t_{ave}}\right)$ from the API equation (Eq. 14.1) or another suitable formula.

3) Compute the cross-sectional properties A_e, I_e, e, c and k from the measured or approximated thickness values.

4) Compute the corresponding axial load to cause local buckling from

$$P_{\ell b} = \frac{F_{cr}}{k} A_e \qquad (14.18)$$

14.5 Future Research on Effect of Corrosion

Results of the limited study on corroded members reported here indicate a need for further research in order to more accurately define engineering rules and methods. The following topics are recommended:

1) More tests and data on the actual thickness variations in corroded members are needed to arrive at a more statistically valid formulation of an engineering method.

2) Additional tests are recommended on Specimens C1 and C2 after repairing or cutting off the portions with local buckles. Each of these specimens has more portions with heavy corrosion where local buckles may be expected to limit column strength. (The advantage of retesting these specimens is that all geometrical and

material properties are already available, and only some additional thickness measurements and instrumentation would be needed to conduct these tests.)

3) There is a possibility that the effect of local corrosion is very similar to the effect of a dent in reducing the ultimate load and causing a more significant reduction in the post-ultimate range. Thus, a method may be found for converting a corroded area to an equivalent dent depth and then using a formula or a program that had been developed for considering the effect of a dent.

15. SUMMARY, CONCLUSIONS AND RECOMMENDATIONS

Twenty tubular columns were tested to investigate the axial load vs. axial shortening relationship of dented or corroded columns. Eighteen of these tubes were large-scale fabricated and salvaged, and two were small-scale manufactured tubes. The purpose of testing large-scale specimens was to determine how dimensions and residual stresses affected the ultimate strength and post-ultimate behavior of damaged tubular columns.

In this group, there were seven newly fabricated and eleven salvaged column specimens. The specimens had lengths from 22 to 35.4 feet and diameters ranging from 10.4 to 24.5 inches. All the fabricated specimens and four of the salvaged specimens were dented at mid-length with dent depths ranging from 5 % to 15 % of the diameter. Of these specimens, two were tested with fixed ends, two with end eccentricity, and seven with pinned ends. The tests on salvaged and fabricated specimens indicated that residual stresses present in the fabricated specimens had little effect on the ultimate strength and post-ultimate behavior of damaged tubular specimens.

The remaining seven salvaged specimens were tested without denting, and of these, three were corroded, one was badly bent and three were non-corroded. Local buckling occurred in two of the corroded specimens before overall yielding. This was due to a significant reduction of thickness at a particular cross section.

Several methods were used to analyze the test specimens. Comparison indicated that the analytical methods could acceptably accurately predict the ultimate strength for dented columns, but were conservative in estimating their post-ultimate behavior, that is, they tended to predict a greater reduction in strength in the post-ultimate range than observed in tests. The analytical methods also predicted the behavior of the uniformly corroded specimens, but could not accurately predict the behavior of specimens with localized corrosion, for which local buckling was the failure mode.

The following areas are recommended for future research based on this study:

1) A study of practical repair methods for damaged members, and formulation of a method(s) for computing the strength and behavior of repaired members.

2) Development of a technique for quick determination of the thickness of a tubular member without surface preparation.

3) An analytical method for evaluating the residual strength of corroded members.

4) An in-depth study of the effects of local reduction of thickness due tocorrosion by using salvaged members and, possibly, by making controlled 'corroded' areas by grinding. This study should include a statistical analysis of the type and extent of corrosion found in existing offshore structures.

5) A computer program that can better predict the post-ultimate behavior of damaged tubular columns.

16. ACKNOWLEDGMENTS

This report describes most of the work conducted on the project "Residual Strength of Damaged and Deteriorated Offshore Structures" at Lehigh University Department of Civil Engineering (I.J. Kugelman, Chairman). This project was within the managerial structure of ATLSS (Advanced Technology for Large Structural Systems, J.W. Fisher, Director) and was administratively guided by W.D. Michalerya. The tests were conducted at Fritz Engineering Laboratory and Imbt Laboratory.

The project was sponsored as a Joint Industry Project by the following: Chevron Oil Field Research Company, EXXON Production Research Company, Mobil Oil Research and Development Corp., Shell Oil Company, Texaco Inc., Minerals Management Service (DOI), Marine Technology Support Unit (MaTSU, U.K.), and American Iron and Steel Institute (AISI). We are grateful for the financial support provided by these organizations. We are also indebted for the advice and guidance of the following Representatives of these organizations: T.M. Hsu (Chevron), J.T. Loh and N. Zettlemoyer (EXXON), J.A. Volker and D.R. Angevine (Mobil), P.W. Marshall (Shell), J.H. Kemper (Texaco), C.E. Smith (MMS/DOI), N.W. Nichols (MaTSU, U.K.), and Kathlene H. Almand (AISI). Special thanks go to EXXON for providing the salvaged tubes and to J.T. Loh (EXXON) for analyzing the test specimen behavior with their computer program BCDENT, and also for making many useful suggestions. Thanks also go to T.M. Hsu of Chevron for providing the DENTA analysis of the behavior of the test specimens.

Gratitude is extended to the following individuals for their help. J.A. Padula, a graduate student, was instrumental in the preparation of the research proposal, and whose previously developed finite element models were used to analyze the test specimens. He also worked on the project at the initial stages. W. Kim and R. Kowalik, graduate students, and S. Dimitrakis, Patti Grossi, P. Luger, Michelle Morgan, and M.Z. Rehman, undergraduate students, were helpful in testing and/or reducing the experimental data.

Sincere gratitude goes to T.W. Berger, a graduate student, who provided tremendous help in the production of this report.

Thanks are also due to F. Stokes, R.R. Dales and C.F. Hittinger, and the technical staff of the laboratories who helped plan, set up, and run the tests. R. Longenbach and E. Tomlinson were most helpful with the test instrumentation. R.N. Sopko attended to the photographic needs of the project, and P. Bryan gave advice on the use of software.

17. REFERENCES

[1] ADINA
"ADINA User's Manual"
Report AE 81-1 edition, ADINA Engineering, Inc., 71 Elton Ave., Watertown, MA 02172, 1981.

[2] AISI
"Specification for the Design of Cold-Formed Steel Structural Members"
American Iron and Steel Institute, Washington, 1986. [pp. I-39]

[3] API
"Recommended Practice for Planning, Designing, and Constructing Fixed Offshore Platforms, API RP2A"
American Petroleum Institute, Washington, D.C., 1989.

[4] ASTM
"Standard Test Methods and Definitions for Mechanical Testing of Steel Products"
ASTM Annual Book of Standards 1992, , Designation: A 370-91a, Vol. 01.01.

[5] DNV
"Rules for the Design, Construction and Inspection of Fixed Offshore Structures"
Det Norske Veritas (DNV), Oslo, 1974.

[6] Ellinas, C.P.
"Ultimate Strength of Damaged Tubular Bracing Members"
J. Struct. Engnrg, American Society of Civil Engineers, Vol. 110, No. 2, February, 1984, pp. 244-259.

[7] Kim, Woobum
"Behavior and Strength of Damaged Tubular Columns with End Restraints"
Ph.D. Dissertation (supervised by A. Ostapenko), Lehigh University, September 1992.

[8] Ostapenko, A.
"Local Buckling of Welded Tubular Columns"
Proceedings of the International Colloquium on Stability of Structures under Static and Dynamic Loads (held in Washington, D.C., May 17-19, 1977), American Society of Civil Engineers, New York, 1977, pp. 367-374.

[9] Padula, J.A. and Ostapenko, A.
"Indentation Behavior and Axial Tests of Two Tubular Columns"
In Proceedings of the 19th Annual Offshore Technology Conference, Offshore Technology Conference, Houston, April, 1987, (Paper OTC 5438), pp. 151-159.

[10] Padula, J.A. and Ostapenko, A.
"Load-Shortening Behavior of Damaged Tubular Columns"
In Proceedings of the 22nd Annual Offshore Technology Conference, Offshore Technology Conference, Houston, May, 1990, (Paper OTC 6382), pp. 317-325.

[11] Padula, J.A. and Ostapenko, A.
"A Load-Indentation Relationship for Tubular Members"
In Proceedings of the 23rd Annual Offshore Technology Conference, Offshore Technology Conference, Houston, May, 1991,(OTC Paper 6651), pp. 45-55.

[12] Rashed, S.M.H., Taby, J. , and Moan, T.
"Theoretical and Experimental Study of the Behavior of Damaged Tubular Members"
In INCOE 81, 1981.

[13] Riehle
"Rockwell Hardness Table"
in "Instruction Manual, Riehle Portable Hardness Tester Model PHT-2"
Riehle Testing Machines, Division of Ametek, Inc.,
East Moline, Illinois; 1963.

[14] Smith, C.S., Kirkwood, W., and Swan, J.W.
"Buckling Strength and Post-Collapse Behaviour of Tubular Bracing Members Including Damage Effects"
In Second International Conference on Behaviour of Offshore Structures, London, August, 1979, pp. 303-326.

[15] Smith, C.S.
"Residual Strength of Tubulars Containing Combined Bending and Dent Damage"
In Offshore Operations Symposium - 1986, American Society of Mechanical Engineers, New Orleans, February, 1986, pp. 221-227.

[16] SSRC-a
"Guide to Stability Design Criteria for Metal Structures"
4th Edition, Editor: T.V. Galambos, John Wiley & Sons, New York, 1988, pp. 473-474.

[17] SSRC-b
"Guide to Stability Design Criteria for Metal Structures"
4th Edition, Editor: T.V. Galambos, John Wiley & Sons, New York, 1988, pp. 708-717.

[18] Taby, J.
"DENTA II – User's Manual (VAX Version 1.01)"
Department of Marine Technology, The Norwegian Institute of Technology, Trondheim, Norway, March, 1988.

[19] Ueda, Y., and Rashed, S.M.H.
"Behavior of Damaged Tubular Structural Members"
In Proceedings of the Fourth International Offshore Mechanics and Arctic Engineering Symposium, Vol. 2, pages 528-536. American Society of Mechanical Engineers,New York, February, 1985 (Symposium held in Dallas, TX, on February 17-21, 1985).

[20] AISC
"Manual of Steel Construction, Allowable Stress Design", 9th Edition
American Institute of Steel Construction, Chicago, IL, 1989.

[21] Duan, L., Loh, J.T., and Chen, W.F.
"Moment-Curvature Relationship for Dented Tubular Sections"
J. Struct. Engnrg, American Society of Civil Engineers, Vol. 119, No. 3, March, 1993, pp. 809-830.

[22] Loh, J.T.
"Ultimate Strength Guidance for Evaluating Dented Members"
EXXON Production Research Company, Offshore Division, Houston, TX, March 31, 1993.

18. NOMENCLATURE

A	Cross-sectional area. [in.^{2}]
A_e	Calculated effective area of corroded tube cross section. [in.^{2}]
B	Known coefficients of approximation functions.
C	Unknown coefficient for regression analysis.
C_1,C_2,etc.	Integration constants.
D	Any use of D refers to mid-thickness diameter D_m. [in.]
D_i	Inside diameter of tube. [in.]
D_m	Mid-thickness diameter of tube. [in.]
D_o	Outside diameter of tube. [in.]
E	Modulus of elasticity. [ksi]
E_{SH}	Strain hardening modulus. [ksi]
$\bar{F}$	Vector of approximated data for regression analysis.
F	Vector of actual data for eccentricity regression analysis.
F_{cr}	Critical average column stress controlled by local buckling. [ksi]
$F_{\ell b}$	Local Buckling Stress. [ksi]
F_y	Yield stress of steel. Used in calculations. [ksi]
F_{yd}	Dynamic yield stress determined from tensile coupons. [ksi]
F_{ys}	Static yield stress determined from tensile coupons. [ksi]
$F_y(h)$	Yield stress estimate calculated from hardness measurements. [ksi]
$F_y(t)_{ave}$	Average of longitudinal and transverse yield stresses from tensile coupons.
F_u	Ultimate tensile stress of steel. Used in calculations. [ksi]
$F_u(h)$	Ultimate stress estimate determined from hardness measurements. [ksi]
$F_u(t)_{ave}$	Average of longitudinal and transverse ultimate stress from tensile coupons.
GL	Gage Length for tensile coupons and stub columns. [in.]
I	Moment of inertia. [in.^{4}]
I_e	Effective moment inertia of corroded tube cross section. [in.^{4}]
L	Length. [in. or ft as noted]
LVDT	Linear Voltage Displacement Transducer
OOS	Out-of-straightness of tube. [in.]
P	Axial load. [kips]
$P_{\ell b}$	Local buckling load. [kips]
P_{exp}	Ultimate axial load from experiment. [kips]
P_{FE}	Ultimate axial load calculated by finite element analysis. [kips]
P_y	Axial load causing yielding of whole cross section. (P_y=AF_y) [kips]
R	Radius [in.]
SC	Stub-column

SG	Strain gage
TC	Tensile coupon
SSRC	Structural Stability Research Council
$\mathbf{W}$	Matrix of weights.
W_E	Weight for south-east LVDT.
W_W	Weight for south-west LVDT.
W_N	Weight for west LVDT.
W_θ	Weight for rotation.
c	Distance from centroid to mid-thickness of thinnest side of tube.[in.]
d	Dent depth [in.]
$d_x(x)$	Dent depth as function of x.
e	End eccentricity; shift of centroid from the center of inside circle. [in.]
e_o	Calculated end eccentricity. [in.]
g	Acceleration of Gravity. [in./sec^2]
k	Stress amplification factor.(Ratio of maximum to average stress.)
ℓ_d	Length of dented portion of column. [in.]
r	Radius of gyration [in.]
s	Distance from center of inside circle to center of outside circle. [in.]
t	Tube thickness, actual. [in.]
t_{ave}	Average thickness of tube for corroded specimens. [in.]
t_{eq}	Calculated equivalent thickness of corroded cross section. [in.]
t_{max}	Maximum thickness of corroded tube cross section. [in.]
t_{min}	Minimum thickness of corroded tube cross section. [in.]
x	Distance along length of member.
y	Lateral deflection at corresponding x.
y'	Rotation (slope) at corresponding x.
y''	Curvature at corresponding x.
α	Parameter used in local buckling formulas.
Δ	Out-of-straightness measured at mid-length of specimen.
δ	Out-of-straightness at distance x.
γ	Unit weight of material.
ε	Strain
η	Non-dimensionalized lateral deflection; $[\eta=y/(D/2)]$
ν	Poisson's ratio
ξ	Distance non-dimensionalized with respect to length L. $[\xi=x/L]$ (Chapter 13)
	Parameter used in local buckling formulas. (Chapter 14)
ϕ	Angle measured around tube cross section. (radians)
ρ	Unit density of material.

TABLES

Spec.	End Con	Dm (in.)	t (in.)	L tube (ft.)	dent (in.)	End Ecc. (in.)	OOS (in.)	Dm/t	L/r	d/Dm	Area (in^2)	Fy (ksi)
1	2	3	4	5	6	7	8	9	10	11	12	13
P1P	Pin	15.00	0.260	35.35	0.71	0.75	-0.30	57.69	80.04	0.047	12.25	42.70
P1F	Fix	15.00	0.260	35.29	0.74		0.37	57.69	79.90	0.049	12.25	42.70
P1PS	Pin	3.94	0.060	9.42	0.20		0.00	65.67	81.11	0.051	0.743	38.54
P2P	Pin	17.03	0.375	34.85	2.37		0.66	45.41	69.47	0.139	20.06	57.13
P2F	Fix	17.01	0.375	34.79	2.31		0.94	45.36	69.35	0.136	20.04	57.13
P2PS	Pin	5.38	0.118	11.33	0.74		0.38	45.61	71.46	0.138	1.995	42.11
P3PA	Pin	24.50	0.321	34.35	1.26		0.02	76.32	47.60	0.052	24.71	59.30
P3PB	Pin	24.50	0.321	34.35	3.64		0.30	76.32	47.60	0.149	24.71	59.30
P4P	Pin	18.75	0.197	31.35	2.58		0.98	95.18	56.74	0.138	11.60	55.32
C1	Pin	10.31	0.314	24.50	N/A		0.09	32.83	80.55	N/A	10.17	40.89
D1	Pin	10.36	0.360	24.50	1.60		0.80	28.78	80.11	0.154	11.72	54.19
E1	Pin	10.38	0.375	24.50	1.40	0.90	1.00	27.67	80.11	0.135	12.23	53.27
S1	Pin	10.36	0.360	24.50	N/A		0.06	28.78	80.11	N/A	11.72	54.40
C2	Pin	13.54	0.415	23.10	N/A		0.06	32.63	57.87	N/A	17.65	40.72
S2	Pin	13.62	0.443	23.20	N/A		0.06	30.74	57.76	N/A	18.96	40.46
B3	Pin	13.57	0.434	28.00	0.73		3.75	31.27	70.00	0.054	18.50	40.50
D3	Pin	13.55	0.444	28.00	2.12		0.26	30.52	70.15	0.156	18.90	43.95
E3	Pin	13.59	0.439	28.00	1.82	2.20	0.59	30.96	69.85	0.134	18.74	40.50
S3	Pin	13.55	0.445	28.00	N/A		0.35	30.45	70.15	N/A	18.94	40.28
C4B	Pin	12.36	0.355	21.70	N/A		0.34	34.82	59.59	N/A	13.78	42.85

B3 - Fy: assumed to be Fy of E3
B3 - d: means ovalization at midspan over 3 Dia.
Dm - mid-thickness diameter

Table 1-1: Long Column Specimen Properties.

Perimeter (in.)	End 'A' thickness (in.)	End 'A' Ultrasonic (in.)	End 'B' thickness (in.)	End 'B' Ultrasonic (in.)
1	2	3	4	5
0	0.379	0.38	0.253	
2	0.372		0.273	
4	0.365		0.14	
6	0.364	0.36	0.115	0.12
8	0.378		0.153	
10	0.375		0.15	
12	0.356		0.18	0.19
14	0.358		0.222	
16	0.358		0.267	0.255
18	0.36		0.342	
20	0.364		0.363	0.36
22	0.334		0.366	
24	0.288		0.332	
26	0.278		0.302	
28	0.278		0.24	0.23
30	0.348		0.216	
32	0.368		0.246	
t ave =	0.348 in		0.245 in	
Area =	11.327 in^2		7.876 in^2	

Table 3-1: Specimen C1 – End Thickness Measurements

Perimeter (in.)	End 'A' thickness (in.)	End 'A' Ulrasonic (in.)	End 'B' thickness (in.)	End 'B' Ultrasonic (in.)
1	2	3	4	5
0	0.374		0.37	
2	0.375		0.373	
4	0.373		0.372	
6	0.373		0.37	
8	0.376		0.375	
10	0.375		0.373	
12	0.371		0.376	
14	0.376		0.375	
16	0.374		0.374	
18	0.372		0.373	
20	0.37		0.371	
22	0.373		0.375	
24	0.37		0.373	
26	0.372		0.375	
28	0.374		0.374	
30	0.375		0.373	
32	0.376		0.371	
t ave =	0.373	in	0.373	in
Area =	12.175	in^2	12.164	in^2

Table 3-2: Specimen E1 – End Thickness Measurements

Perimeter (in.)	End 'A' thickness (in.)	End 'A' Ulrasonic (in.)	End 'B' thickness (in.)	End 'B' Ultrasonic (in.)
1	2	3	4	5
0	0.369	0.371	0.369	
2	0.367		0.361	
4	0.367		0.369	
6	0.366	0.371	0.368	0.367
8	0.37		0.37	
10	0.367		0.372	
12	0.362		0.328	
14	0.363		0.308	
16	0.368		0.295	0.297
18	0.369		0.361	
20	0.369	0.367	0.371	
22	0.37		0.369	0.367
24	0.36	0.362	0.371	
26	0.366	0.367	0.371	
28	0.37		0.377	
30	0.364		0.368	
32	0.367		0.37	0.371
t ave =	0.367	in	0.359	in
Area =	11.962	in^2	11.710	in^2

Table 3-3: Specimen S1 – End Thickness Measurements

Perimeter (in.)	End 'A' thickness (in.)	End 'A' Ulrasonic (in.)	End 'B' thickness (in.)	End 'B' Ultrasonic (in.)
1	2	3	4	5
0	0.416	0.41	0.434	0.43
2	0.452	0.45	0.412	0.42
4	0.418	0.42	0.415	0.42
6	0.403	0.4	0.4	0.4
8	0.367	0.37	0.391	0.39
10	0.387	0.39	0.389	0.37
12	0.339	0.34	0.35	0.35
14	0.3	0.3	0.342	0.33
16	0.344	0.34	0.384	0.38
18	0.359	0.36	0.403	0.41
20	0.326	0.33	0.395	0.39
22	0.362	0.36	0.384	0.39
24	0.349	0.36	0.38	0.38
26	0.357	0.36	0.335	0.34
28	0.288	0.3	0.342	0.35
30	0.362	0.36	0.362	0.37
32	0.364	0.37	0.293	0.29
34	0.335	0.34	0.332	0.33
36	0.362	0.37	0.354	0.35
38	0.363	0.37	0.401	0.4
40	0.367	0.36	0.365	0.36
42	0.376	0.38	0.436	0.44
t ave =	0.363	in	0.377	in
Area =	15.384	in^2	15.984	in^2

Table 3-4: Specimen C2 – End Thickness Measurements

Perimeter (in.)	End 'A' thickness (in.)	End 'A' Ulrasonic (in.)	End 'B' thickness (in.)	End 'B' Ultrasonic (in.)
1	2	3	4	5
0	0.442	0.444	0.444	0.444
2	0.44	0.44	0.449	0.44
4	0.438	0.43	0.442	0.44
6	0.448	0.44	0.441	0.44
8	0.455	0.45	0.445	0.44
10	0.469	0.47	0.458	0.46
12	0.472	0.46	0.476	0.47
14	0.437	0.43	0.45	0.45
16	0.433	0.43	0.438	0.44
18	0.43	0.43	0.432	0.43
20	0.437	0.43	0.425	0.42
22	0.431	0.43	0.431	0.43
24	0.453	0.45	0.452	0.45
26	0.44	0.47	0.462	0.46
28	0.433	0.48	0.486	0.48
30	0.445	0.44	0.475	0.47
32	0.442	0.44	0.461	0.46
34	0.434	0.43	0.458	0.45
36	0.46	0.45	0.444	0.44
38	0.484	0.48	0.489	0.49
40	0.457	0.45	0.461	0.46
42	0.455	0.45	0.475	0.47
44	0.444	0.44	0.444	0.44
t ave =	0.447	in	0.454	in
Area =	19.113	in^2	19.399	in^2

Table 3-5: Specimen S2 – End Thickness Measurements

Perimeter (in.)	End 'A' thickness (in.)	End 'A' Ulrasonic (in.)	(1/4) pt Ult. (in.)	(1/2) pt Ult. (in.)	(3/4) pt Ult. (in.)	End 'B' thickness (in.)	End 'B' Ultrasonic (in.)
1	2	3	4	5	6	7	8
0	0.392	0.39	0.41	0.41	0.42	0.43	0.43
2	0.404	0.41	0.41	0.41	0.43	0.423	0.42
4	0.415	0.42	0.42	0.42	0.43	0.432	0.44
6	0.434	0.44	0.44	0.44	0.45	0.45	0.45
8	0.432	0.44	0.43	0.43	0.43	0.434	0.44
10	0.45	0.45	0.45	0.46	0.45	0.457	0.46
12	0.443	0.47	0.48	0.48	0.48	0.478	0.48
14	0.437	0.44	0.45	0.46	0.46	0.475	0.47
16	0.423	0.43	0.43	0.44	0.43	0.427	0.43
18	0.422	0.42	0.42	0.43	0.43	0.419	0.42
20	0.441	0.44	0.43	0.43	0.43	0.417	0.42
22	0.475	0.47	0.46	0.47	0.47	0.462	0.46
24	0.462	0.46	0.46	0.48	0.48	0.475	0.47
26	0.43	0.44	0.45	0.46	0.46	0.45	0.45
28	0.427	0.43	0.42	0.43	0.43	0.404	0.41
30	0.438	0.44	0.44	0.45	0.45	0.446	0.45
32	0.428	0.43	0.43	0.44	0.43	0.422	0.43
34	0.433	0.43	0.42	0.42	0.42	0.41	0.41
36	0.435	0.44	0.44	0.43	0.43	0.427	0.43
38	0.452	0.45	0.46	0.44	0.45	0.445	0.45
40	0.45	0.45	0.46	0.45	0.46	0.465	0.47
42	0.418	0.42	0.43	0.44	0.44	0.452	0.45
t ave =	0.434	in	0.438	0.442	0.444	0.441	in
Area =	18.565	in^2				18.865	in^2

Table 3-6: Specimen B3 – End Thickness Measurements

Perimeter (in.)	End 'A' thickness (in.)	End 'A' Ult. (in.)	End 'B' thickness (in.)	End 'B' Ult. (in.)
1	2	3	4	5
0	0.427	0.43	0.427	0.43
2	0.452	0.45	0.436	0.44
4	0.461	0.46	0.459	0.45
6	0.445	0.44	0.469	0.47
8	0.4	0.4	0.448	0.45
10	0.413	0.41	0.41	0.41
12	0.425	0.42	0.4	0.43
14	0.454	0.45	0.452	0.45
16	0.459	0.46	0.482	0.48
18	0.44	0.43	0.471	0.47
20	0.41	0.41	0.453	0.45
22	0.431	0.43	0.449	0.45
24	0.416	0.41	0.448	0.45
26	0.416	0.41	0.437	0.44
28	0.424	0.42	0.427	0.43
30	0.454	0.44	0.439	0.43
32	0.457	0.46	0.466	0.47
34	0.44	0.44	0.469	0.47
36	0.427	0.42	0.448	0.45
38	0.424	0.43	0.439	0.44
40	0.436	0.44	0.425	0.43
42	0.45	0.45	0.436	0.44
t ave =	0.435	in	0.445	in
Area =	18.603	in^2	19.034	in^2

Table 3-7: Specimen E3 – End Thickness Measurements

Perimeter (in.)	End 'A' thickness (in.)	End 'A' Ulrasonic (in.)	End 'B' thickness (in.)	End 'B' Ultrasonic (in.)
1	2	3	4	5
0	0.444	0.447	0.433	0.428
2	0.432		0.43	
4	0.431		0.41	0.4
6	0.455	0.451	0.463	
8	0.483	0.479	0.465	
10	0.452	0.453	0.441	0.437
12	0.434		0.439	
14	0.459		0.447	
16	0.444		0.441	
18	0.434		0.431	
20	0.432		0.436	
22	0.448		0.456	
24	0.469		0.469	
26	0.444		0.464	
28	0.426		0.444	
30	0.416	0.418	0.441	
32	0.43		0.44	0.437
34	0.442		0.447	0.442
36	0.427	0.423	0.44	
38	0.447		0.459	
40	0.476	0.475	0.471	
42	0.473		0.47	0.465
44	0.442		0.432	

t ave =	0.445	in	0.446	in
Area =	19.043	in^2	19.095	in^2

Table 3-8: Specimen S3 – End Thickness Measurements

Perimeter (in.)	End 'A' thickness (in.)	End 'A' Ulrasonic (in.)	End 'B' thickness (in.)	End 'B' Ultrasonic (in.)
1	2	3	4	5
0	0.397	0.4	0.364	0.37
2	0.391		0.361	
4	0.401	0.4	0.367	0.38
6	0.4		0.36	
8	0.33	0.33	0.374	0.37
10	0.373		0.376	
12	0.382	0.38	0.381	0.38
14	0.378		0.372	
16	0.384	0.38	0.369	0.37
18	0.382		0.373	
20	0.378		0.358	
22	0.377	0.38	0.351	0.37
24	0.372		0.361	
26	0.376		0.36	
28	0.372	0.37	0.358	0.37
30	0.372		0.363	
32	0.375	0.37	0.367	0.37
34	0.384		0.364	
36	0.379	0.38	0.375	
38	0.381		0.37	0.37
t ave =	0.379 in		0.366 in	
Area =	13.844 in^2		13.384 in^2	

Table 3-9: Specimen C4B – End Thickness Measurements

0 is the 0 datum.

To 270 Degree Datum, Distance in Inches.

Circum. Longitud	-1	1	3	5	7	9	11	13	15	17	19	21	23	25	27*	t ave	area
217	0.25	0.285	0.28	0.3	0.245	0.25	0.275	0.265	0.25	0.25	0.26	0.255	0.22	0.245	0.3	0.263	8.47
215	0.28	0.3	0.32	0.265	0.175	0.145	0.18	0.22	0.19	0.17	0.185	0.145	0.2	0.3	0.255	0.221	7.09
213	0.28	0.25	0.26	0.22	0.195	0.17	0.17	0.17	0.18	0.125	0.13	0.145	0.135	0.23	0.235	0.193	6.18
211	0.23	0.17	0.195	0.225	0.17	0.15	0.16	0.16	0.13	0.1	0.12	0.16	0.18	0.23	0.14	0.168	5.37
209	0.24	0.215	0.25	0.3	0.22	0.2	0.18	0.19	0.18	0.13	0.14	0.15	0.26	0.325	0.25	0.215	6.91
207	0.275	0.265	0.26	0.33	0.3	0.305	0.28	0.215	0.19	0.175	0.18	0.25	0.325	0.36	0.36	0.269	8.69
205	0.215	0.18	0.26	0.345	0.355	0.32	0.255	0.265	0.245	0.25	0.245	0.26	0.34	0.37	0.33	0.282	9.10
203	0.225	0.245	0.285	0.34	0.37	0.365	0.295	0.295	0.29	0.285	0.31	0.31	0.345		0.27	0.302	9.78

* note: column was installed with the 'B' end at the bottom

Table 3-10: Specimen C1 – Thickness Grid Measurements of Buckled Section

Table 3-11: Specimen C1 -- Thickness Grid Measurements for Area Near Hole

Near Hole

t ave other half = 0.3

0 is the 0 datum.

circum	-1	1	3	5	7	9	11	13	t ave	area
longit										
253	0.28	0.315	0.295	0.28	0.25	0.21	0.215	0.265	0.282	9.10
251	0.285	0.26	0.27	0.24	0.27	0.225	0.275	0.26	0.280	9.05
249	0.275	0.33	0.265	0.235	0.17	0.16	0.22	0.245	0.269	8.67
247	0.32	0.33	0.27	0.16	0.16	0.15	0.24	0.255	0.268	8.64
245	0.29	0.3	0.21	0.14	0.18	0.255	0.285	0.23	0.268	8.65
243	0.245	0.31	0.26	0.2	0.225	0.315	0.31	0.265	0.283	9.15

^ /\ — — — — to bot of col.

——————>

To 270 Degree Datum. Distance in inches.

Table 3-12: Specimen C2 -- Thickness Grid Measurements for Buckled Section

^ /\ —— to top of col

——> Toward 90 degree R.L. Dist. in Inches.

Circum.	6	8	10	12	14	16	18	20	22	24	26
Longitun											
269	0.455	0.435	0.39	0.355	0.285	0.27	0.27	0.305	0.36	0.4	
267	0.385	0.4	0.385	0.34	0.33	0.31	0.3	0.345	0.36	0.405	
265	0.345	0.35	0.36	0.355	0.3	0.31	0.29	0.305	0.315	0.365	0.36
263	0.32	0.32	0.275	0.3	0.25	0.15	0.27	0.285	0.33	0.335	0.26
261	0.345	0.34	0.335	0.33	0.3	0.275	0.27	0.29	0.32	0.325	0.275
259	0.36	0.37	0.345	0.375	0.32	0.28	0.27	0.32	0.36	0.32	0.295
257	0.365	0.35	0.355	0.39	0.335	0.3	0.3	0.32	0.395	0.39	0.34
255	0.355	0.325	0.35	0.395	0.395	0.31	0.34	0.355	0.36	0.36	0.33
253	0.395	0.385	0.385	0.42	0.395	0.345	0.34	0.34	0.32	0.295	0.31
251	0.42	0.4	0.36	0.39	0.4	0.34	0.33	0.325	0.29	0.275	0.295

t ave = 0.35 for other half

t ave	area
0.351	14.89
0.353	14.96
0.341	14.46
0.316	13.35
0.330	13.97
0.339	14.38
0.350	14.82
0.351	14.89
0.354	15.00
0.349	

Table 3-13: Specimen C4B – Thickness Grid Measurements for Buckled Section

0 is the 0 datum.

t ave = 0.36 for other half

——> Toward 90 Degree R.L. Dist. in inches.

Circum.	-12	-10	-8	-6	-4	-2	0	2	4	6	8	10	t ave	area
Longit.														
167	0.35	0.36	0.365	0.37	0.365	0.375	0.365	0.365	0.375	0.37	0.37	0.37	0.364	14.14
165	0.355	0.35	0.355	0.365	0.38	0.375	0.365	0.365	0.37	0.365	0.37	0.365	0.363	14.10
163	0.35	0.35	0.36	0.35	0.22	0.39	0.125	0.375	0.37	0.37	0.27	0.365	0.339	13.13
161	0.355	0.355	0.36	0.365	0.365	0.375	0.125	0.37	0.36	0.365	0.27	0.37	0.346	13.41
159	0.355	0.355	0.355	0.36	0.355	0.38	0.375	0.375	0.36	0.365	0.37	0.375	0.363	14.10
157	0.36	0.355	0.355	0.365	0.37	0.385	0.385	0.375	0.355	0.37	0.37	0.37	0.365	14.17

^ /\ — — — — to top of col

Specimen	Average Load Voltage	Standard Deviation of Voltage	Calculated Weight (lbs.)	Column Length (ft.)	Column Inside Dia. (in.)	Calculated Thickness (in.)	Average End Thickness (in.)
1	2	3	4	5	6	7	8
C1	3.545	2.6 %	834.0	24.50	10.00	0.309	0.314
S1	4.099	1.5 %	964.5	24.50	10.00	0.356	0.360
C2	5.46	.46 %	1307.9	23.10	13.13	0.392	0.415
C4B	4.27	.6 %	1019.8	21.70	12.00	0.356	0.355

Table 3-14: Comparison of Micrometer Thickness and Weighing Thickness

Specimen	Rockwell B Scale Hardness Readings	Average Hardness	Fu(h) (ksi)	Fy(h) (ksi)	Average Fy(h) (ksi)	Average Fy(t) (ksi)
1	2	3	4	5	6	7
C1	83 83 84	83.3	78.3	54.81		
	82 83 83	82.7	77.4	54.18	54.5	40.9
D1	84 87 87 86	86.0	83	58.1		
	86 85 87	86.0	83	58.1	58.1	54.2
E1C	87 86 87 85 85	86.0	83	58.1		
	84 87 87 87 86	86.2	83.4	58.38	58.2	53.3
E1S	86 85 86 88 88	86.6	84.2	58.94		
	87 86 87 87 87	86.8	84.6	59.22	59.1	57
S1	88 86 87	87.0	85	59.5		
	87 87 87	87.0	85	59.5	59.5	54.4
C2	78 78 78	78.0	70	49		
	78 79 78	78.3	70.3	49.21	49.1	40.72
S2	76 77 76	76.3	67.6	47.32		
	77 77 77	77.0	69	48.3	47.8	40.46

Table 4-1: Hardness – Salvaged Specimens in Series 1 and 2

Specimen	Rockwell B Scale Hardness Readings	Average Hardness	Fu(h) (ksi)	Fy(h) (ksi)	Average Fy(h) (ksi)	Average Fy(t) (ksi)
1	2	3	4	5	6	7
B3	75 78 78 79 80	78.0	70	49		
	74 76 76 78 80	76.8	68.6	48.02		
E3C	79 80 80 81 82	80.4	73.8	51.66		
	82 82 83 83 83	82.6	77.2	54.04	52.9	
E3S	78 79 77 80 83	79.4	71.8	50.26		
	82 84 80 81 83	82.0	76	53.2	51.7	40.5
S3	81 82 81	81.3	75.6	52.92	52.92	40.28
				0		
C4A	77 80 76 77 77	77.4	69.4	48.58		
	63 62 63	62.7	53.7	37.59		
C4B	64 64 65 67 67	65.4	55.4	38.78		
	69 70 74 74 77	72.8	63.8	44.66	41.7	42.8

Table 4-2: Hardness – Salvaged Specimens in Series 3 and 4

Specimen	Hardness Readings	Average Hardness	Fu(h) (ksi)	Fy(h) (ksi)	Average Fy(h) (ksi)	Fy(t)ave (ksi)
1	2	3	4		6	7
P1	74 75 76	75.0	66.5	46.55		
	71 72 72	71.7	62.7	43.89	45.2	42.0
P1S	68 66 66 61 65	65.2	55	27.92		
	65 67 68 62	65.5	56	28.71	28.3	38.54
P2	80 81 82	81.0	75	52.5		
	81 82 83	82.0	76	53.2	52.9	56.2
P2S	72 72 72 72	72.0	63	34.69		
	72 72 72	72.0	63	34.69	34.69	42.11
P3	88 89 88	88.3	87.6	61.32		
	83 84 87 86 83	84.6	80.2	56.14		
	87 87 87	87.0	85	59.5		
	82 84 87 84	84.3	79.6	55.72	58.2	59.2
P4	86 86 87	86.3	83.6	58.52		
	84 86 87	85.7	82.4	57.68		
	83 83 83	83.0	78	54.6	56.9	54.3

Table 4-3: Hardness - Fabricated Specimens.

Coupon	Fy (static) ksi	Fy (dynamic) ksi	Fu (static) ksi	Fu (dynamic) ksi	Percent Elongation	% Area Reduction
1	2	3	4	5	6	7
P1L	41.22	43.13	57.92	61.11	41.7	54.2
P1T	42.70	44.05	61.60	65.37	37.5	54.0
P1R	44.26	45.60	62.30	65.34	32.3	60.7
P1S	38.54	39.87	52.08	53.74	30.3	69.6
P2L	55.32	57.13	67.47	70.73	36.8	64.4
P2T	57.13	58.84	68.44	71.78	34.1	63.5
P2R	58.06	60.36	69.26	72.44	34.4	65.3
P2S	42.11	42.84	50.88	53.47	36.4	73.5
P3L	59.17	62.02	82.40	87.39	30.1	49.3
P3T	59.30	61.09	81.69	86.23	32.5	54.7
P3R	55.38	57.33	80.34	85.36	30.4	61.0
P4L	53.37	57.41	61.66	72.75	33.4	60.5
P4T	55.32	57.62	67.07	72.14	32.7	57.6
P4R	57.90	60.14	70.26	73.40	30.7	65.6
C1	40.89	42.37	62.66	69.45	32.3	50.5
D1	54.19	55.47	66.00	69.38	27.1	48.9
E1-C	53.27	55.39	65.97	68.57	25.6	51.2
E1-S	57.00	59.45	69.87	73.50	26.2	48.2
S1	54.40	55.79	67.35	70.43	27.0	49.0
C2	40.72	42.39	69.72	74.10	33.3	50.8
S2	40.46	41.85	66.48	69.63	32.2	47.1
D3	43.95	45.28	65.24	69.43	34.8	46.5
E3	40.50	42.37	69.87	73.37	38.2	50.6
S3	40.28	41.87	67.73	71.48	33.8	49.9
C4B	42.85	44.32	50.04	52.91	28.8	55.9

Table 4-4: Tensile Coupons - Average Properties

Coupon	Fy (static) ksi	Fy (dynamic) ksi	Fu (static) ksi	Fu (dynamic) ksi	Percent Elongation	% Area Reduction
1	2	3	4	5	6	7
C1-1	41.09	42.61	63.59	70.05	33.2	50.4
C1-2	40.69	42.13	61.73	68.85	31.3	50.5
D1-1	54.48	55.77	66.2	69.56	28.7	49.2
D1-2	53.9	55.17	65.8	69.2	25.5	48.5
E1-TC1	52.9	55.17	65.3	68	23.7	49.8
E1-TC2	54.1	56.1	67.2	69.7	27.9	51.1
E1-TC3	52.8	54.9	65.4	68	25.1	52.7
E1-TS1						
E1-TS2	56.6	59.4	69.4	73.32	25.9	48.9
E1-TS3	57.4	59.5	70.34	73.67	26.4	47.5
S1-1	54.4	55.62	67.7	70.38	26.5	46.6
S1-2	54.4	55.95	67	70.48	27.5	51.3
C2-1	40.89	42.39	70.5	74.3	35	51.7
C2-2	40.55	42.39	68.93	73.9	31.5	49.8
S2-1	40.46	42.03	66.88	69.19	31	44.7
S2-2	39.46	40.68	65.74	69.63	35.5	47.9
S2-3	41.45	42.85	66.83	70.08	30	48.8
D3-1	43.59	44.79	65.52	69.53	36	49.2
D3-2	44.3	45.76	64.95	69.33	33.6	43.7
E3-T1	40.8	43.2	70.3	73.7	38.1	50.4
E3-T2	40.5	42.6	69.6	73.4	39.5	49.8
E3-T3	40.2	41.3	69.7	73	36.9	51.5
S3-1	40.46	42.01	67.62	71.45	34.3	46.8
S3-2	40.1	41.73	67.83	71.51	33.2	52.9
C4B-1	43.8	45.06	52.37	55.63	29	51.4
C4B-2	41.89	43.58	47.7	50.18	28.5	60.4

Table 4-5: Tensile Coupons – Salvaged Specimens

Coupon	Fy (static) ksi	Fy (dynamic) ksi	Fu (static) ksi	Fu (dynamic) ksi	Percent Elongation	% Area Reduction
1	2	3	4	5	6	7
P1L-A	42.09	44.20	61.77	64.94	53.8	56.4
P1L-B	41.80	43.75	52.96	55.43	50.2	58.9
P1L-C	39.77	41.43	59.04	62.95	52.5	47.2
P1T-A	42.06	43.52	60.91	64.80	47.5	56.6
P1T-B	43.30	44.40	62.03	65.93	45.5	53.6
P1T-C	42.74	44.24	61.87	65.37	47.5	51.7
P1R-1	45.38	47.35	62.97	66.09	28.8	64.1
P1R-2	43.13	43.84	61.62	64.59	35.8	57.3
P1S-1	38.07	39.40	51.36	52.86	31.4	71.6
P1S-2	39.01	40.34	52.79	54.62	29.3	67.6
P2L-A	54.11	56.02	67.27	70.31	50.4	57.3
P2L-B	56.13	57.92	67.64	71.07	47.0	68.3
P2L-C	55.73	57.46	67.50	70.82	40.6	67.5
P2T-A	55.95	57.91	68.37	71.78	42.6	66.0
P2T-B	57.84	59.47	68.57	71.88	42.5	61.5
P2T-C	57.60	59.15	68.38	71.69	42.8	63.0
P2R-1	57.08	59.34	69.03	72.09	34.4	63.0
P2R-2	59.03	61.38	69.49	72.78	34.4	67.6
P2S-1	42.20	42.95	50.92	53.45	36.3	73.3
P2S-2	42.01	42.73	50.84	53.50	36.5	73.8
P3L-A	58.02	63.00	-	88.40	29.2	51.5
P3L-B	59.86	61.57	81.84	86.54	29.2	48.2
P3L-C	59.64	61.49	82.95	87.22	31.8	48.1
P3T-A	59.10	60.78	80.96	85.35	32.2	54.0
P3T-B	59.37	61.24	82.37	86.83	32.7	55.2
P3T-C	59.42	61.24	81.73	86.50	32.5	54.8
P3R-1	55.61	57.56	79.88	85.84	30.7	60.3
P3R-2	55.15	57.10	80.79	84.87	30.0	61.7
P4L-A	52.81	56.53	61.11	73.10	33.0	59.7
P4L-B	53.40	57.59	62.41	73.60	33.5	60.0
P4L-C	53.90	58.12	61.45	71.56	33.8	61.8
P4T-A	55.90	58.90	66.09	74.12	32.8	60.0
P4T-B	53.37	55.57	65.98	69.68	29.7	55.9
P4T-C	56.68	58.40	69.13	72.61	35.6	56.8
P4R-1	57.30	59.31	70.10	73.14	32.3	63.8
P4R-2	58.49	60.97	70.42	73.66	29.1	67.4

Table 4-6: Tensile Coupons - Fabricated Specimens

Rockwell B Hardness	Fu(h) (ksi)
1	2
83	78
82	76
81	75
80	73
79	71
78	70
77	69
76	67
74	66
73	64
72	63
71	62
70	60
69	59
68	58
67	57
66	56
65	55
64	54
62	53
61	52
60	51
59	50
57	49
56	48

Table 4-7: Rockwell Hardness (B Scale) Conversion Chart to Fu(h)

Tube	Average Hardness	Fu(h) ksi	Fu(t) ksi	Fy(t) ksi	Fy(t) /Fu(t)	Fy(t) /Fu(h)
1	2	3	4	5	6	7
P1	73.35	64.60	59.76	42.70	0.71	0.66
P1S	65.35	55.00	52.15	38.54	0.74	0.70
P2	81.50	75.50	67.96	57.13	0.84	0.76
P2S	72.00	63.00	50.89	42.11	0.83	0.67
P3	86.05	83.10	82.05	59.30	0.72	0.71
P4	85.00	81.33	64.40	55.32	0.86	0.68
C1	83.00	77.85	62.66	50.52	0.81	0.65
D1	86.00	83.00	66.00	54.18	0.82	0.65
E1C	86.10	83.20	65.90	53.27	0.81	0.64
E1S	86.70	84.40	69.80	57.00	0.82	0.68
S1	87.00	85.00	67.35	54.40	0.81	0.64
C2	78.20	70.00	69.72	40.72	0.58	0.58
S2	76.60	68.20	66.50	40.46	0.61	0.59
D3	82.20	76.40	65.24	43.95	0.67	0.58
E3S	70.70	75.50	65.40	40.50	0.62	0.54
S3	81.30	75.60	67.70	40.28	0.59	0.53
C4B	69.10	59.60	50.04	42.80	0.86	0.72

Fu(h) is the Hardness Estimated Ultimate Stress
Fu(t) is the Tensile Coupon Measured Ultimate Stress
Fy(t) is the Tensile Coupon Measured Yield Stress

Table 4-8: Comparison of Hardness and Tensile Coupon Properties

Specimen	Dm/t	Tensile Coupon Tests		Stub Column Tests			
		Fy(t) (static) ksi	Fu(t) (static) ksi	Fy(s) (static) ksi	Fy(s) (dynamic) ksi	Fu(s) (static) ksi	Fu(s) (dynamic ksi
1	2	3	4	5	6	7	8
P1-SC	57.7	42.7	61.6	38.3	39.2	42.1	43.2
P1S-SC	65.7	38.5	52.1	37.8	39.4	37.8	39.4
P2-SC	45.4	57.1	68.4	56.3	57.3	57.2	58.5
P2S-SC	45.6	42.1	50.9	40.6	42.1	44.5	46.3
P3-SC	76.3	59.3	81.7	55.8	57.0	56.3	57.4
P4-SC	95.2	55.3	67.1	48.1	49.5	48.1	49.5
E1-SC	27.7	57.0	69.9	50.0	51.3	59.5	60.6
S2-SC	30.7	40.5	66.5	40.1	41.2	54.1	55.3
E3-SC	31.0	40.5	69.9	40.7	41.8	55.9	58.0
C4B-SC	34.8	42.9	50.0	39.3	41.1	42.5	44.4

Dm : Mid-thickness diameter

Table 5-1: Summary of Stub Column and Tensile Coupon Properties

Spec.	End Con	D (in.)	t (in.)	L tube (ft.)	dent (in.)	End Ecc. (in.)	OOS (in.)	Fy (ksi)	P exp (kips)	P exp / Py
1	2	3	4	5	6	7	8	9	10	11
P1P	Pin	15.00	0.26	35.35	0.71	0.75	-0.30	42.7	328	0.627
P1F	Fix	15.00	0.26	35.29	0.74		0.37	42.7	415.5	0.794
P1S	Pin	3.94	0.06	9.42	0.2		0	38.5	23.3	0.814

Table 10-1: Specimens P1P, P1F, and P1PS
Comparison of Pin-Ended and Fixed-Ended Tests

Spec.	End Con	D (in.)	t (in.)	L tube (ft.)	dent (in.)	End Ecc. (in.)	OOS (in.)	Fy (ksi)	P exp (kips)	P exp / Py
1	2	3	4	5	6	7	8	9	10	11
P2P	Pin	17.03	0.375	34.85	2.37		0.66	57.1	516	0.450
P2F	Fix	17.01	0.375	34.79	2.31		0.94	57.1	768	0.671
P2S	Pin	5.38	0.118	11.33	0.74		0.375	42.11	43.4	0.517

Table 10-2: Specimens P2P, P2F, and P2PS
Comparison of Pin-Ended and Fixed-Ended Tests

Spec.	End Con	D (in.)	t (in.)	L tube (ft.)	dent (in.)	End Ecc. (in.)	OOS (in.)	Fy (ksi)	P exp (kips)	P exp / Py
1	2	3	4	5	6	7	8	9	10	11
P3PA	Pin	24.5	0.321	34.35	1.26		0.02	59.3	950	0.648
P3PB	Pin	24.5	0.321	34.35	3.64		0.30	59.3	620	0.423

Table 10-3: Specimens P3PA and P3PB
Comparison of Varied Dent Depth Tests

Spec.	End Con	D (in.)	t (in.)	L tube (ft.)	dent (in.)	End Ecc. (in.)	OOS (in.)	Fy (ksi)	P exp (kips)	P exp / Py
1	2	3	4	5	6	7	8	9	10	11
P4P	Pin	18.75	0.197	31.35	2.58		0.98	55.3	283	0.441

Table 10-4: Specimen P4P Test Results

Spec.	End Con	D (in.)	t (in.)	L tube (ft.)	dent (in.)	End Ecc. (in.)	OOS (in.)	Fy (ksi)	P exp (kips)	P exp / Py
1	2	3	4	5	6	7	8	9	10	11
C1	Pin	10.31	0.314	24.50	N/A		0.09	40.9	177	0.426
D1	Pin	10.36	0.36	24.50	1.60		0.80	54.2	188	0.296
E1	Pin	10.375	0.375	24.50	1.40	0.903	1.00	53.3	237	0.364
S1	Pin	10.36	0.36	24.50	N/A		0.06	54.4	459	0.720

Table 10-5: Comparison of Series 1 Specimens C1, D1, E1 and S1 Test Results

Spec.	End Con	D (in.)	t (in.)	L tube (ft.)	dent (in.)	End Ecc. (in.)	OOS (in.)	Fy (ksi)	P exp (kips)	P exp / Py
1	2	3	4	5	6	7	8	9	10	11
C2	Pin	13.54	0.415	23.10	N/A		0.06	40.7	556	0.773
S2	Pin	13.62	0.443	23.20	N/A		0.06	40.5	766	0.999

Table 10-6: Comparison of Series 2 Specimens C2 and S2 Test Results

Spec.	End Con	D (in.)	t (in.)	L tube (ft.)	dent (in.)	End Ecc. (in.)	OOS (in.)	Fy (ksi)	P exp (kips)	P exp / Py
1	2	3	4	5	6	7	8	9	10	11
B3	Pin	13.57	0.434	28.00	0.73		3.75	40.5	392	0.523
D3	Pin	13.55	0.444	28.00	2.12		0.26	44.0	444	0.535
E3	Pin	13.59	0.439	28.00	1.82	2.202	0.59	40.5	337	0.444
S3	Pin	13.55	0.445	28.00	N/A		0.35	40.3	690	0.904

Table 10-7: Comparison of Series 3 Specimens B3, D3, E3 and S3 Test Results

Spec.	End Con	D (in.)	t (in.)	L tube (ft.)	dent (in.)	End Ecc. (in.)	OOS (in.)	Fy (ksi)	P exp (kips)	P exp / Py
1	2	3	4	5	6	7	8	9	10	11
C4B	Pin	12.36	0.355	21.70	N/A		0.34	42.9	480	0.813

Table 10-8: Specimen C4B Test Results

Name	P1PS	IAI	P1P	P2PS	PIA	P2P
Reference	Lehigh	Taby-81	Lehigh	Lehigh	Smith-79	Lehigh
Scale	Small	Small	Large	Small	Small	Large
Dm (in.)	3.940	4.847	15.000	5.382	1.717	17.030
Thickness; t (in.)	0.060	0.080	0.260	0.118	0.038	0.375
Length; L (in.)	113.0	137.8	424.2	136.0	42.4	418.2
Area; A	0.743	1.223	12.252	1.995	0.204	20.063
r (in.)	1.393	1.714	5.304	1.903	0.607	6.022
L / r	81.110	80.401	79.976	71.456	69.850	69.440
Yield Stress (ksi)	38.54	29.58	42.70	42.11	51.33	57.13
Dent Depth; d (in.)	0.200	0.247	0.710	0.740	0.165	2.370
OOS (in.)	0.000	0.102	-0.300	0.380	0.081	0.660
Dent Type	SHARP	SHARP	SHARP	SHARP	SHARP	SHARP
Dm / t	65.667	60.348	57.692	45.610	45.417	45.413
L / Dm	28.680	28.430	28.280	25.269	24.702	24.557
d / Dm (%)	5.076	5.101	4.733	13.750	9.587	13.917
OOS / L (%)	0.000	0.074	-0.071	0.279	0.190	0.158
Pu / Py	0.814	0.666	0.611	0.517	0.635	0.450

Dm: Mid-thickness diameter (OD-t)

Table 10-9: Summary of Properties of Large Scale and Small Scale Specimens

Specimen Name	Length (ft)	Diameter (in.)	Yield Stress (ksi)	End Eccentr. (in.)	Dent Depth (in.)	Out-of-Str. (OOS) (in.)
P1P	35.35	15.000	42.700	0.600	0.710	-0.300
P1F	35.29	15.000	42.700	0.000	0.740	0.370
P1PS	9.42	3.940	38.540	0.000	0.200	0.000
P2P	34.85	17.030	57.130	-0.250	2.370	0.660
P2F	34.79	17.010	57.130	0.000	2.310	0.940
P2PS	11.33	5.380	42.110	0.000	0.740	0.380
P3PA	34.35	24.500	59.300	0.300	1.260	0.020
P3PB	34.35	24.500	59.300	-0.400	3.640	0.300
P4P	31.35	18.750	55.320	0.000	2.580	0.980
C1	24.50	10.310	40.890	-0.268	N/A	0.090
D1	24.50	10.360	54.190	0.500	1.600	0.800
E1	24.50	10.380	53.270	0.903	1.400	1.000
S1	24.50	10.360	54.400	0.074	N/A	0.060
C2	23.10	13.540	40.720	-0.121	N/A	0.060
S2	23.10	13.620	40.460	-0.003	N/A	0.060
B3	28.00	13.570	40.500	0.000	0.730	3.750
D3	28.00	13.550	43.950	0.094	2.120	0.260
E3	28.00	13.590	40.500	1.750	1.820	0.590
S3	28.00	13.550	40.280	0.349	N/A	0.350
C4B	21.70	12.360	42.850	0.060	N/A	0.340

Table 11-1: Data used in the Finite Element Models of the Test Specimens

Specimen Name	Py (kips)	Pexp (kips)	Pfe (kips)	Pexp/Py	Pfe/Py	Pfe/Pexp
P1P	522.0	328.0	339.0	0.628	0.649	1.034
P1F	523.0	415.0	427.0	0.793	0.816	1.029
P1PS	28.6	23.3	22.4	0.815	0.783	0.961
P2P	1145.0	516.0	490.0	0.451	0.428	0.950
P2F	1145.0	768.0	703.0	0.671	0.614	0.915
P2PS	84.0	43.4	35.8	0.517	0.426	0.825
P3PA	1464.0	950.0	984.0	0.649	0.672	1.036
P3PB	1464.0	620.0	620.0	0.423	0.423	1.000
P4P	651.0	283.0	227.0	0.435	0.349	0.802
C1	515.0	177.0	359.0	0.344	0.697	2.028
D1	635.0	188.0	221.0	0.296	0.348	1.176
E1	651.0	237.0	243.0	0.364	0.373	1.025
S1	637.0	459.0	451.0	0.721	0.708	0.983
C2	719.0	556.0	684.0	0.773	0.951	1.230
S2	766.0	766.0	734.0	1.000	0.958	0.958
B3	754.0	392.0	315.0	0.520	0.418	0.804
D3	830.0	444.0	418.0	0.535	0.504	0.941
E3	759.0	337.0	303.0	0.444	0.399	0.899
S3	763.0	690.0	555.0	0.904	0.727	0.804
C4B	605.0	480.0	496.0	0.793	0.820	1.033

Table 11-2: Comparison of the Ultimate Capacities from Finite Element Analysis and Tests

	Pu / Py					P analysis / P test			
SPECIMEN	TEST	DENTA	BCDENT	FE	WBK	DENTA	BCDENT	FE	WBK
P1P	0.627	0.581	0.621	0.648	0.616	0.927	0.991	1.034	0.983
P1F	0.794	0.777	0.737	0.817	0.821	0.978	0.928	1.029	1.034
P1PS	0.814	0.680	0.669	0.782	0.665	0.835	0.821	0.961	0.817
P2P	0.450	0.421	0.429	0.427	0.424	0.935	0.953	0.950	0.942
P2F	0.671	0.628	0.511	0.614	0.705	0.936	0.762	0.915	1.051
P2PS	0.517	0.407	0.426	0.426	0.452	0.788	0.816	0.825	0.875
P3PA	0.648	0.697	0.685	0.672	0.674	1.075	1.056	1.036	1.039
P3PB	0.423	0.453	0.382	0.423	0.482	1.070	0.903	1.000	1.139
P4P	0.441	0.403	0.323	0.354	0.419	0.914	0.733	0.802	0.950
C1	0.426	0.810	0.754	0.863	-	1.903	1.772	2.028	-
D1	0.296	0.365	0.420	0.348	0.356	1.233	1.418	1.176	1.202
E1	0.364	0.345	0.310	0.373	0.376	0.948	0.852	1.025	1.033
S1	0.720	0.820	0.742	0.708	-	1.139	1.030	0.983	-
C2	0.773	0.980	0.968	0.952	-	1.267	1.251	1.230	-
S2	0.999	0.983	0.973	0.957	-	0.984	0.974	0.958	-
B3	0.523	0.484	0.435	0.420	-	0.925	0.832	0.804	-
D3	0.535	0.466	0.538	0.503	0.521	0.872	1.007	0.941	0.975
E3	0.444	0.322	0.363	0.399	0.513	0.725	0.818	0.899	1.156
S3	0.904	0.865	0.812	0.727	-	0.957	0.898	0.804	-
C4B	0.813	0.886	0.856	0.840	-	1.090	1.053	1.033	-
ALL SPECIMENS					Average	0.963	0.936	0.954	1.015
(C1 and C2 are excluded)*					Std. Dev.	0.121	0.152	0.098	0.105
DENTED SPECIMENS					Average	0.941	0.927	0.969	1.015
					Std. Dev.	0.127	0.170	0.095	0.105
FABRICATED SPECIMENS					Average	0.977	0.904	0.966	1.020
(P-series with P1PS and P2PS excluded)**					Std. Dev.	0.064	0.109	0.080	0.063

* Specimens C1 and C2 are excluded because they cannot be properly analyzed by the methods used.

** Specimens P1PS and P2PS are small-scale manufactured specimens, not fabricated.

Table 12-1: Comparison of Ultimate Loads from Tests and Computer Programs

	Pu / Py				P analysis / P test		
SPECIMEN	TEST	ELLINAS	LOH	AISC	ELLINAS	LOH	AISC
P1P	0.627	0.479	0.615	0.761	0.764	0.981	1.214
P1F	0.794	--	0.688	0.940	--	0.866	1.184
P1PS	0.814	0.462	0.563	0.779	0.567	0.821	0.956
P2P	0.450	0.333	0.361	0.759	0.740	0.801	1.686
P2F	0.671	--	0.485	0.940	--	0.723	1.401
P2PS	0.517	0.350	0.423	0.812	0.678	0.816	1.572
P3PA	0.648	0.537	0.590	0.883	0.829	0.909	1.361
P3PB	0.423	0.351	0.378	0.883	0.830	0.893	2.086
P4P	0.441	0.348	0.296	0.844	0.789	0.672	1.915
C1	0.426	0.702	1.094	0.768	1.650	2.572	1.805
D1	0.296	0.314	0.301	0.696	1.061	1.016	2.351
E1	0.364	0.339	0.290	0.701	0.931	0.798	1.928
S1	0.720	0.602	0.622	0.695	0.836	0.864	0.965
C2	0.773	0.860	0.903	0.881	1.112	1.167	1.139
S2	0.999	0.861	0.867	0.882	0.862	0.868	0.883
B3	0.523	0.545	0.368	0.827	1.042	0.704	1.580
D3	0.535	0.345	0.487	0.811	0.645	0.911	1.517
E3	0.444	0.381	0.342	0.827	0.859	0.770	1.864
S3	0.904	0.787	0.661	0.827	0.871	0.731	0.914
C4B	0.813	0.842	0.757	0.867	1.036	0.932	1.067
ALL SPECIMENS				Average	0.834	0.838	1.469
(C1 and C2 are excluded)*				Std. Dev.	0.136	0.093	0.427
DENTED SPECIMENS				Average	0.790	0.844	1.618
				Std. Dev.	0.131	0.094	0.384
FABRICATED SPECIMENS				Average	0.790	0.835	1.550
(P-series with P1PS and P2PS excluded)**				Std. Dev.	0.035	0.101	0.326

* Specimens C1 and C2 are excluded because they cannot be properly analyzed by the methods used.

** Specimens P1PS and P2PS are small-scale manufactured specimens, not fabricated.

Table 12-2: Comparison of Ultimate Loads from Tests and Manual Methods

Device Name	Type	Weight	x (in.)	Value	Units
Gage 01	Strain Gage	0.999164	13.25	-625.354	in/in * 10^{-6}
Gage 02	Strain Gage	0.999999	13.25	-668.554	in/in * 10^{-6}
Gage 03	Strain Gage	0.999330	13.25	-540.280	in/in * 10^{-6}
Gage 04	Strain Gage	0.999767	13.25	-700.312	in/in * 10^{-6}
Gage 11	Strain Gage	0.999172	69.7	-805.459	in/in * 10^{-6}
Gage 12	Strain Gage	0.999748	69.7	-649.428	in/in * 10^{-6}
Gage 13	Strain Gage	0.999963	69.7	-501.214	in/in * 10^{-6}
Gage 14	Strain Gage	0.999439	69.7	-620.898	in/in * 10^{-6}
Gage 21	Strain Gage	0.998997	139.4	-857.463	in/in * 10^{-6}
Gage 22	Strain Gage	0.999981	139.4	-616.057	in/in * 10^{-6}
Gage 23	Strain Gage	0.999999	139.4	-405.386	in/in * 10^{-6}
Gage 24	Strain Gage	0.999869	139.4	-590.341	in/in * 10^{-6}
L03	LVDT	0.993486	0	0.042381	inches
L13	LVDT	0.990355	69.7	0.424657	inches
L23	LVDT	0.993212	139.4	0.770341	inches
Rot.Bottom	Rotation	0.992469	0	0.312744	degrees

Table 13-1: Sample Data from Long Column Test
P2P at static load of P=395.594 kips

Specimen Name	Length (ft)	Diameter (in.)	Design End Eccentricity (in.)	Computed Eccentricity (in.)	Deviation from Design (% of Dia)
P1P	35.35	15.00	0.75	+0.564	-1.24
P2P	34.85	17.03	--	+0.215	+1.52
P3PA	34.35	24.50	--	+0.259	+1.06
P3PB	34.35	24.50	--	-0.153	-0.62
P4P	31.35	18.75	--	+0.057	+0.30
D1	24.50	10.36	--	0.500	+4.83
E1	24.50	10.38	0.903	+0.795	-1.04
B3	28.00	13.57	--	+0.025	+0.18
D3	28.00	13.55	--	+0.094	+0.69
E3	28.00	13.59	2.202	+1.737	-3.42

Table 13-2: Computed End Eccentricities for Pinned Long Columns Specimens using Cylindrical Bearings

Specimen Name	Length (ft)	Diameter (in.)	Design End Eccentricity (in.)	Computed Eccentricity (in.)	Deviation from Design (% of Dia)
C1	24.50	10.31	--	-0.268	-2.60
S1	24.50	10.36	--	+0.074	+0.71
C2	23.10	13.54	--	-0.121	-0.89
S2	23.20	13.62	--	-0.003	-0.02
S3	28.00	13.55	--	+0.349	+2.58
C4B	21.70	12.36	--	0.060	+0.49

Table 13-3: Computed End Eccentricities for Pinned Lomg Column Specimens using Spherical Bearings

	Specimens	
	C1	C2
D_i [in.]=	10.00	13.125
t_{min}[in.]=	0.10	0.15
F_y[ksi]=	40.89	40.72
E[ksi]=	29,500	29,500
D_o/t_{min}=	102	89.5
D_m/t_{min}=	101	88.5
α =	7.073	8.095
ξ =	0.0888	0.10148

Source [Refs]	Formula for $\frac{F_{cr}}{F_y}$	C1	C2
API [3]	$1.64 - 0.23\sqrt[4]{\frac{D_o}{t}}$	0.909066	0.93257
DNV [5,8]	$1 - \frac{1}{3}\left(\frac{1.5 + 0.001(D_o/t)}{\alpha}\right)^2$	0.9829	0.987147
AISI [2,16]	$0.667 + 0.037\,\alpha$	0.925287	0.962878
SSRC [16]	$0.610 + 0.043\,\alpha$	0.870287	0.907878
AO [8,16]	1.0 or $38\,\xi - 480\,\xi^2 + 2020\,\xi^3$	1.000	1.000

where D_i = Inside diameter.

D_o = Outside diameter.

D_m = D = Mid-thickness diameter.

F_{cr} = Local buckling stress.

F_y = Yield stress.

$$\alpha = \frac{1}{(D_o/t)}\frac{E}{F_y} \qquad \xi = \frac{1}{(D_m/t)}\sqrt[3]{\frac{E}{F_y}}$$

Table 14.1: Local Buckling Stress According to Design Formulas

FIGURES

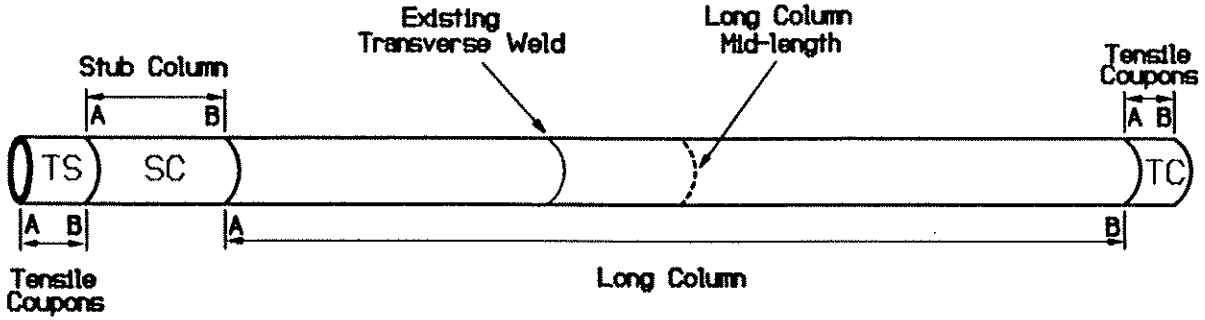

	Long Column						
			Transverse Weld		Length Of Long Column		
	TS	SC	(Yes/No)	From Mid-length		Condition	TC
C1	None	None	No		24'- 6"	Corroded	14"
D1	15"	None	Yes	6' - 0"	24'- 6"	Good Condition	None
E1	15"	42"	Yes	4' - 7"	24'- 6"	Good Condition	14"
S1	None	None	No		24'- 6"	Good Condition	14"
C2	None	None	Yes	2' - 6"	23'- 2.5"	Corroded	11"
S2	15"	42"	No		24'- 6"	Good Condition	None
B3	None	None	No		28'- 0"	Bent	None
D3	15"	None	No		28'- 0"	Good Condition	None
E3	11"	42"	Yes	4' - 1"	28'- 0"	Good Condition	None
S3	14"	None	No		28'- 0"	Good Condition	None
C4B	12"	36"	Yes	2' - 0"	21'- 8.5"	Corroded	None

Figure 2-1: Layout of Salvaged Specimens

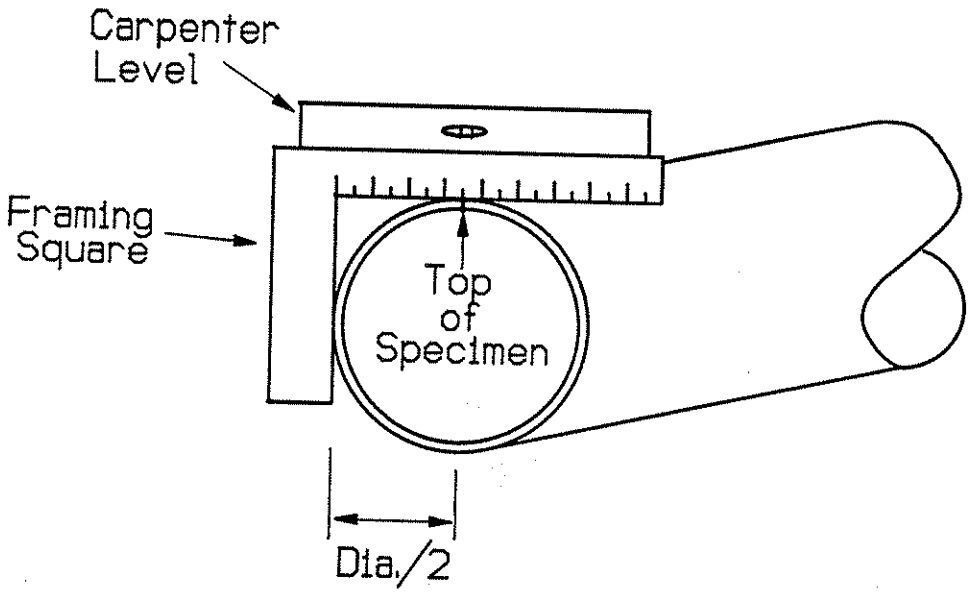

Figure 2-2: Determination of the 'Top' of the Specimens

Figure 2-3: Scheme for Labeling Reference Reference Lines

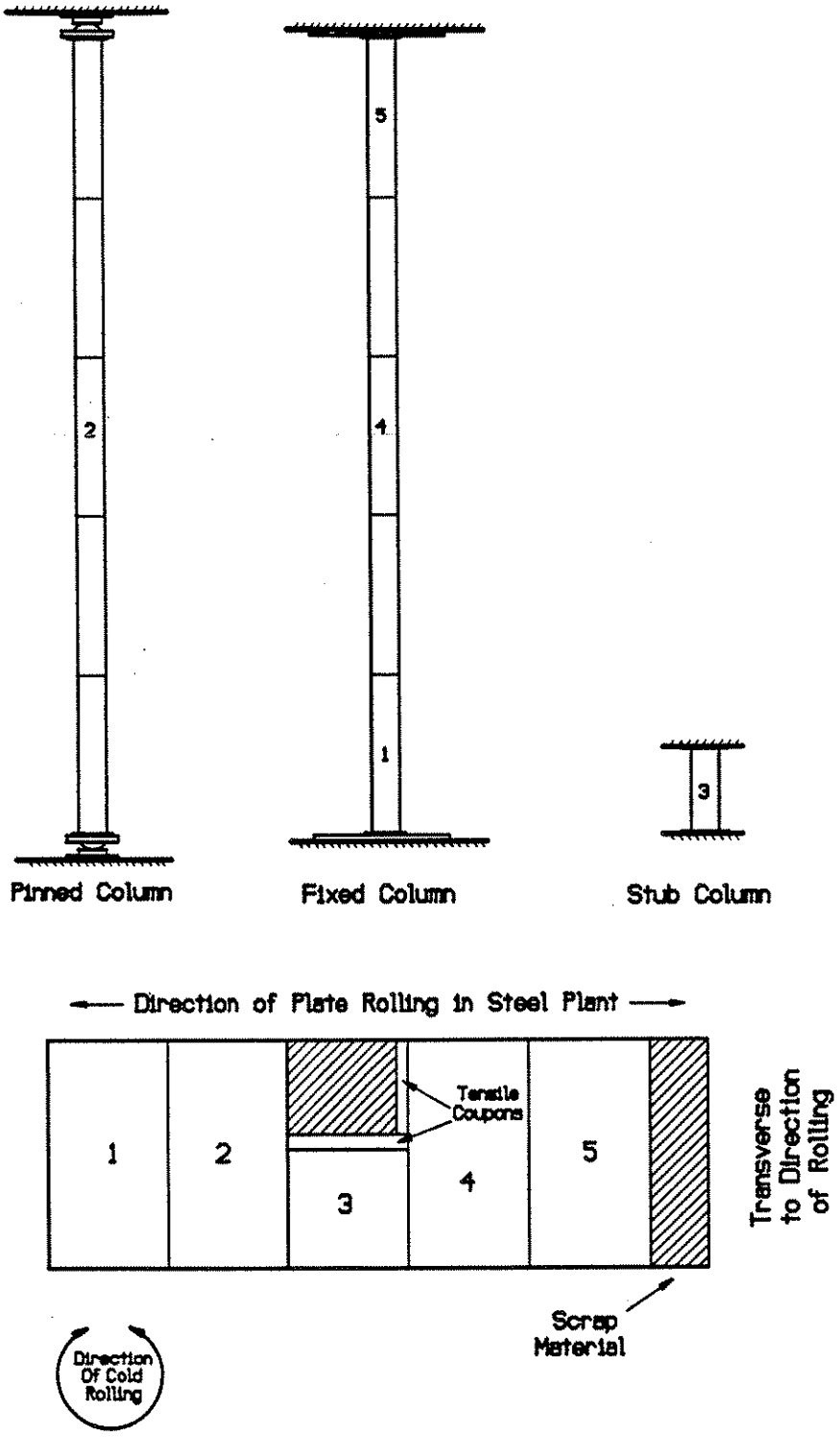

Figure 2-4: Layout of Steel Plate for Fabricated Specimens

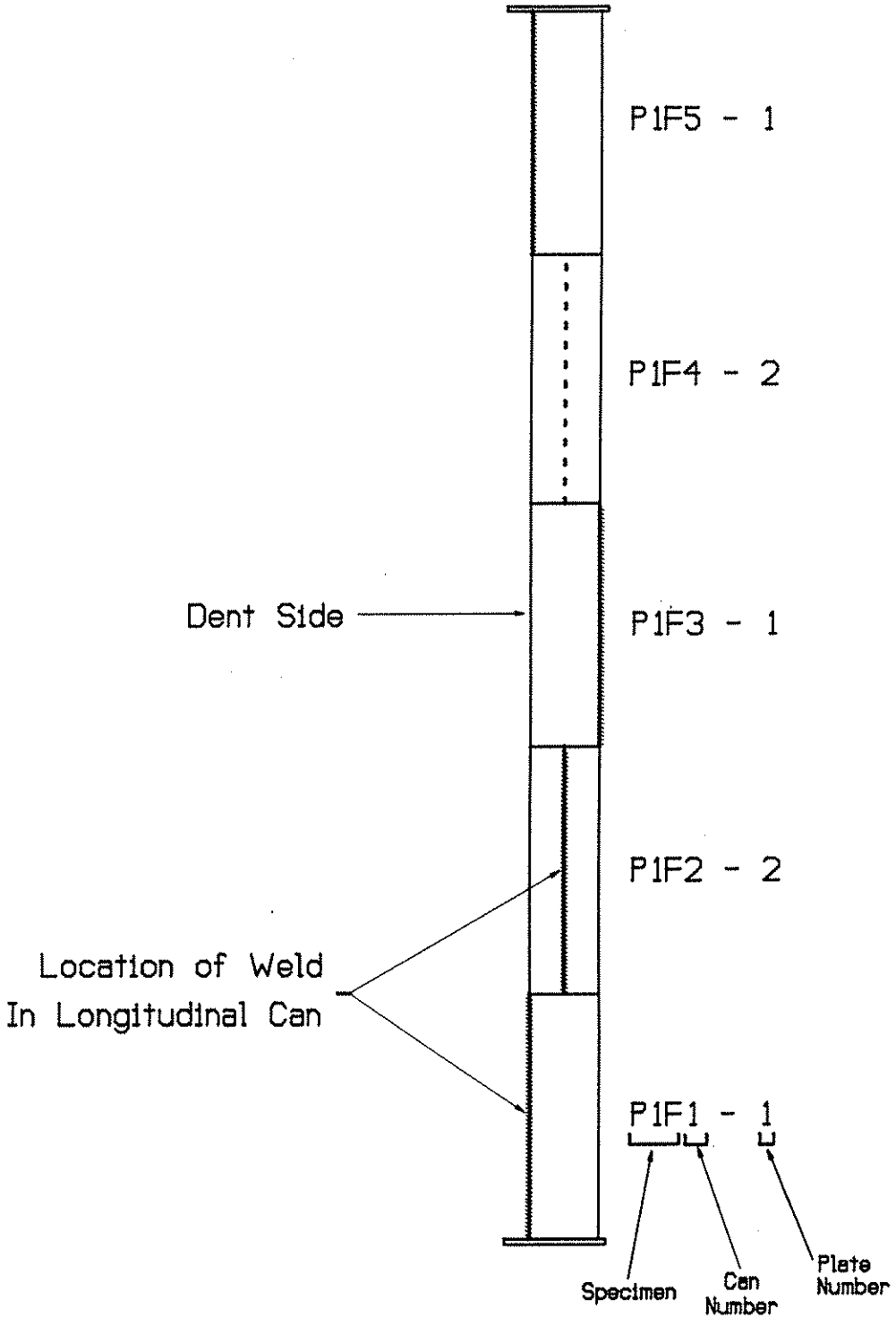

Figure 2-5: Layout of Cans and Longitudinal Welds for Fabricated Specimens

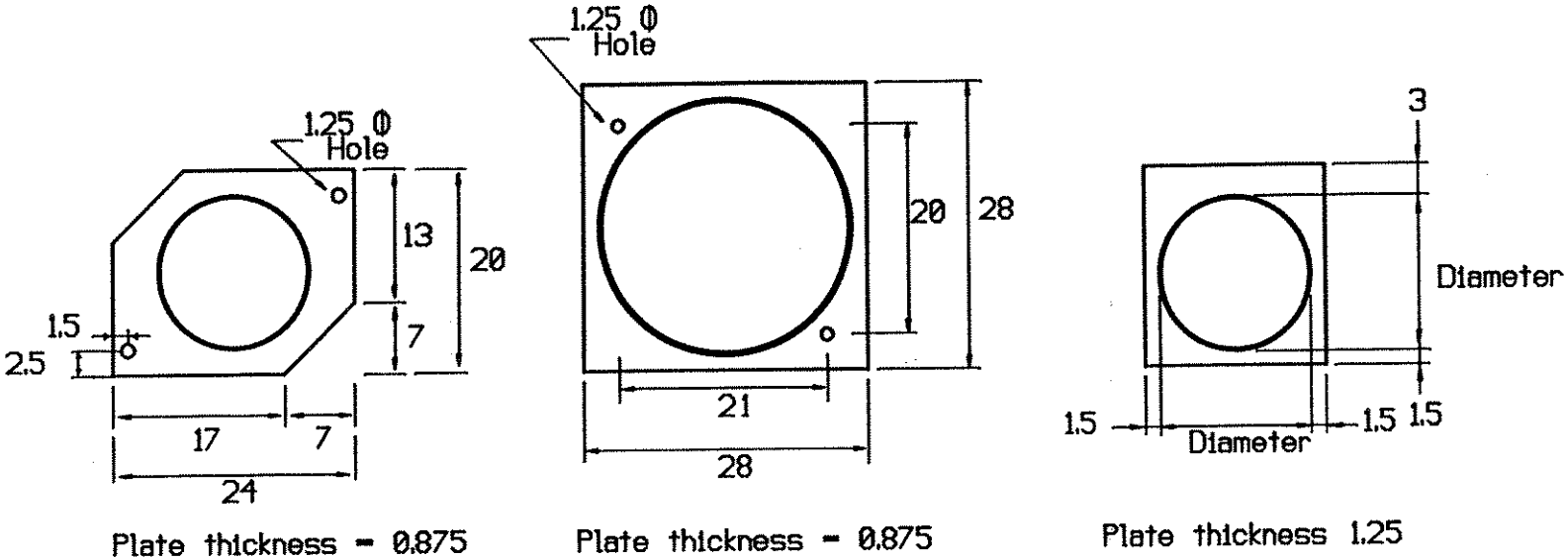

Figure 2-6: Dimensions of End Plates for Long-Column Specimens

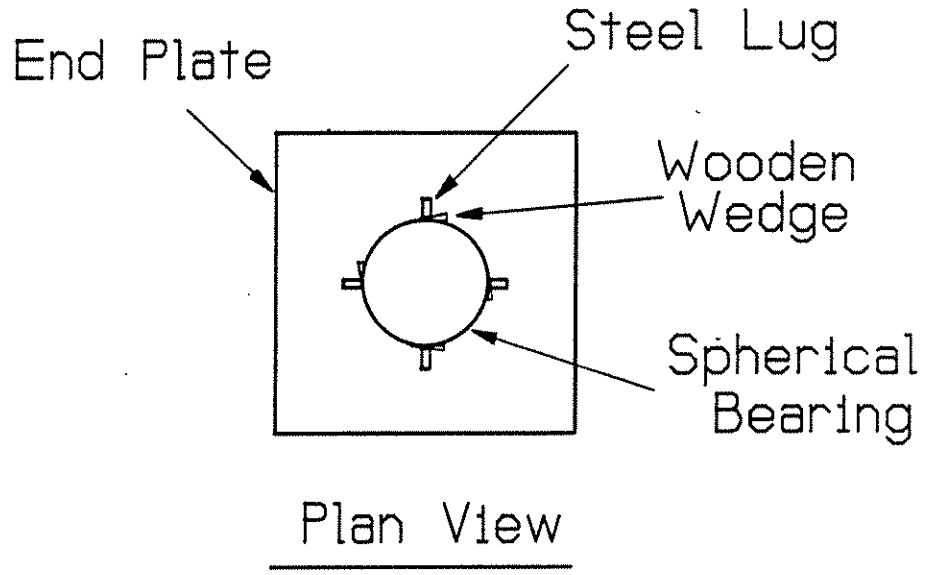

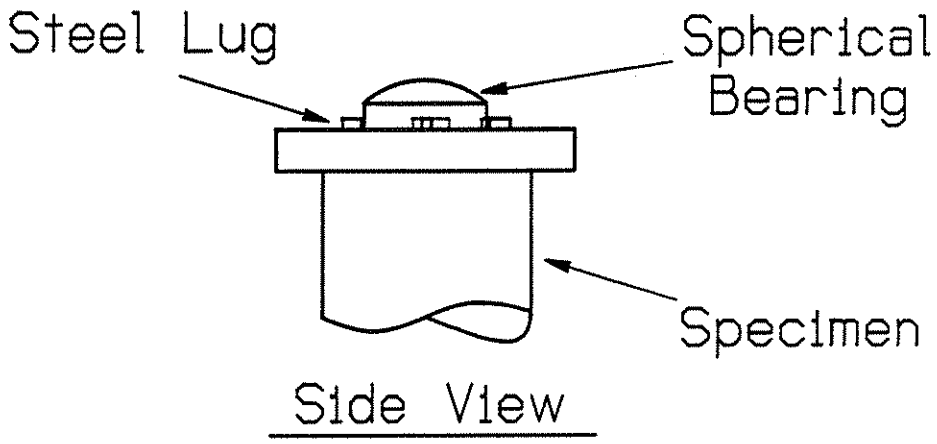

Figure 2-7: End Plates for Spherical Bearings of Long-Column Specimens

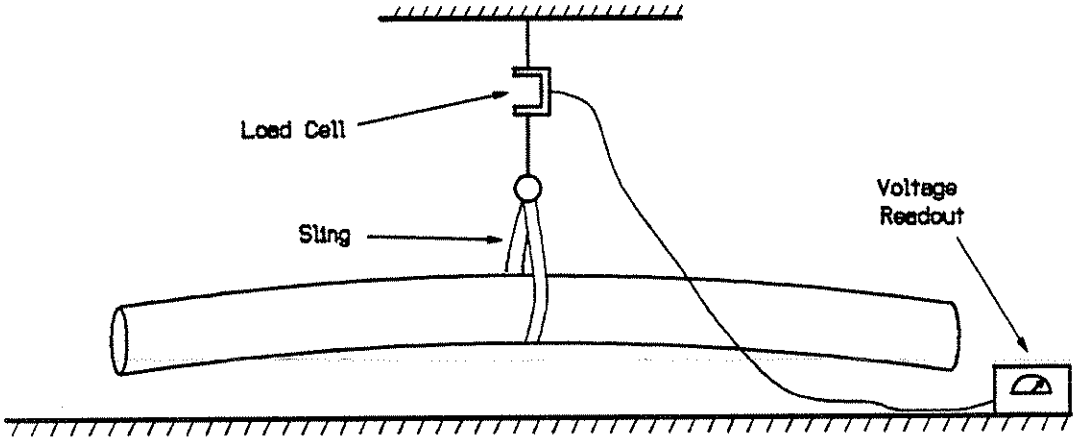

Figure 3-1: Weighing Method for Corroded Salvaged Specimens

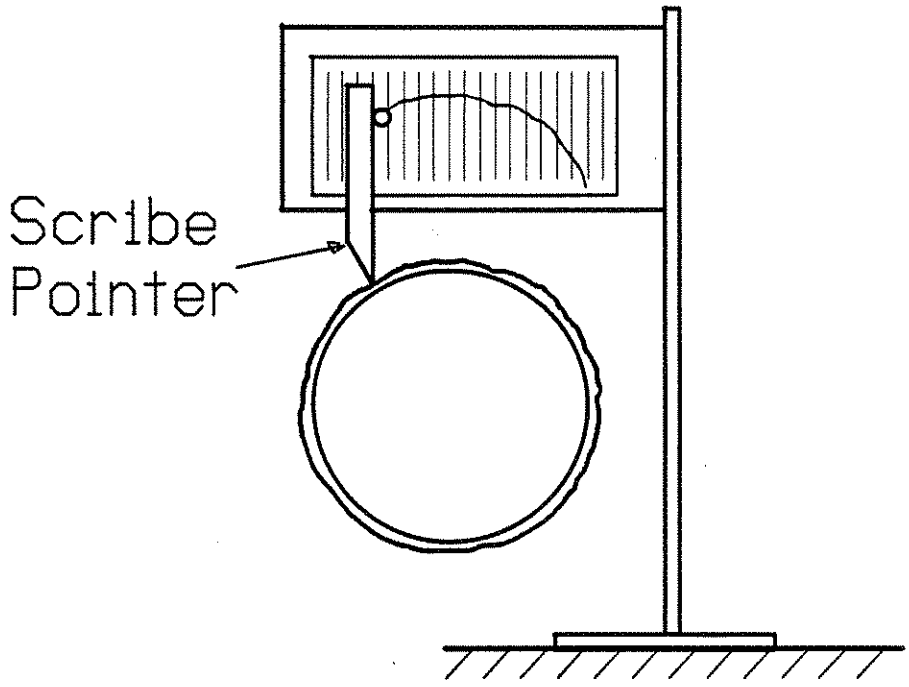

Figure 3-2: Scribing Method for Corroded Specimens

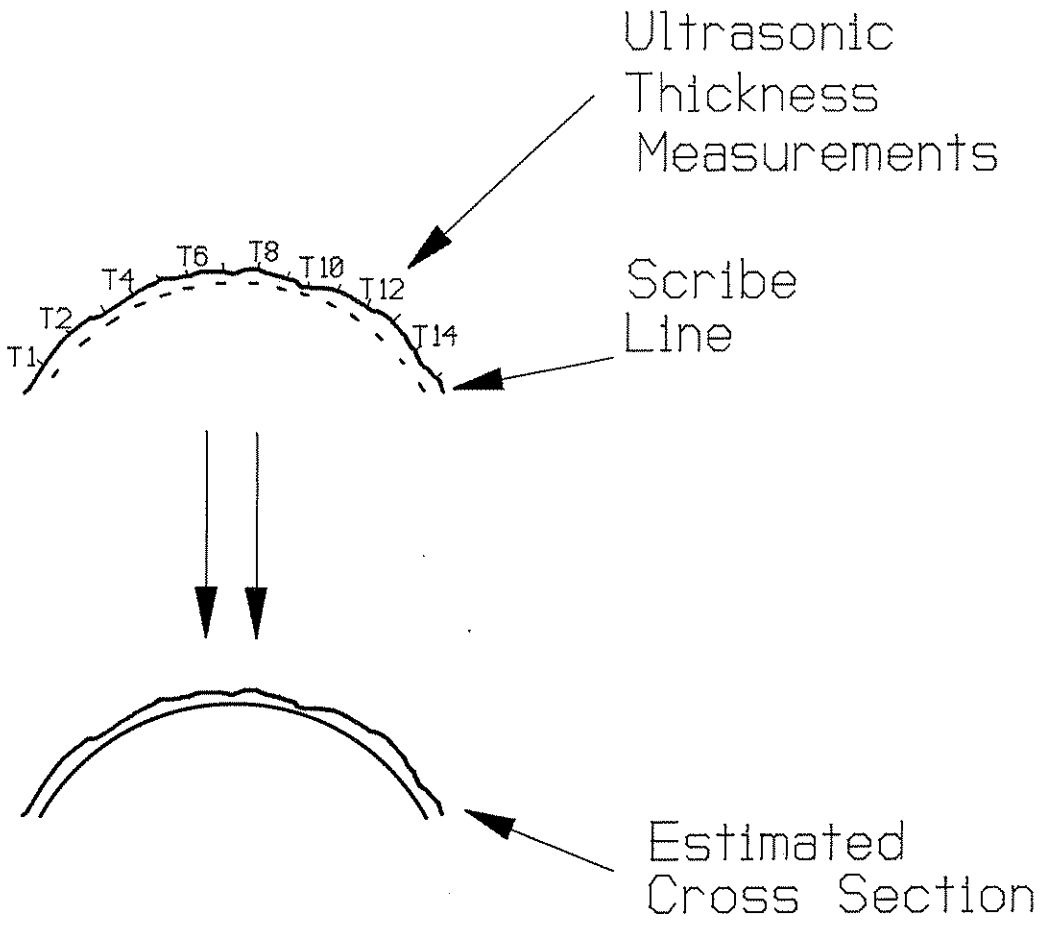

Figure 3-3: Cross Section Measurement by Using the Scribe and Ultrasound Measurements

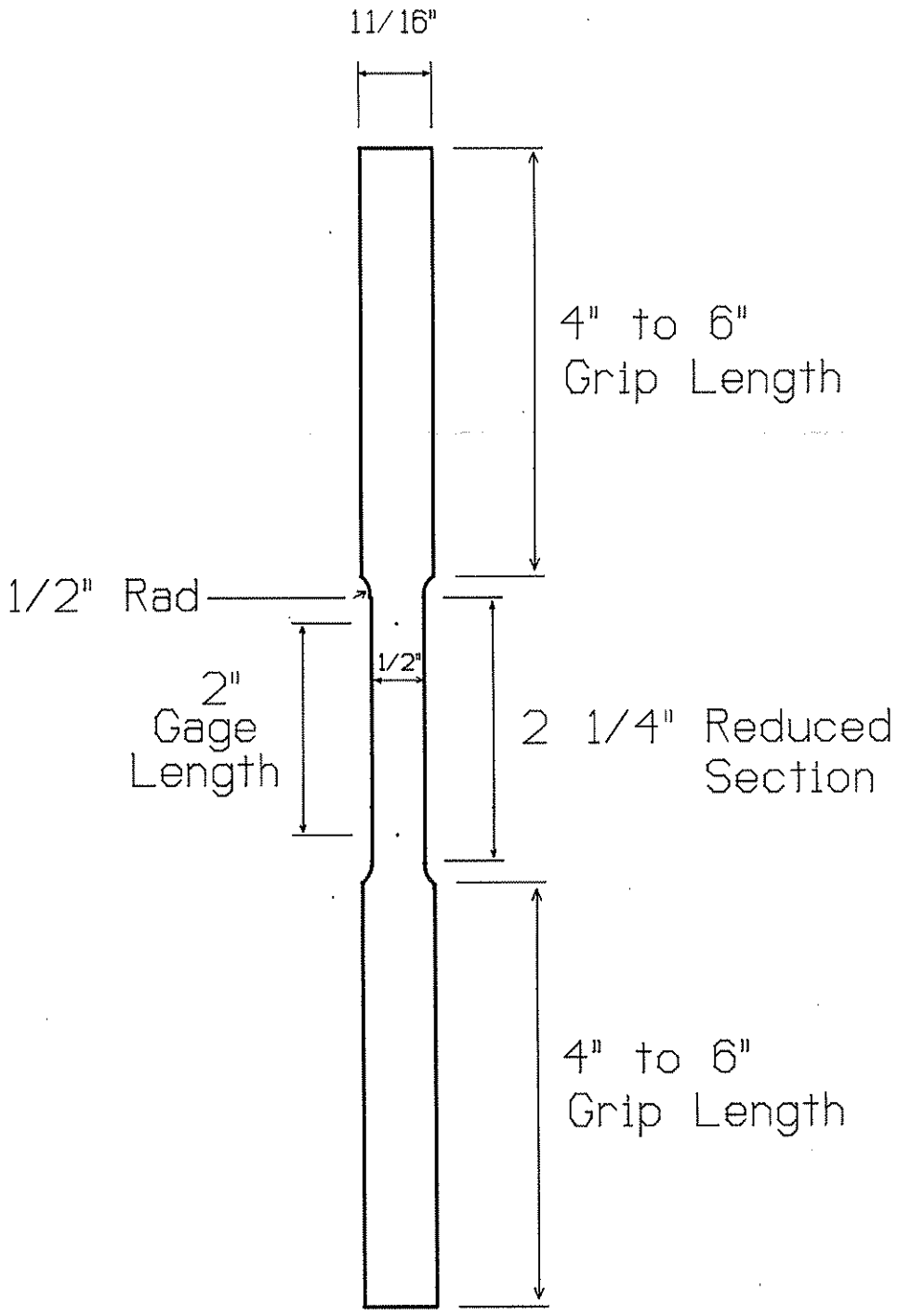

Figure 4-1: Tensile Coupon

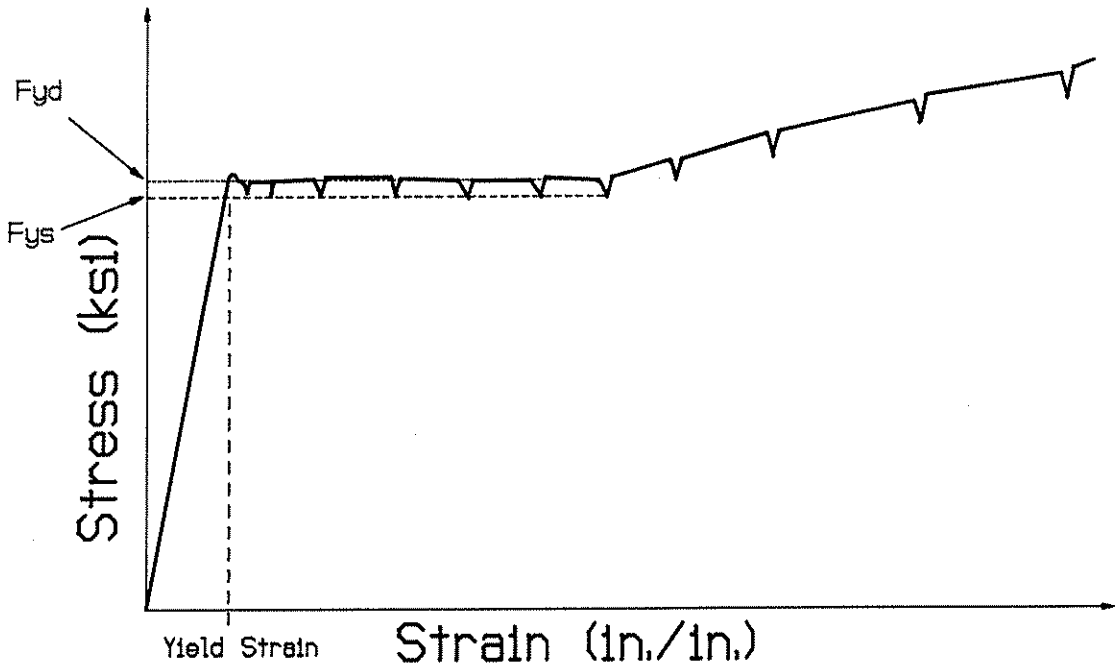

Figure 4-2: Typical Stress-Strain Diagram of Tensile Coupons

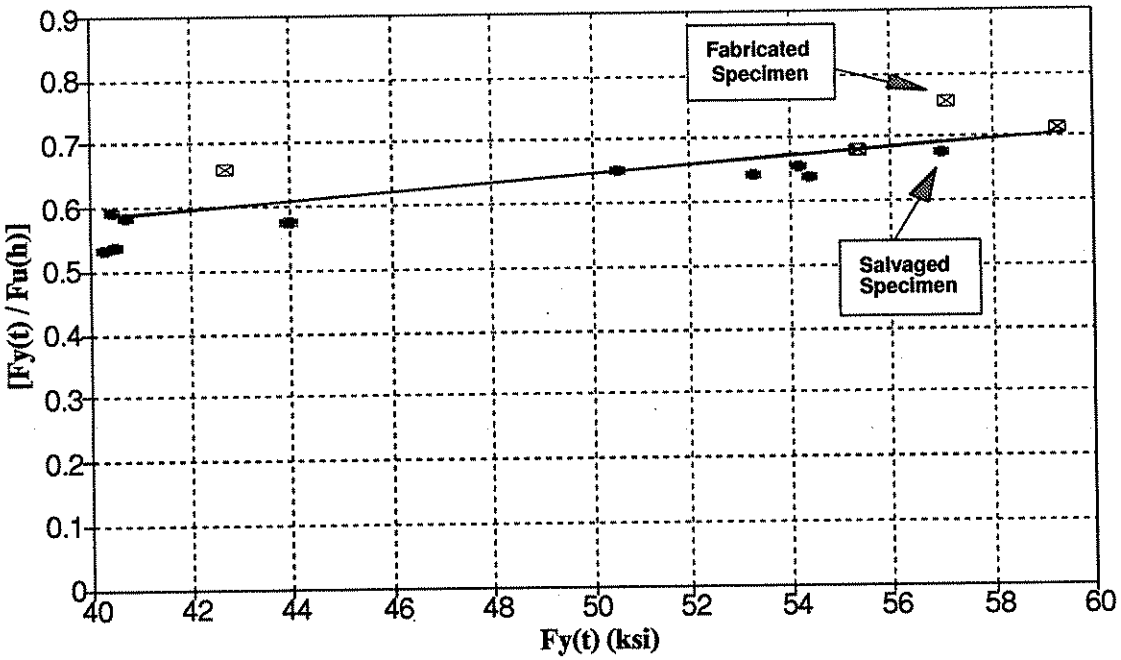

Figure 4-3: Relationship of Ultimate Stresses Estimated From Hardness Readings and Tensile Coupons

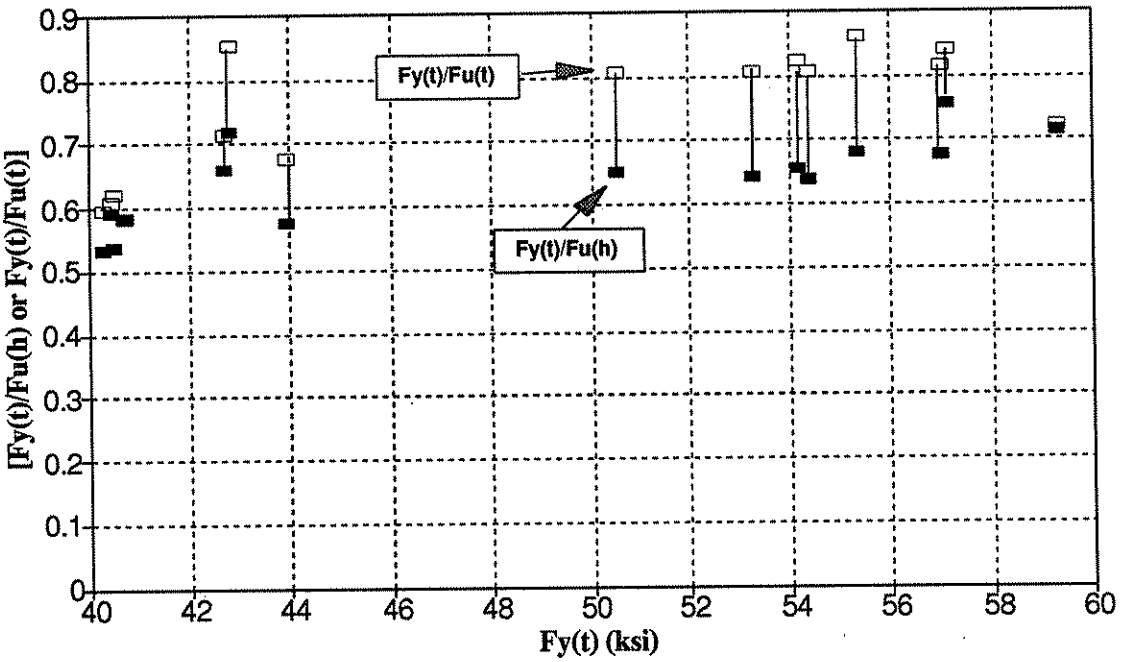

Figure 4-4: Ratio of Tensile Yield Stress to Hardness Estimated Ultimate Stress and to Tensile Ultimate Stress vs. Tensile Yield Stress

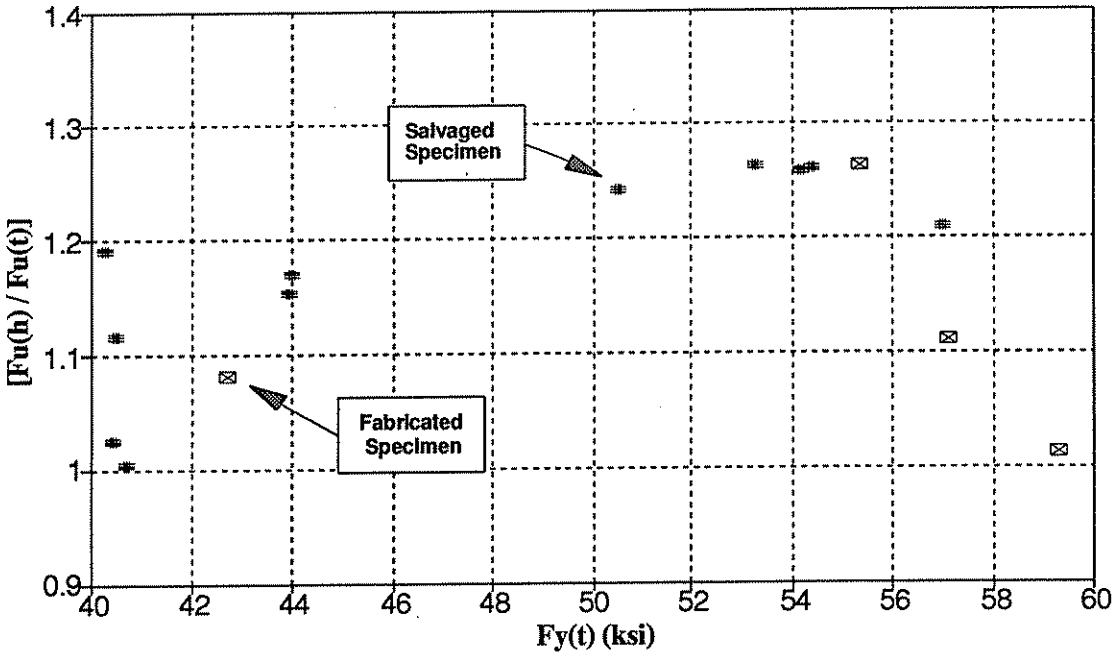

Figure 4-5: Ratio of Hardness Ultimate Stress to Tensile Ultimate Stress vs. Tensile Yield Stress

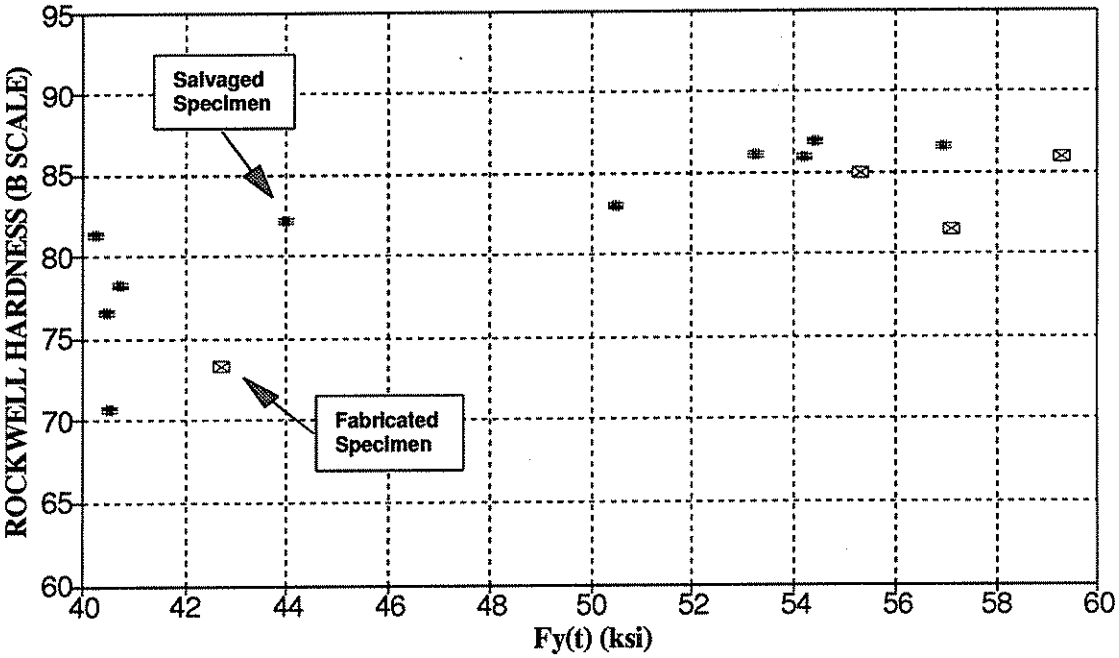

Figure 4-6: Rockwell Hardness (B Scale) Readings vs. Tensile Yield Stress

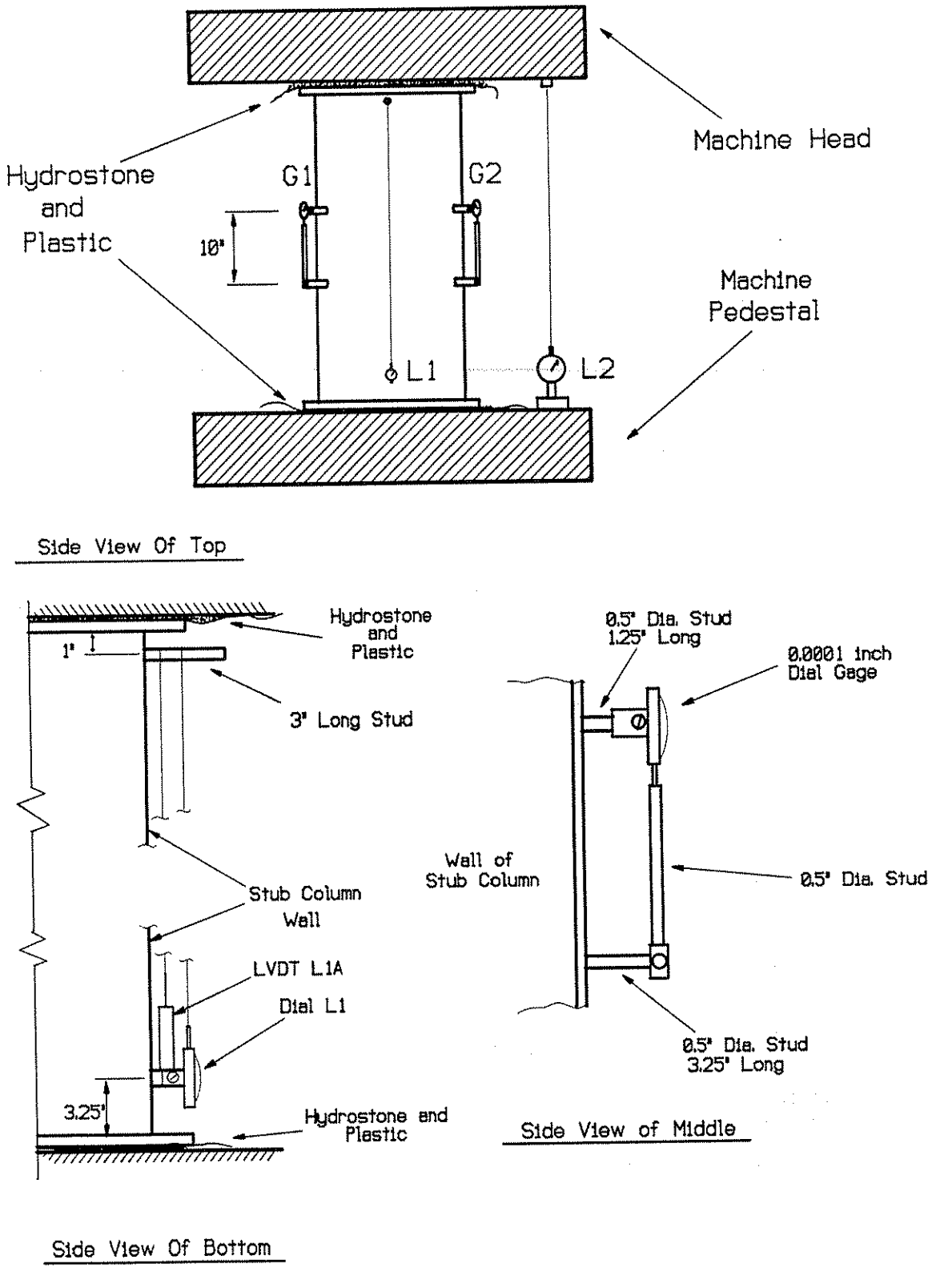

Figure 5-1: Setup of Stub Columns with Two End Plates

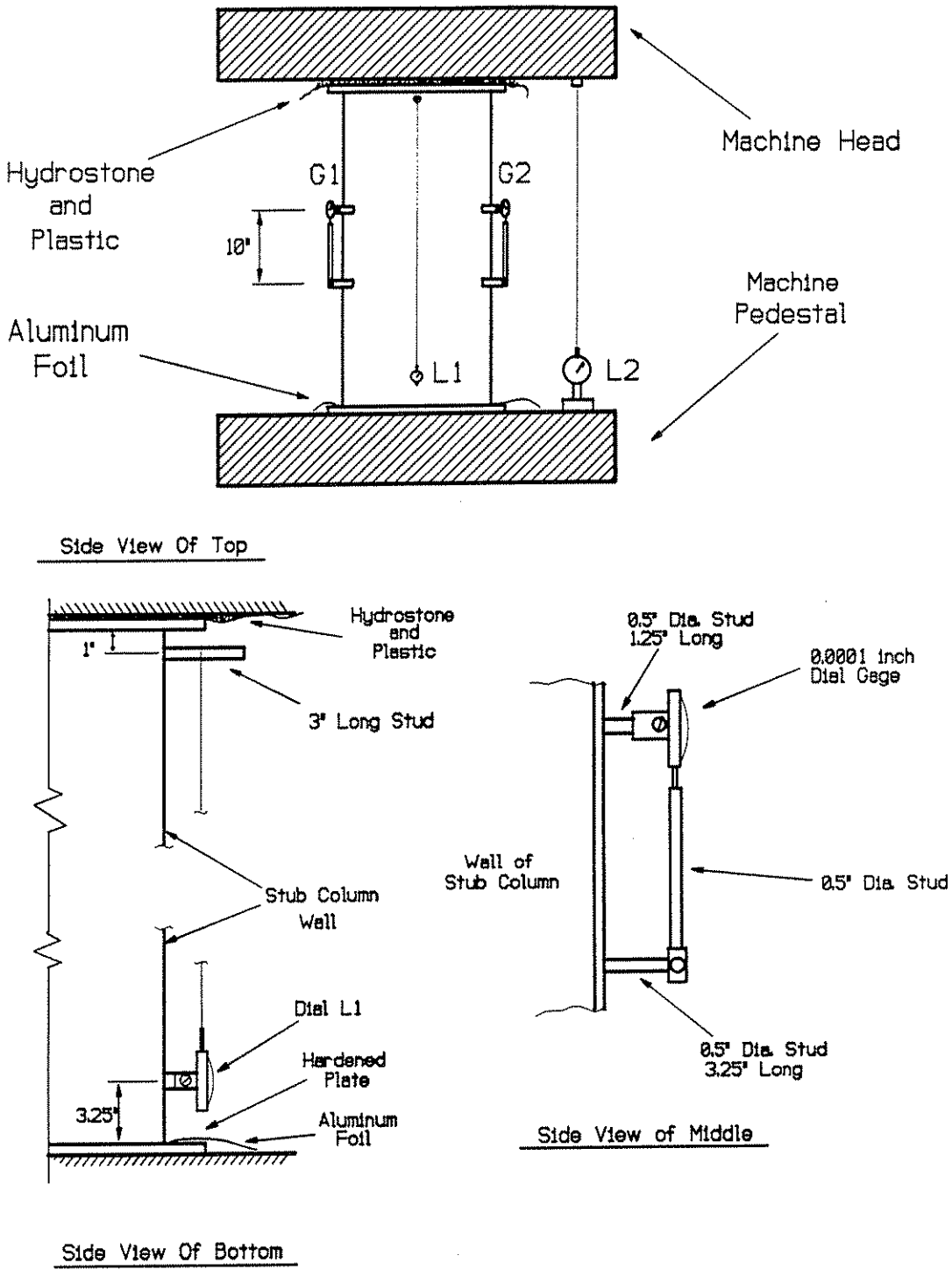

Figure 5-2: Setup of Stub Column with One End Plate

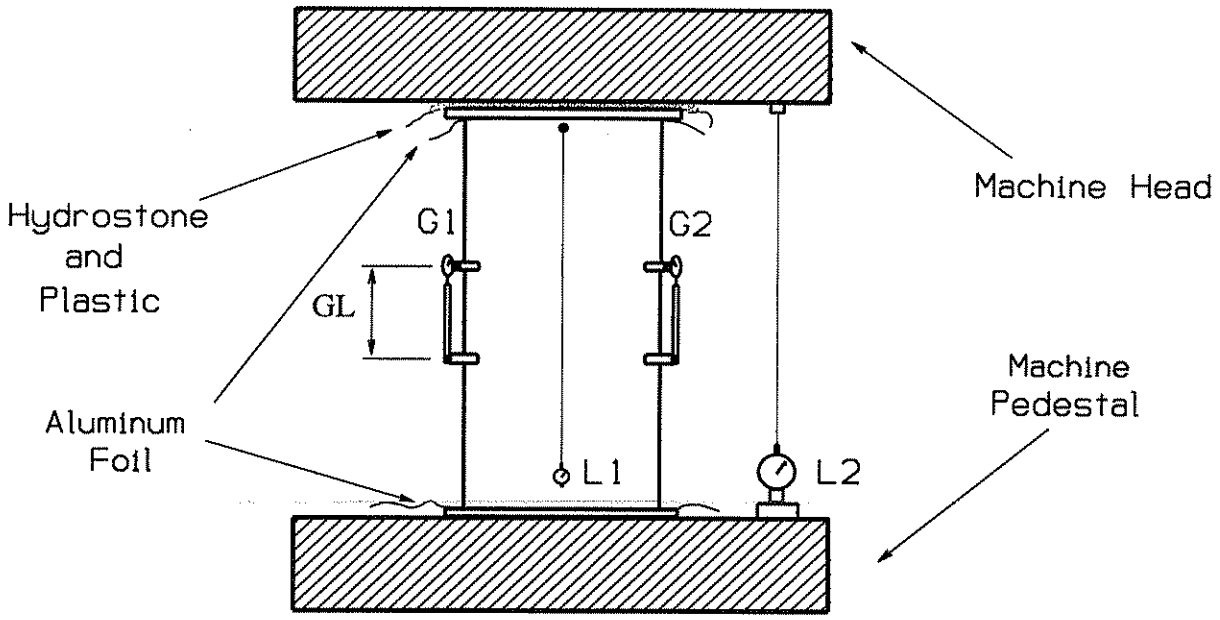

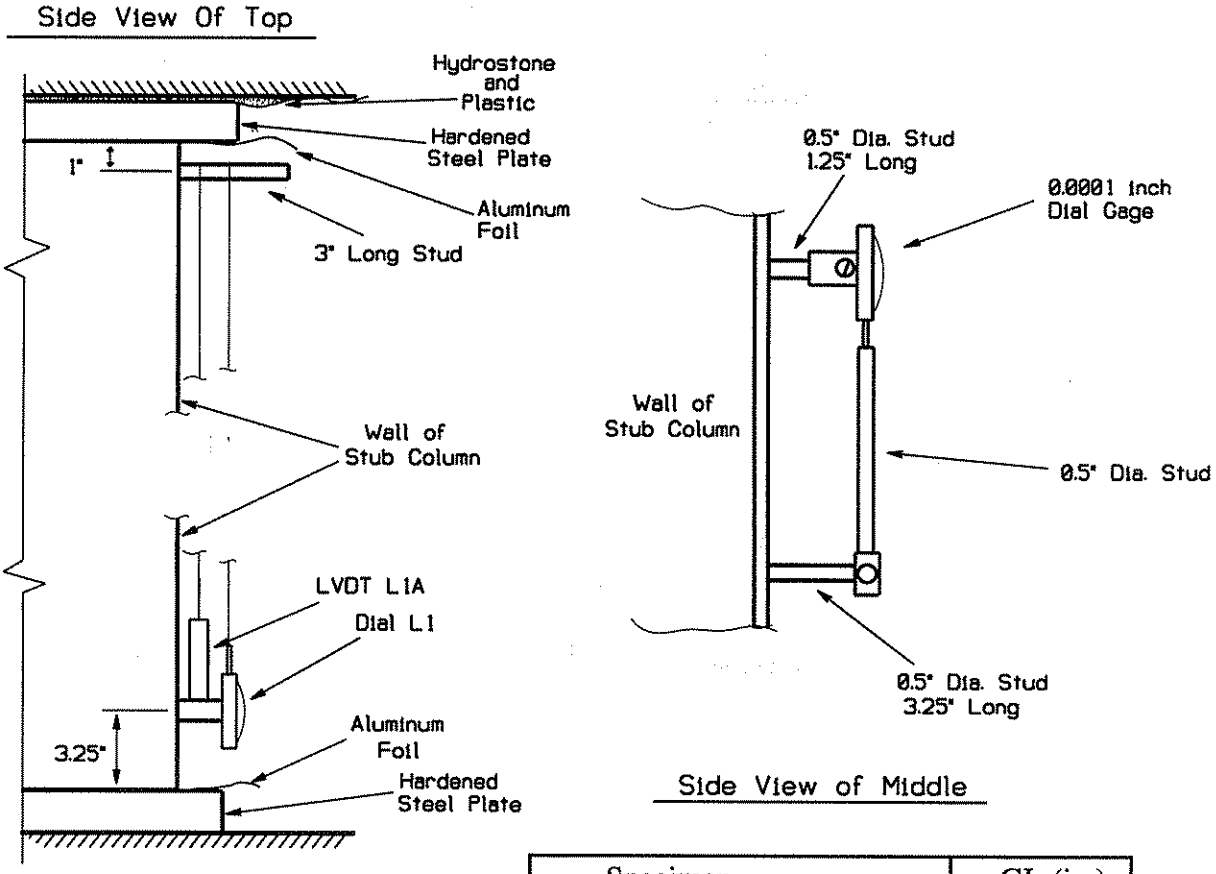

Specimen	GL (in.)
All Large Scale Specimens	10
P1PS	7
P2PS	8

Figure 5-3: Setup of Stub Column without End Plates

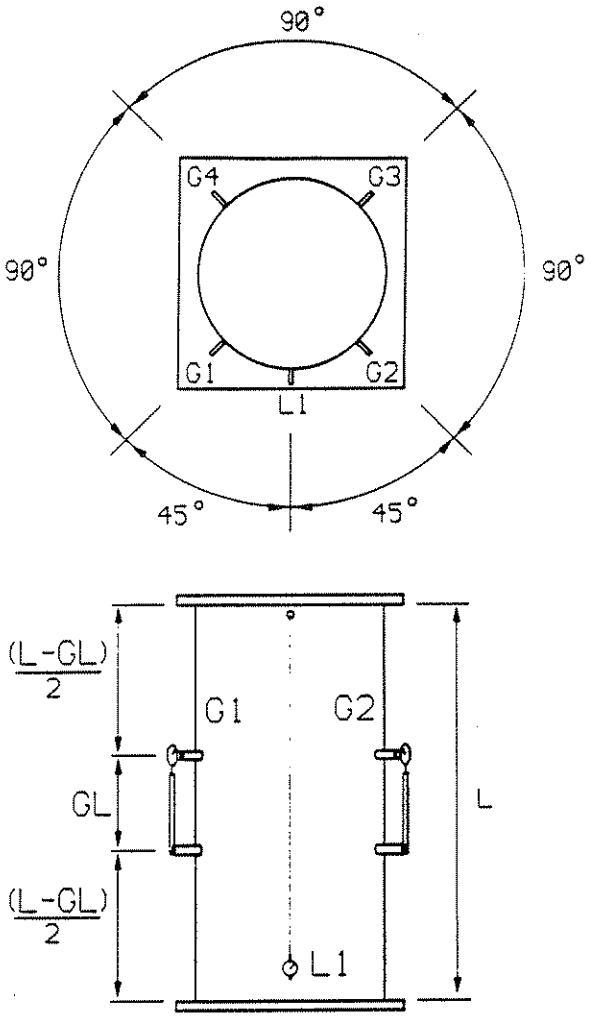

Specimen	GL (in.)
All Full Scale Specimens	10
P1PS	7
P2PS	8

Figure 5-4: Arrangement of Gages for Stub Columns

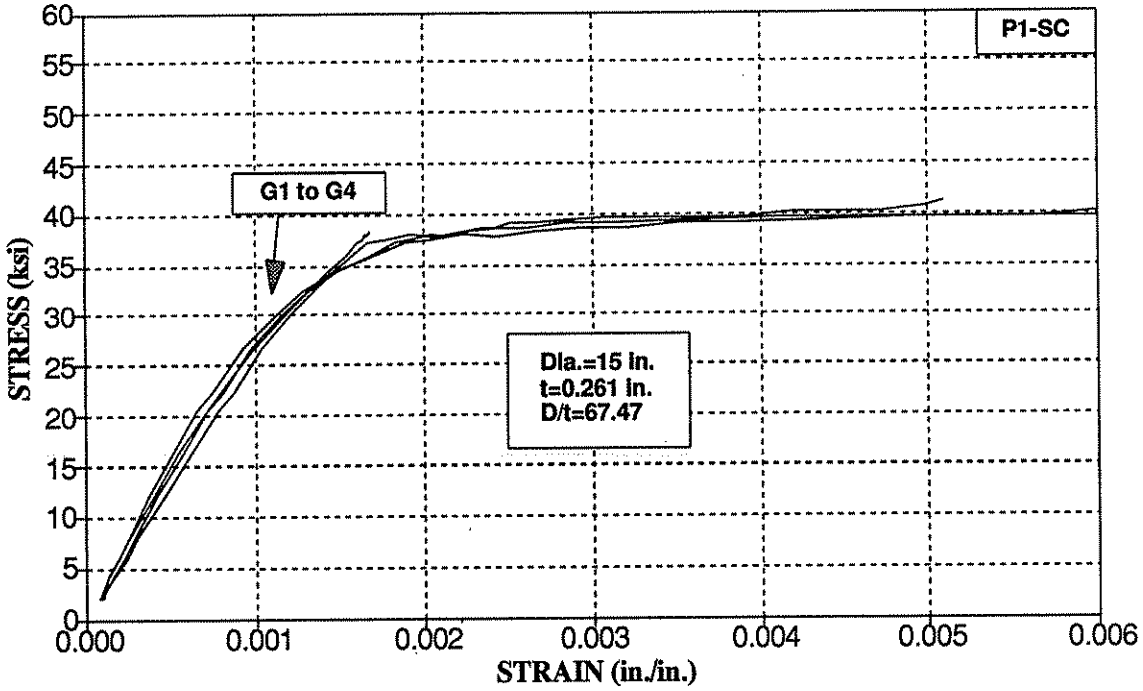

Figure 5-5: Stub Column P1-SC – Axial Load vs. Gage Readings

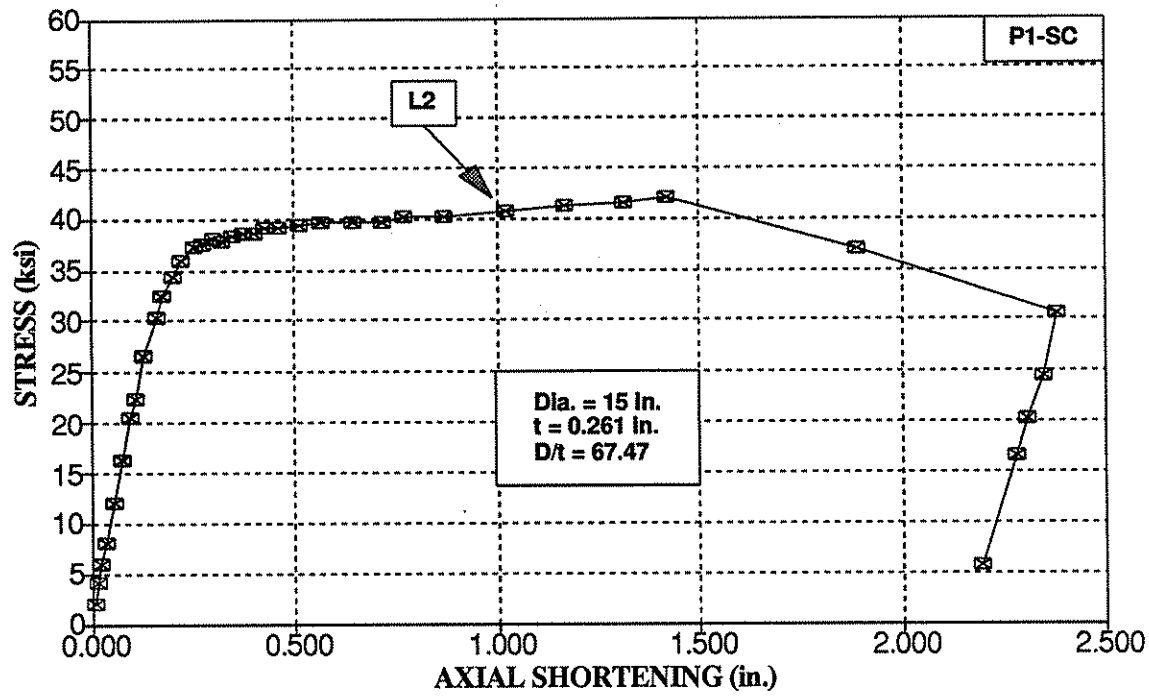

Figure 5-6: Stub Column P1-SC – Axial Load vs. Axial Shortening

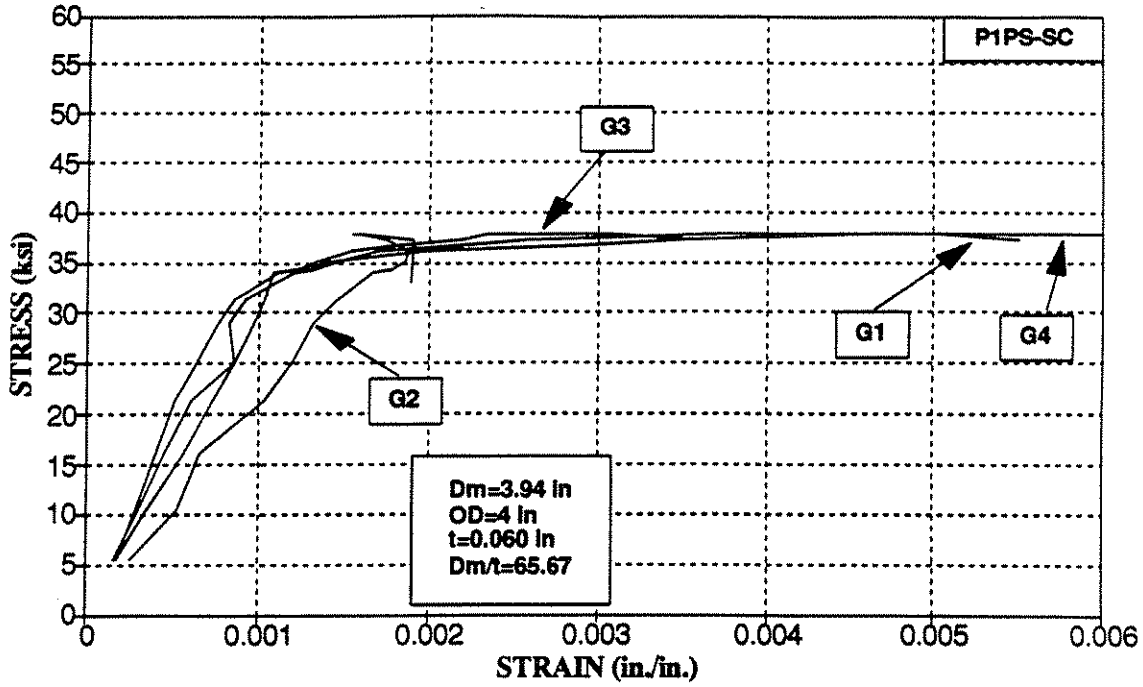

Figure 5-5a: Stub Column P1S-SC - Axial Load vs. Gage Readings

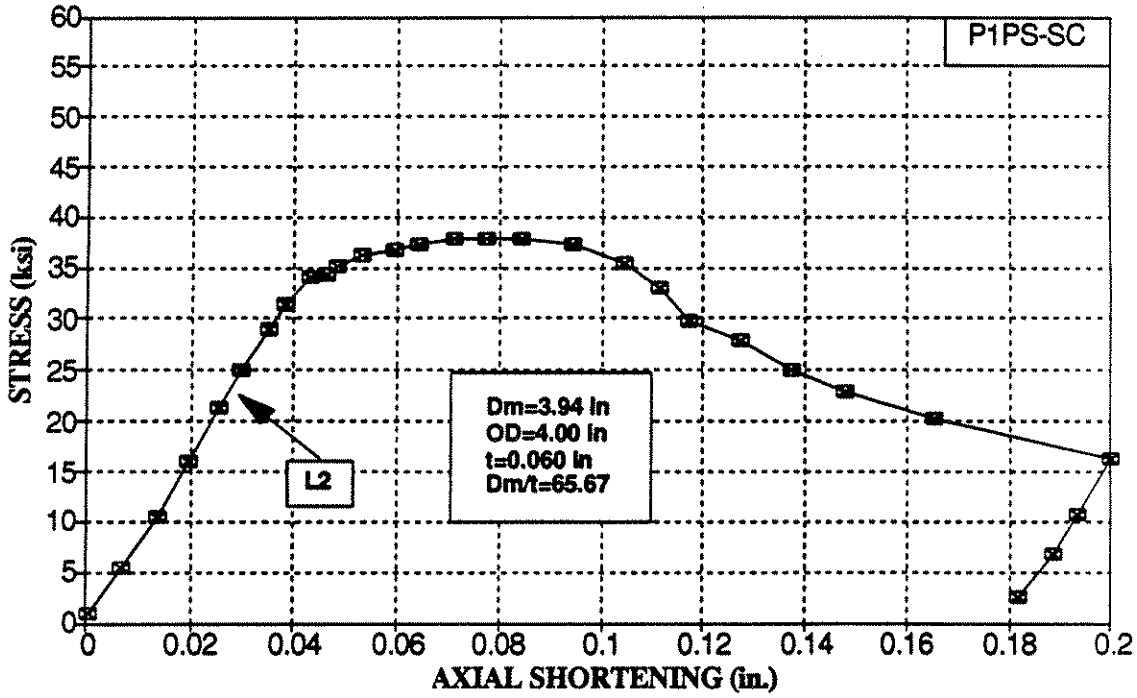

Figure 5-6a: Stub Column P1S-SC - Axial Load vs. Axial Shortening

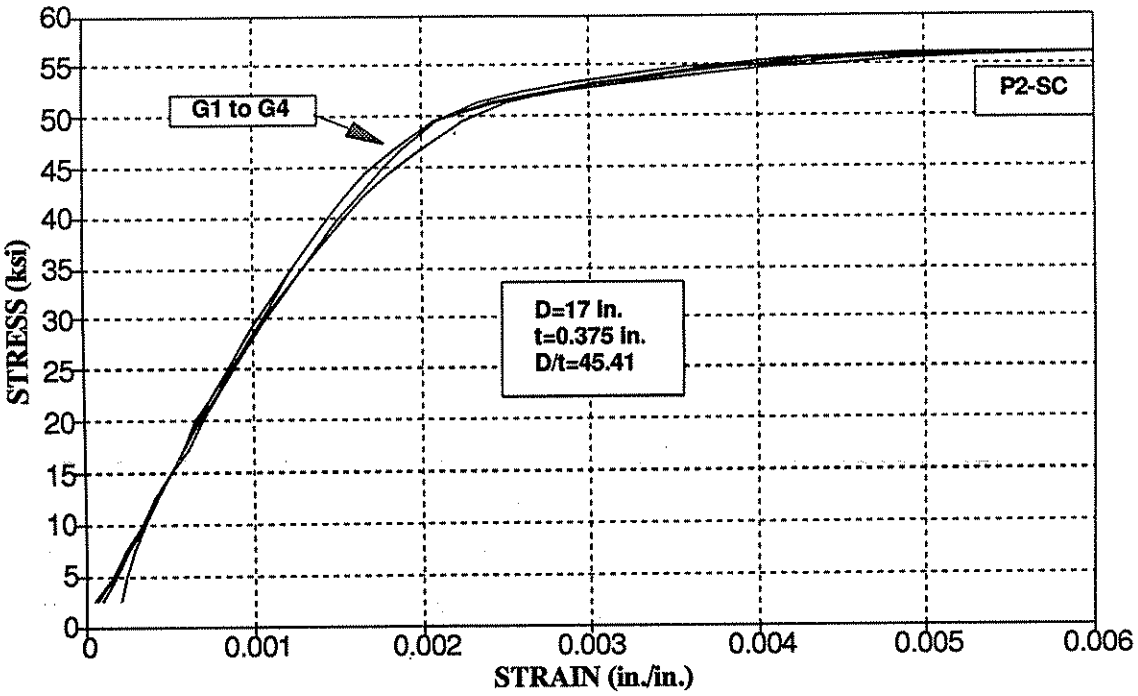

Figure 5-7: Stub Column P2-SC – Axial Load vs. Gage Readings

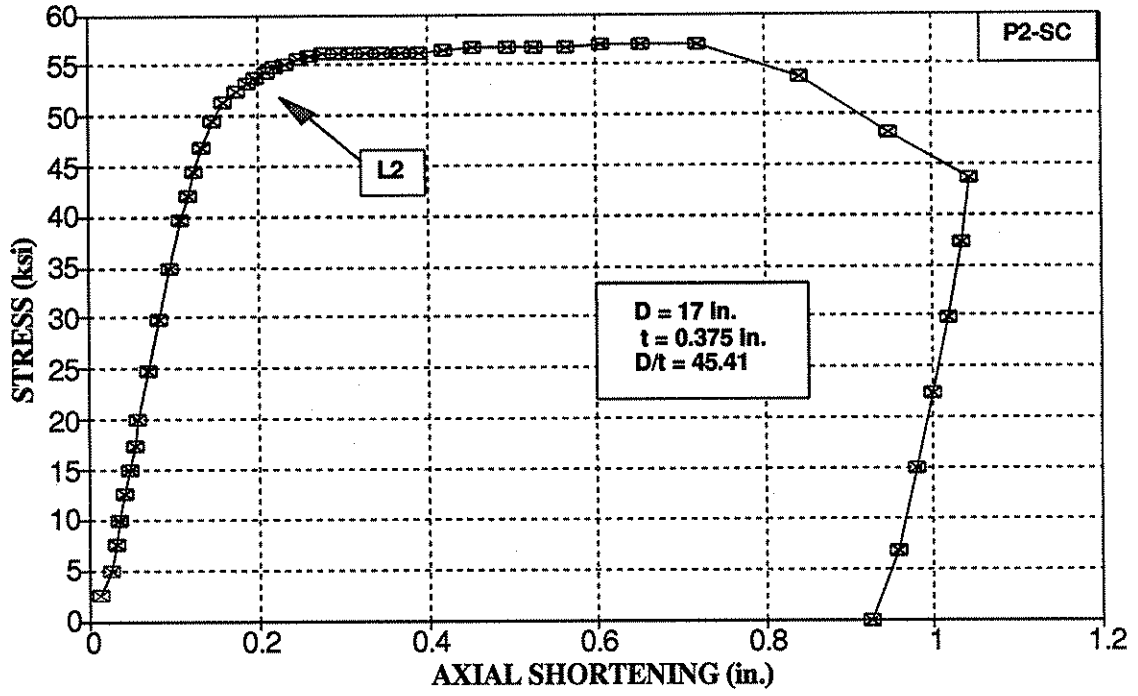

Figure 5-8: Stub Column P2-SC – Axial Load vs. Axial Shortening

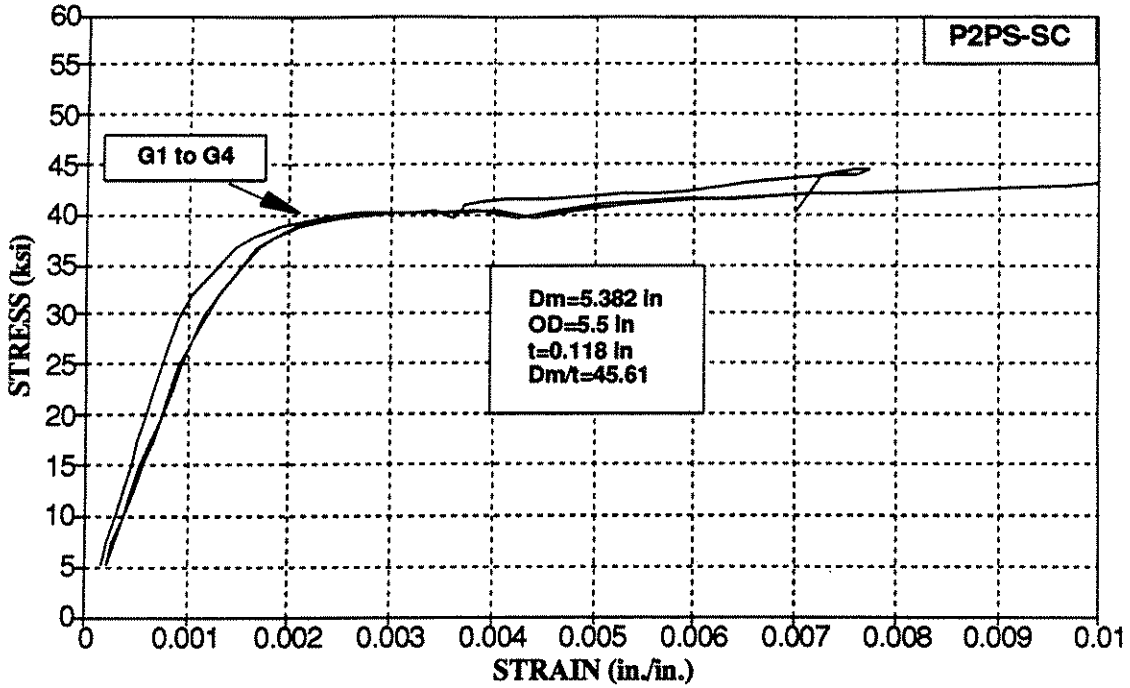

Figure 5-7a: Stub Column P2S-SC - Axial Load vs. Gage Readings

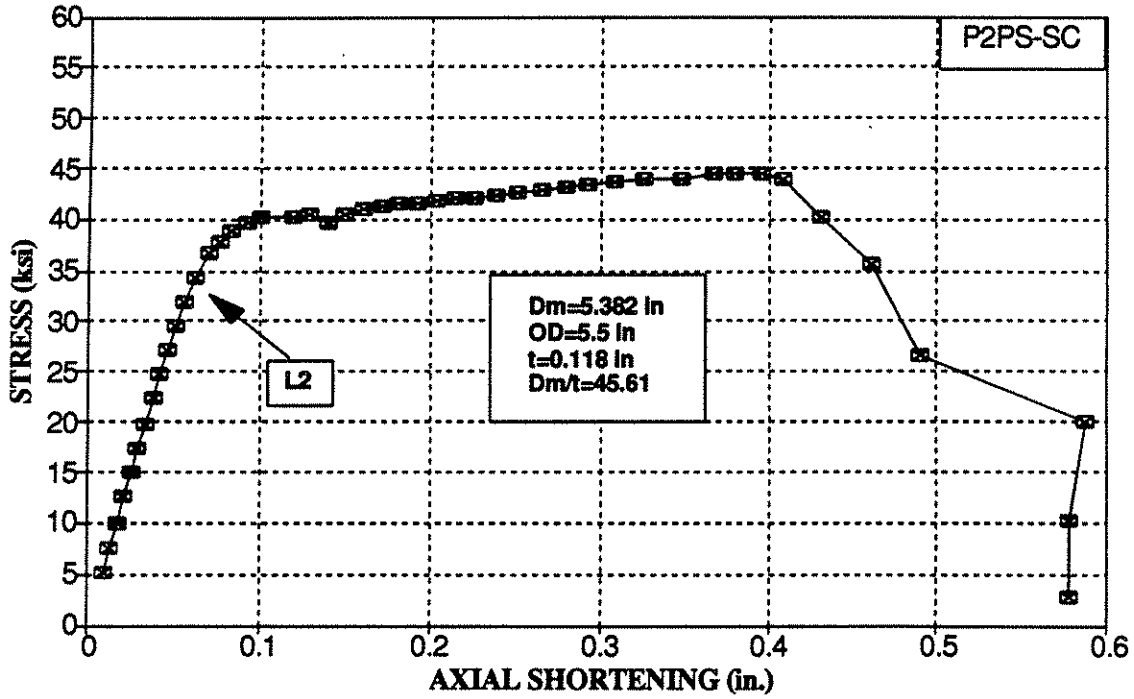

Figure 5-8a: Stub Column P2S-SC - Axial Load vs. Axial Shortening

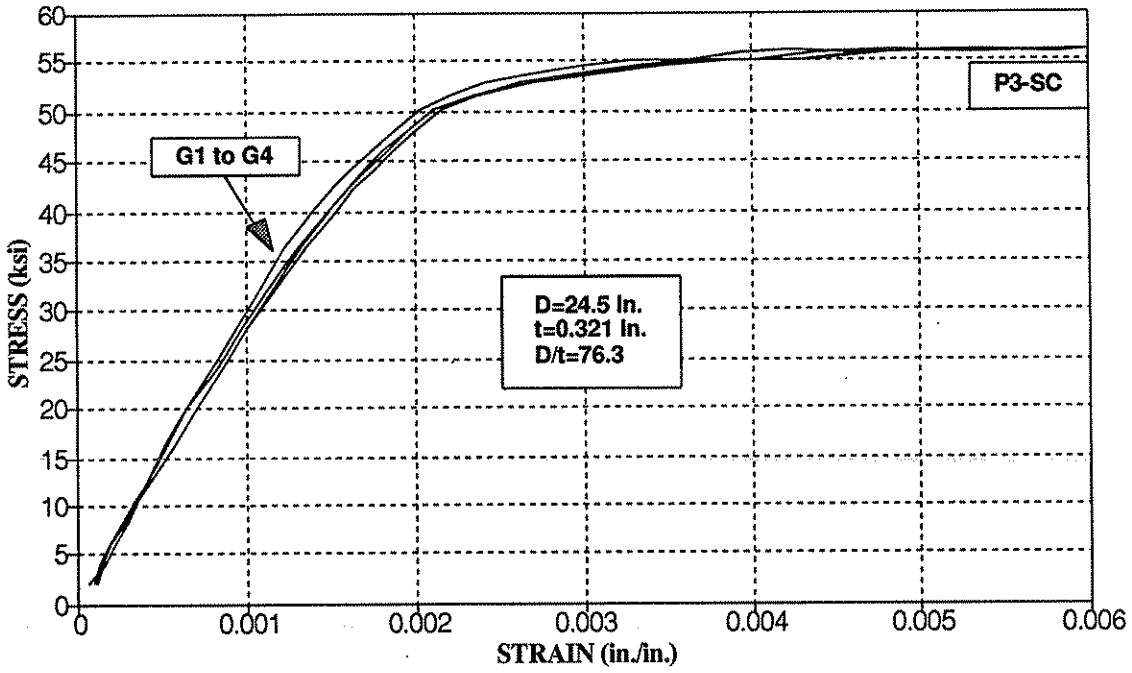

Figure 5-9: Stub Column P3-SC – Axial Load vs. Gage Readings

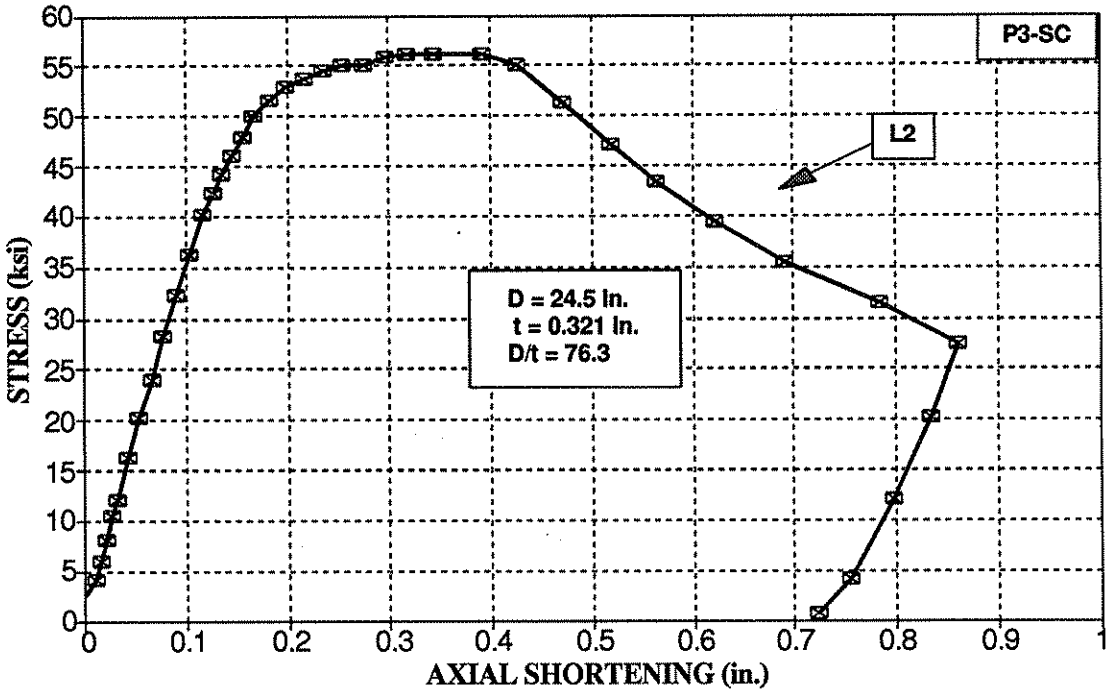

Figure 5-10: Stub Column P3-SC – Axial Load vs. Axial Shortening

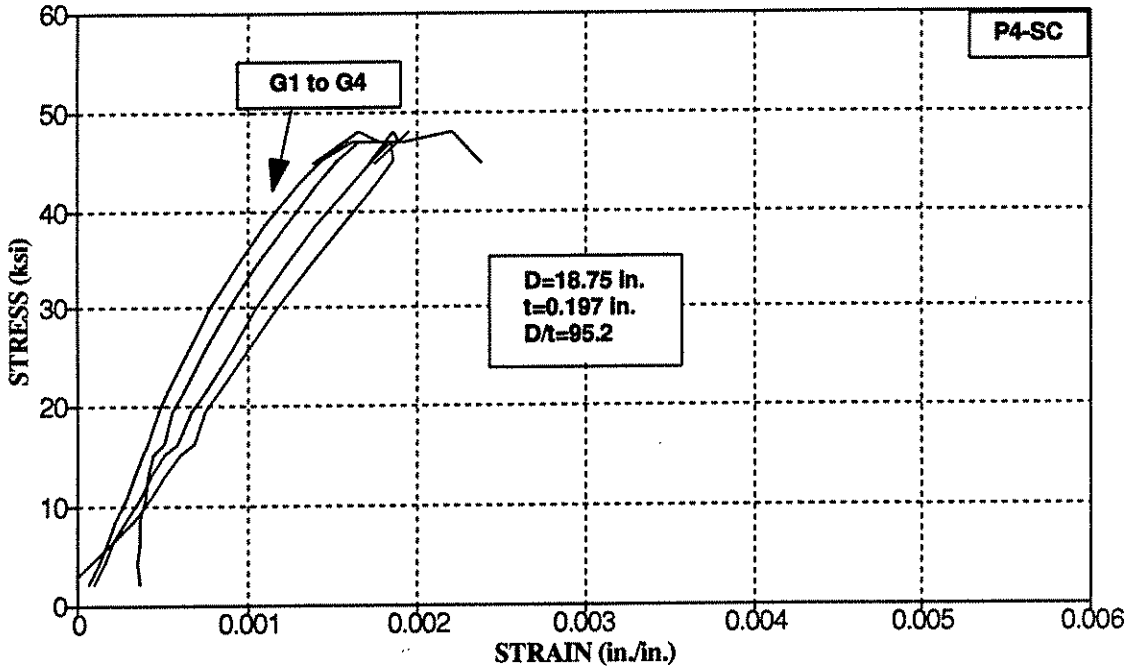

Figure 5-11: Stub Column P4-SC – Axial Load vs. Gage Readings

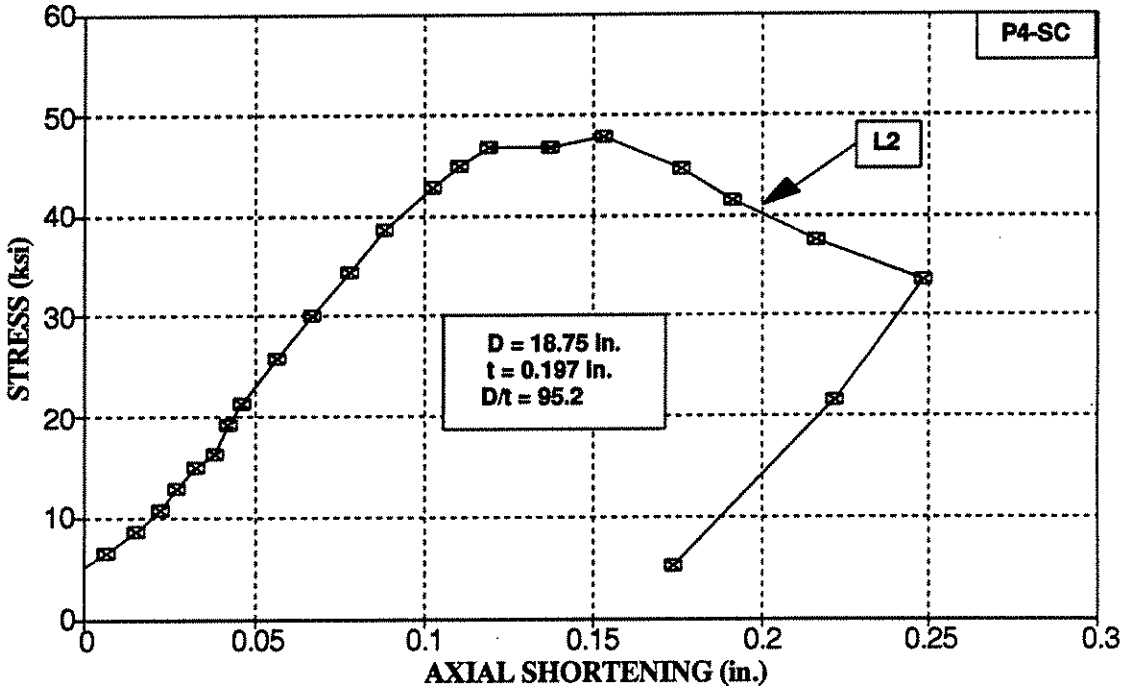

Figure 5-12: Stub Column P4-SC – Axial Load vs. Axial Shortening

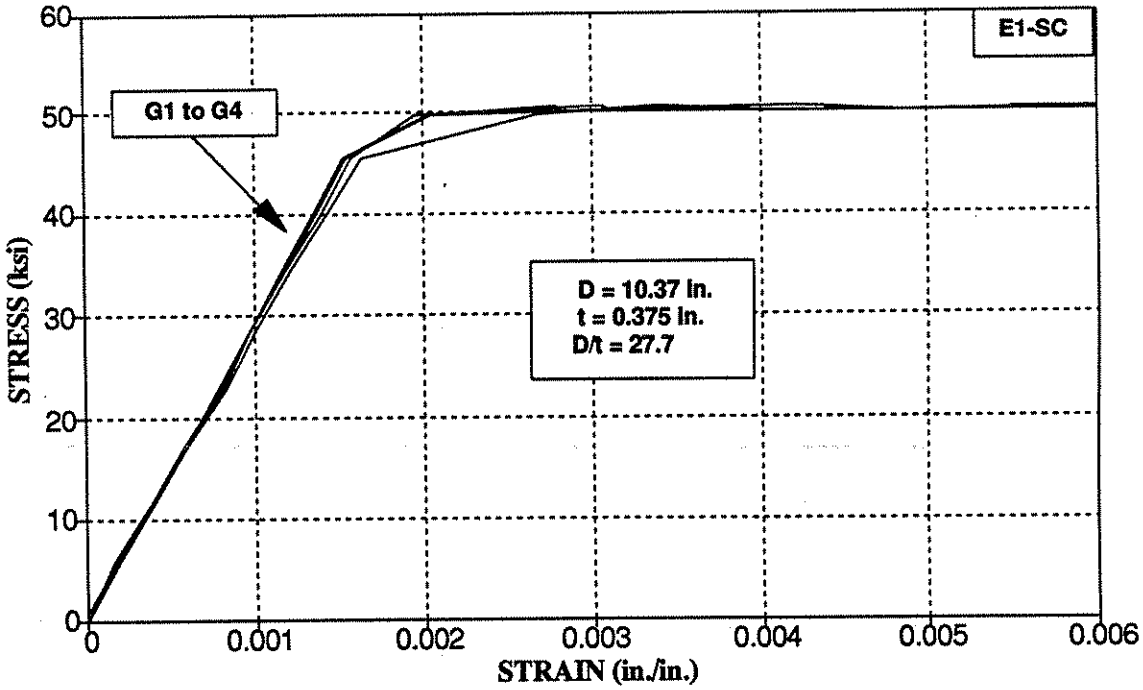

Figure 5-13: Stub Column E1-SC – Axial Load vs. Gage Readings

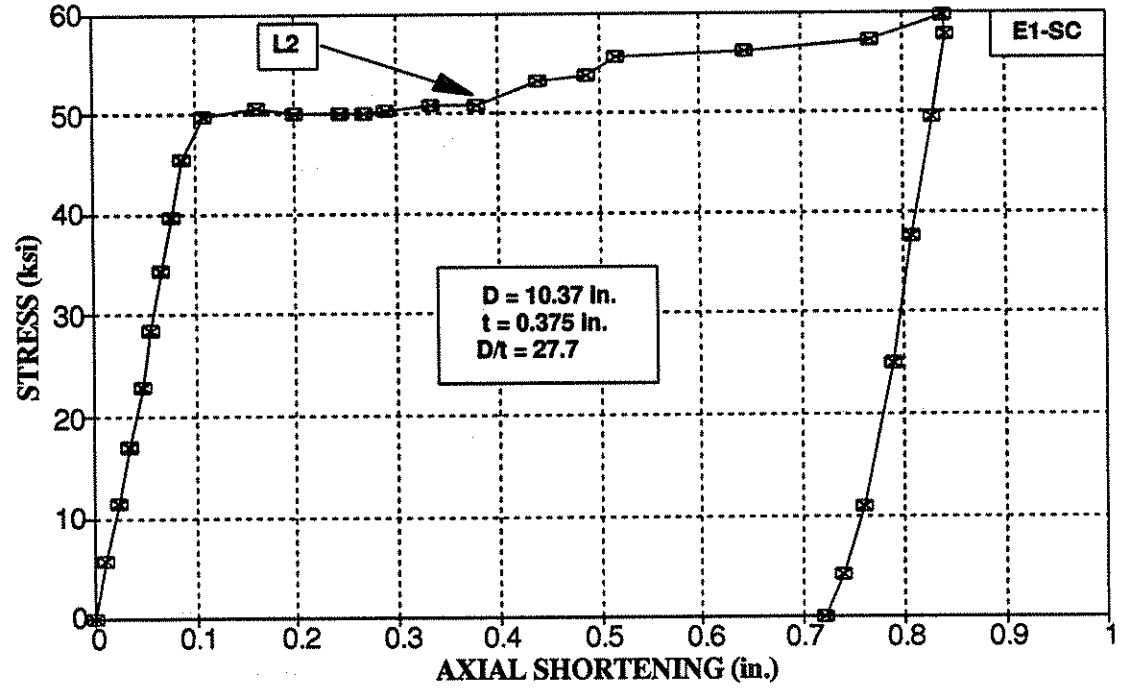

Figure 5-14: Stub Column E1-SC – Axial Load vs. Axial Shortening

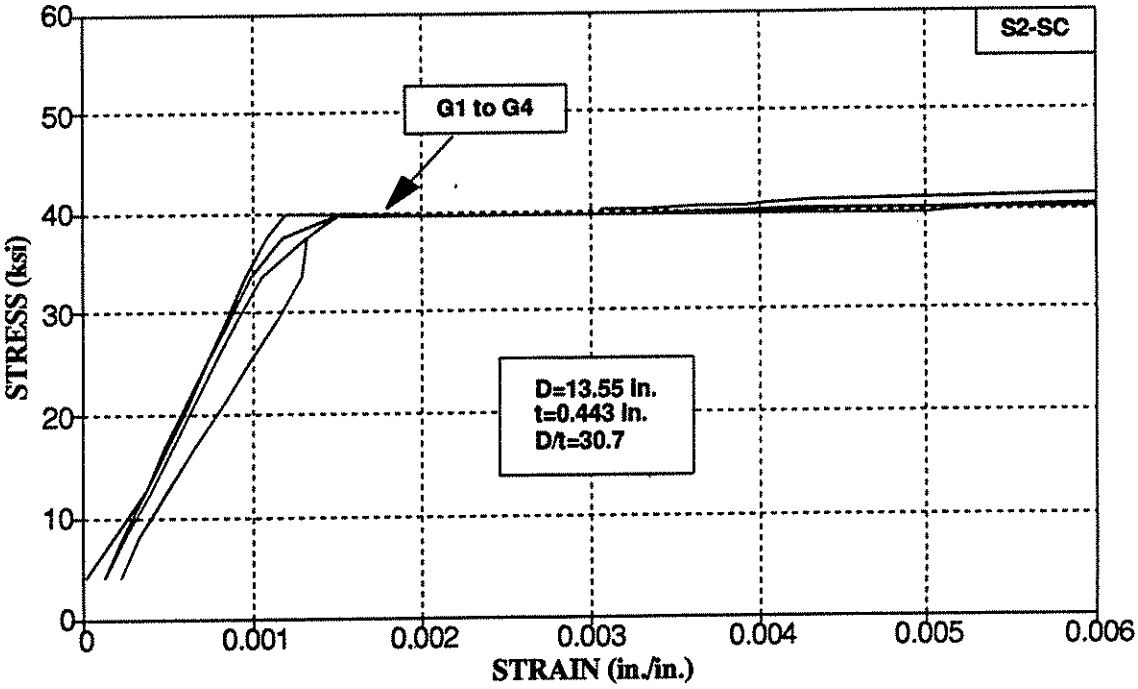

Figure 5-15: Stub Column S2-SC – Axial Load vs. Gage Readings

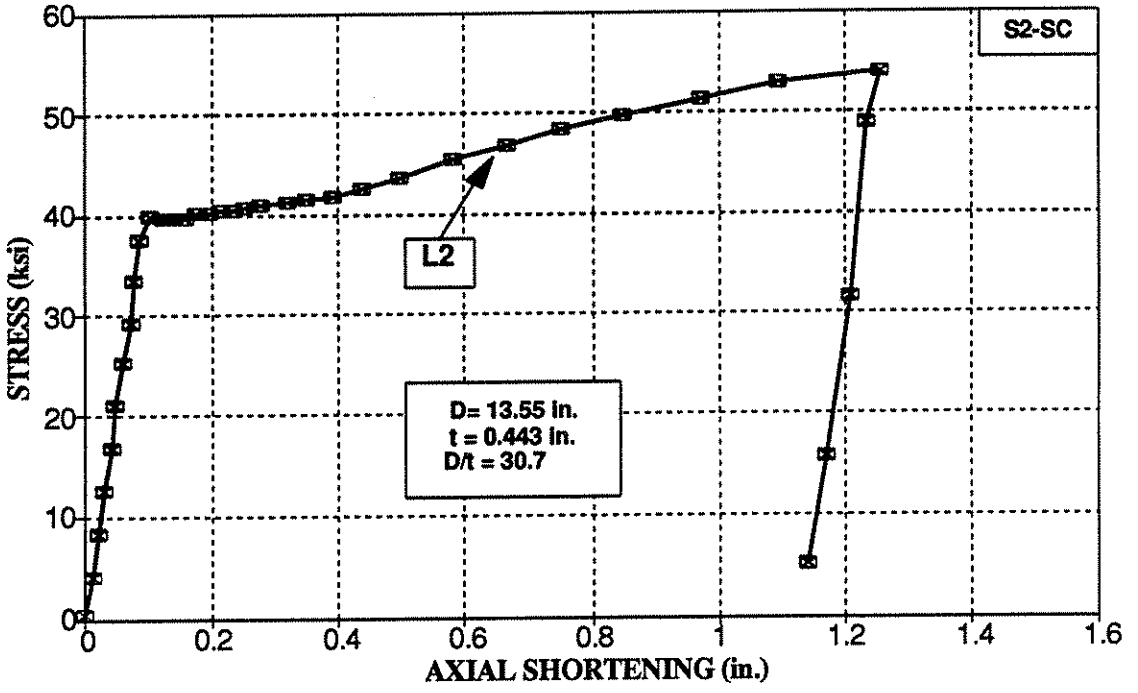

Figure 5-16: Stub Column S2-SC – Axial Load vs. Axial Shortening

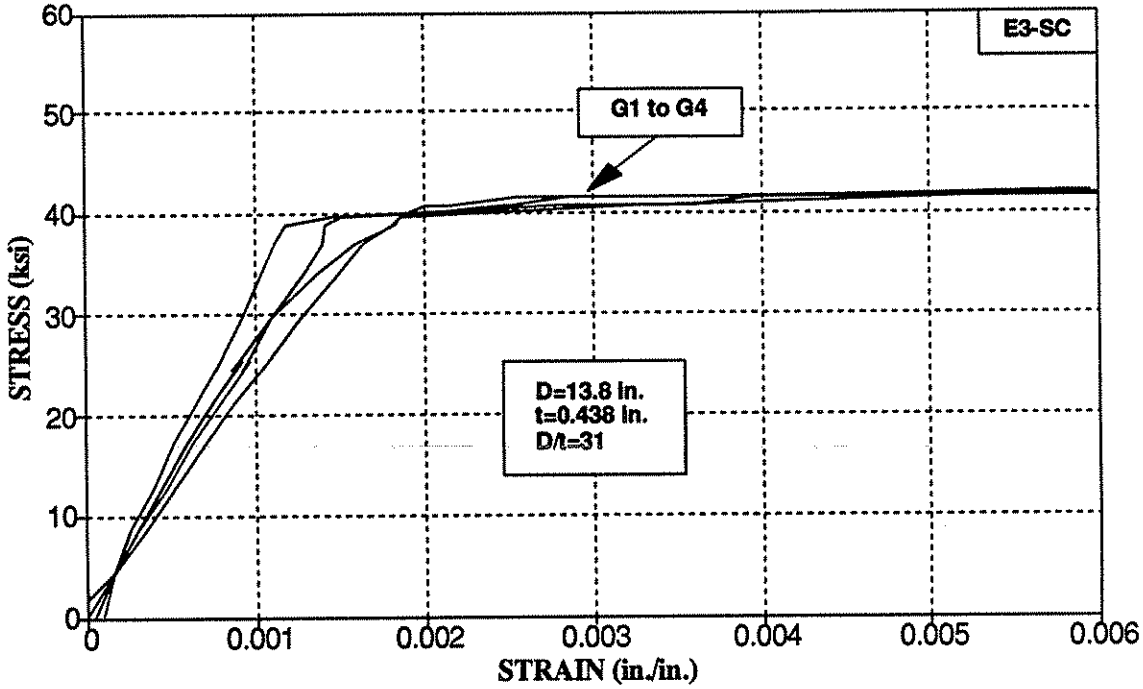

Figure 5-17: Stub Column E3-SC – Axial Load vs. Gage Readings

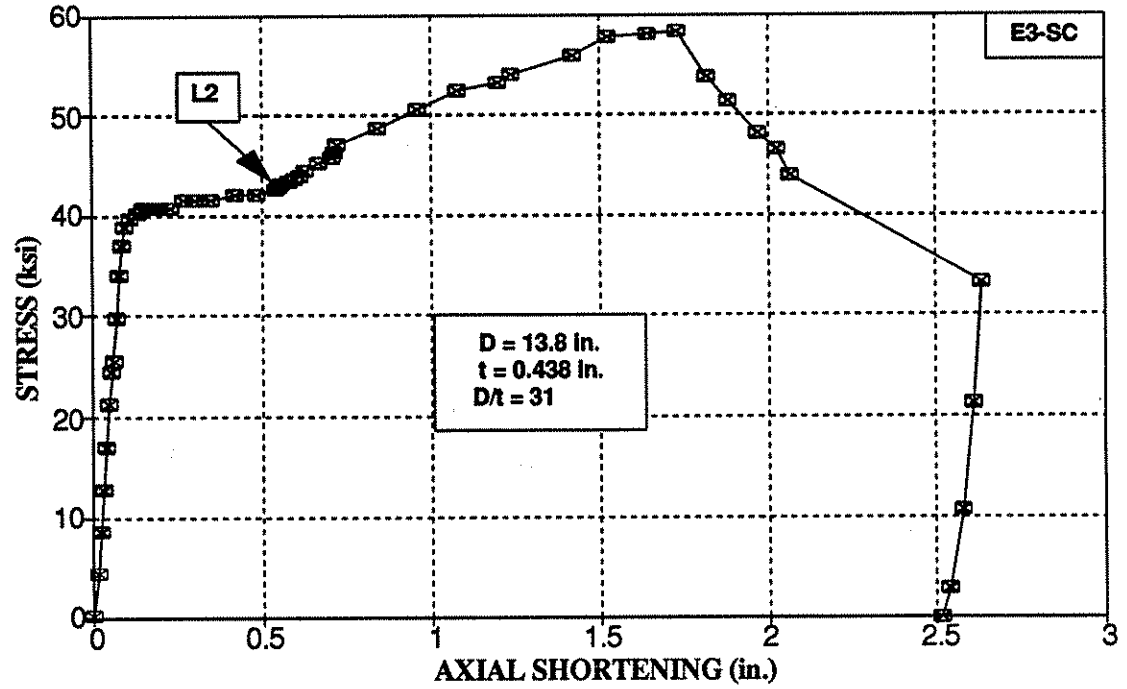

Figure 5-18: Stub Column E3-SC – Axial Load vs. Axial Shortening

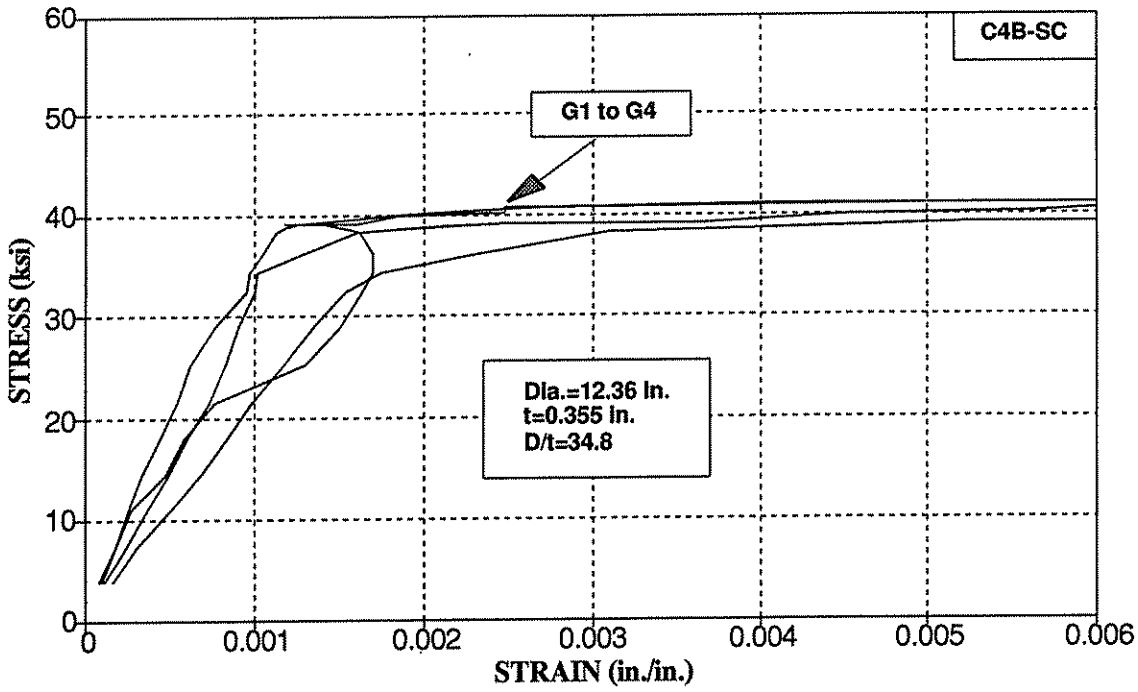

Figure 5-19: Stub Column C4B-SC – Axial Load vs. Gage Readings

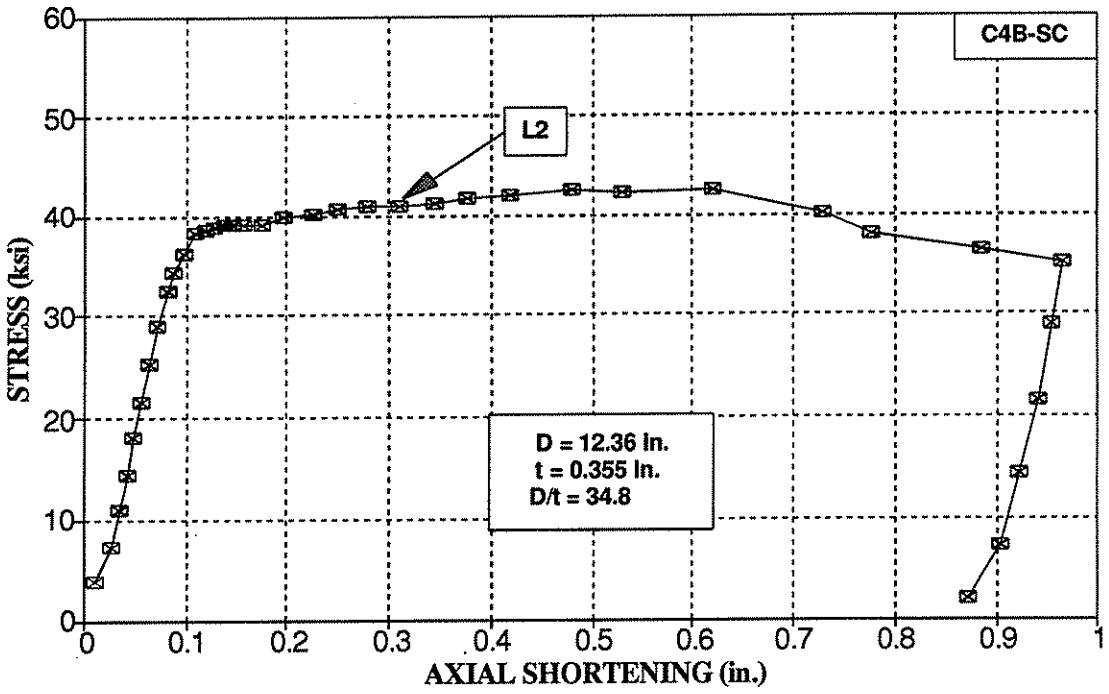

Figure 5-20: Stub Column C4B-SC – Axial Load vs. Axial Shortening

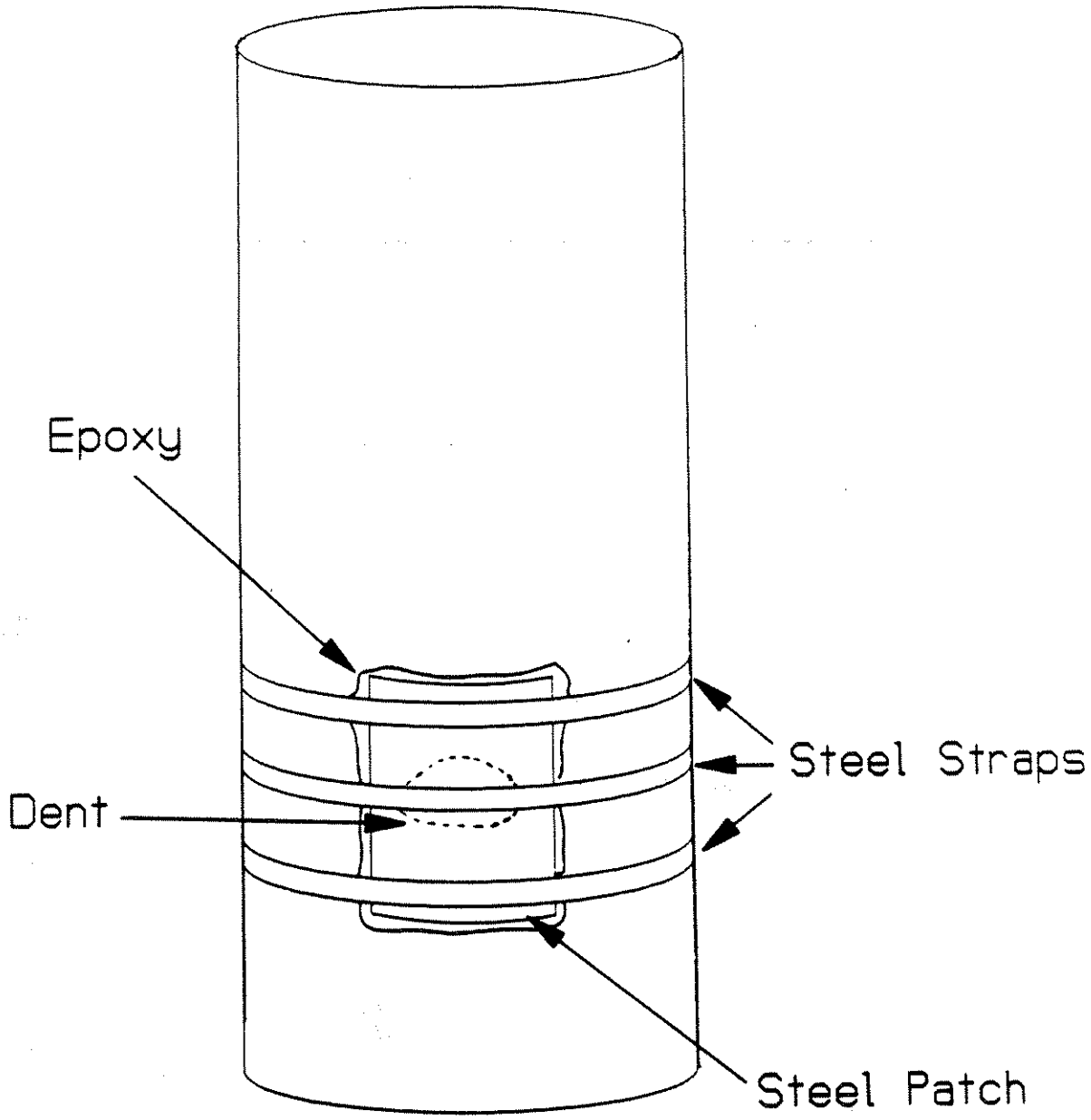

Figure 5-21: Specimen P1S-SC - Patch Used to Repair Dent in Stub Column

Figure 6-1: Supports for Denting Procedure Checked on Small-Scale Specimens

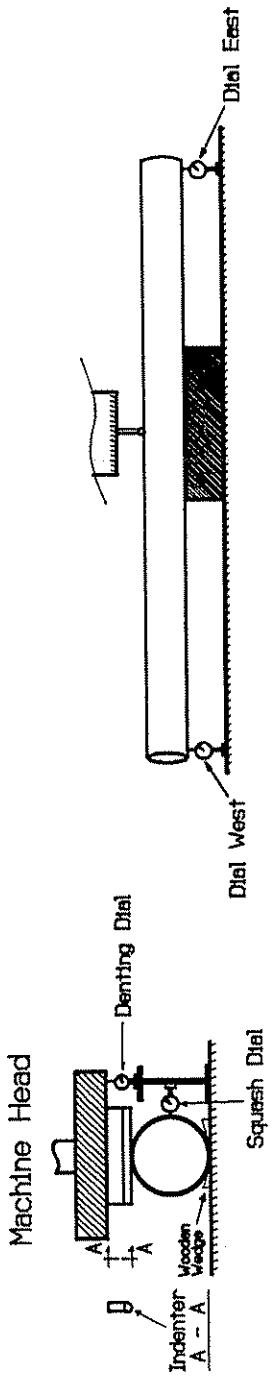

Figure 6-2: Setup For Denting of Specimens in 800-Kip Machine

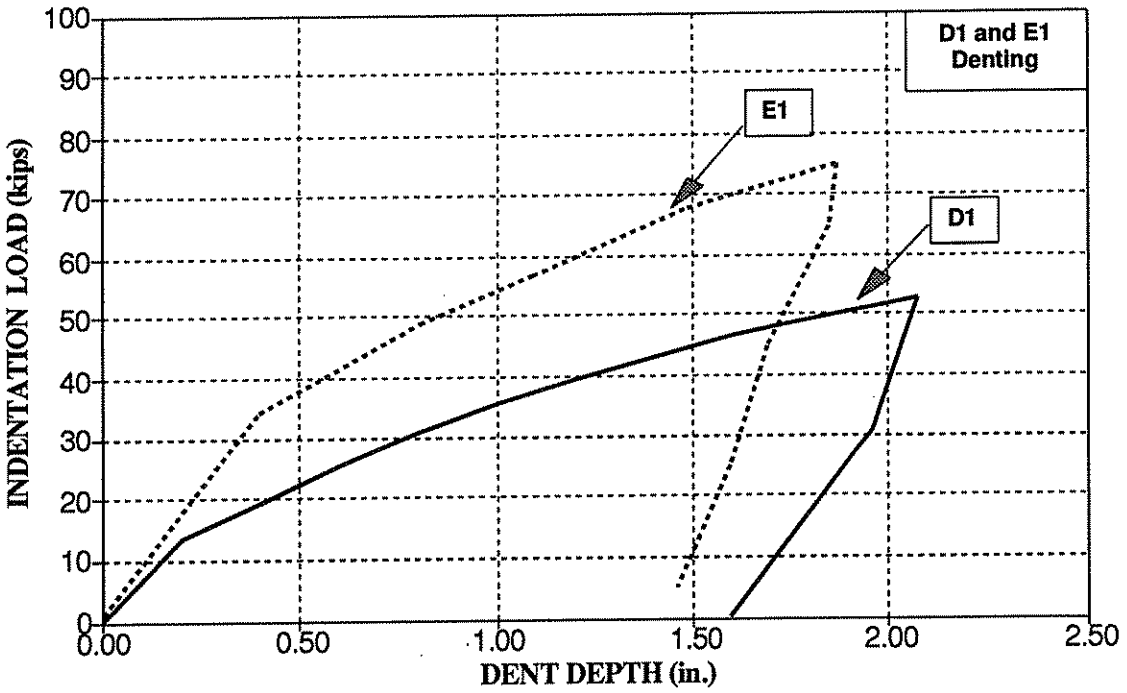

Figure 6-3: Load-Response For Denting of Specimens D1 and E1

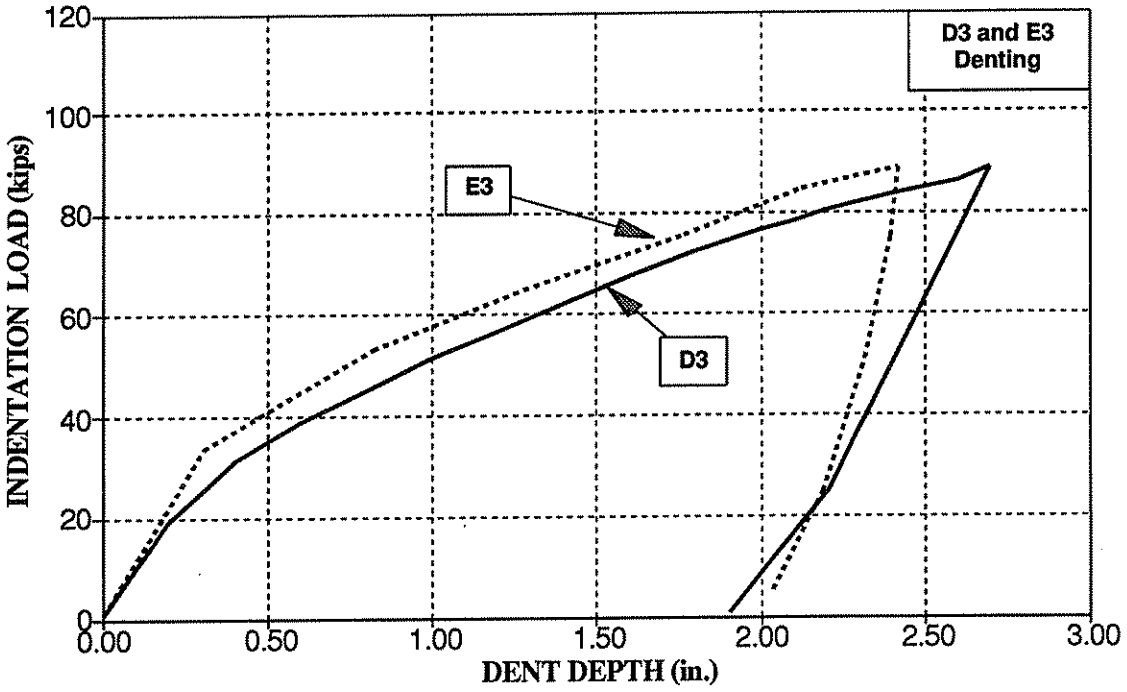

Figure 6-4: Load-Response for Denting of Specimens D3 and E3

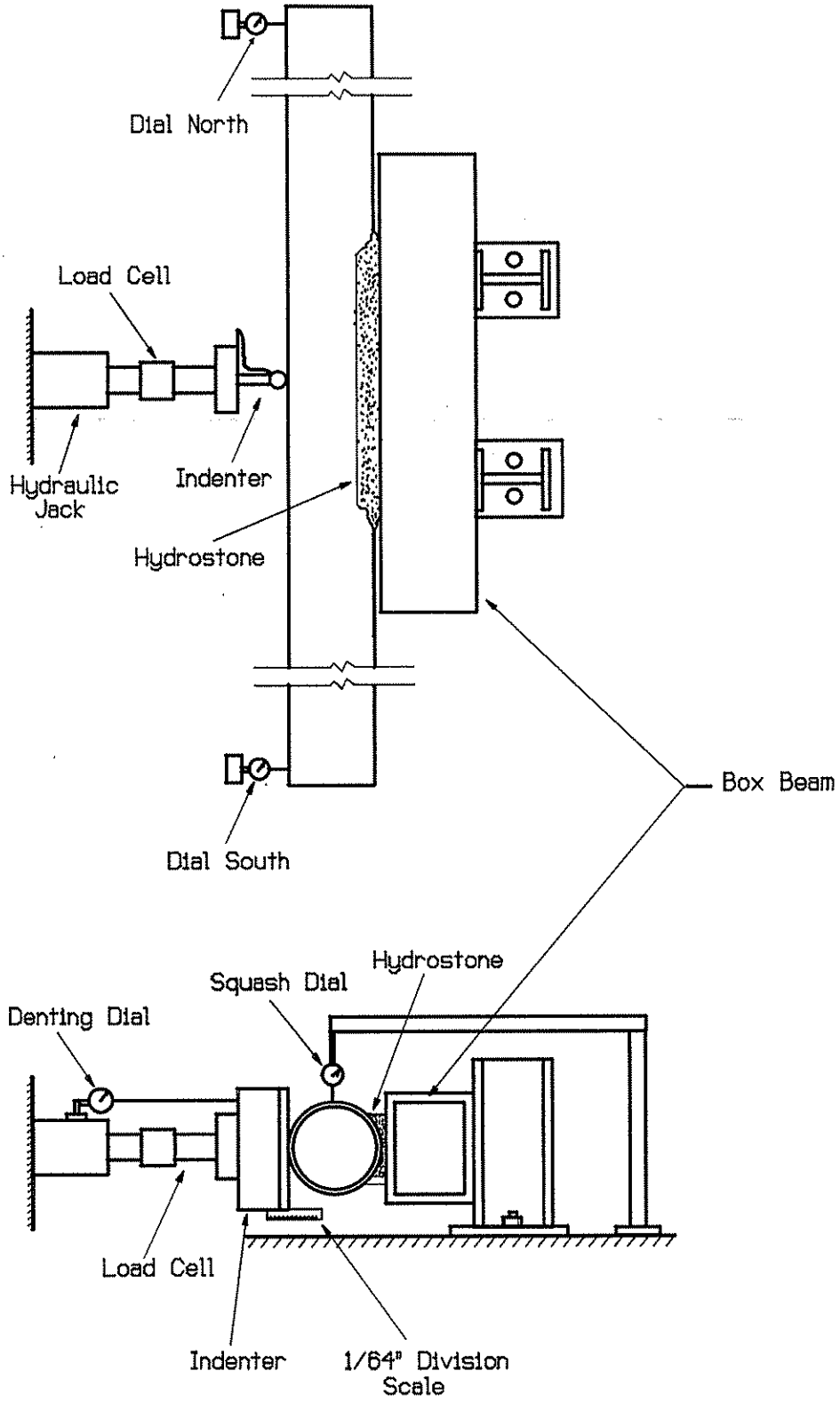

Figure 6-5: Setup for Denting Specimens with Hydraulic Jack

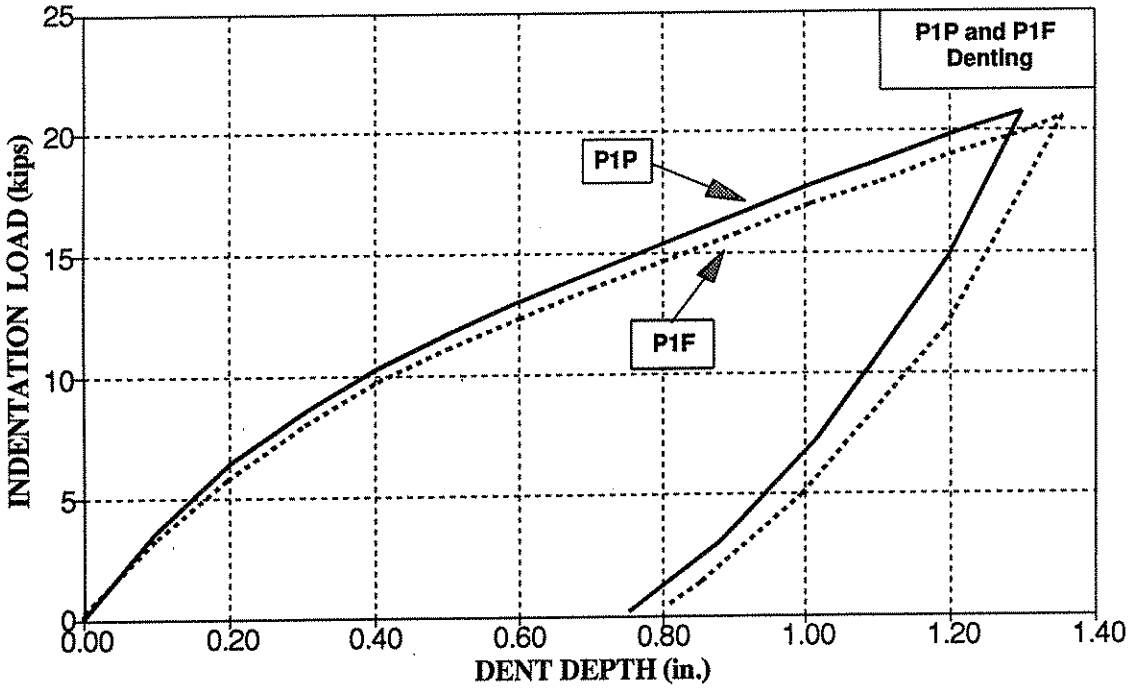

Figure 6-6: Load-Response For Denting Specimens P1P and P1F

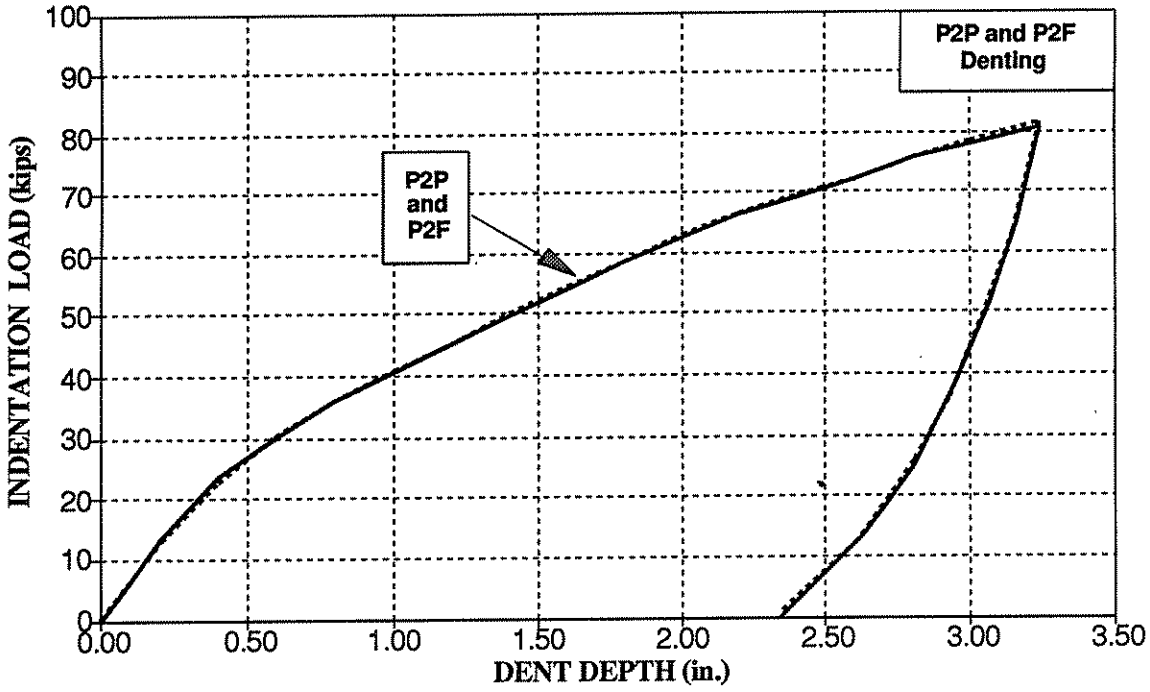

Figure 6-7: Load-Response for Denting Specimens P2P and P2F

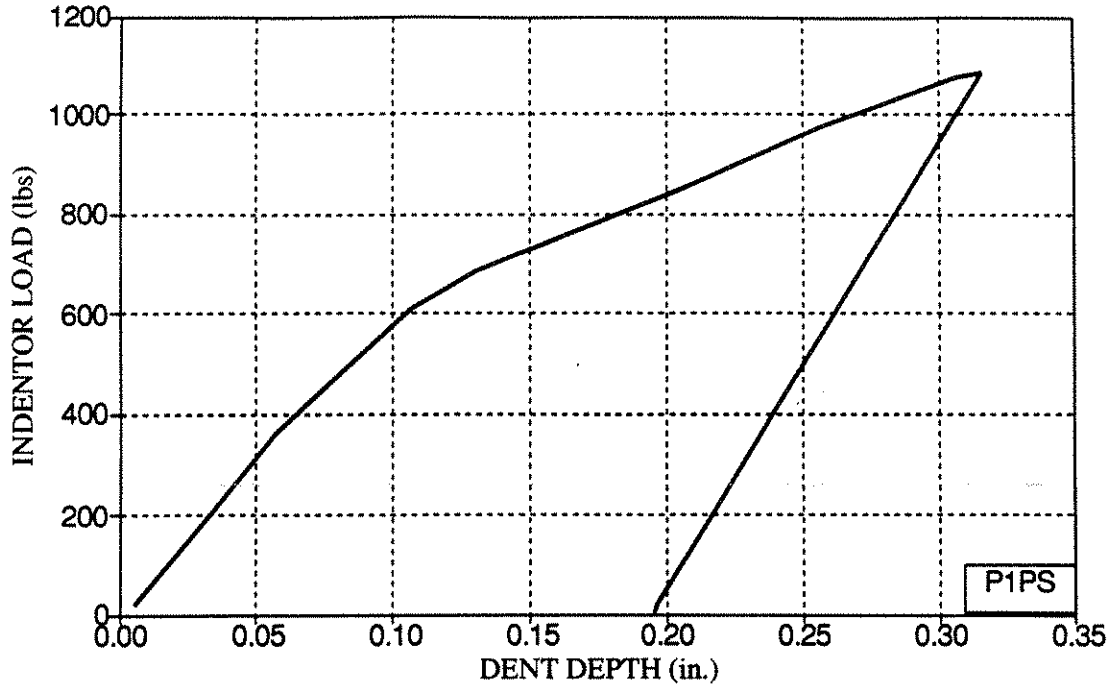

Figure 6-6a: Load Response for Denting of Specimen P1PS

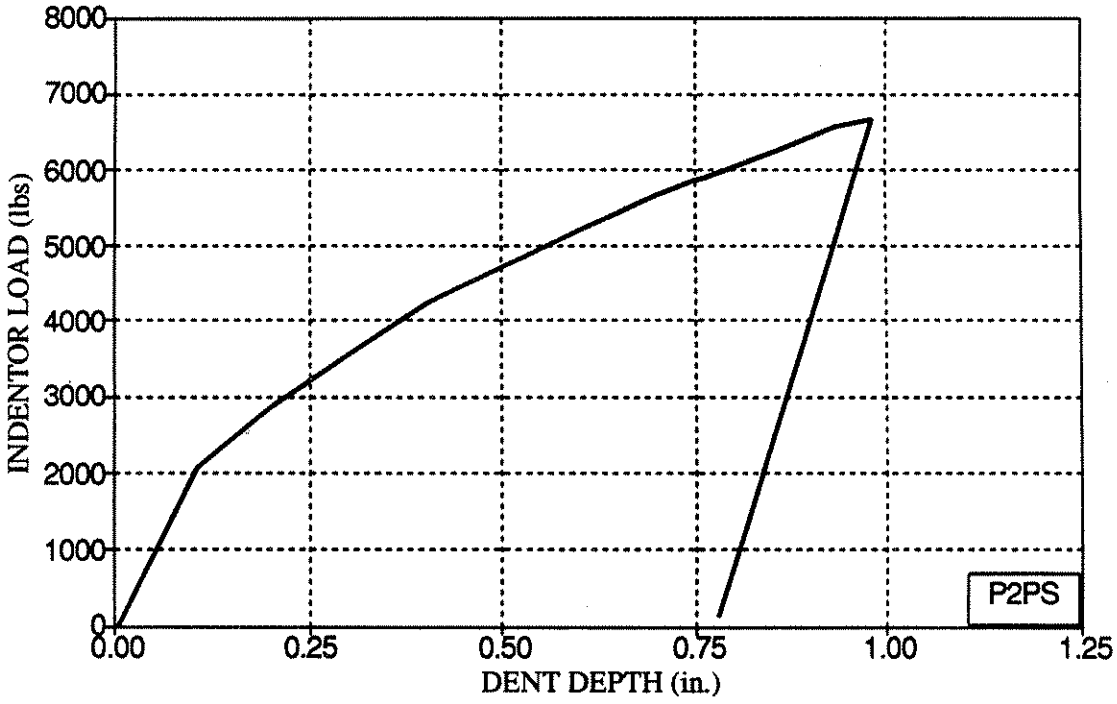

Figure 6-7a: Load Response for Denting of Specimen P2PS

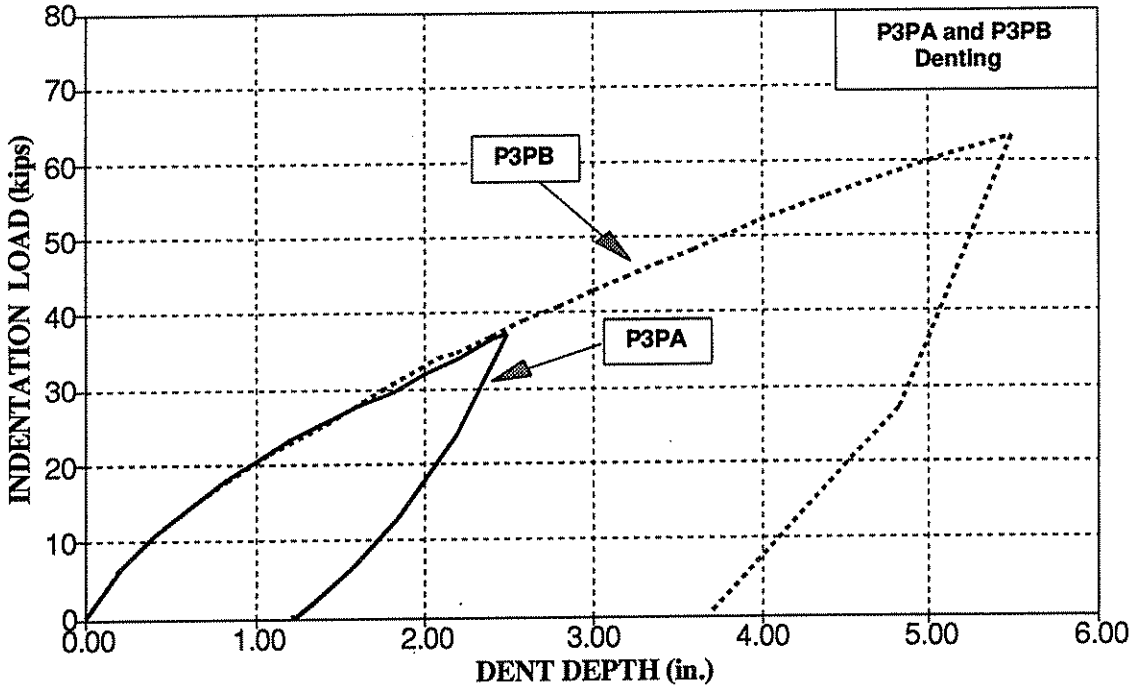

Figure 6-8: Load-Response for Denting Specimens P3PA and P3PB

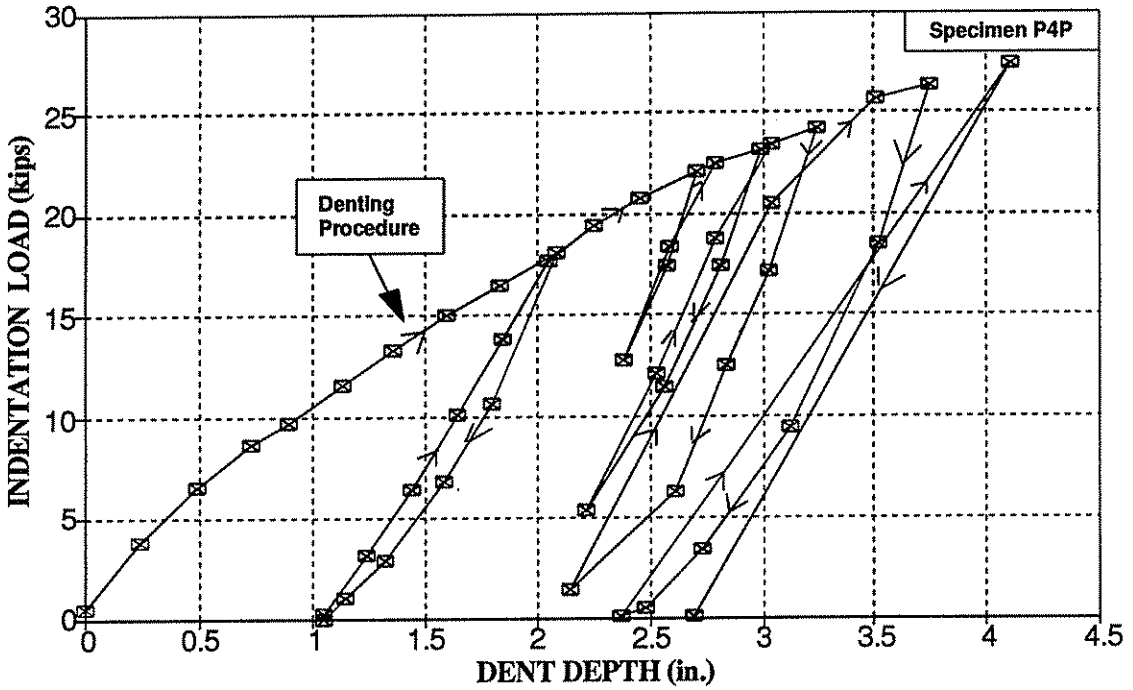

Figure 6-9: Load-Unload Response for Denting Specimen P4P

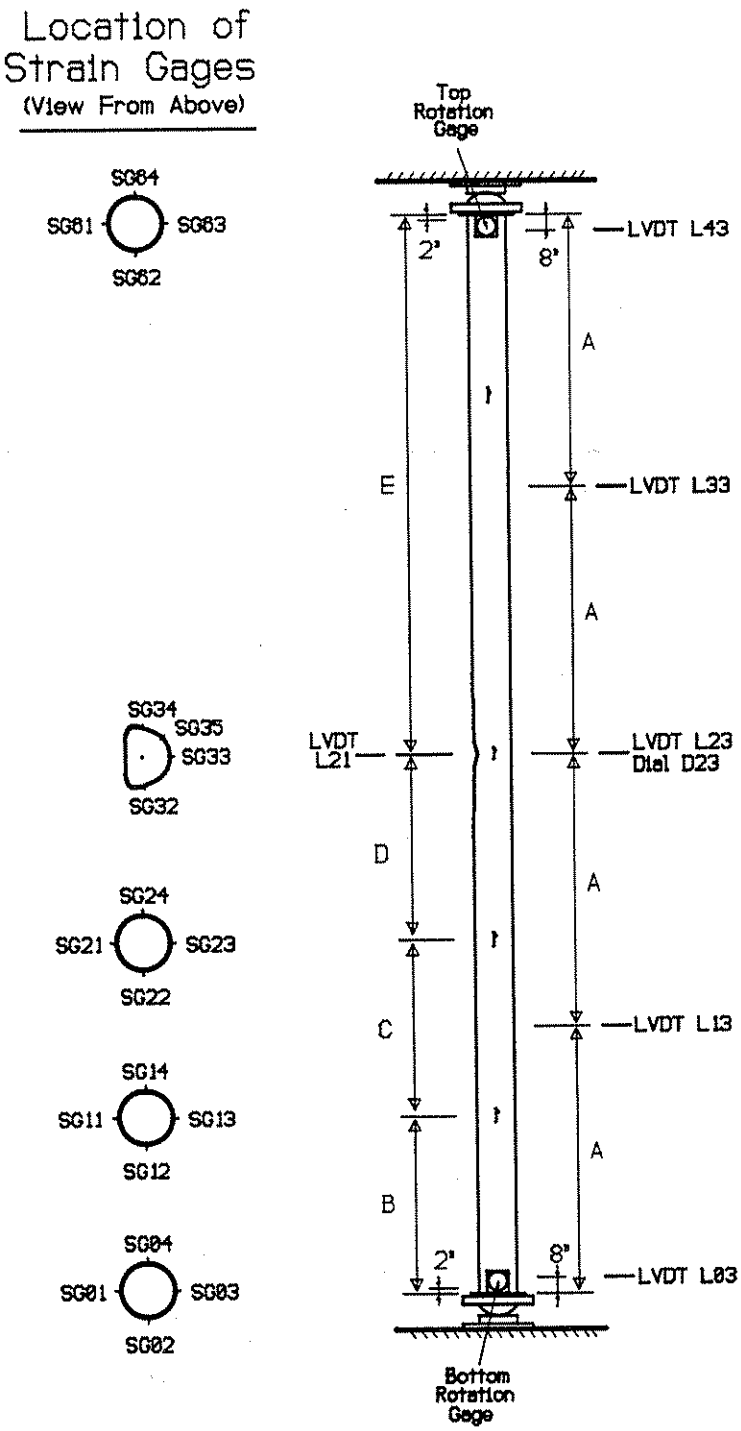

Specimen	Length	A	B	C	D	E
E1	24'-6"	73.5"	60"	38"	49"	145"
E3	28'-0"	84"	56"	56"	56"	166"

Figure 7-1: Location of Gages for Long-Column Specimens E1 and E3

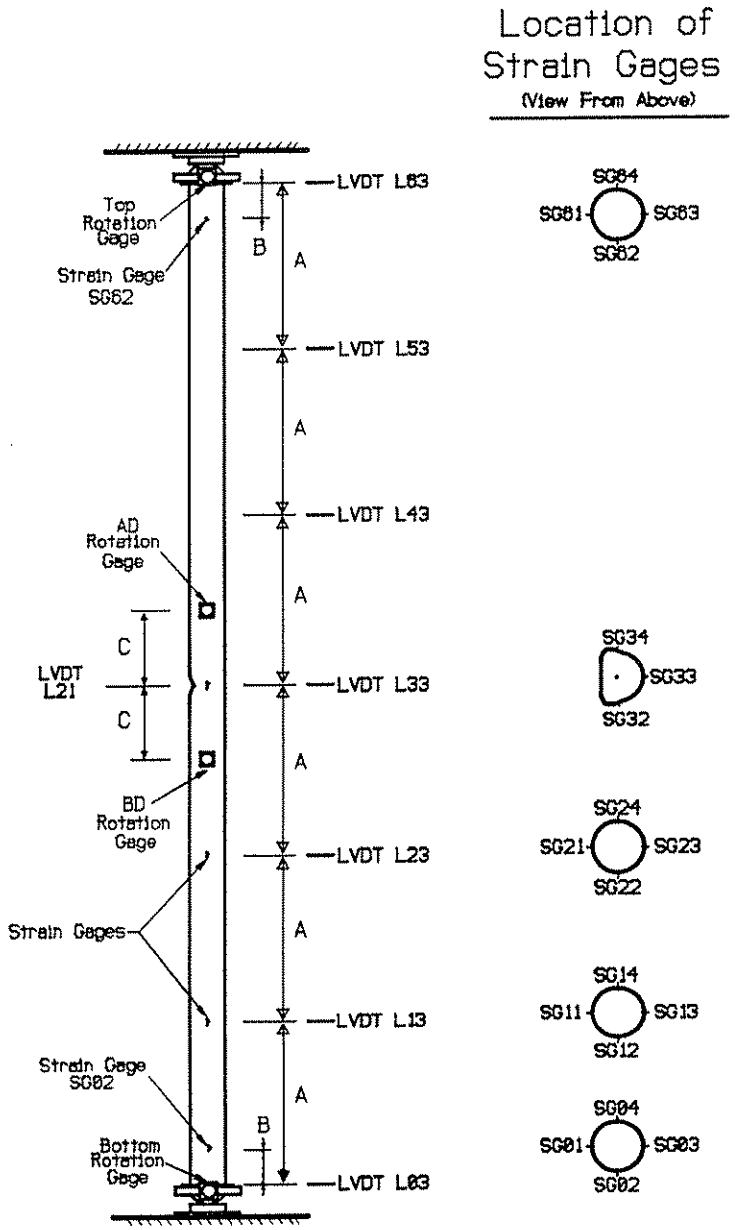

Specimen	Length	A	B	C
D1	24'-6"	49"	8"	22"
D3	28'-0"	56"	10.5"	28"
P1P	35'-4"	70.5"	10.5"	30"
P2P	34'-10"	70"	13.25"	35"
P3PA	34'-4"	69"	17"	48"
P3PB	34'-4"	69"	17"	48"
P4P	31'-4"	63"	13"	36"

Figure 7-2: Location of Gages for Fabricated Long-Column Specimens

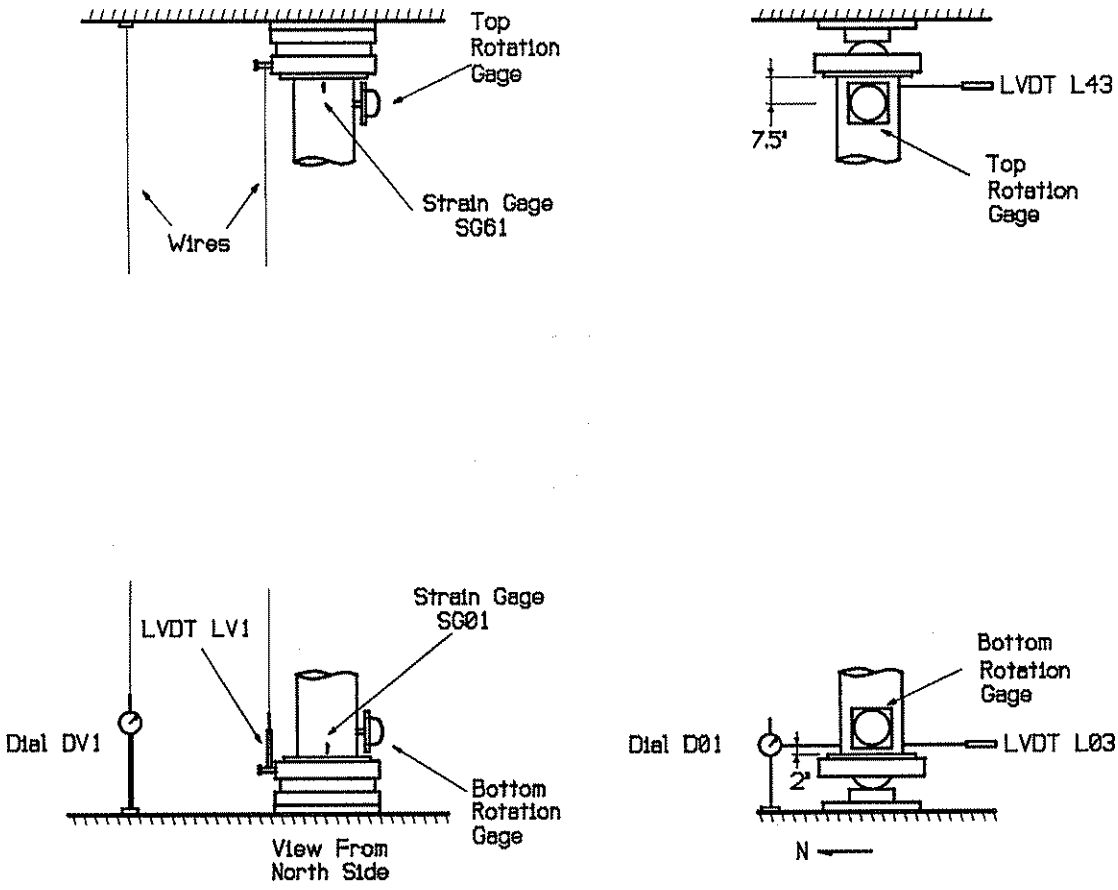

Figure 7-3: Location of Gages for Ends of Long-Column Specimens E1, B3 and E3

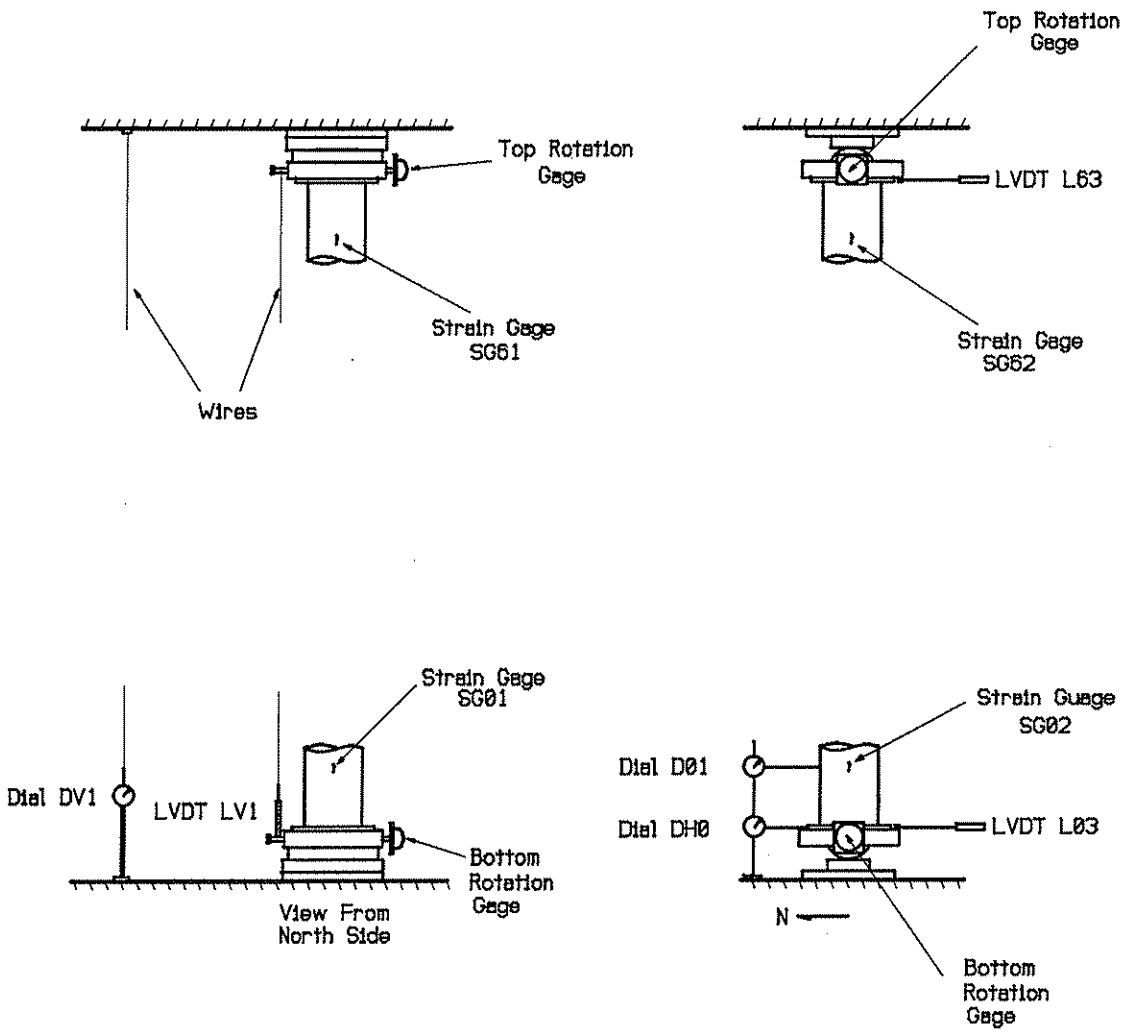

Figure 7-4: Location of Gages for Fabricated Pin-Ended Specimens

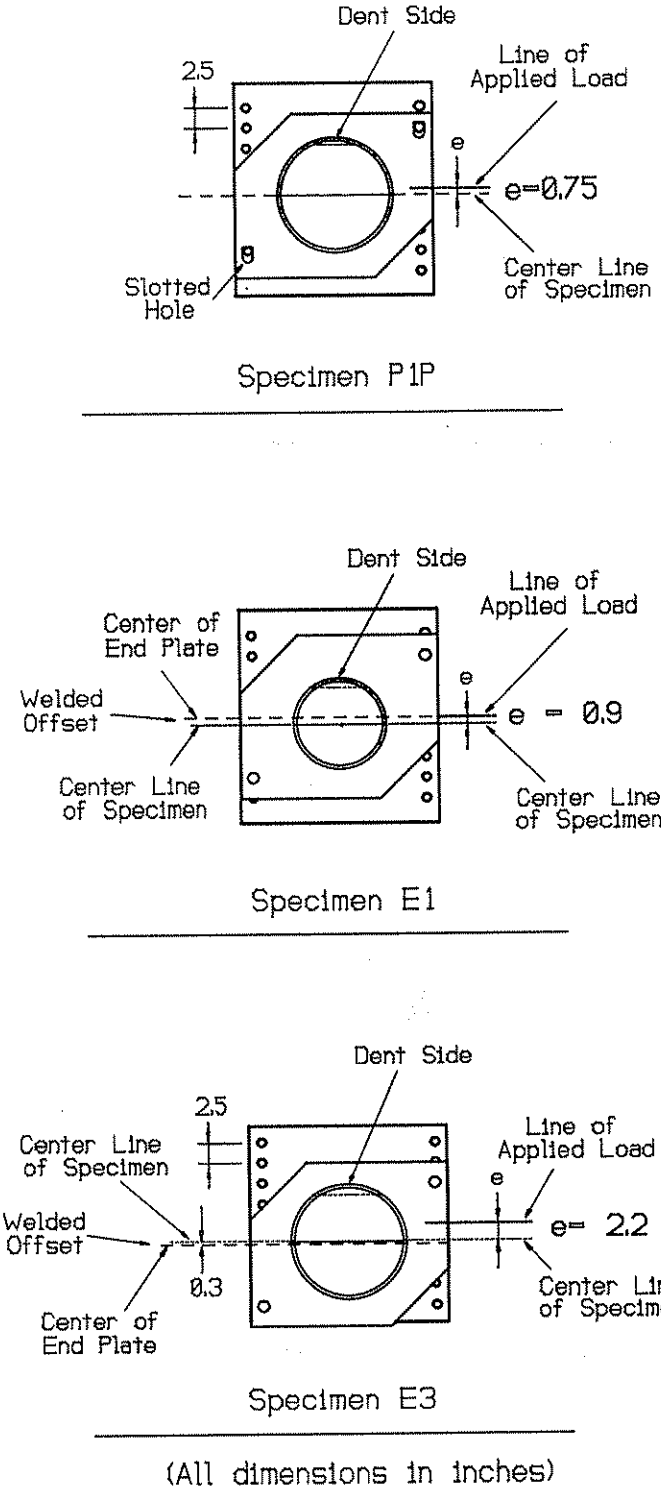

Figure 7-5: Geometric End Eccentricity for Long-Columns Specimens – P1P, E1 and E3

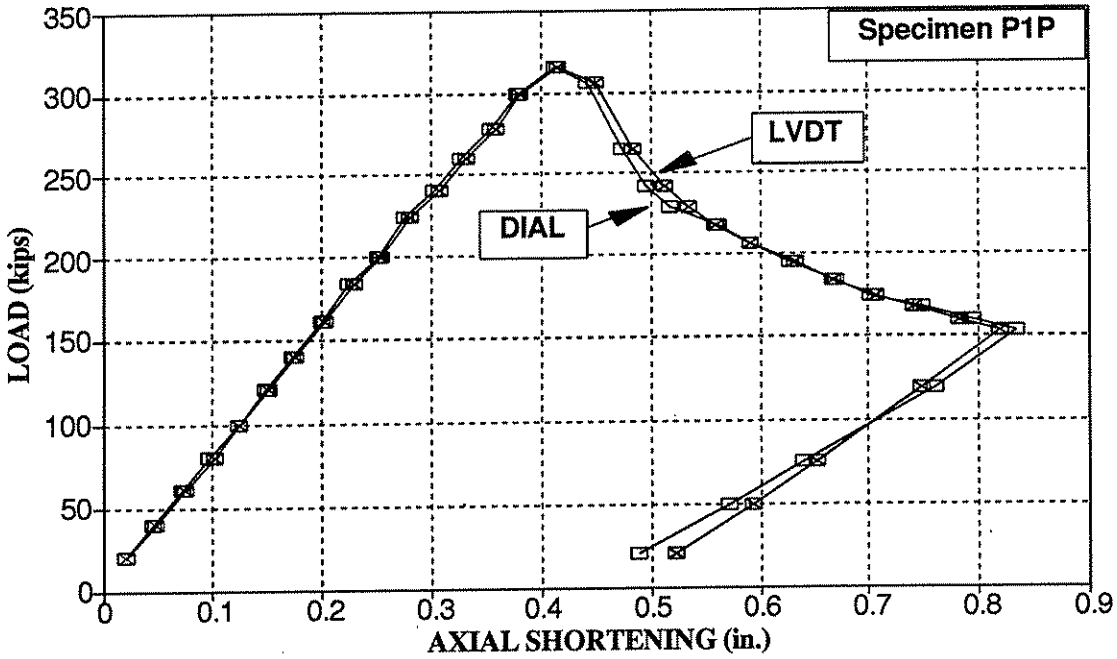

Figure 7-6: Specimen P1P – Axial Shortening

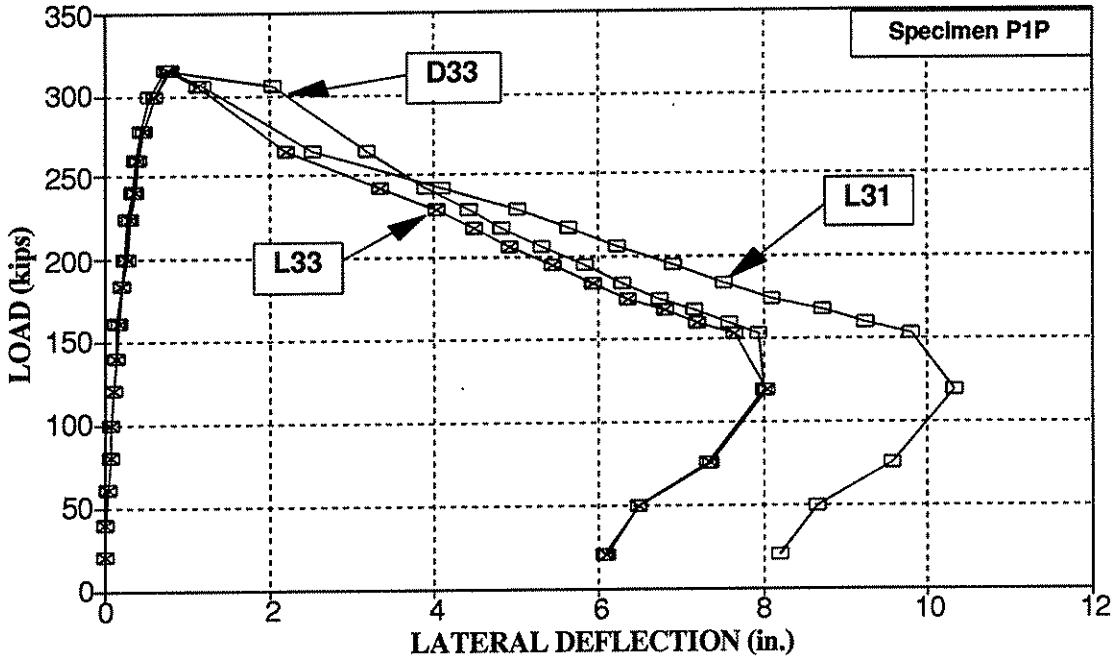

Figure 7-7: Specimen P1P – Lateral Deflection at Mid-Length

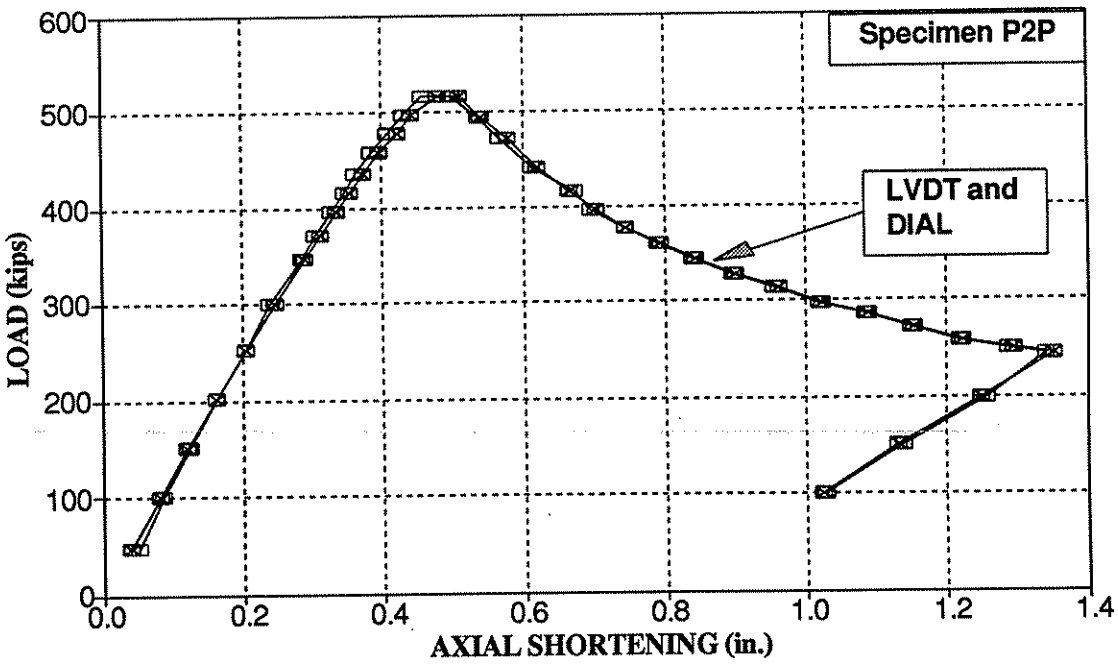

Figure 7-8: Specimen P2P – Axial Shortening

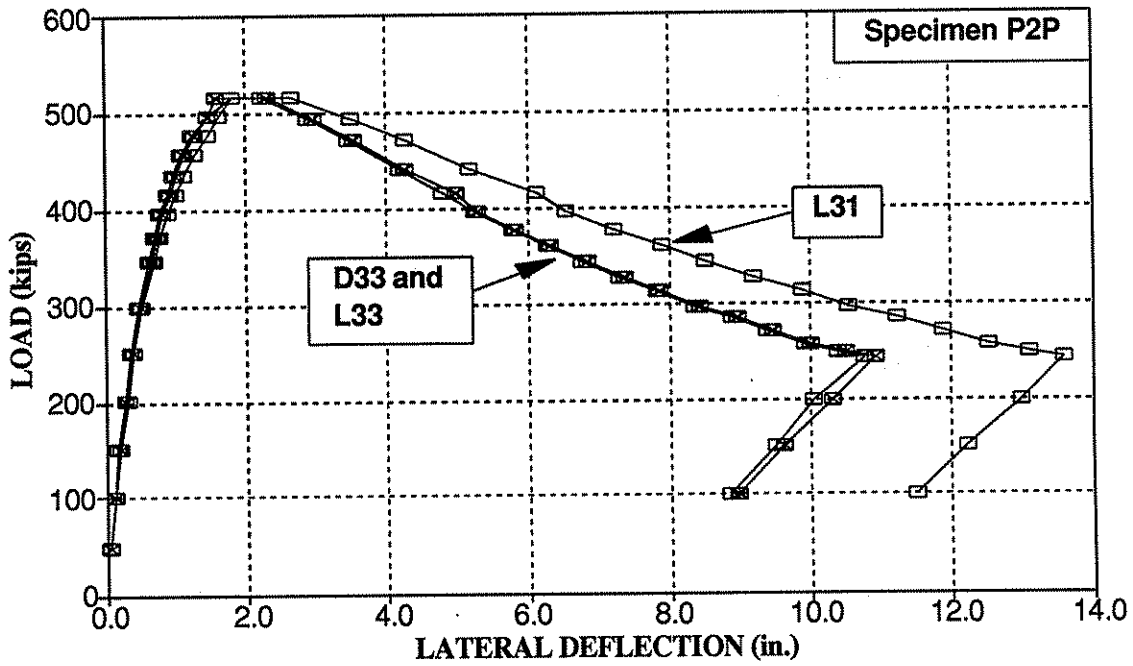

Figure 7-9: Specimen P2P – Lateral Deflection at Mid-Length

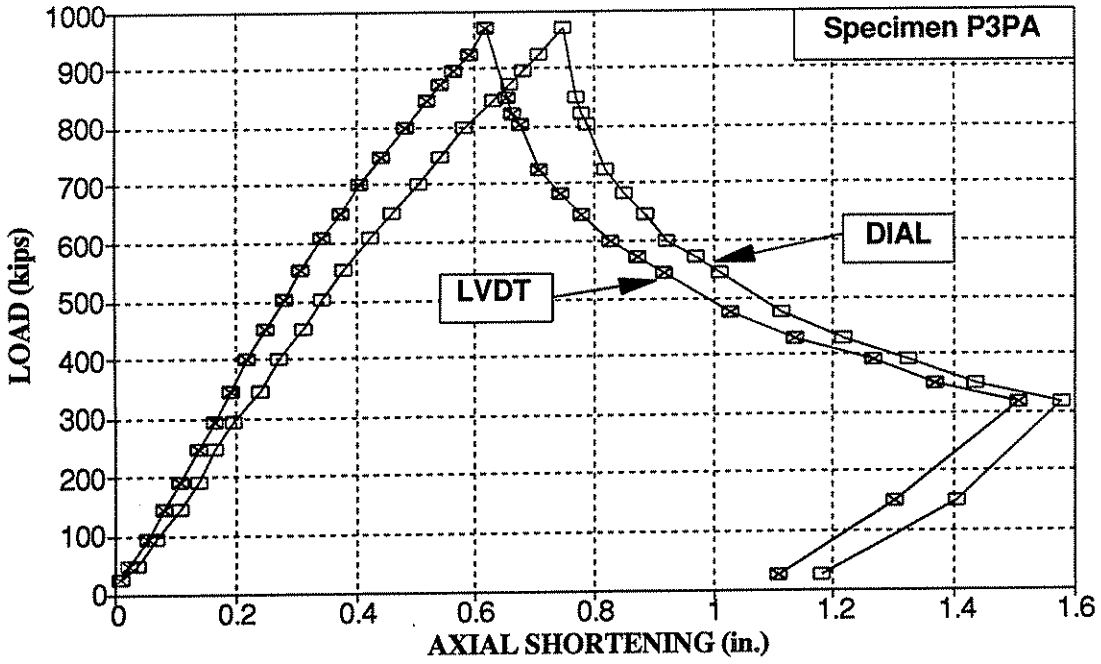

Figure 7-10: Specimen P3PA – Axial Shortening

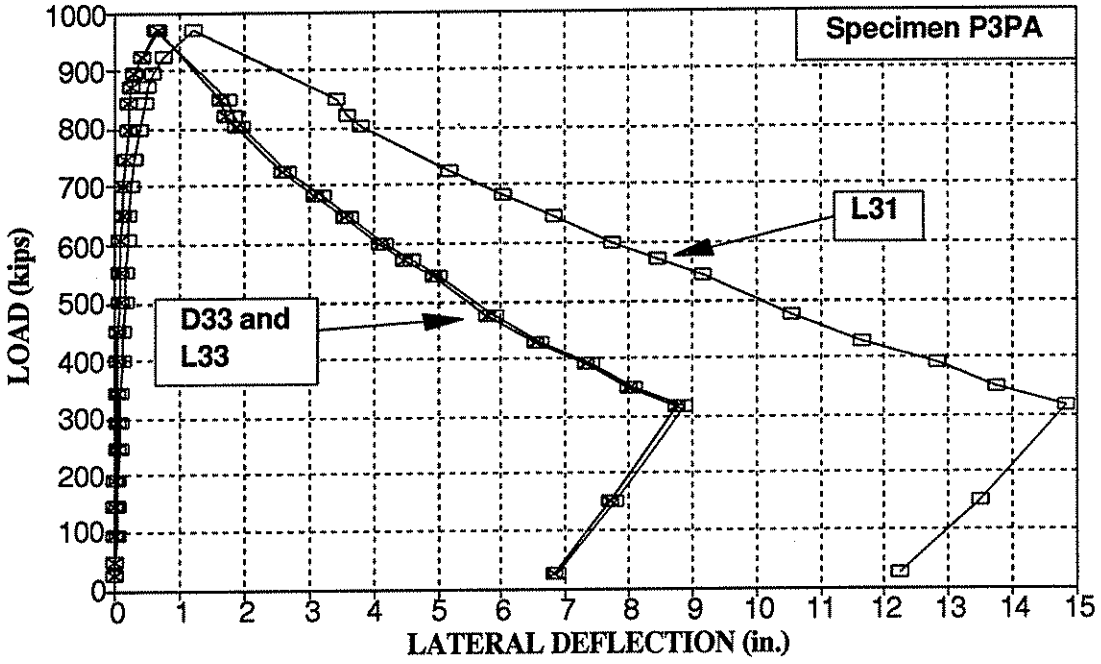

Figure 7-11: Specimen P3PA – Lateral Deflection at Mid-Length

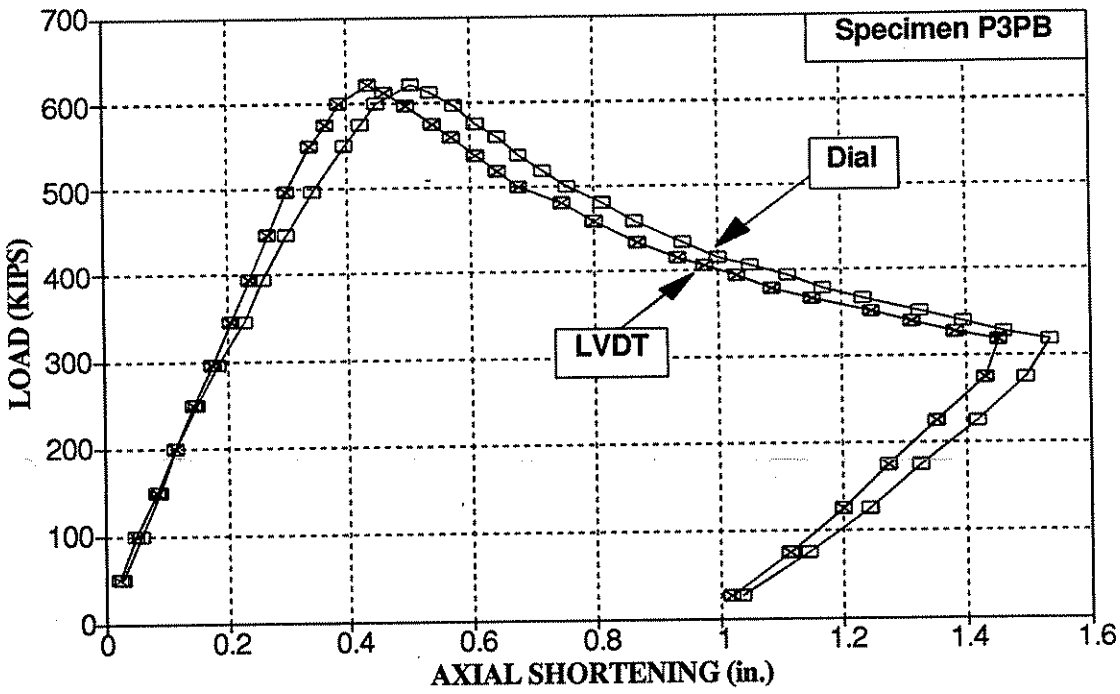

Figure 7-12: Specimen P3PB – Axial Shortening

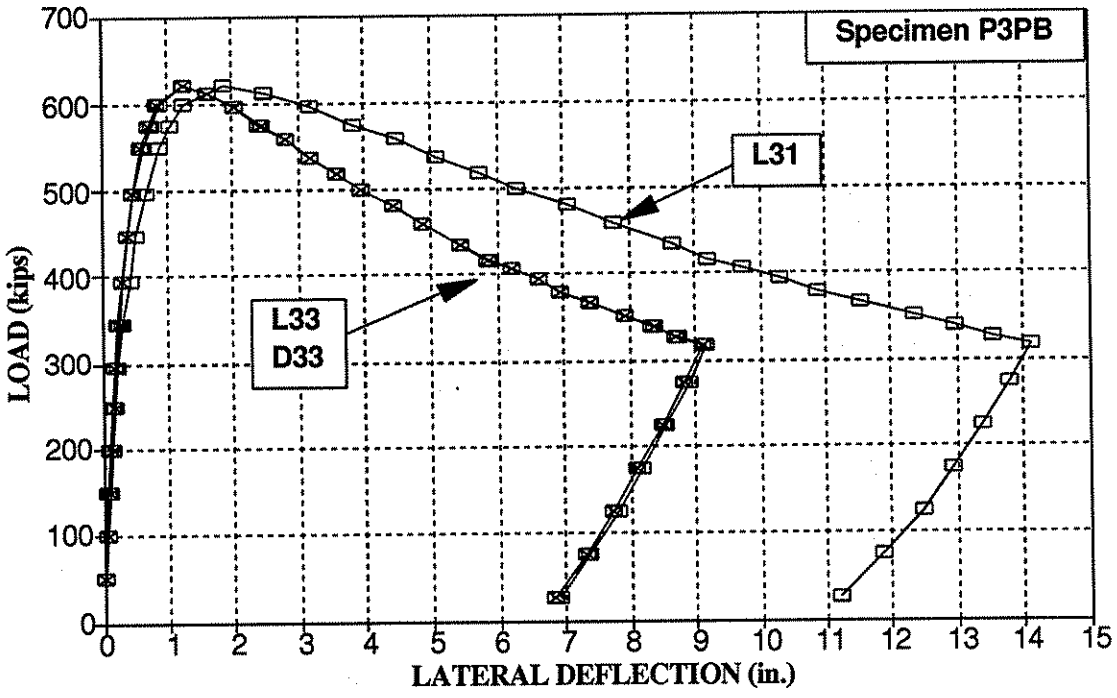

Figure 7-13: Specimen P3PB – Lateral Deflection at Mid-Length

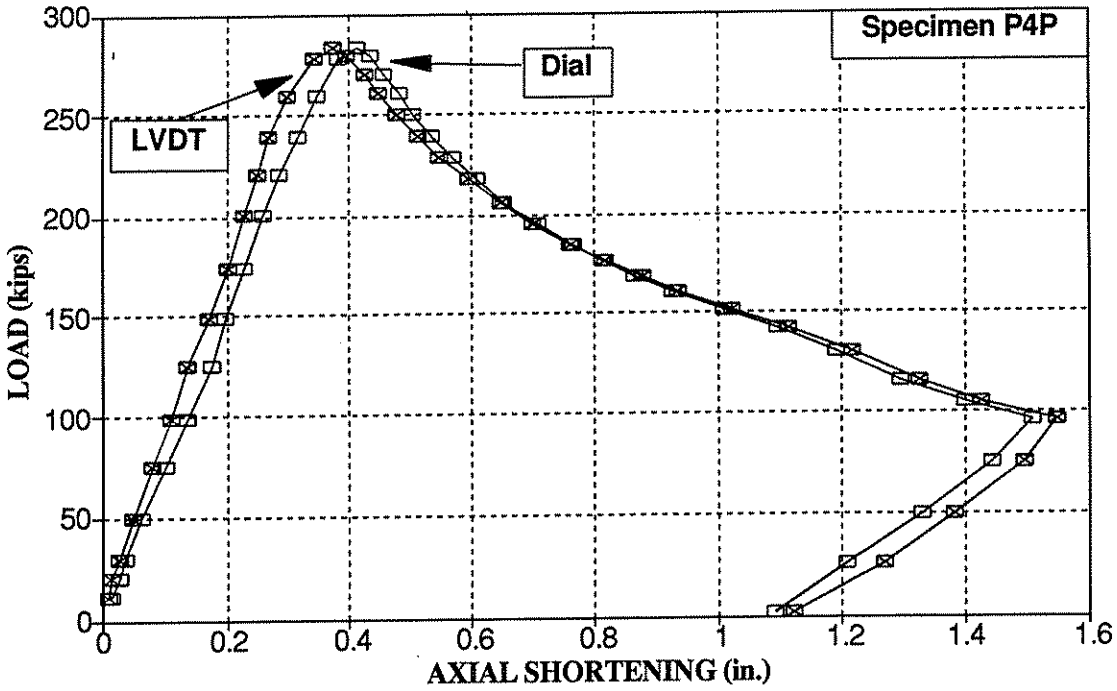

Figure 7-14: Specimen P4P – Axial Shortening

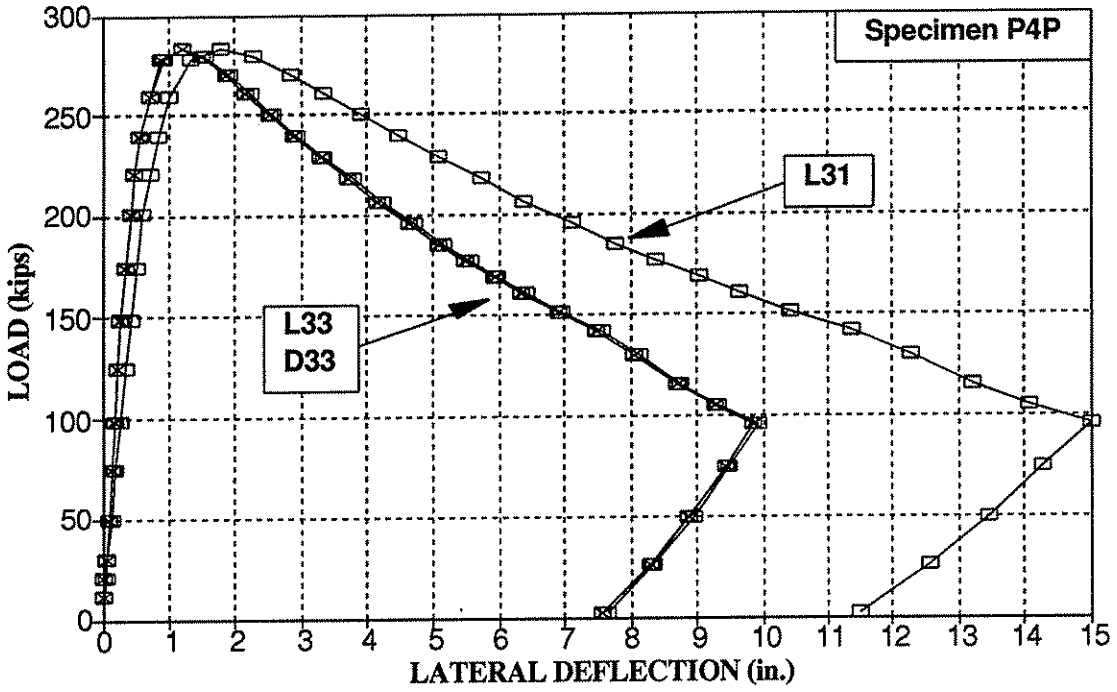

Figure 7-15: Specimen P4P – Lateral Deflection at Mid-Length

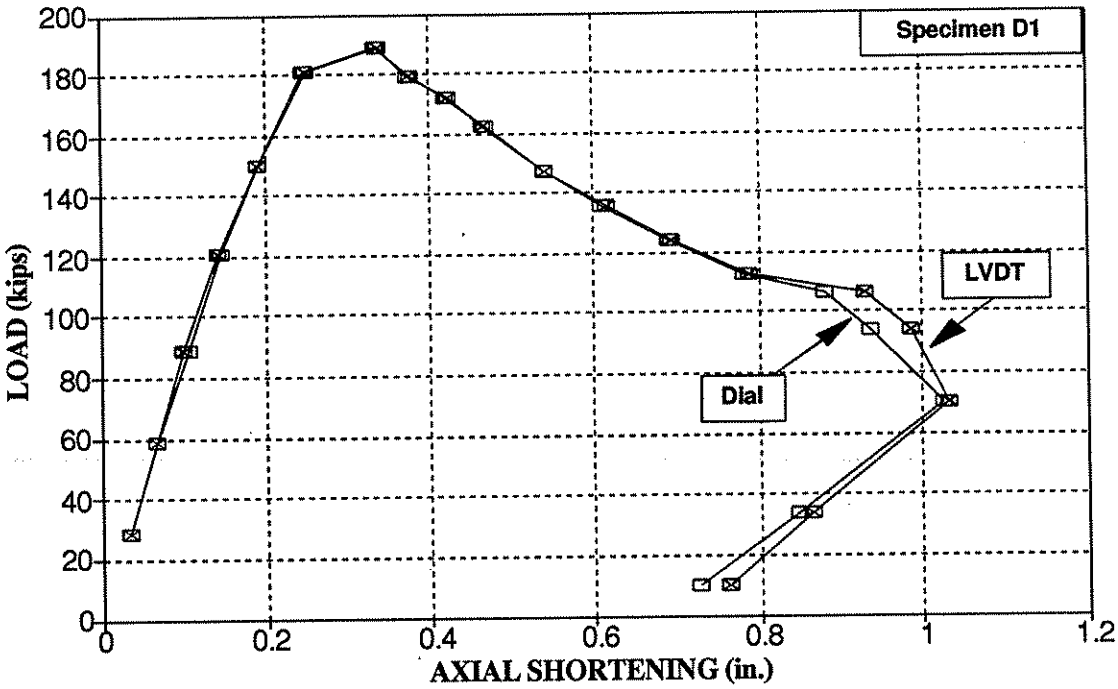

Figure 7-16: Specimen D1 – Axial Shortening

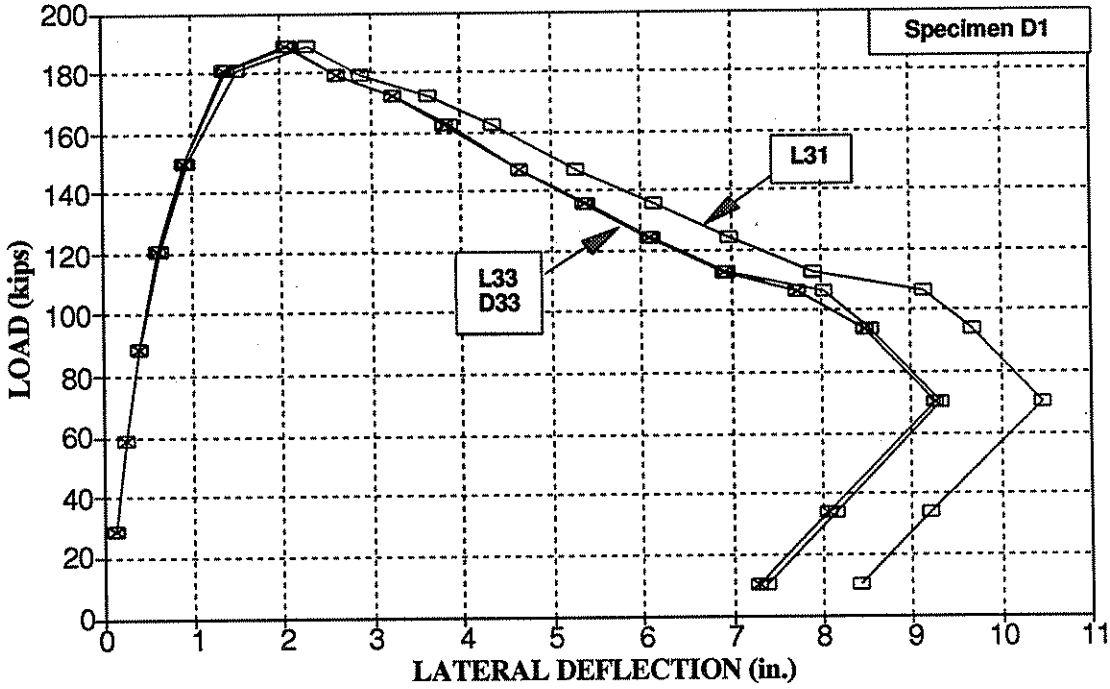

Figure 7-17: Specimen D1 – Lateral Deflection at Mid-Length

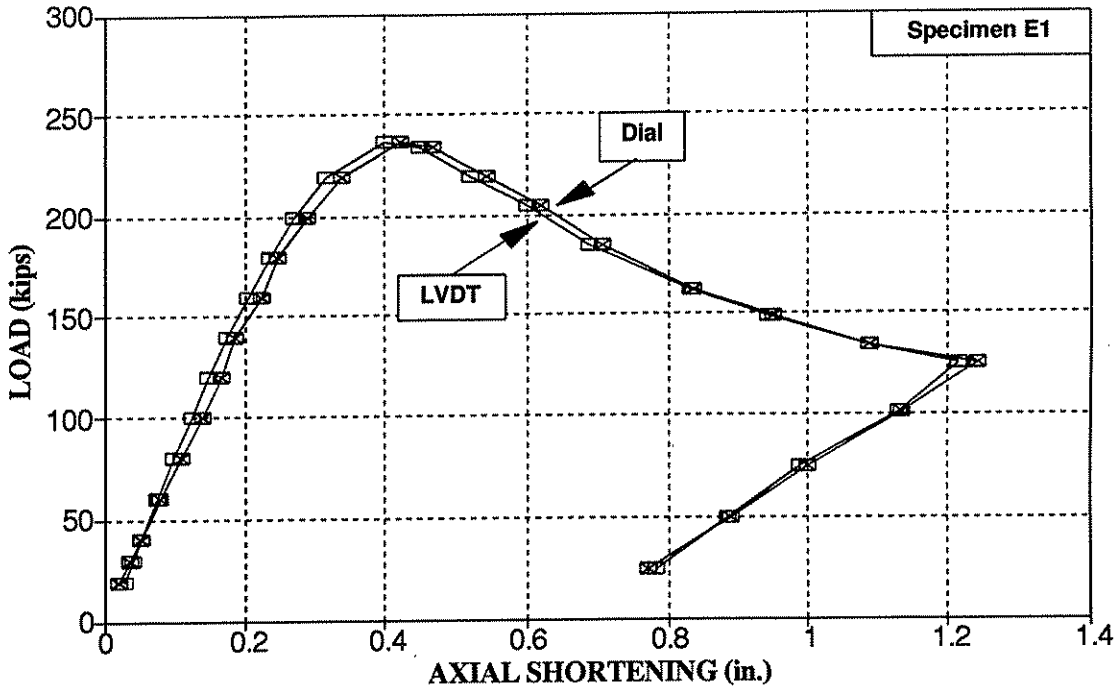

Figure 7-18: Specimen E1 – Axial Shortening

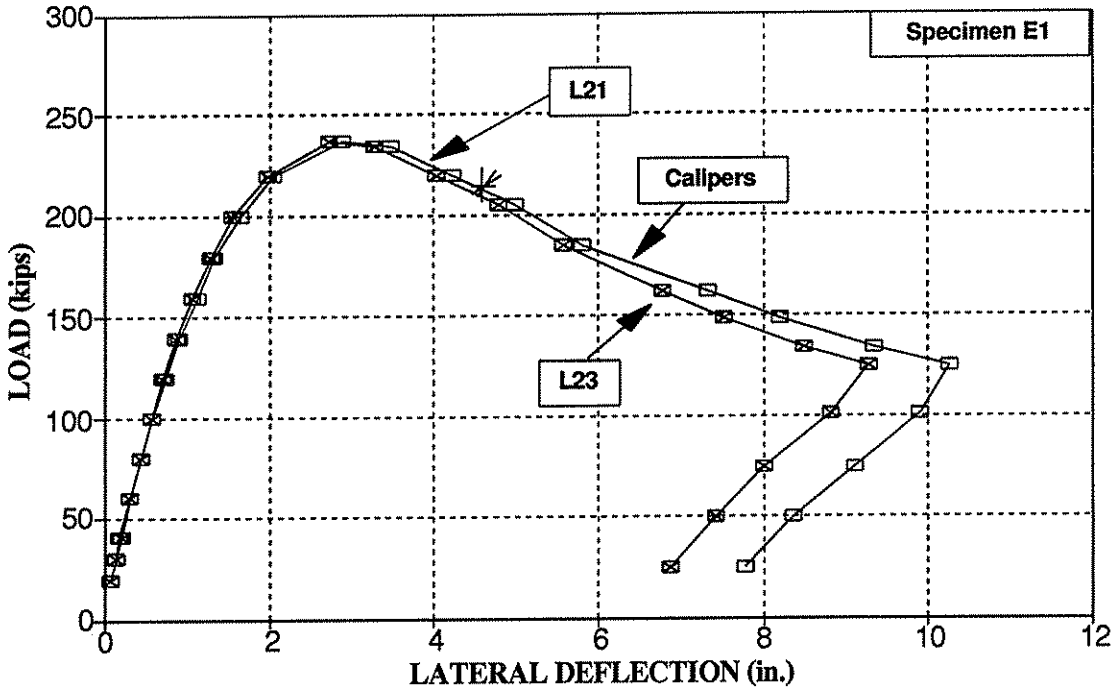

Figure 7-19: Specimen E1 – Lateral Deflection at Mid-Length

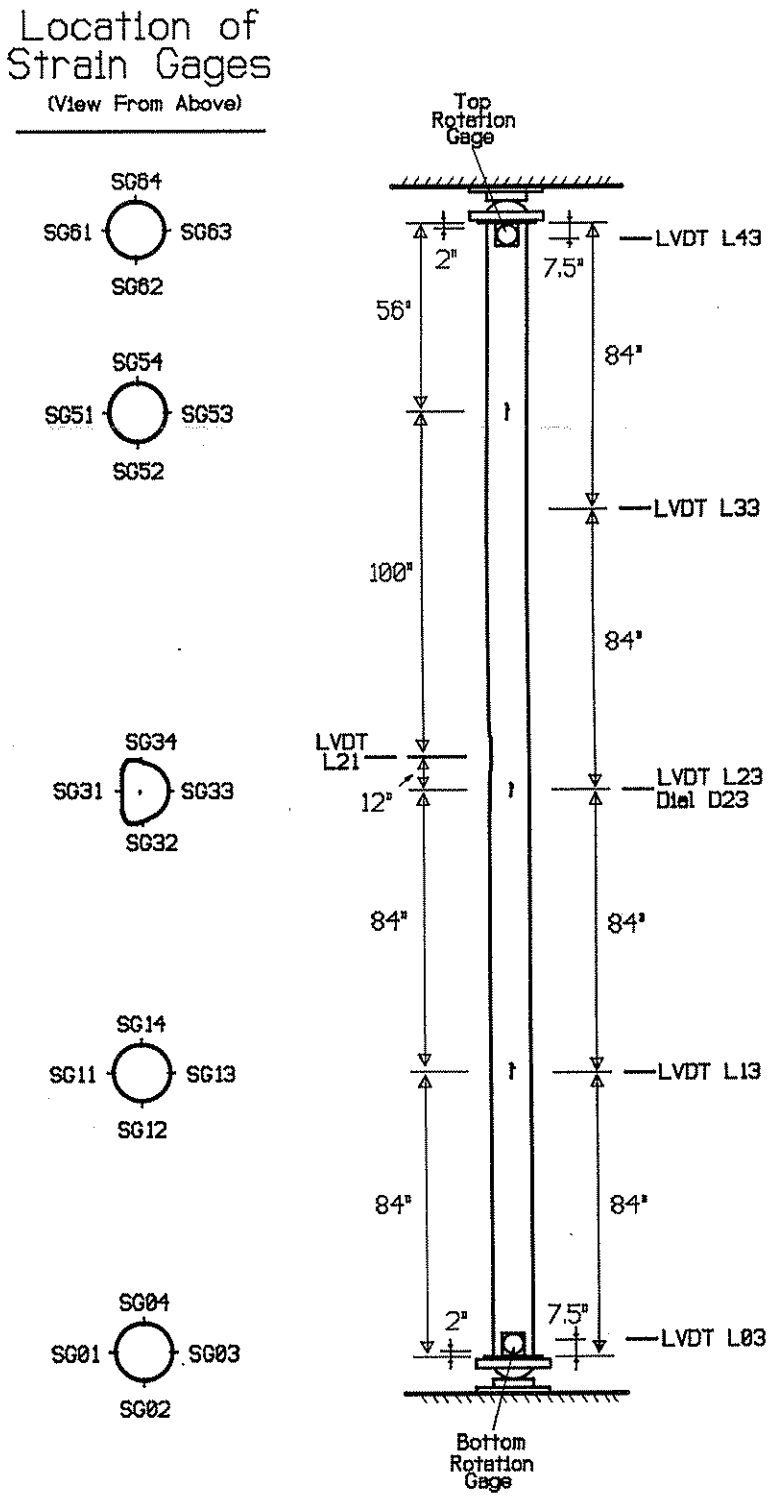

Figure 7-20: Specimen B3 – Location of Gages

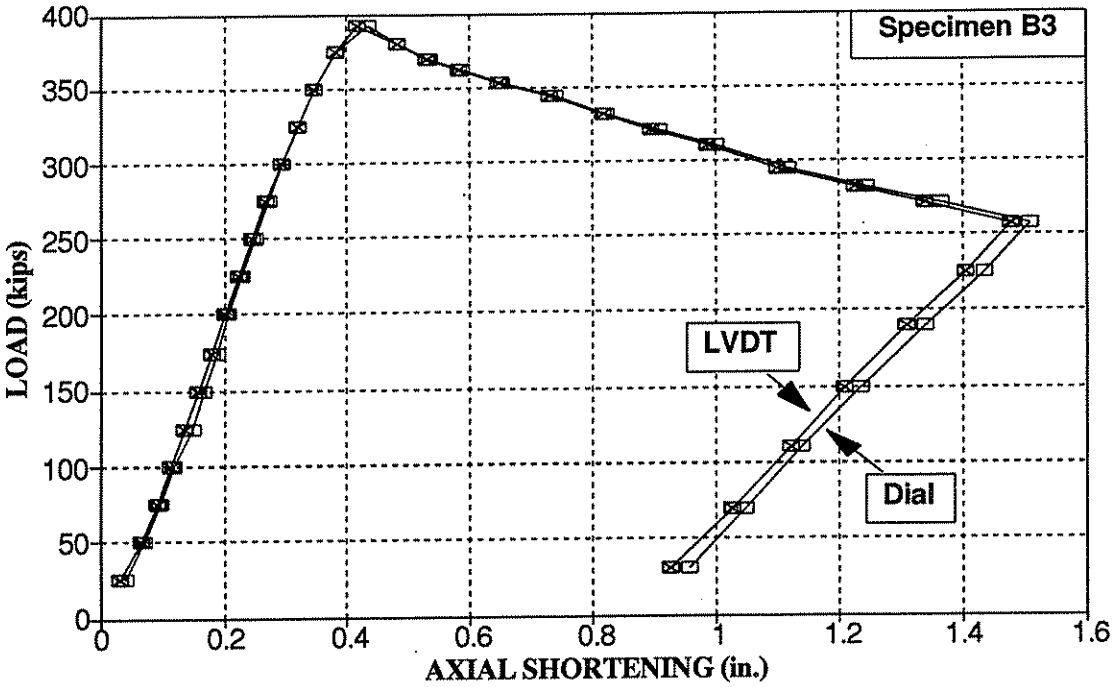

Figure 7-21: Specimen B3 – Axial Shortening

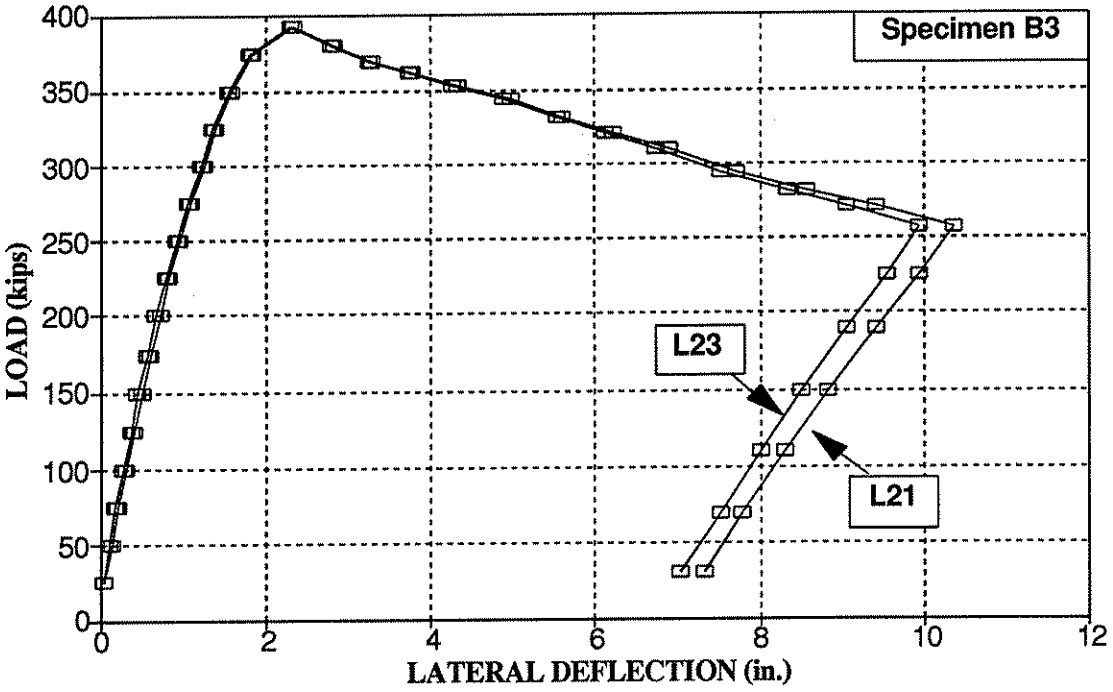

Figure 7-22: Specimen B3 – Lateral Deflection at Mid-Length

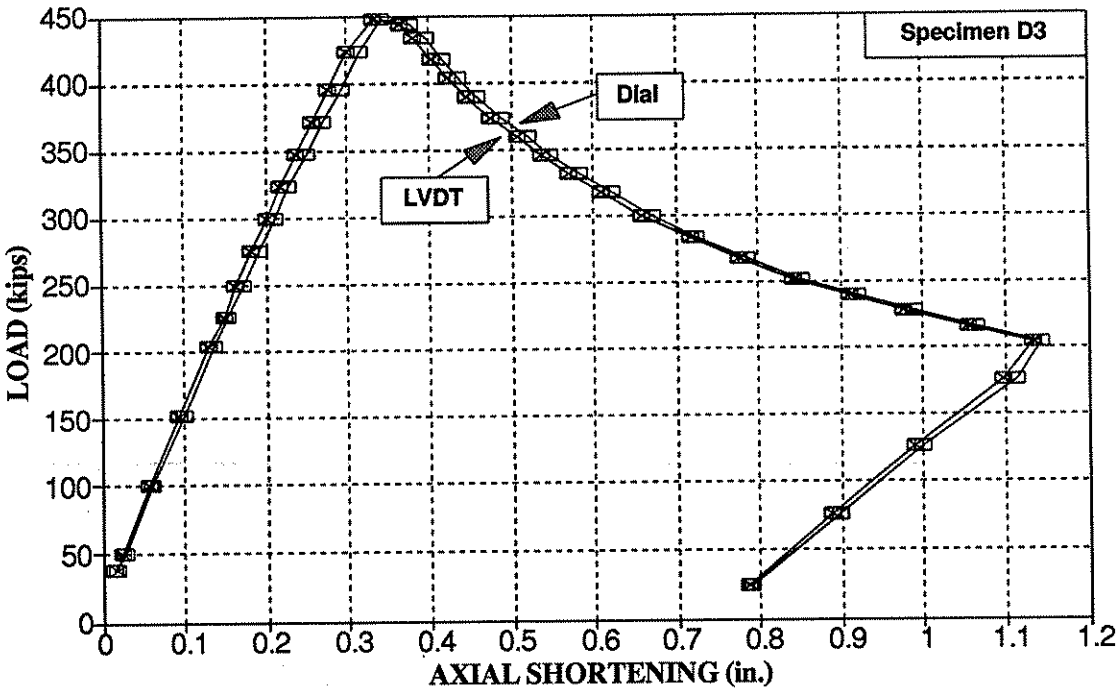

Figure 7-23: Specimen D3 – Axial Shortening

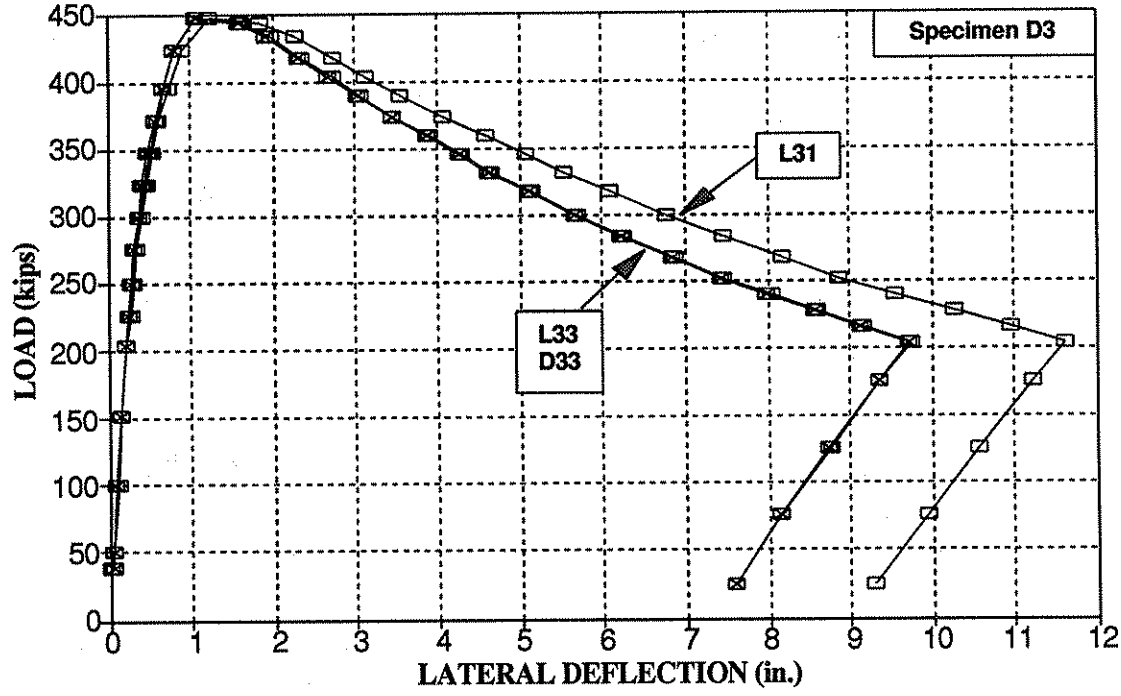

Figure 7-24: Specimen D3 – Lateral Deflection at Mid-Length

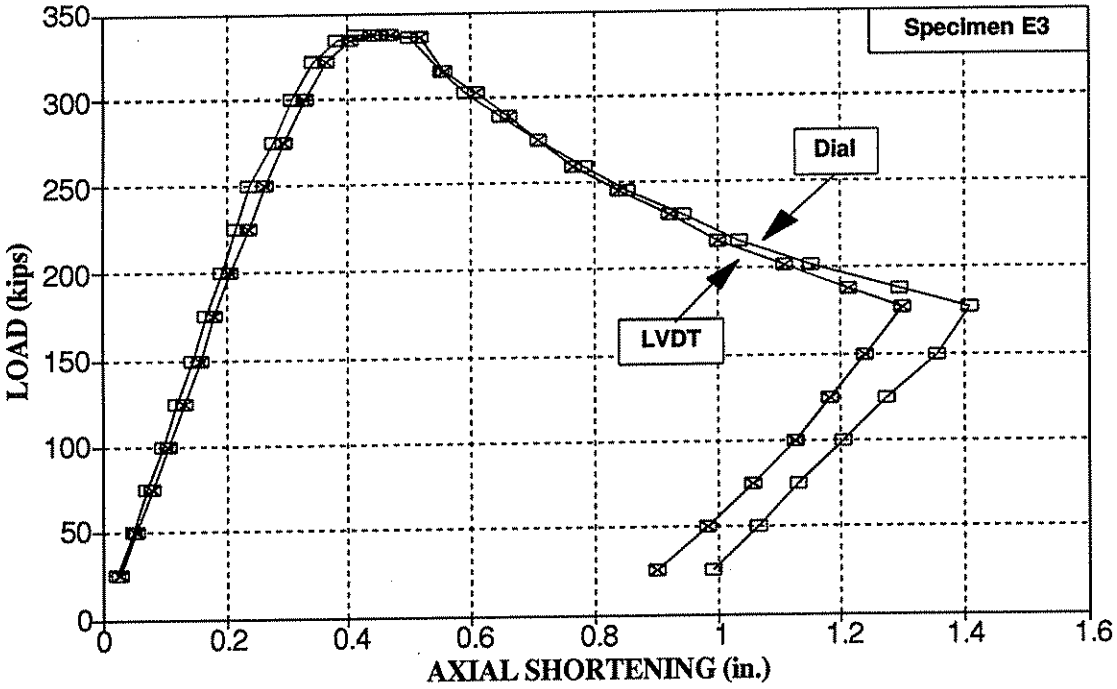

Figure 7-25: Specimen E3 – Axial Shortening

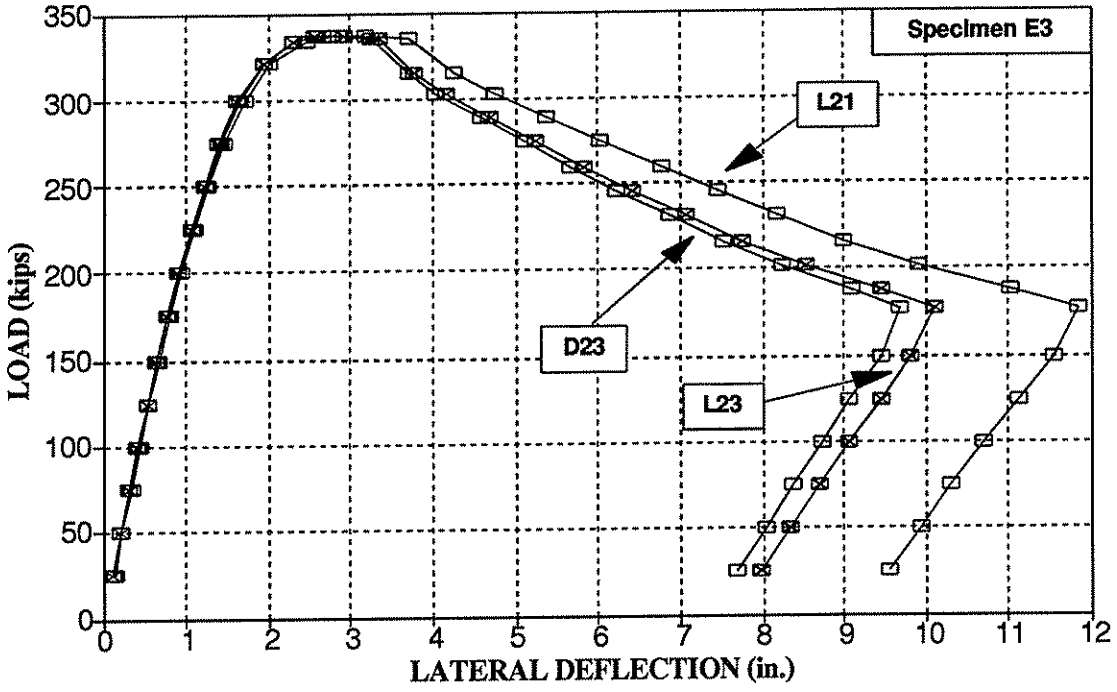

Figure 7-26: Specimen E3 – Lateral Deflection at Mid-Length

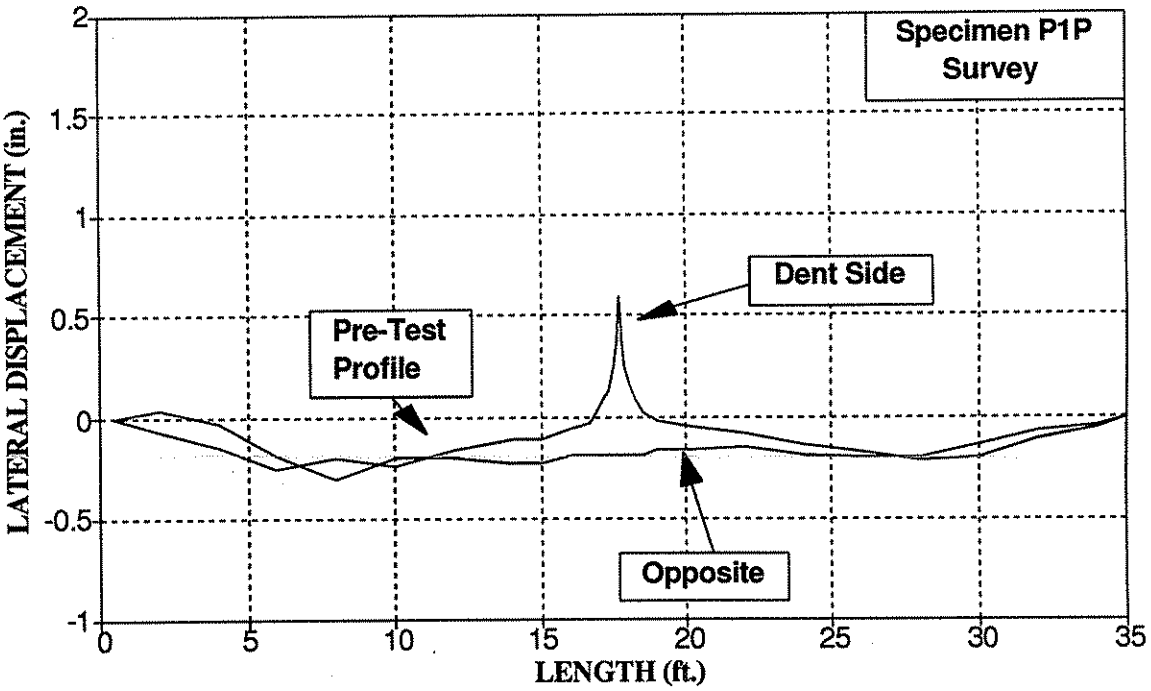

Figure 7-27: Specimen P1P – Pre-Test Surface Profile

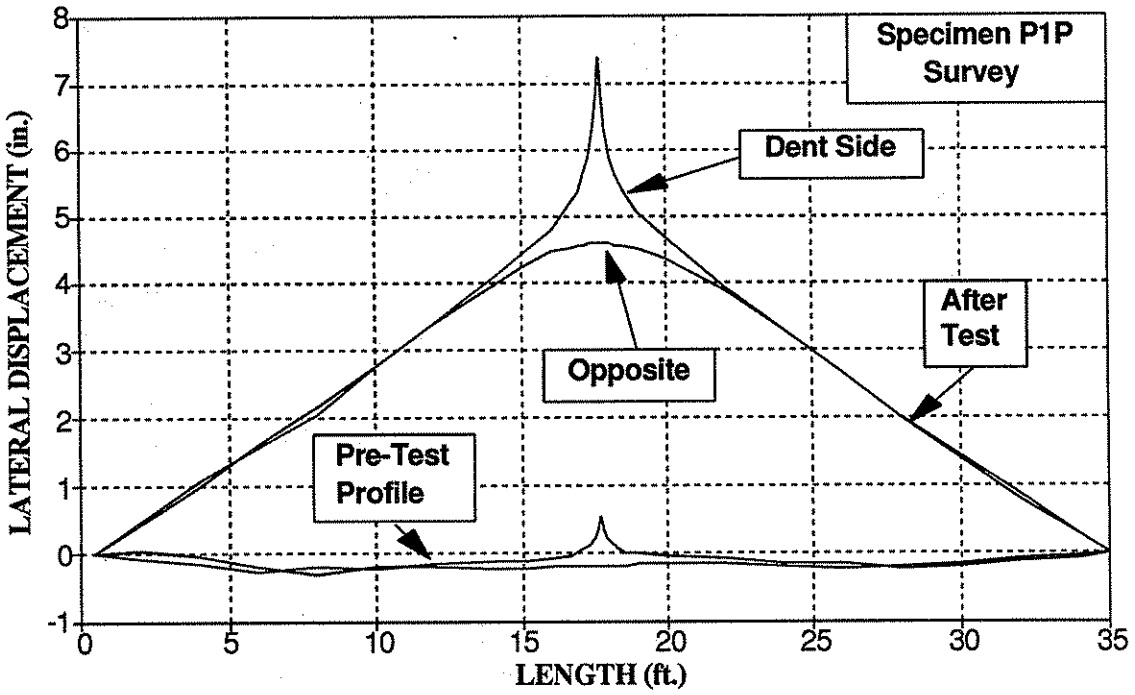

Figure 7-28: Specimen P1P – Pre- and Post-Test Surface Profiles

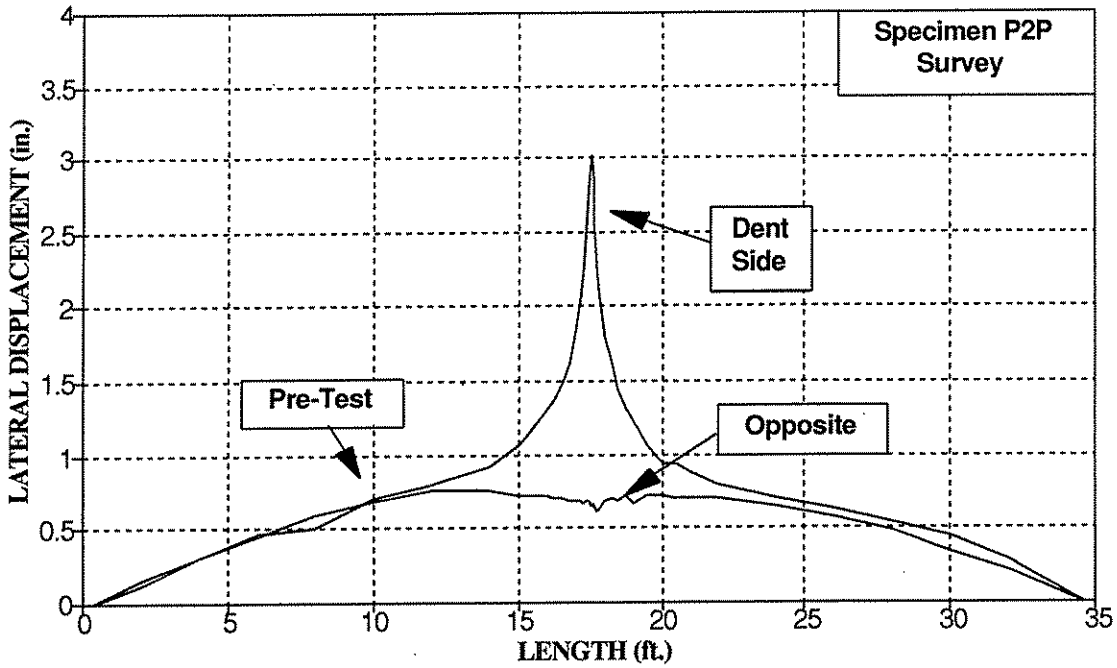

Figure 7-29: Specimen P2P – Pre-Test Surface Profile

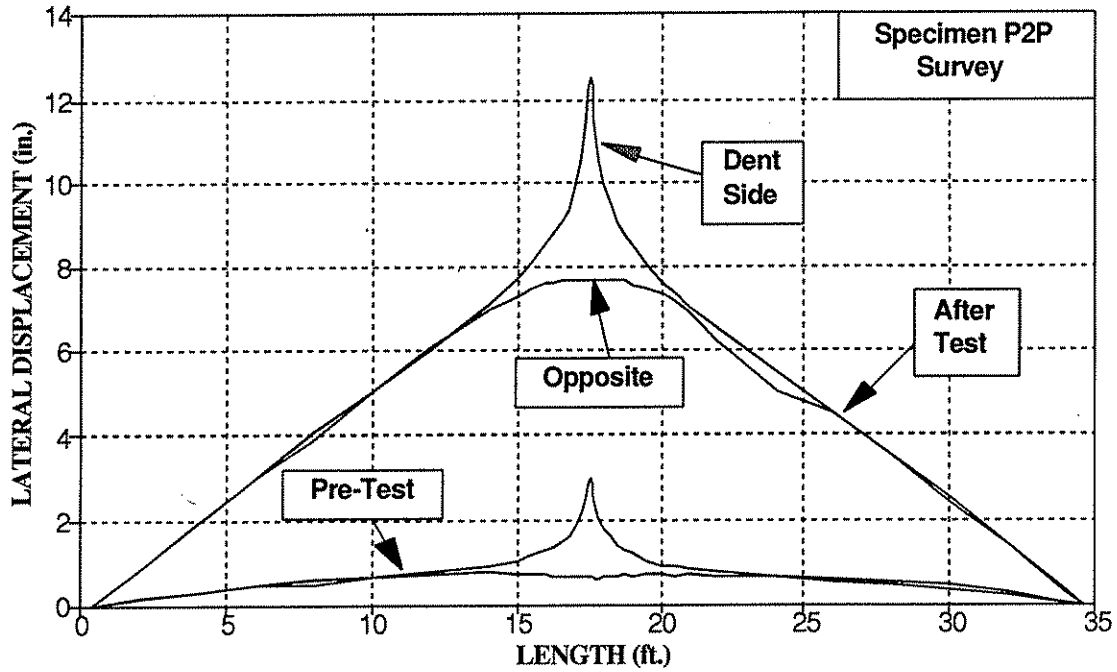

Figure 7-30: Specimen P2P – Pre- and Post-Test Surface Profiles

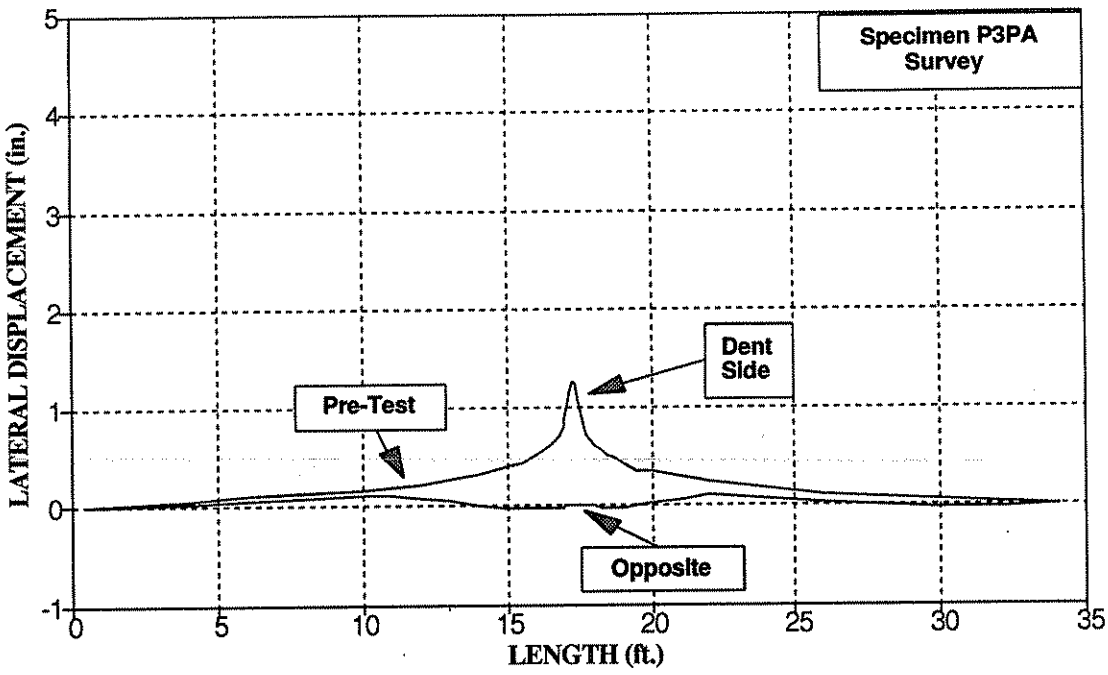

Figure 7-31: Specimen P3PA – Pre-Test Surface Profile

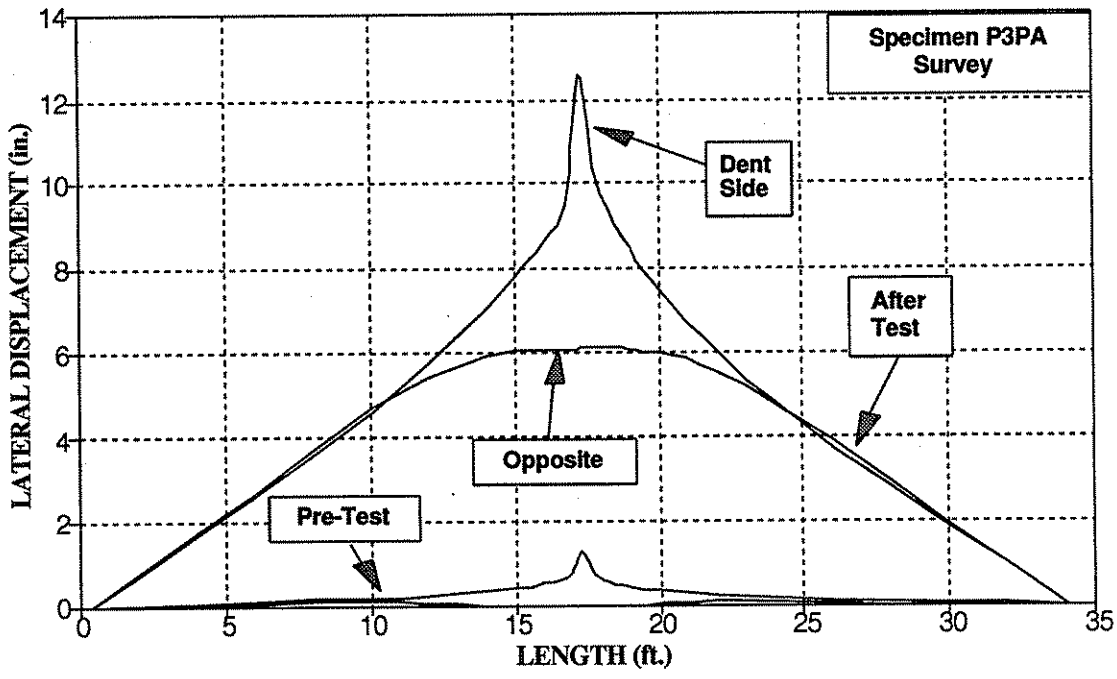

Figure 7-32: Specimen P3PA – Pre- and Post-Test Surface Profiles

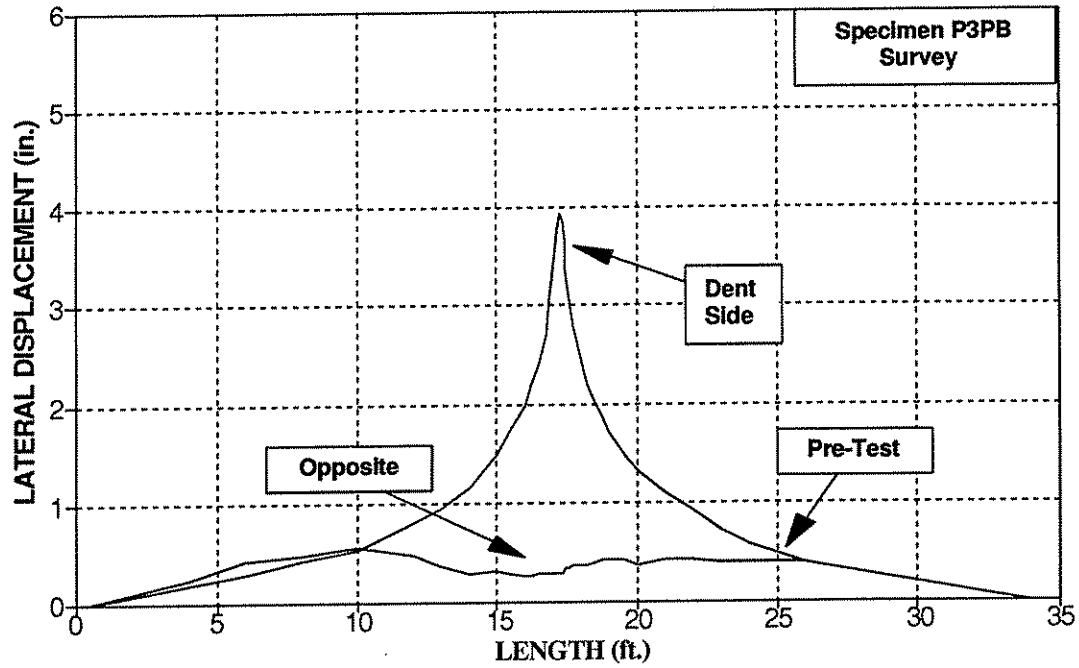

Figure 7-33: Specimen P3PB – Pre-Test Surface Profile

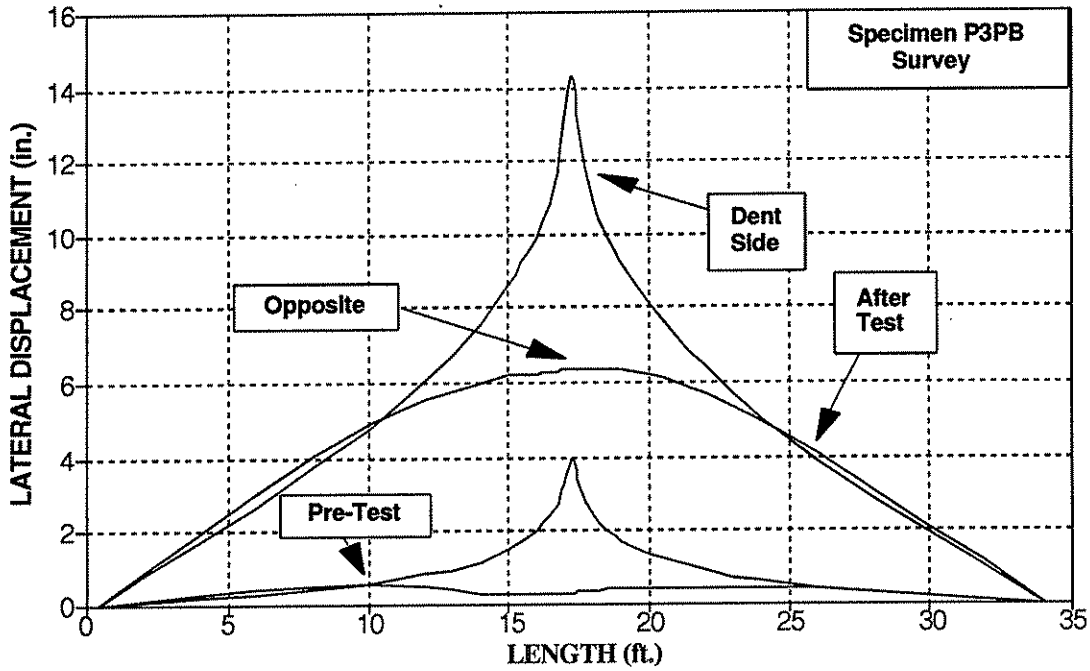

Figure 7-34: Specimen P3PB – Pre- and Post-Test Surface Profiles

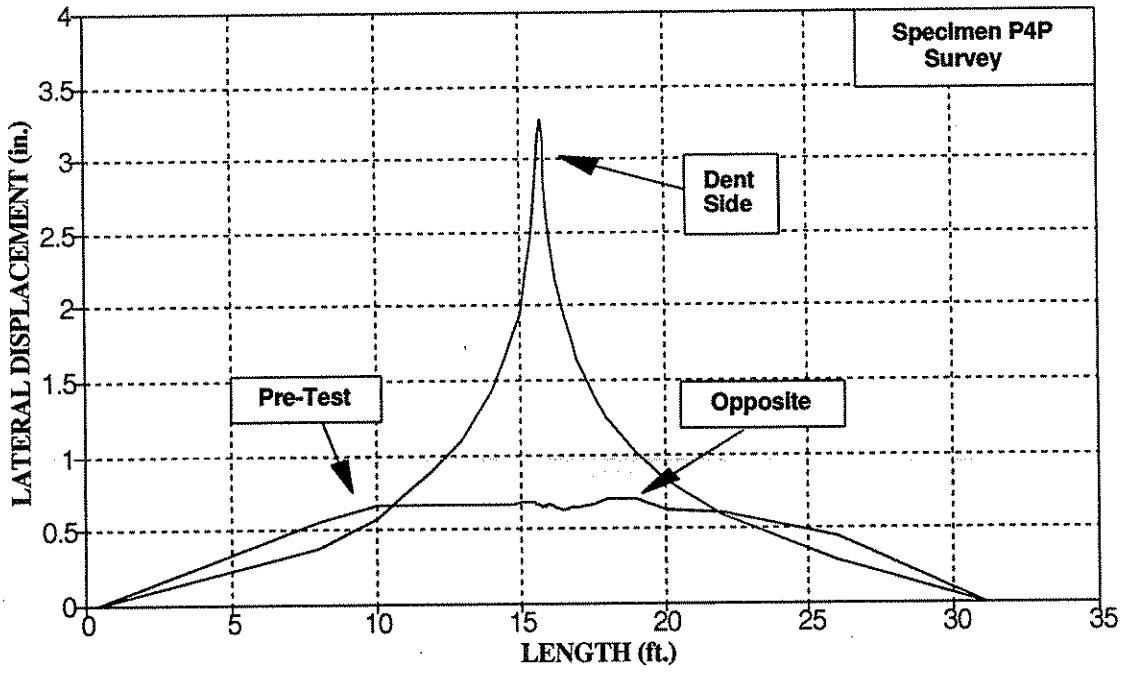

Figure 7-35: Specimen P4P – Pre-Test Surface Profile

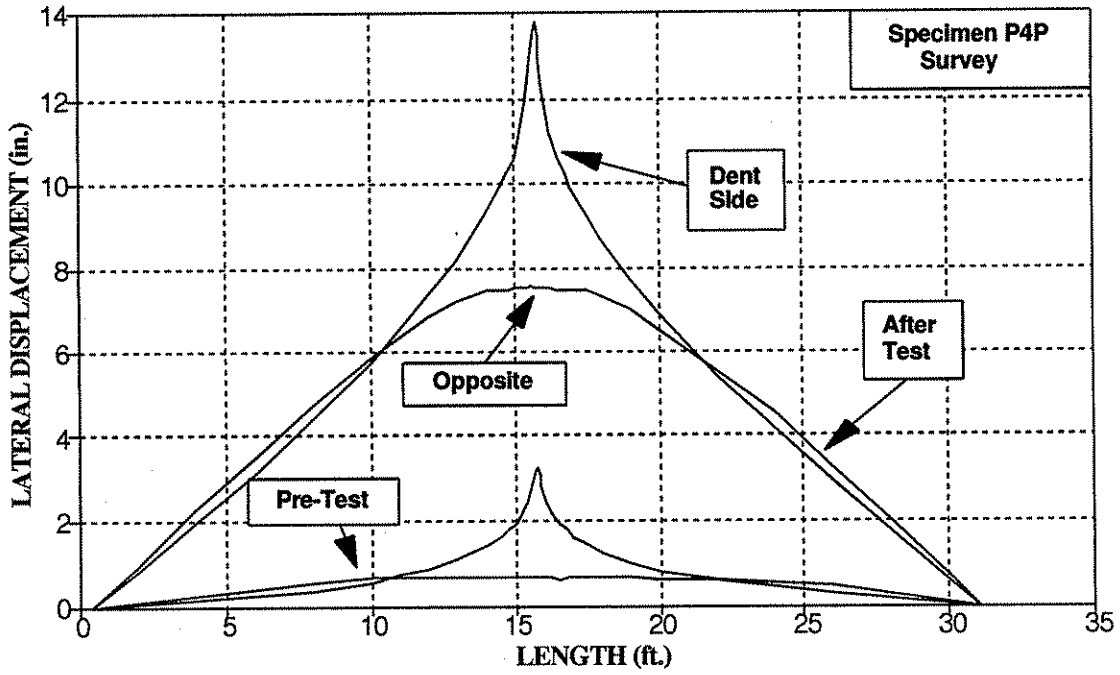

Figure 7-36: Specimen P4P – Pre- and Post-Test Surface Profiles

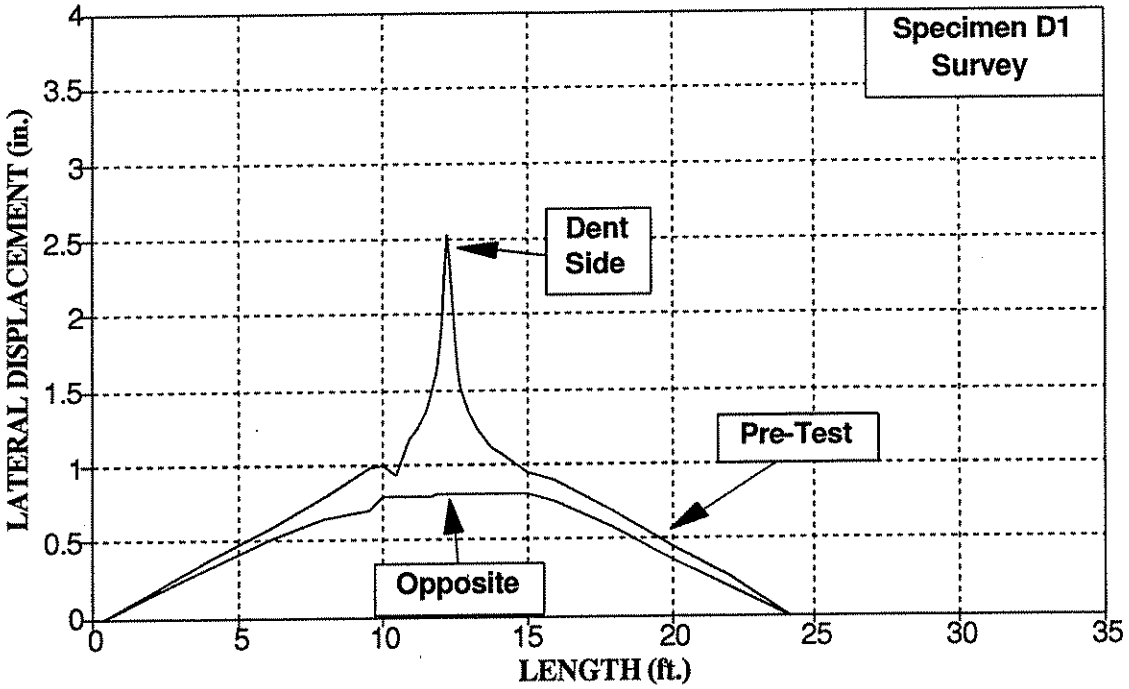

Figure 7-37: Specimen D1 – Pre-Test Surface Profile

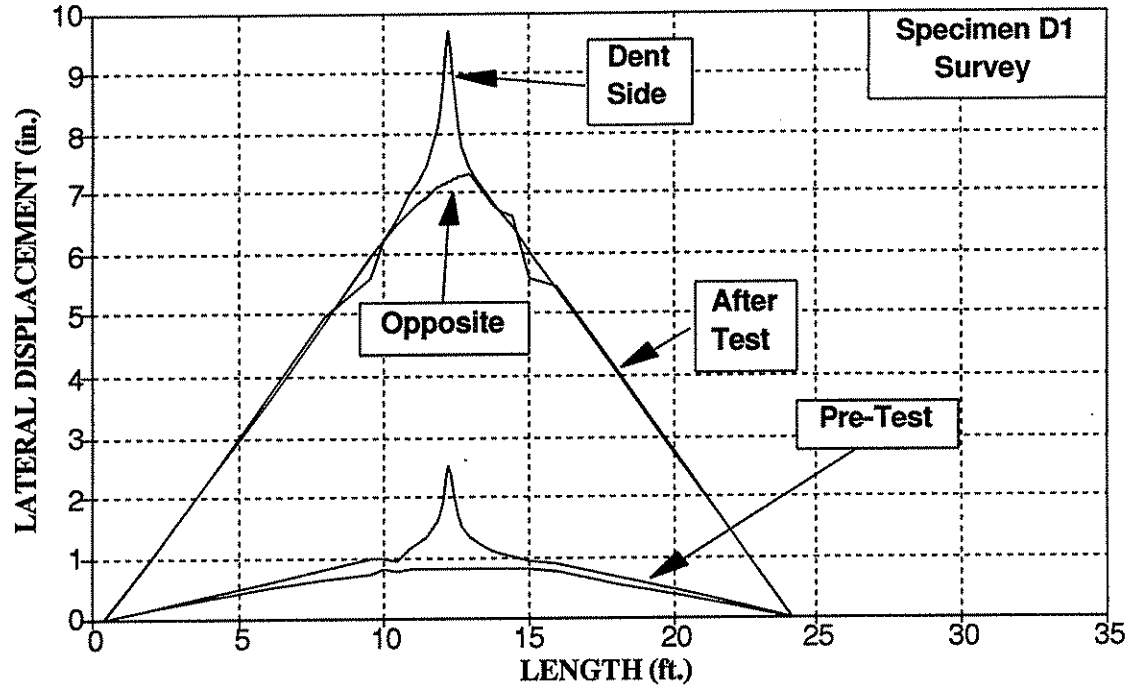

Figure 7-38: Specimen D1 – Pre- and Post-Test Surface Profiles

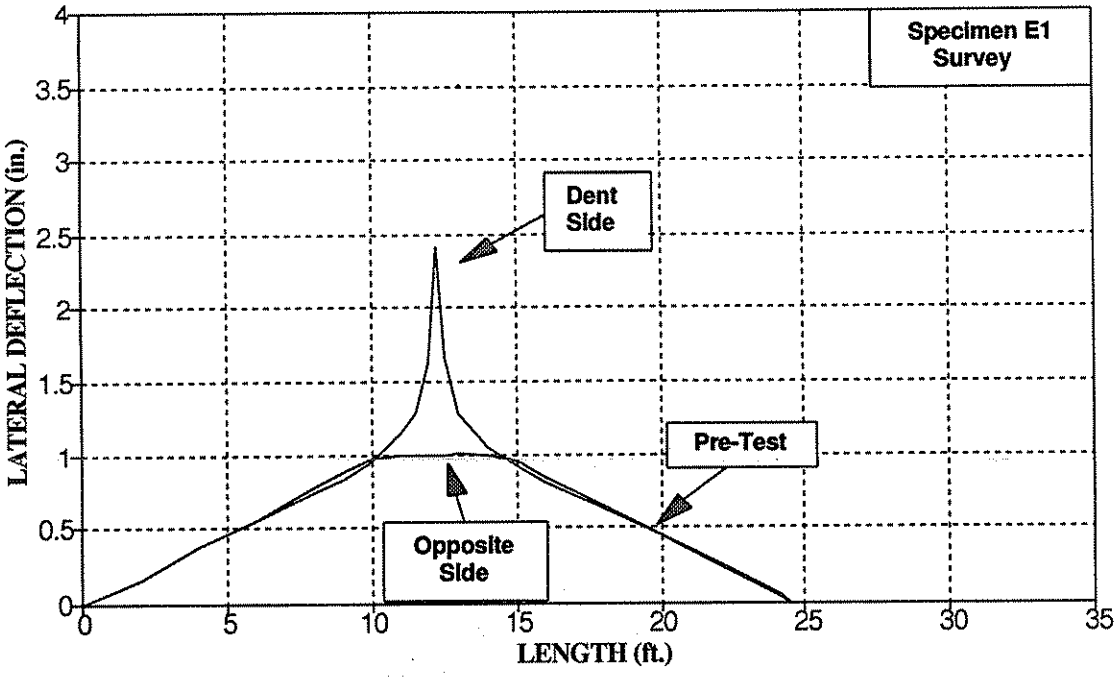

Figure 7-39: Specimen E1 – Pre-Test Surface Profile

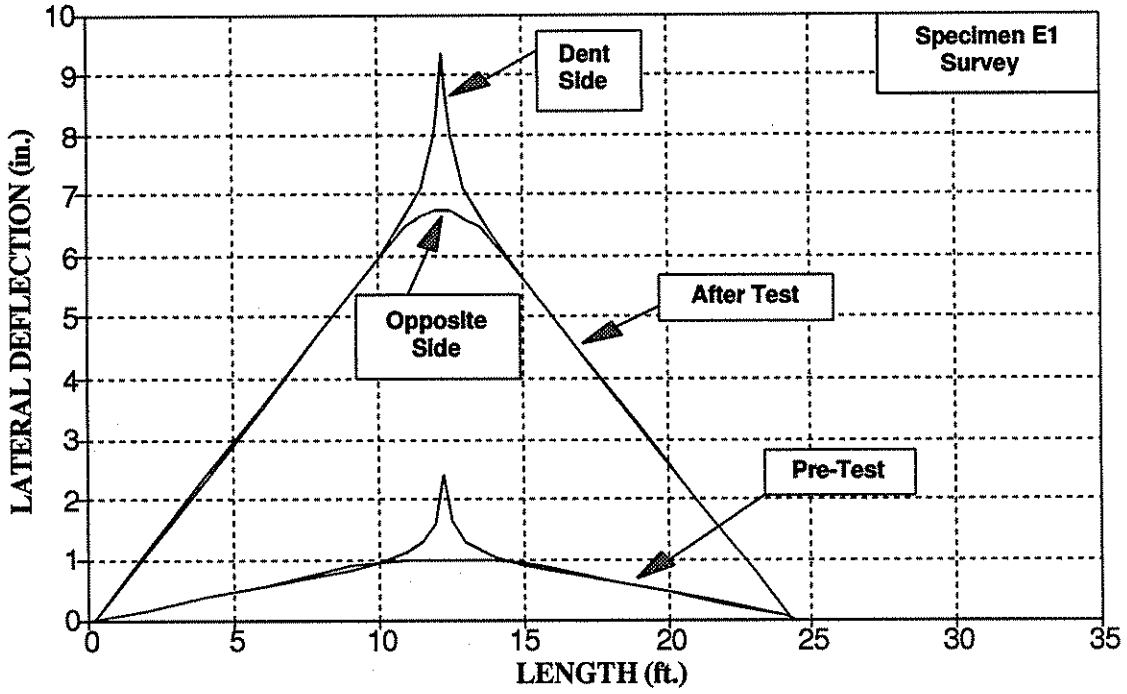

Figure 7-40: Specimen E1 – Pre- and Post-Test Surface Profiles

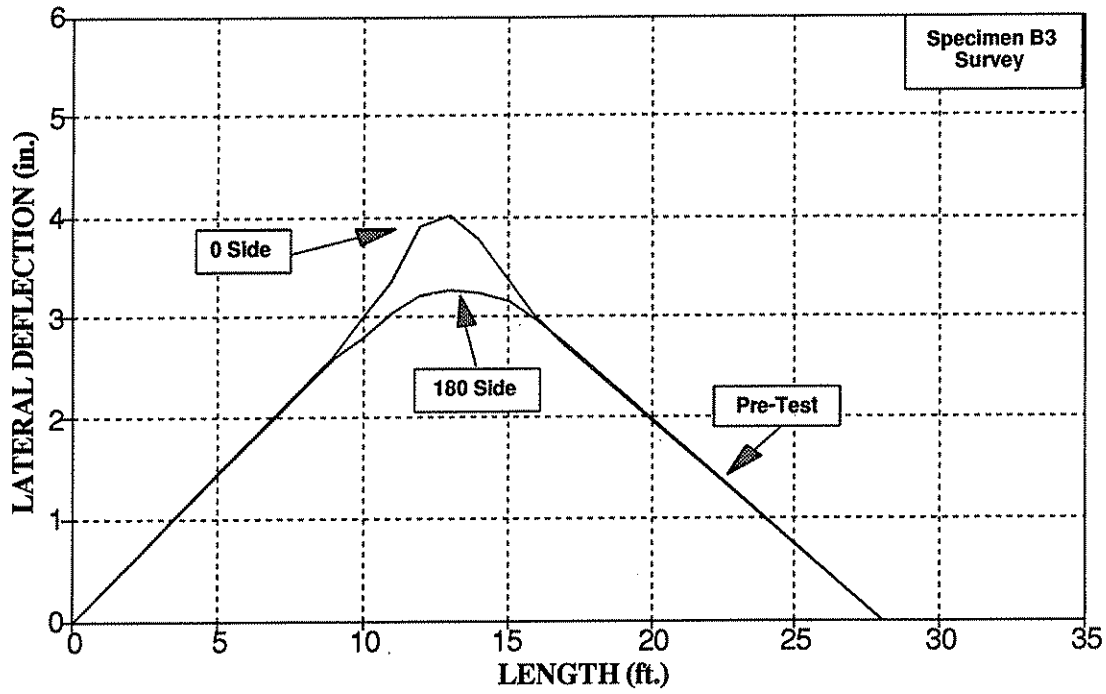

Figure 7-41: Specimen B3 – Pre-Test Surface Profile

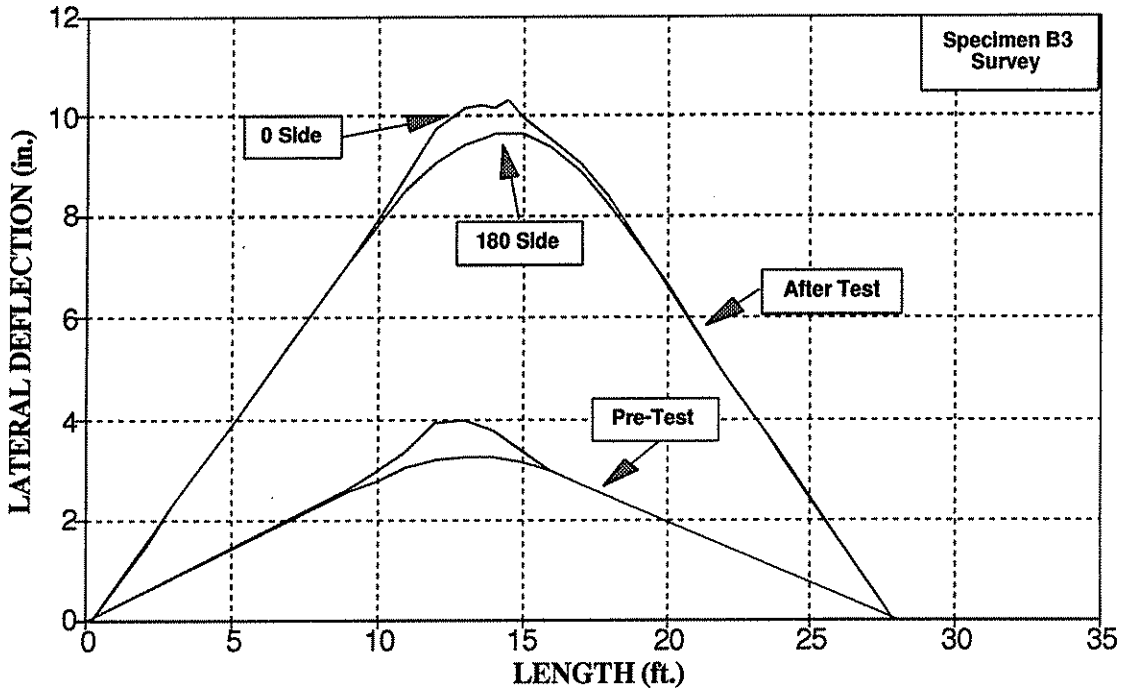

Figure 7-42: Specimen B3 – Pre- and Post-Test Surface Profiles

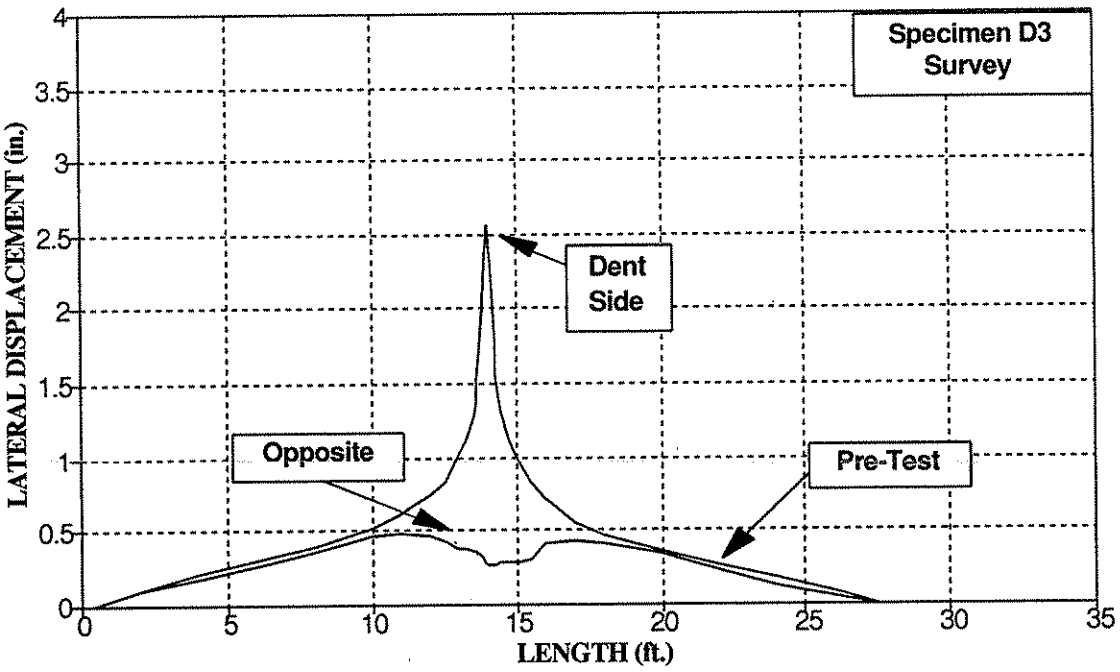

Figure 7-43: Specimen D3 – Pre-Test Surface Profile

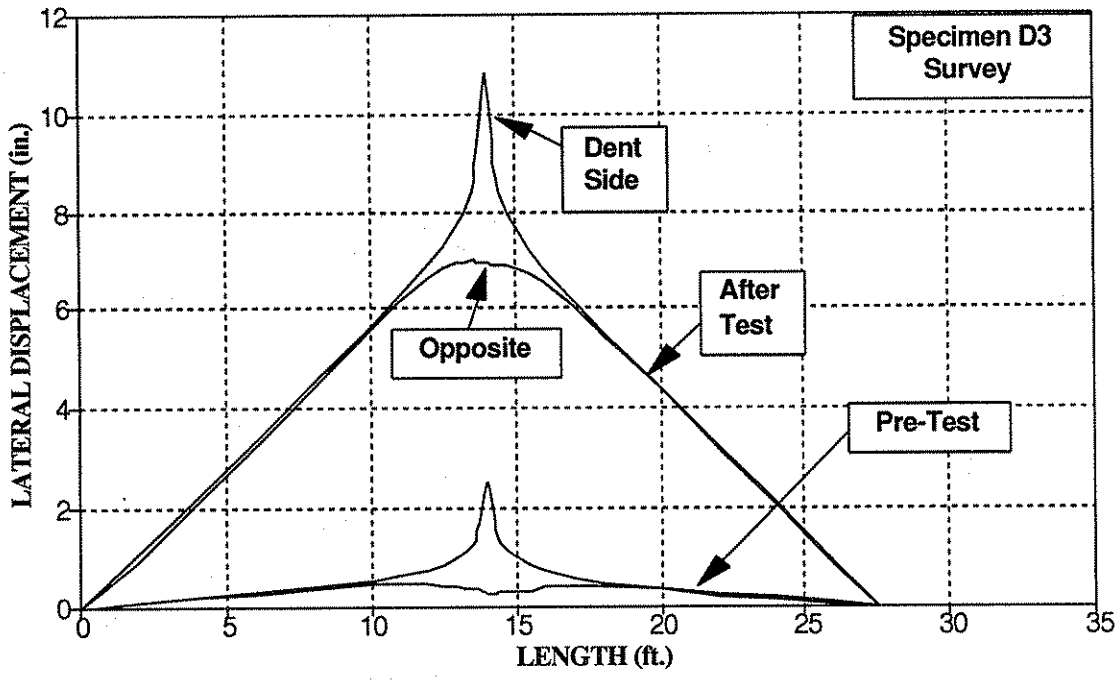

Figure 7-44: Specimen D3 – Pre- and Post-Test Surface Profiles

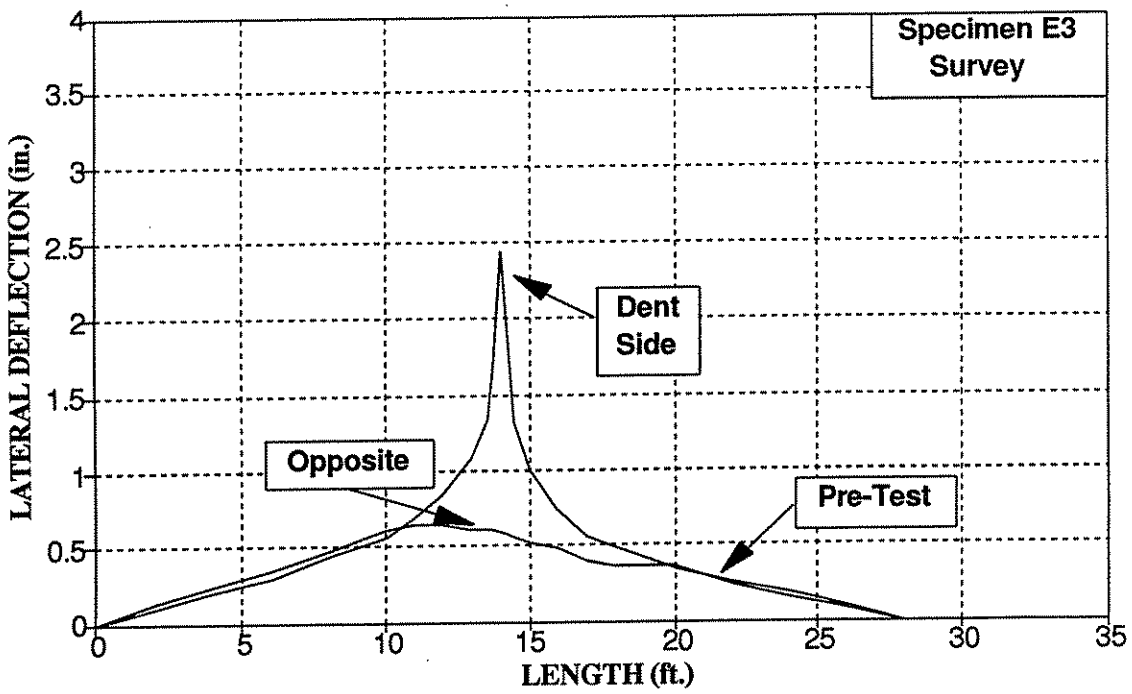

Figure 7-45: Specimen E3 – Pre-Test Surface Profile

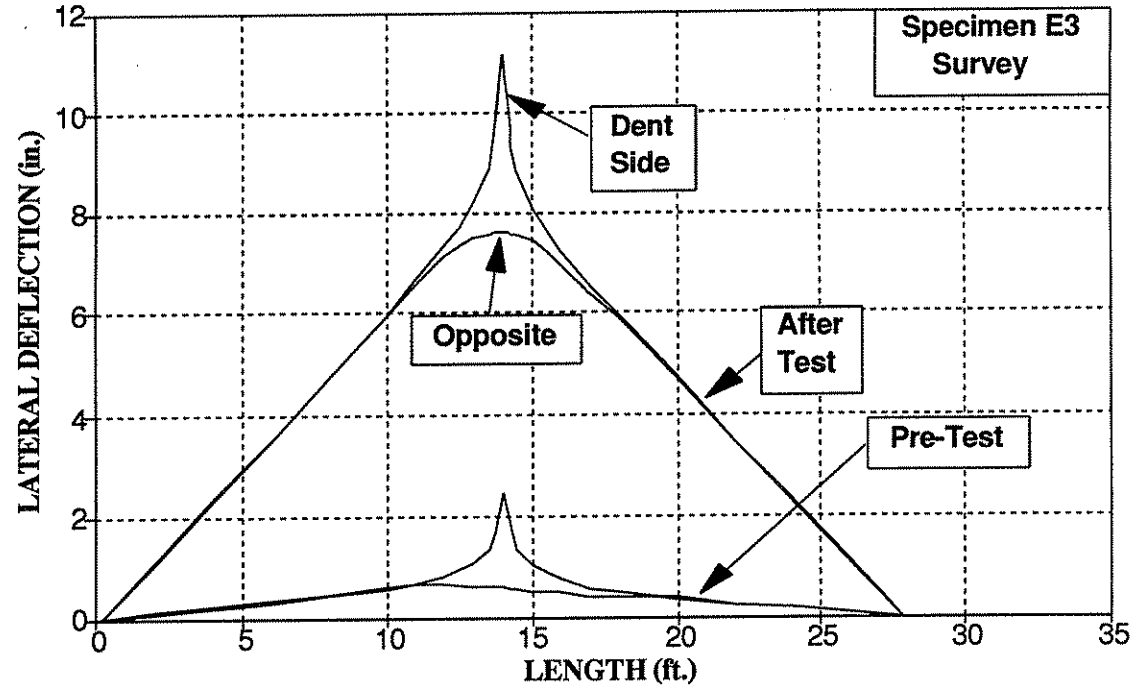

Figure 7-46: Specimen E3 – Pre- and Post-Test Surface Profiles

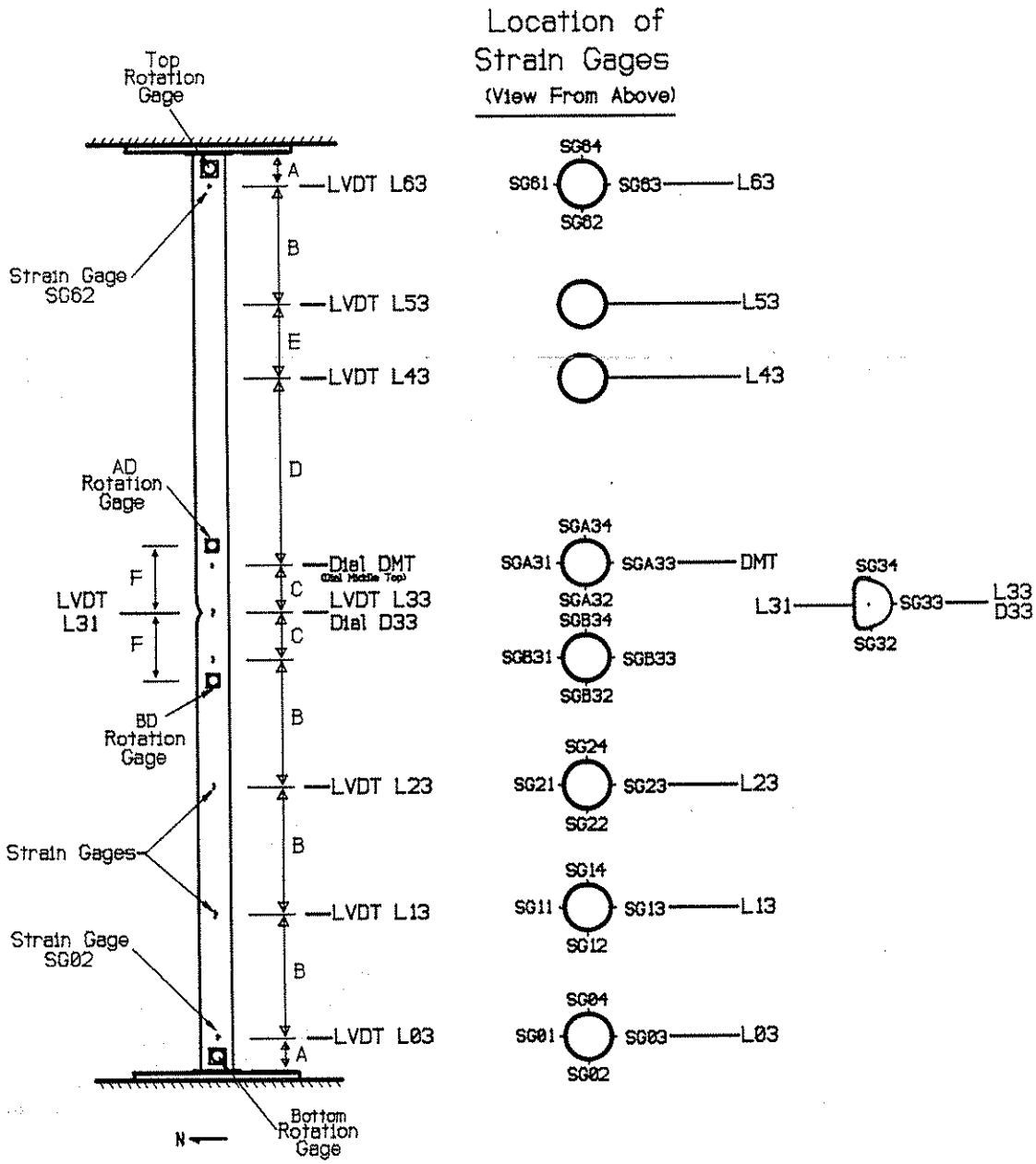

Specimen	Length	A	B	C	D	E	F
P1F	35'-3.5"	15"	58"	22.5"	106"	73"	30"
P2F	34'-8"	17"	55.5"	25.5"	79"	32"	34"

Figure 8-1: Fixed Ended Specimens P1F and P2F – Location of Gages

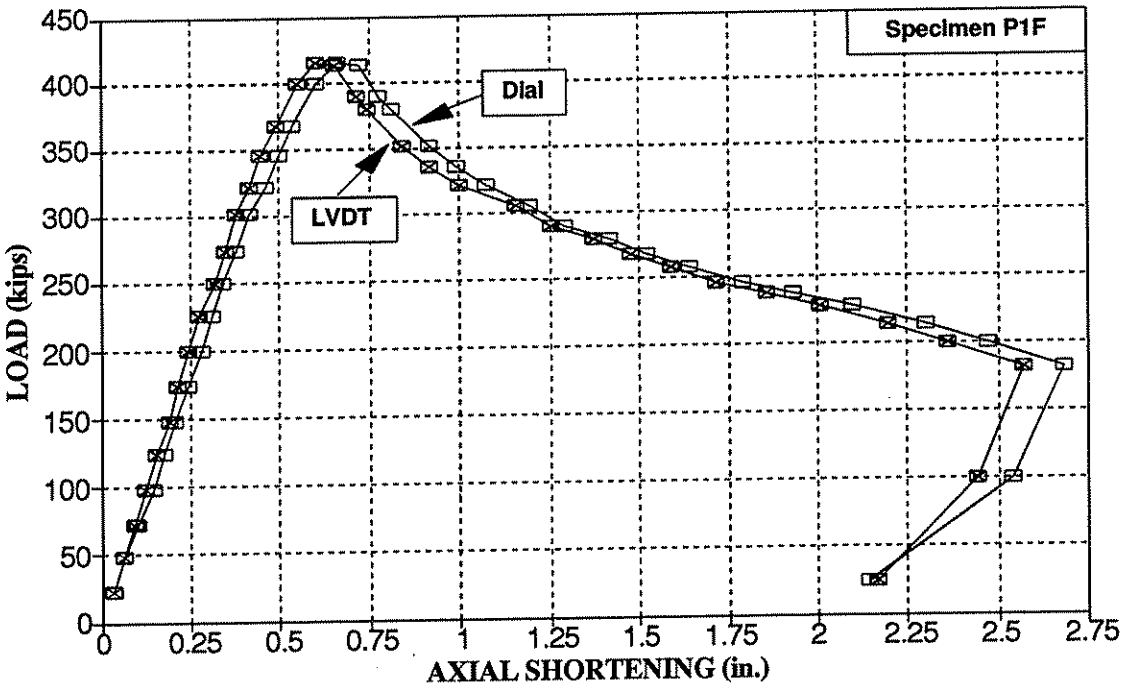

Figure 8-2: Specimen P1F – Axial Shortening

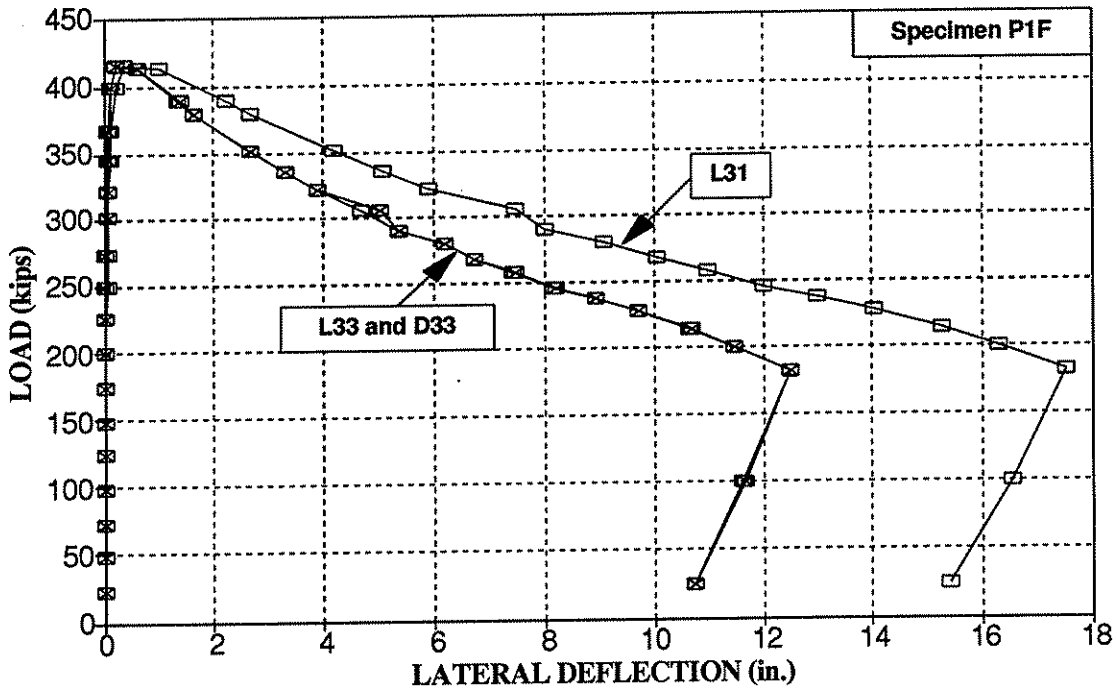

Figure 8-3: Specimen P1F – Lateral Deflection at Mid-Length

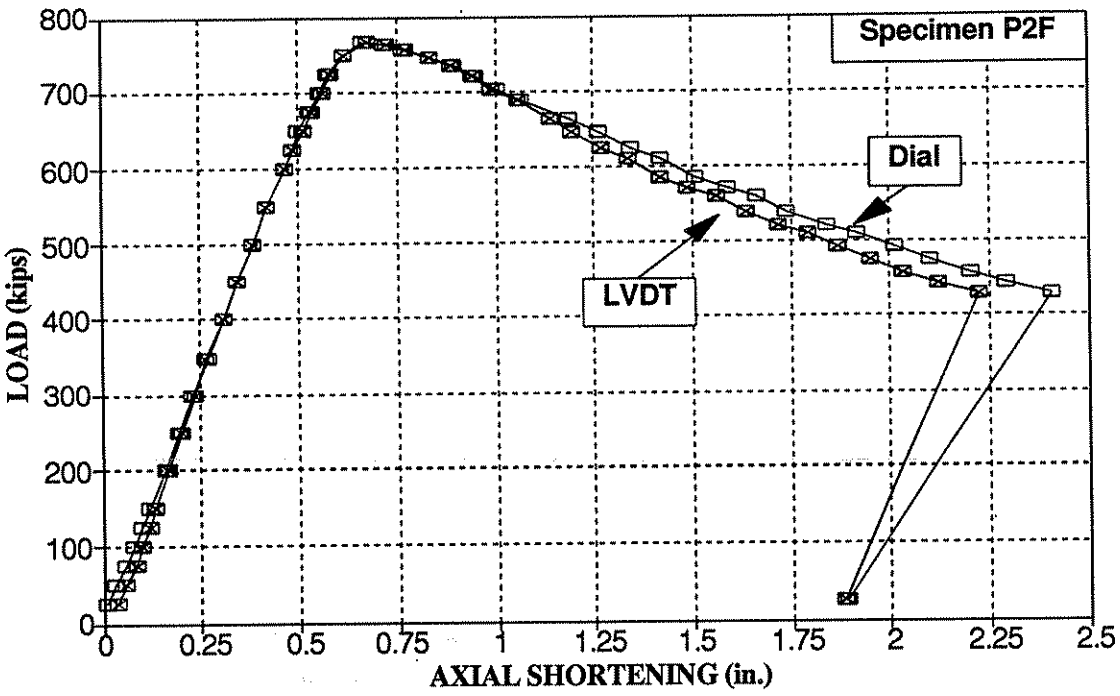

Figure 8-4: Specimen P2F – Axial Shortening

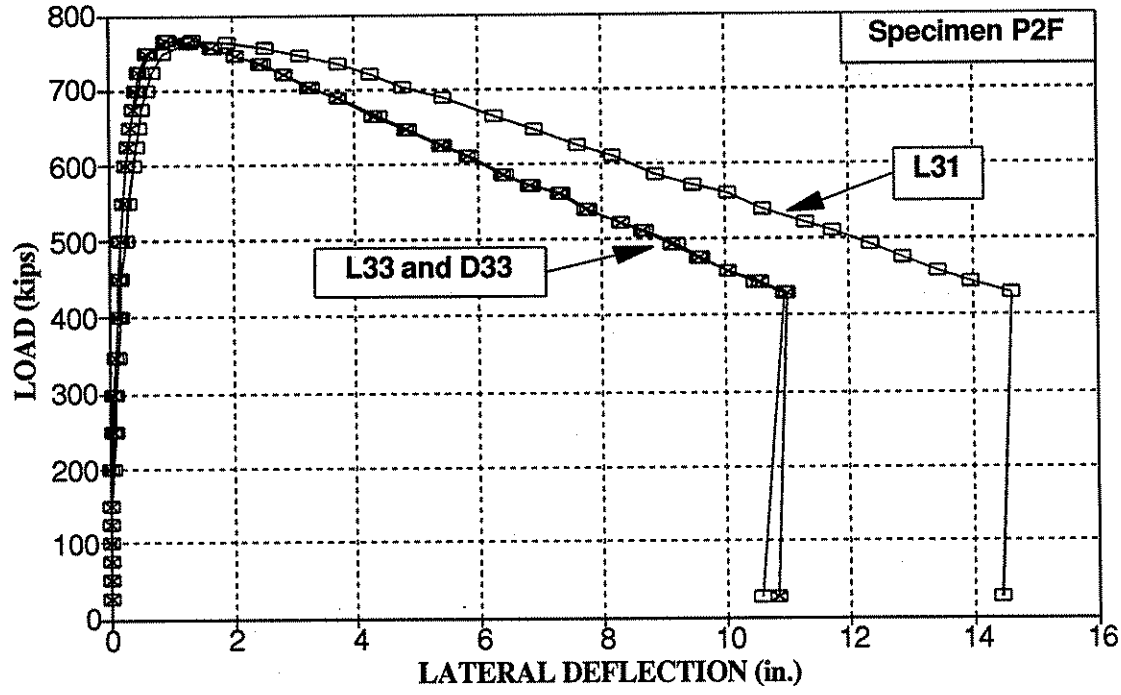

Figure 8-5: Specimen P2F – Lateral Deflection at Mid-Length

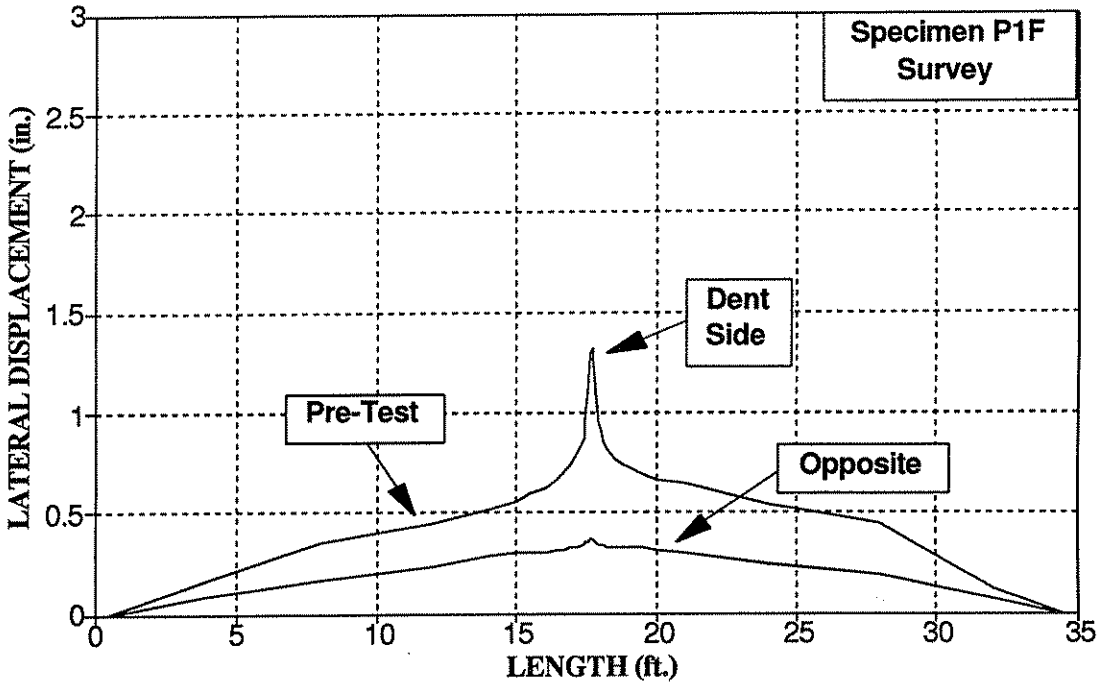

Figure 8-6: Specimen P1F – Pre-Test Surface Profile

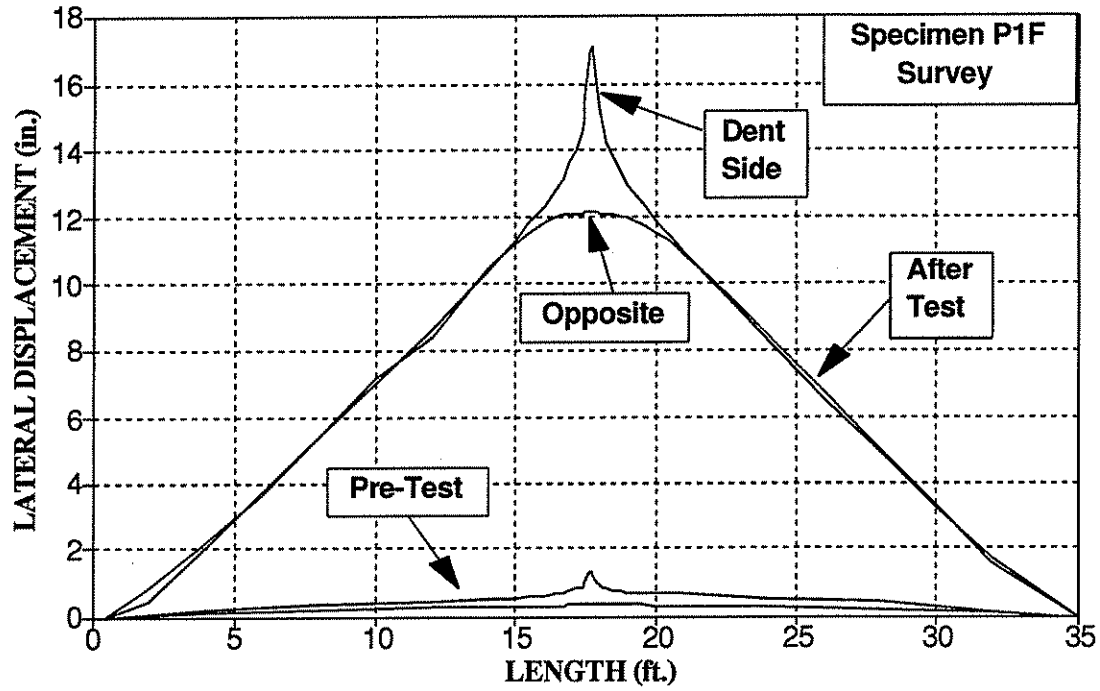

Figure 8-7: Specimen P1F – Pre- and Post-Test Surface Profiles

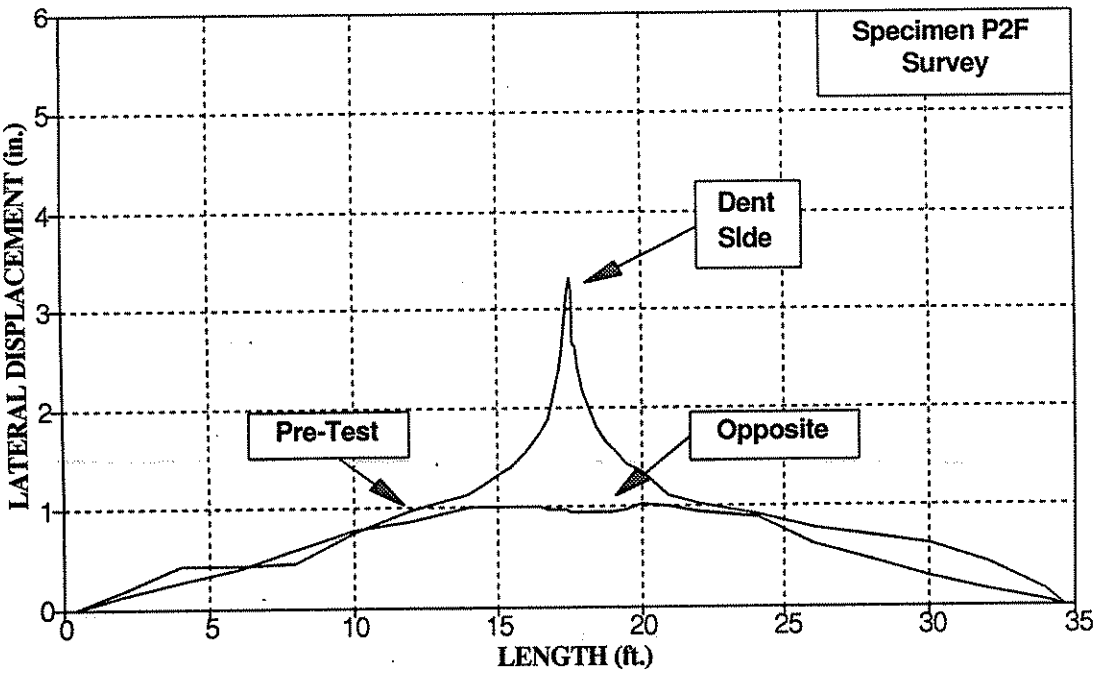

Figure 8-8: Specimen P2F – Pre-Test Surface Profile

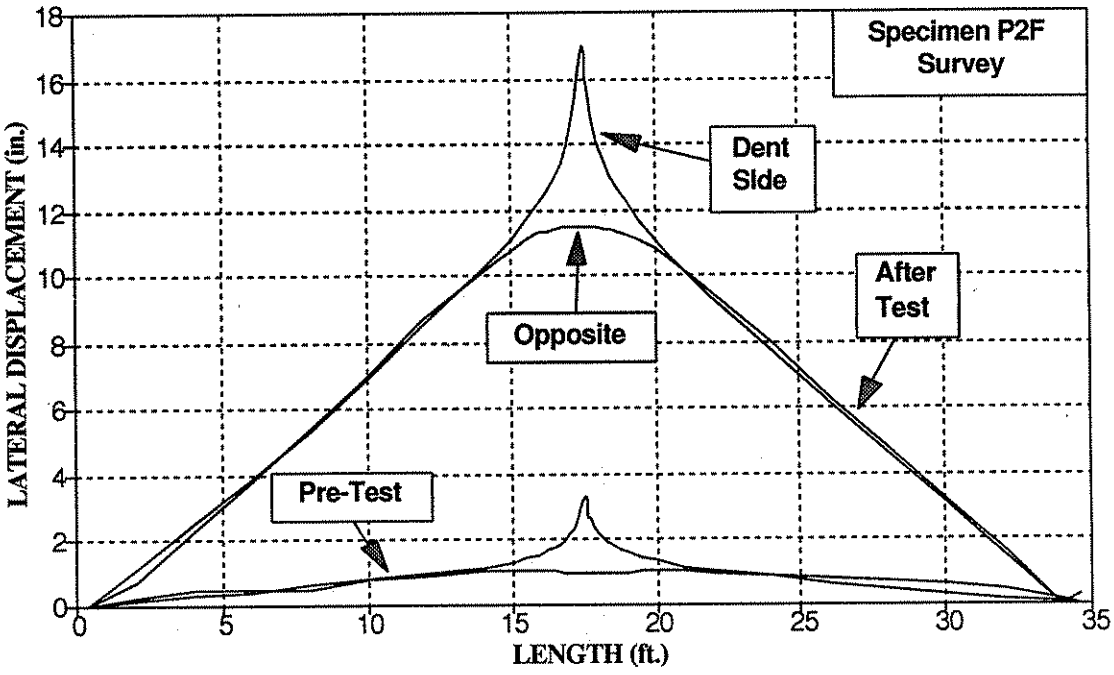

Figure 8-9: Specimen P2F – Pre- and Post-Test Surface Profiles

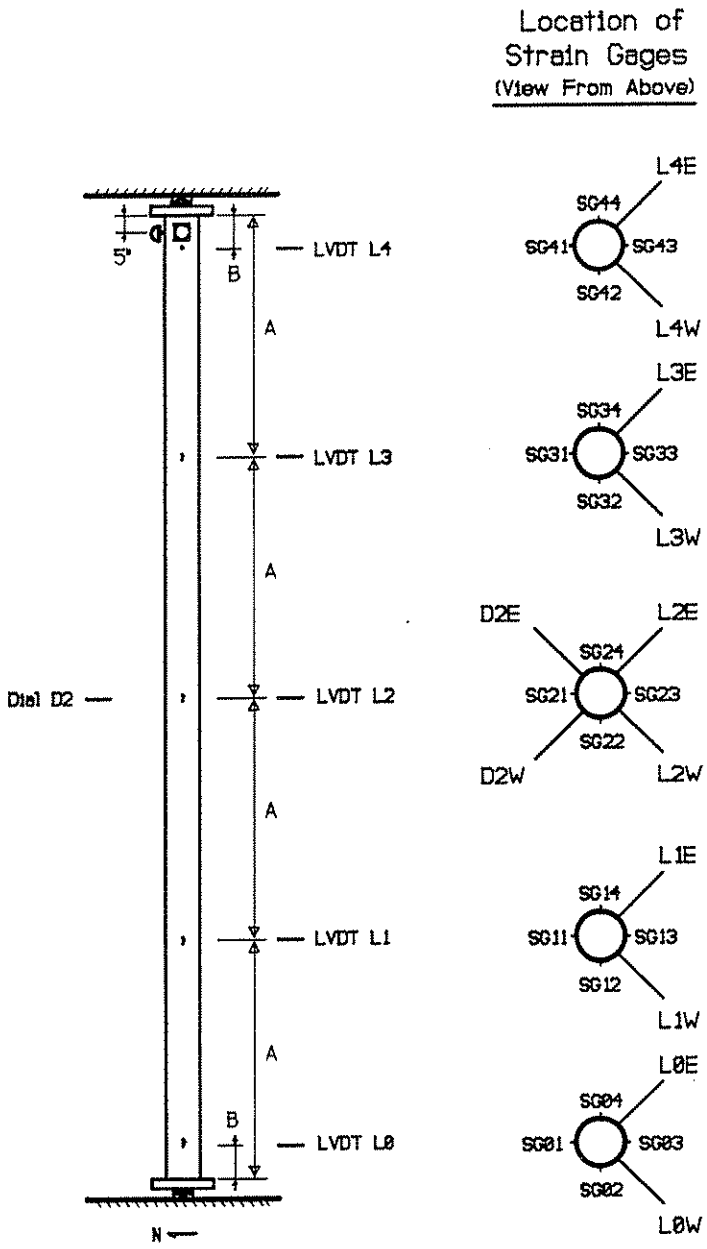

Specimen	Length	A	B
C1	24'-6"	73.5"	11"
S1	24'-6"	73.5"	11"
C2	24'-1"	72.2"	14"
S2	24'-2"	72.2"	14"
S3	28'-0"	84"	14"
C4B	21'-8"	65.1"	12"

Figure 9-1: Location of Gages For Specimens Tested with Spherical Bearings

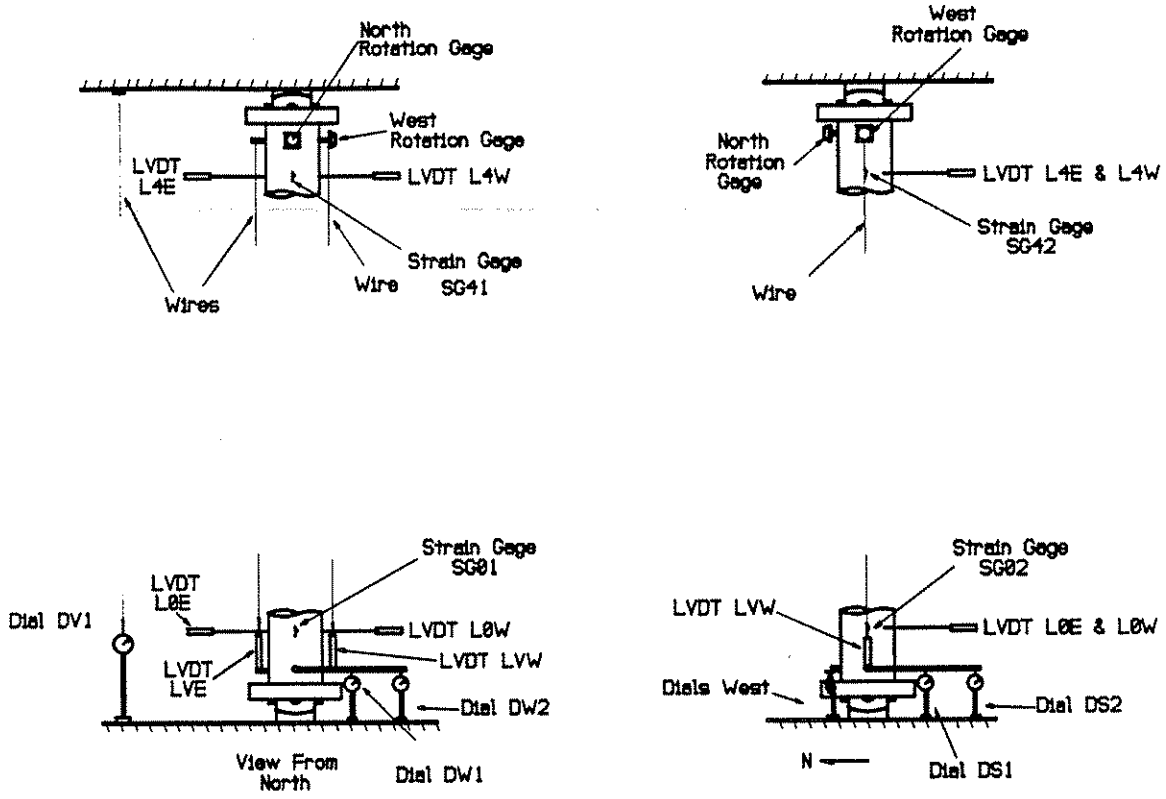

Figure 9-2: Location of Gages for Ends of Straight Specimen Tests

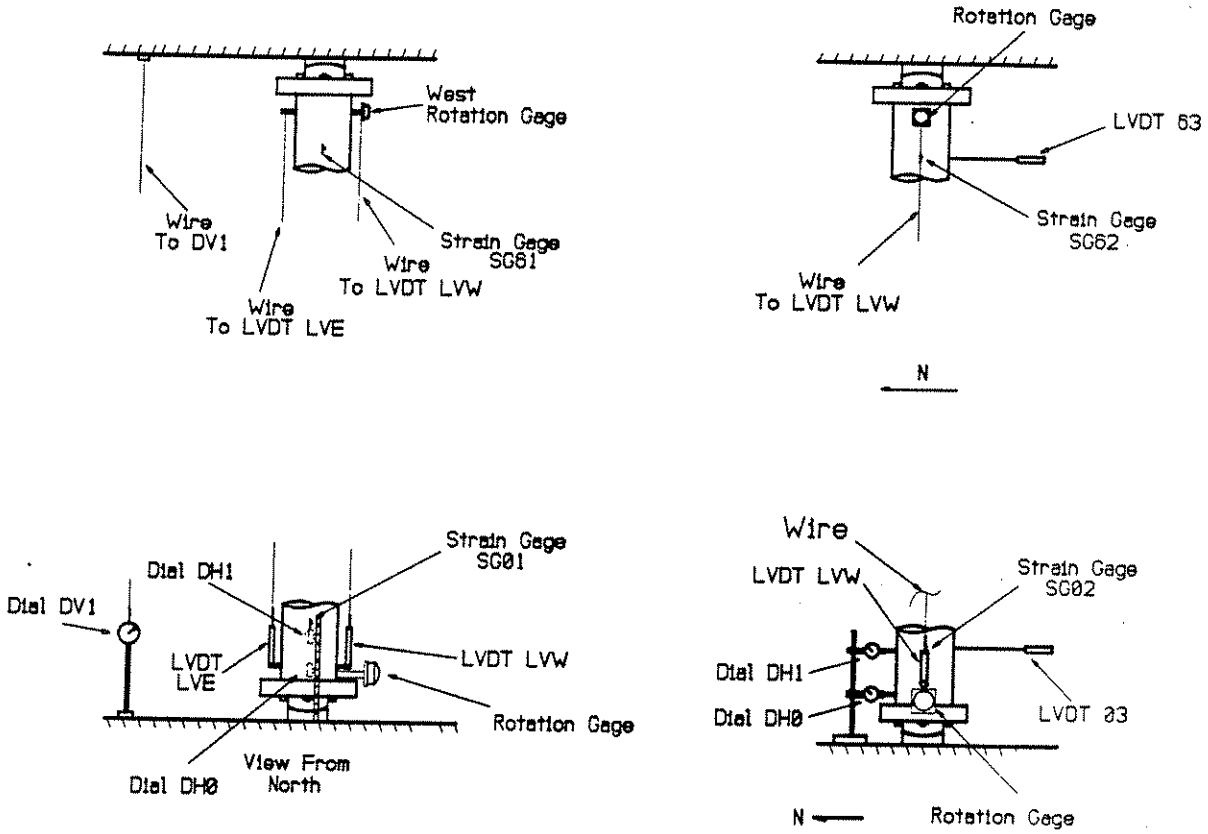

Figure 9-2a: Location of Gages for Ends of Small Scale Specimens P1PS and P2PS

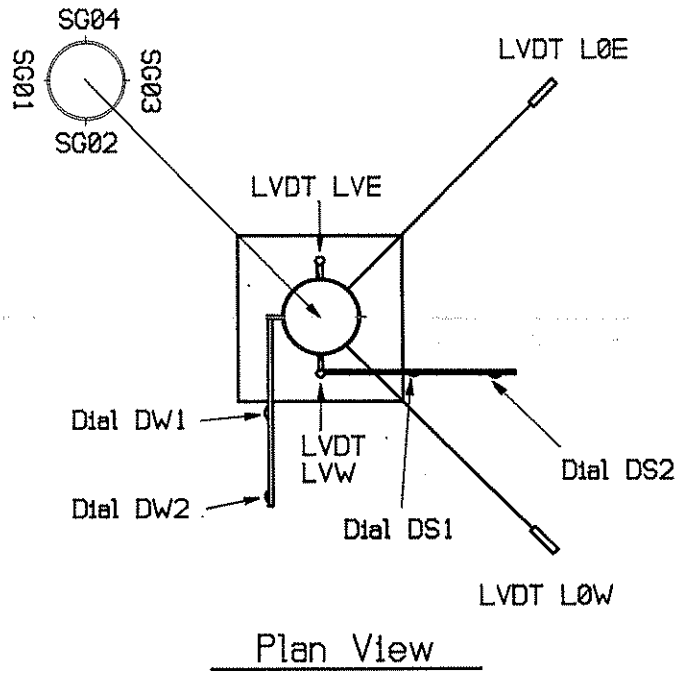

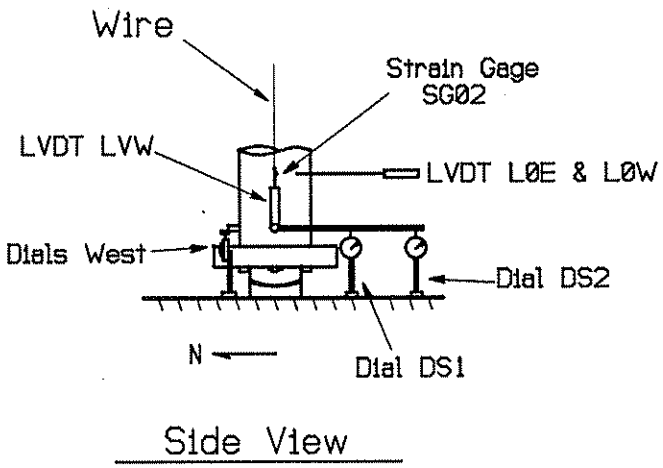

Figure 9-3: Detailed View of Setup for Rotation at Lower End

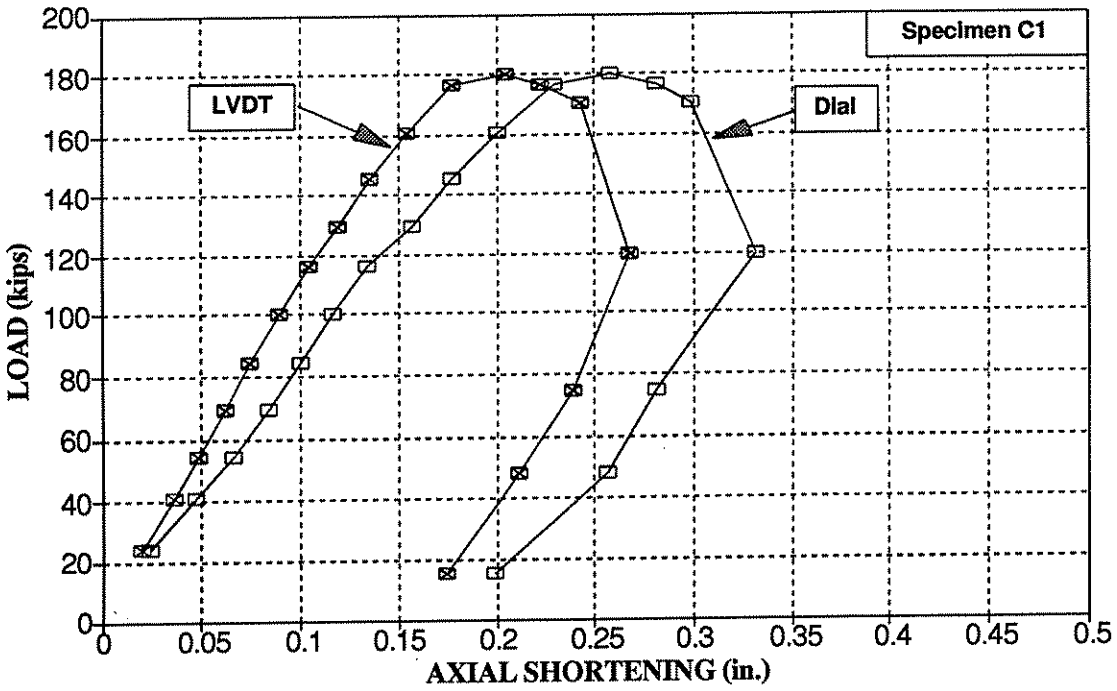

Figure 9-4: Specimen C1 – Axial Shortening

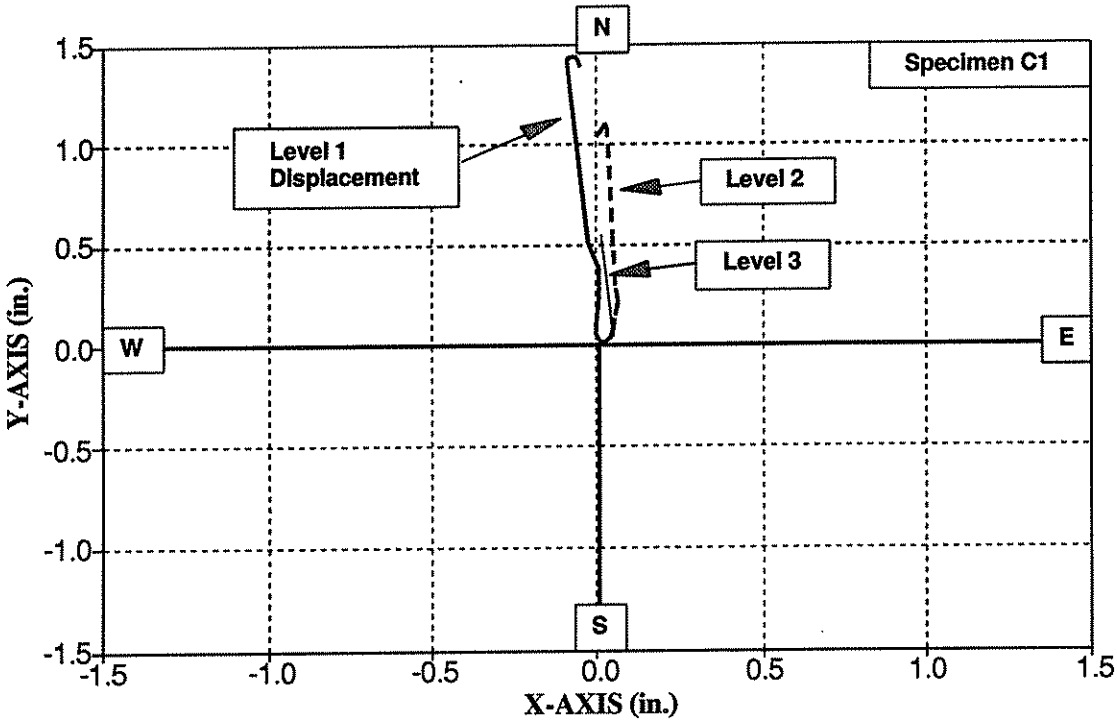

Figure 9-5: Specimen C1 – Lateral Deflection

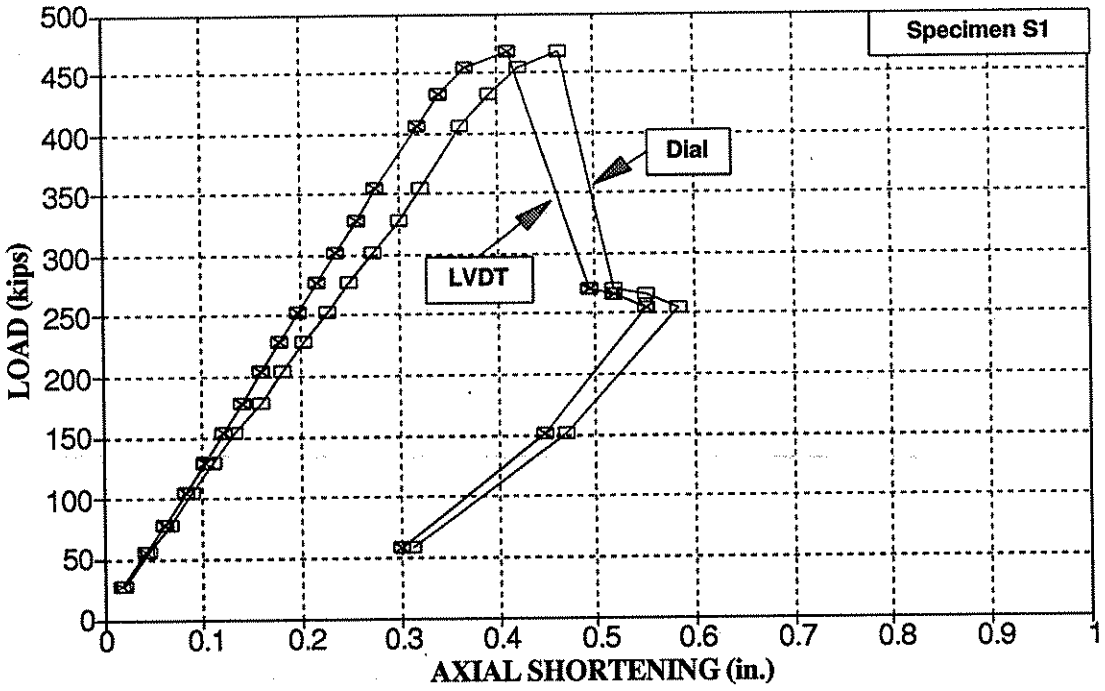

Figure 9-6: Specimen S1 – Axial Shortening

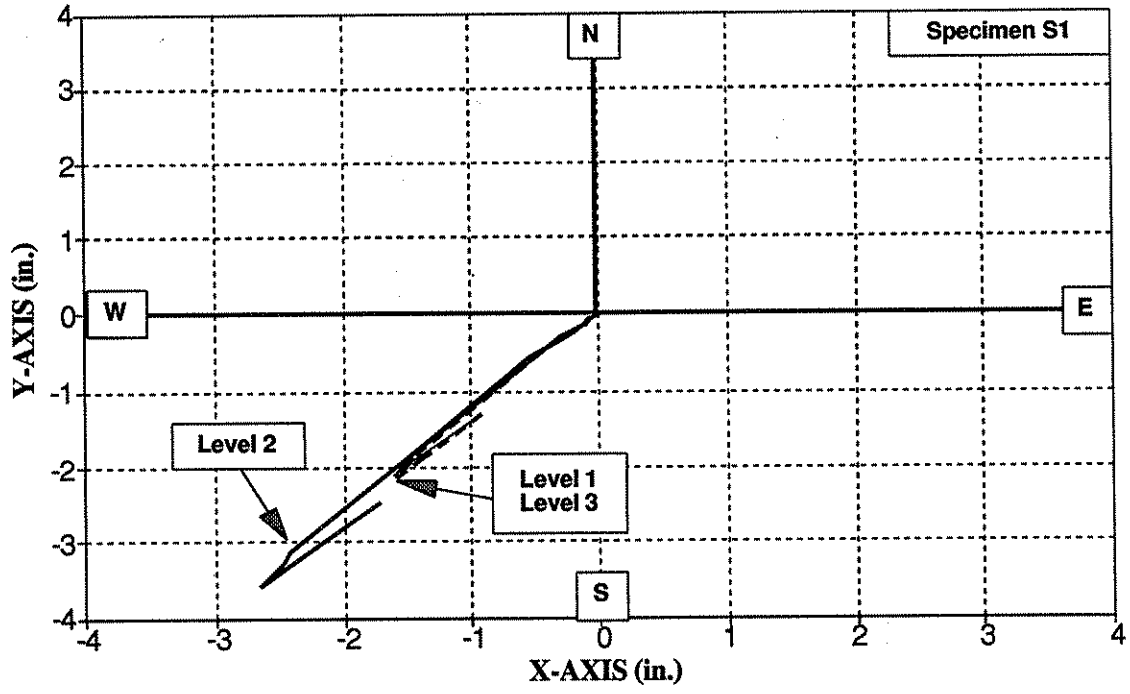

Figure 9-7: Specimen S1 – Lateral Deflection

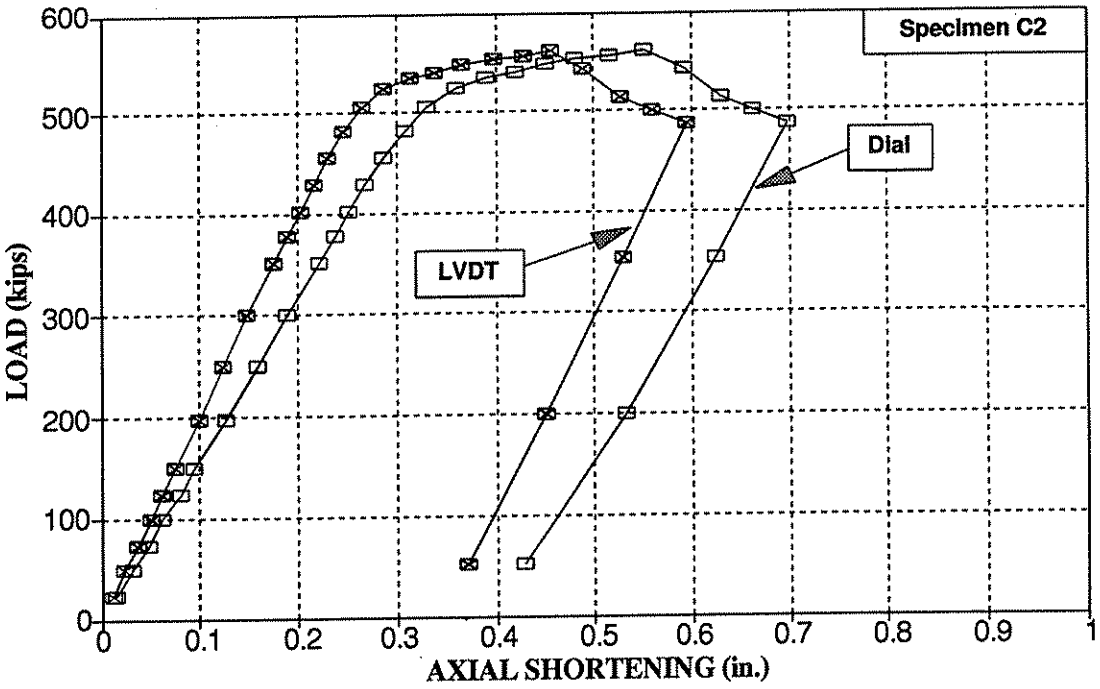

Figure 9-8: Specimen C2 – Axial Shortening

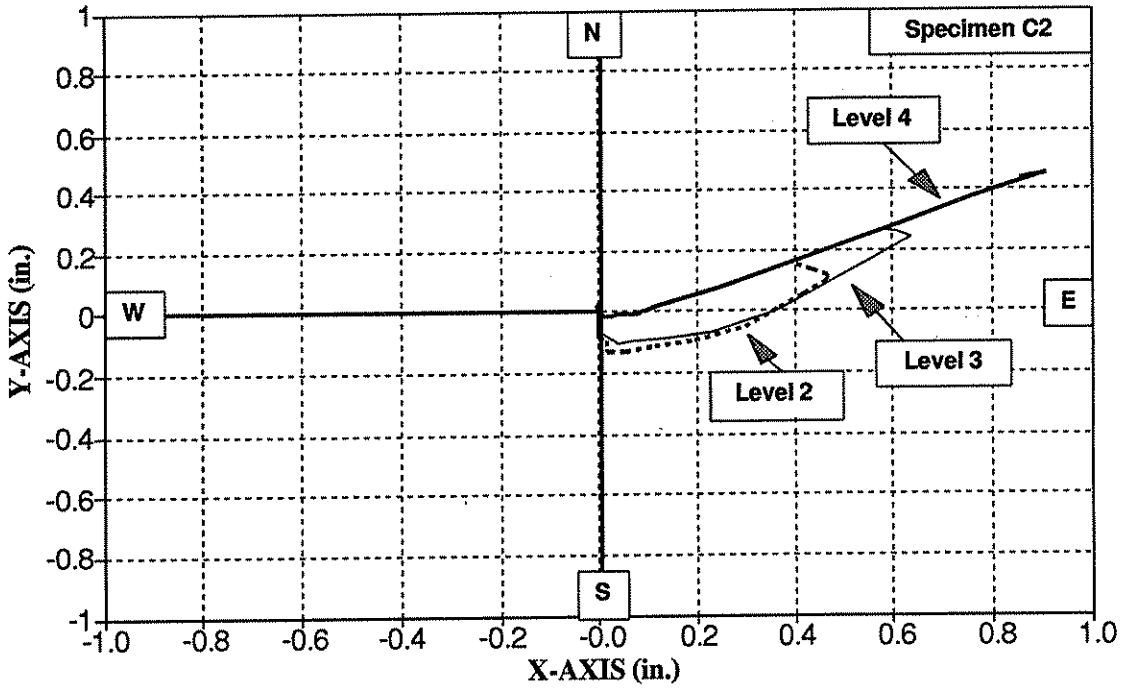

Figure 9-9: Specimen C2 – Lateral Deflection

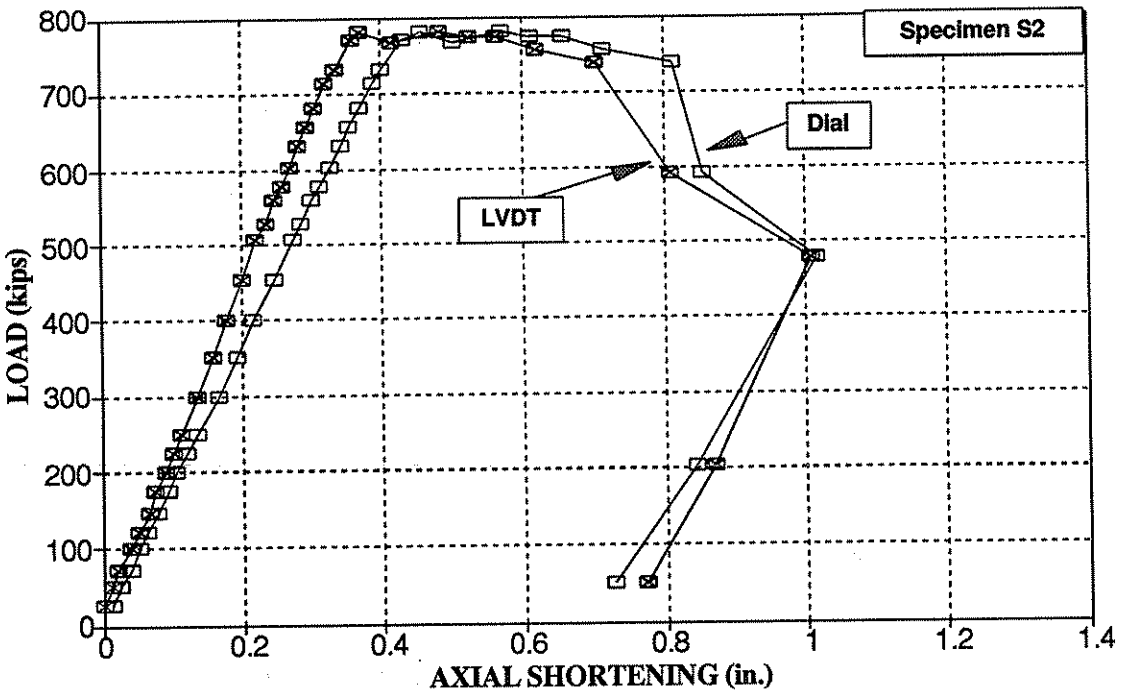

Figure 9-10: Specimen S2 – Axial Shortening

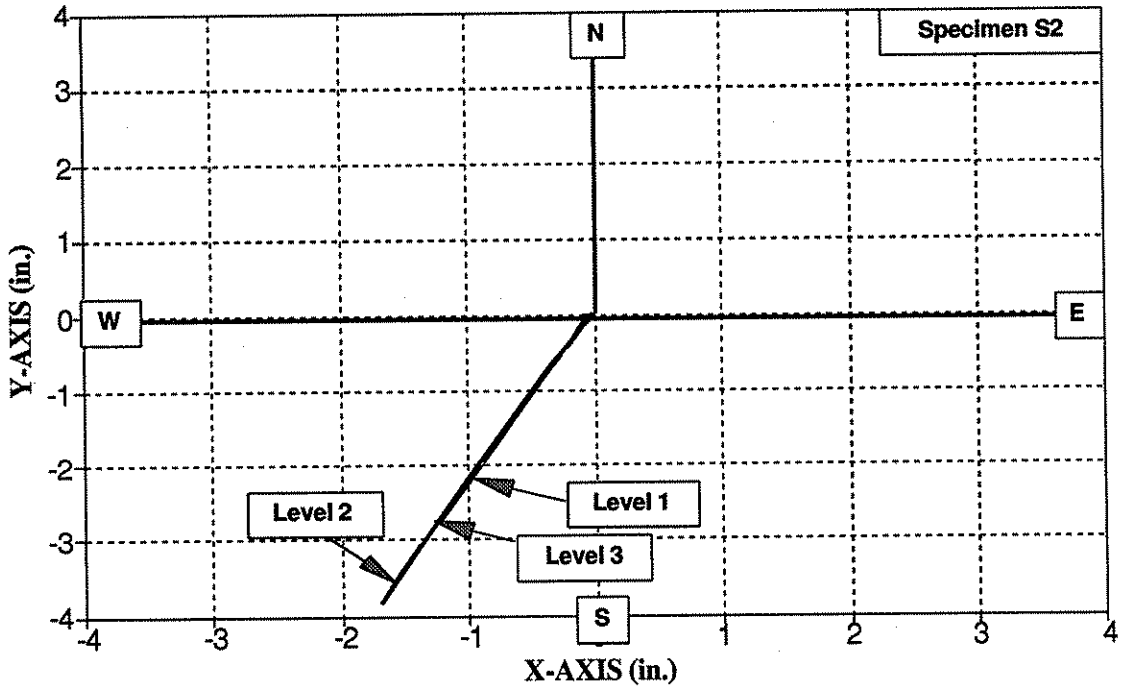

Figure 9-11: Specimen S2 – Lateral Deflection

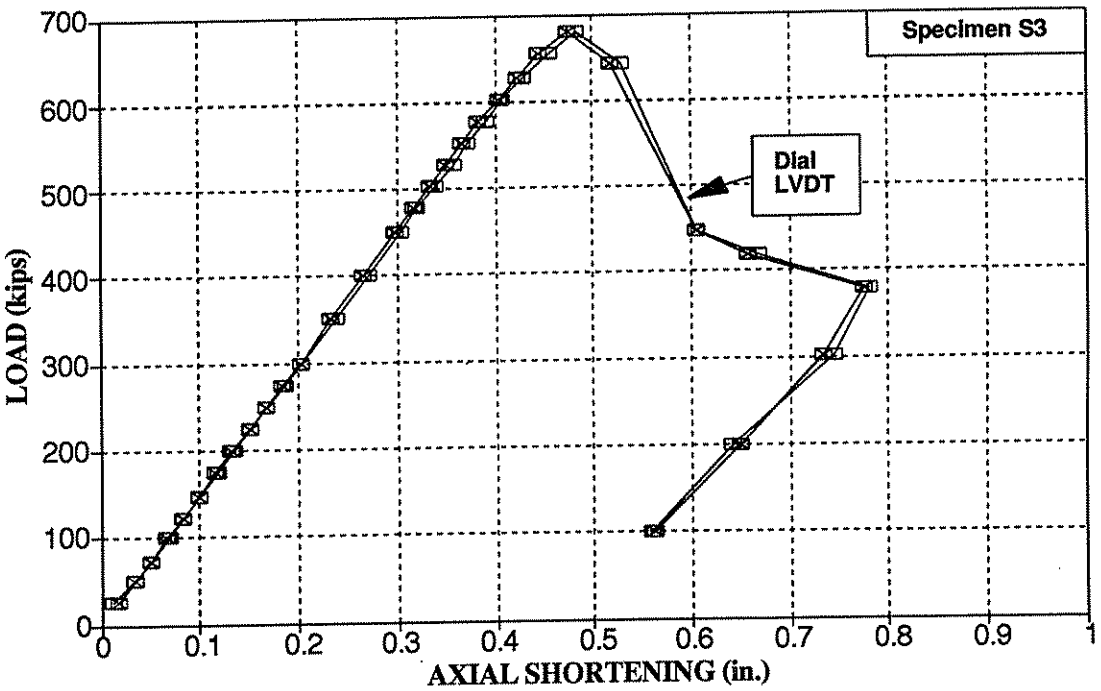

Figure 9-12: Specimen S3 – Axial Shortening

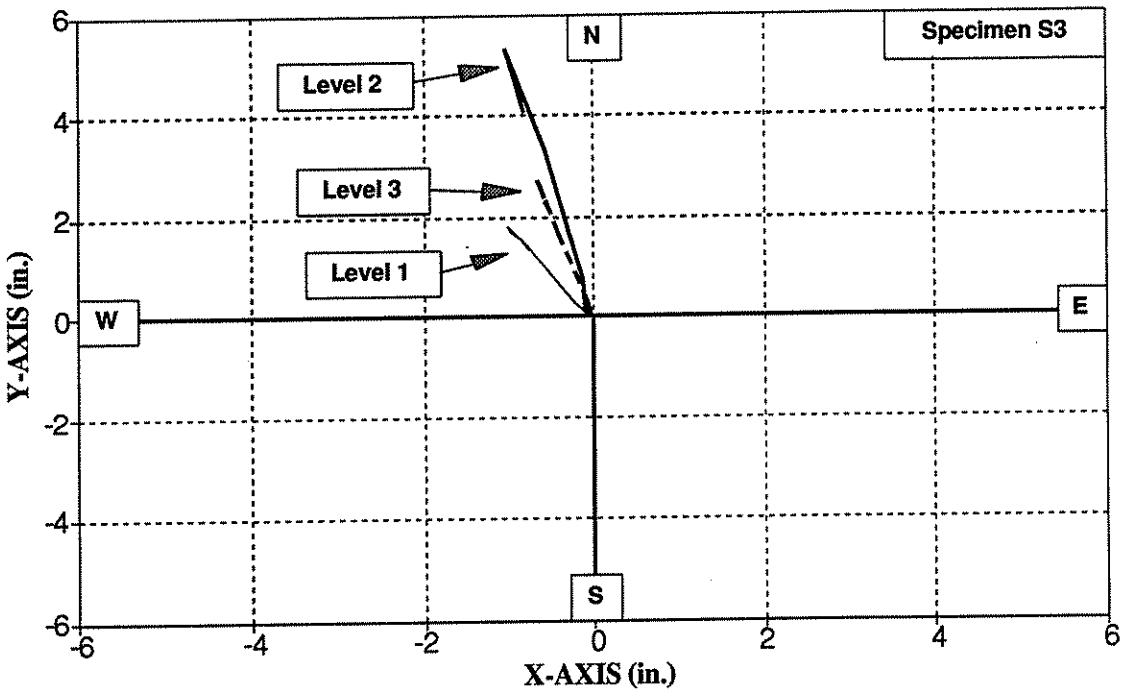

Figure 9-13: Specimen S3 – Lateral Deflection

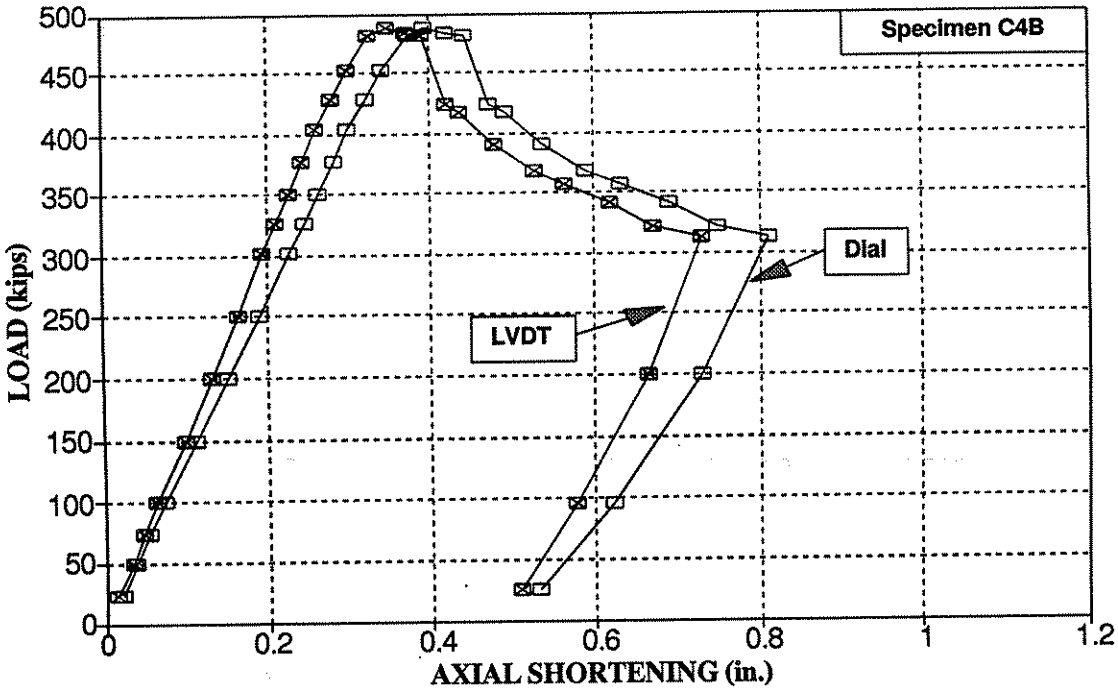

Figure 9-14: Specimen C4B – Axial Shortening

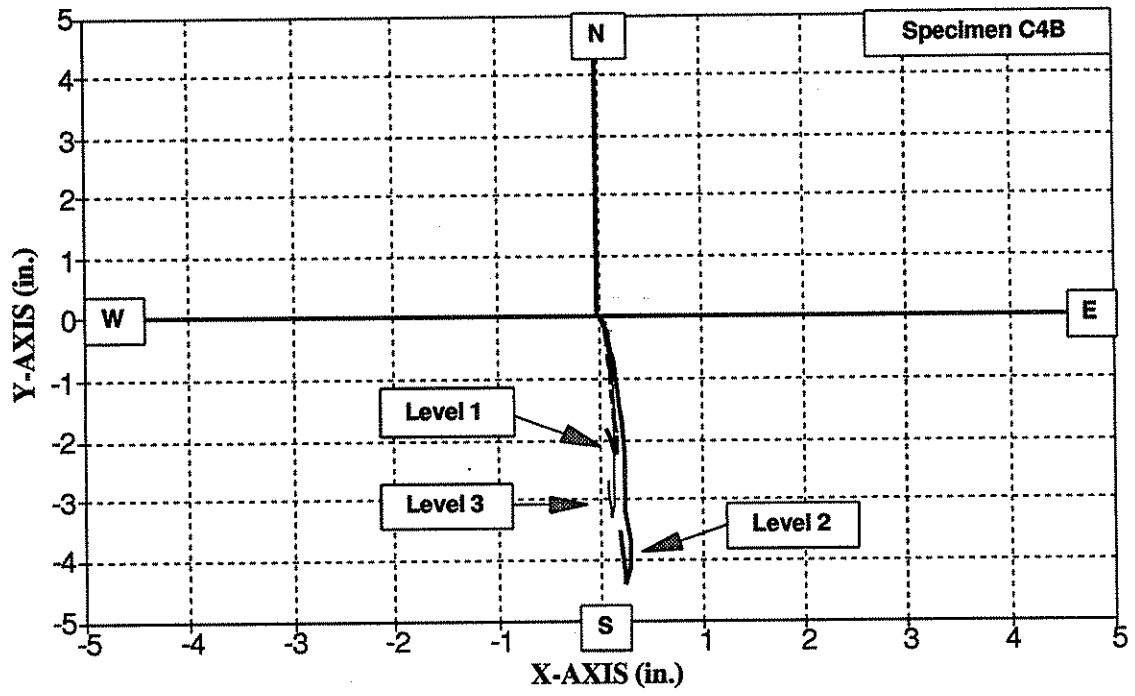

Figure 9-15: Specimen C4B – Lateral Deflection

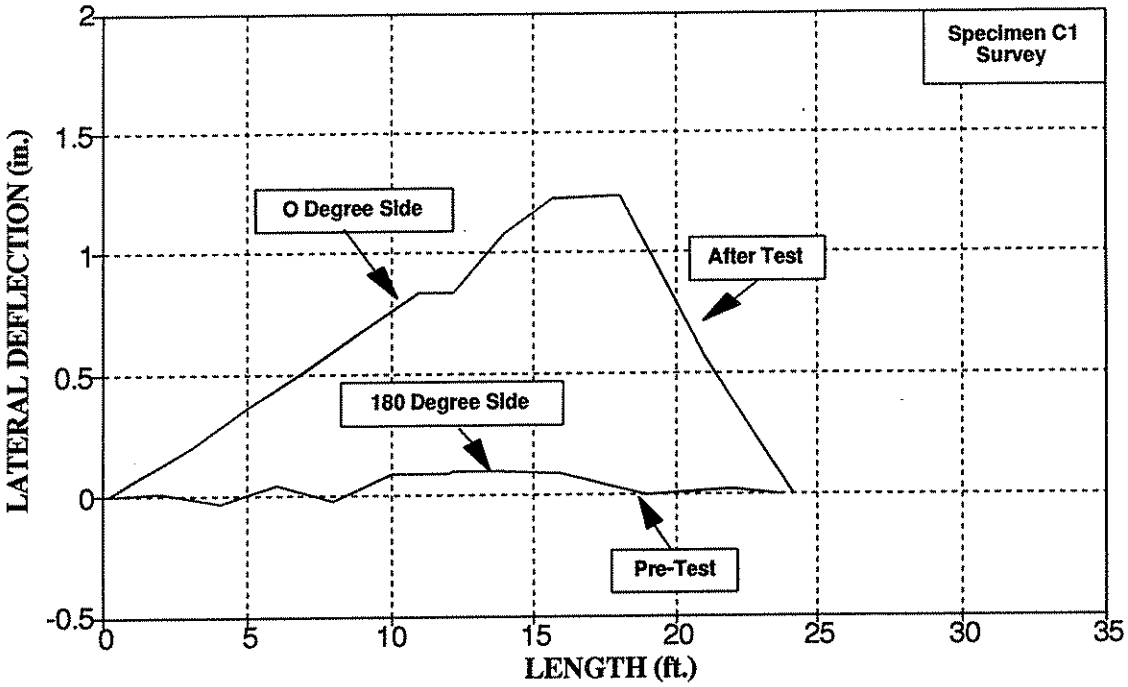

Figure 9-16: Specimen C1 – Pre- and Post-Test Surface Profiles

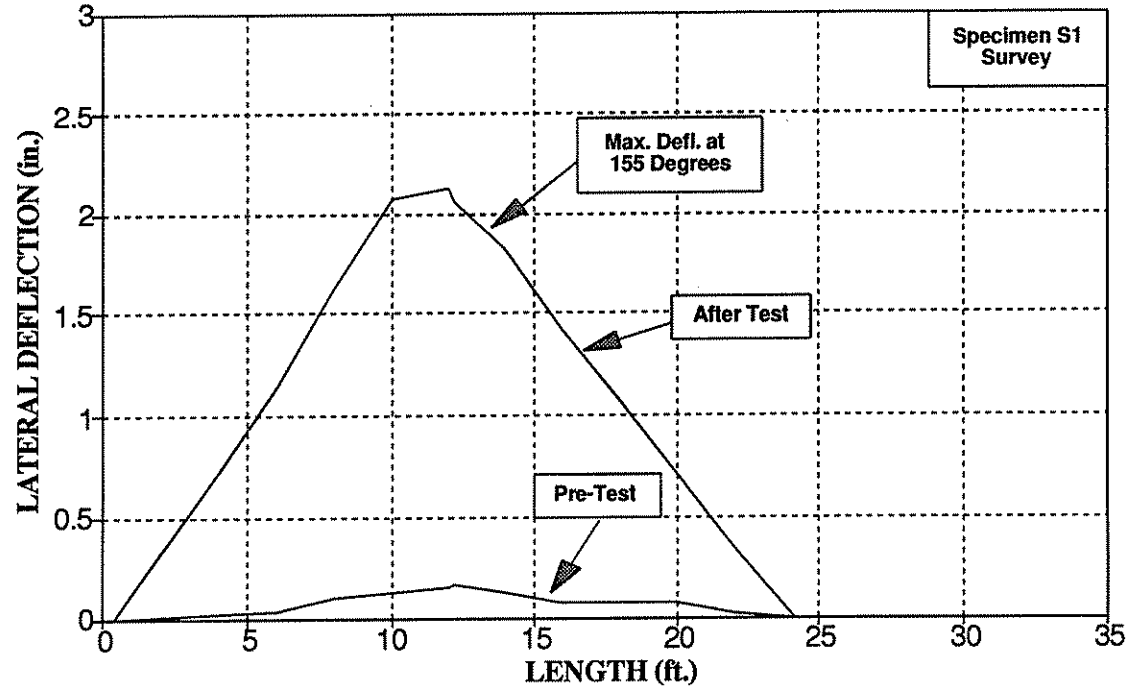

Figure 9-17: Specimen S1 – Pre- and Post-Test Surface Profiles

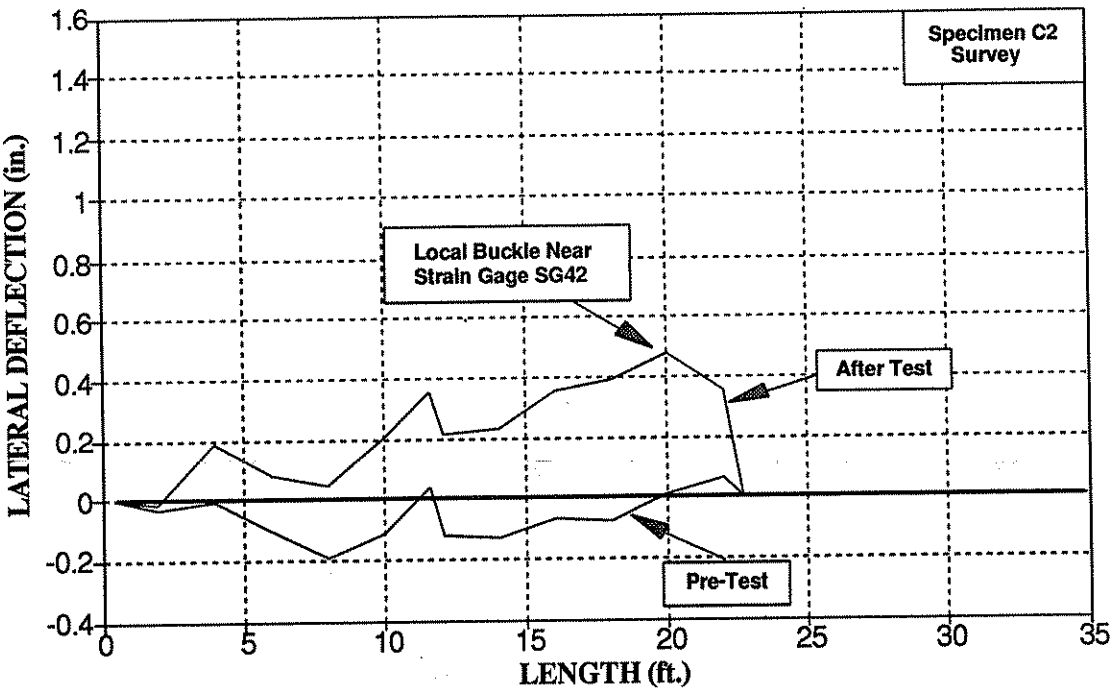

Figure 9-18: Specimen C2 – Pre- and Post-Test Surface Profiles

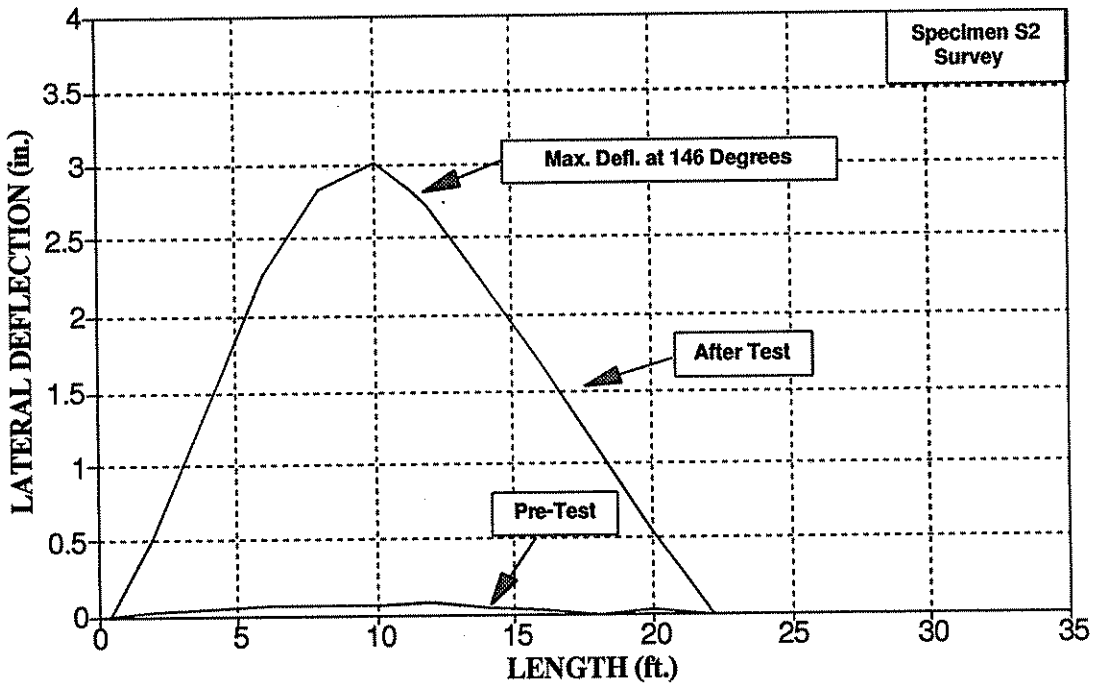

Figure 9-19: Specimen S2 – Pre- and Post-Test Surface Profiles

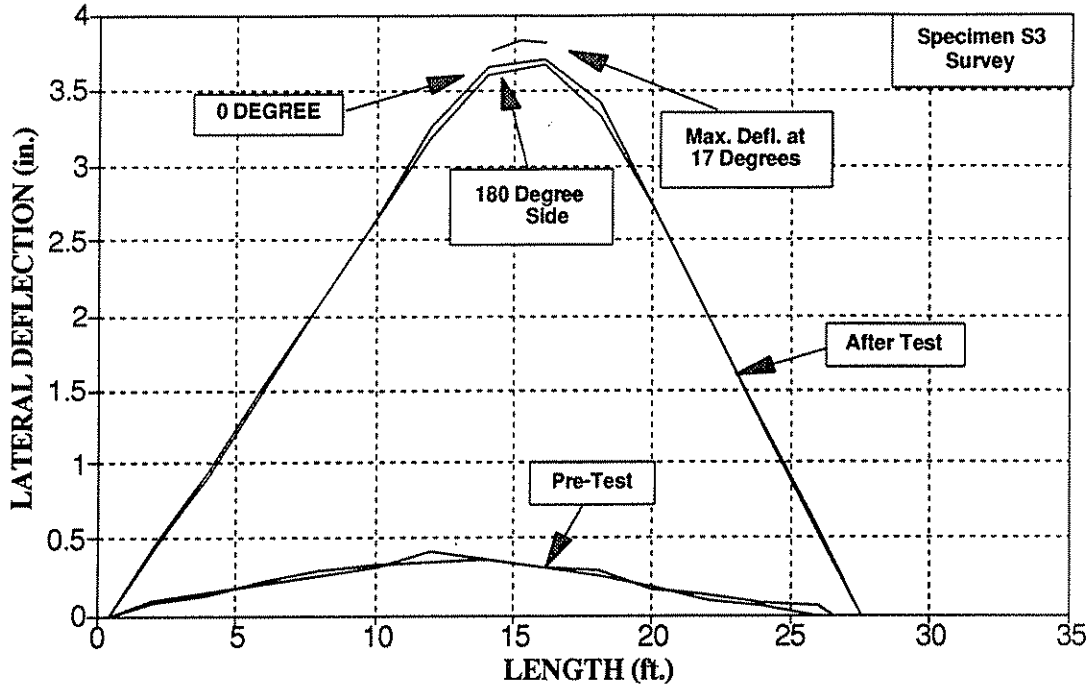

Figure 9-20: Specimen S3 – Pre- and Post-Test Surface Profiles

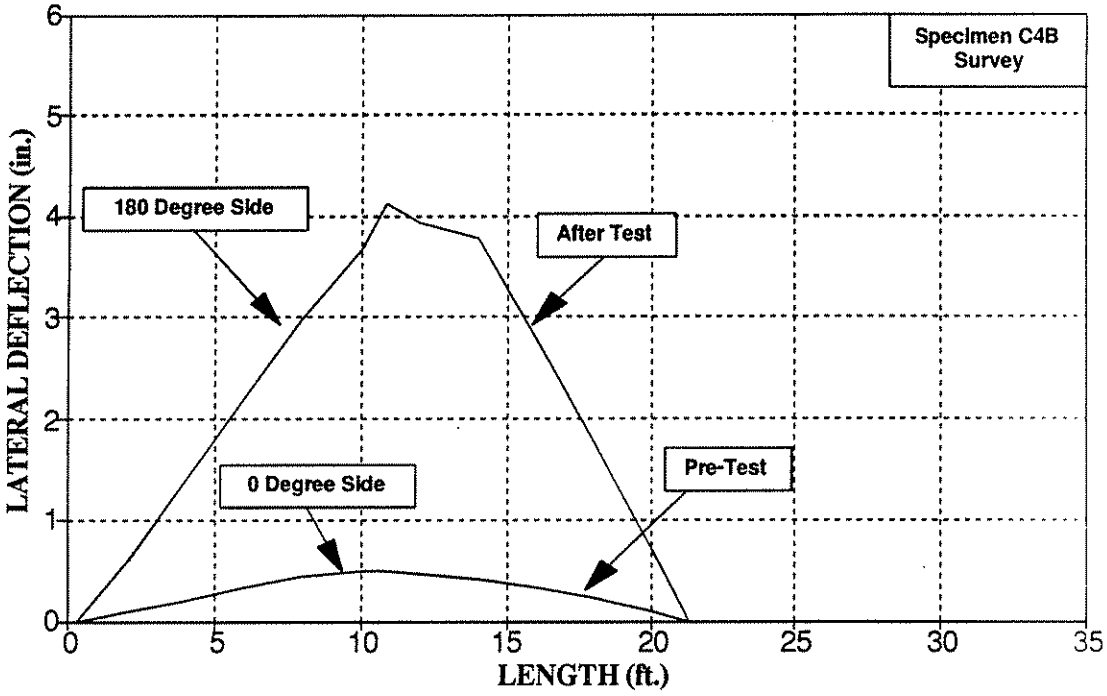

Figure 9-21: Specimen C4B – Pre- and Post-Test Surface Profiles

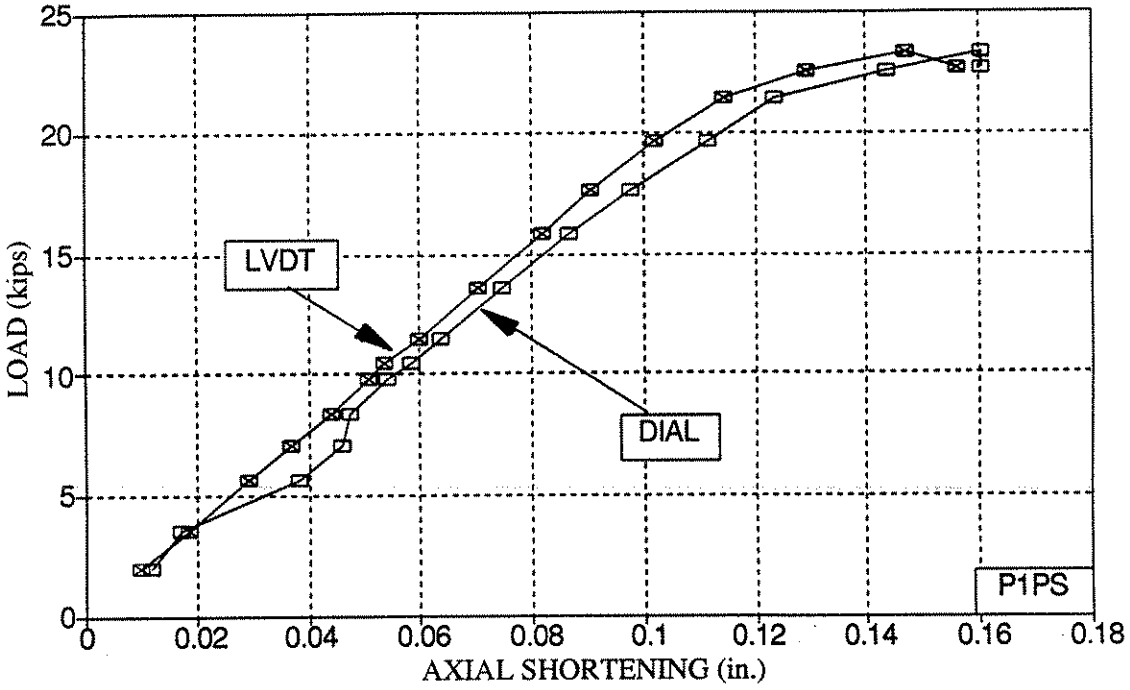

Figure 9-22: Specimen P1PS - Axial Shortening

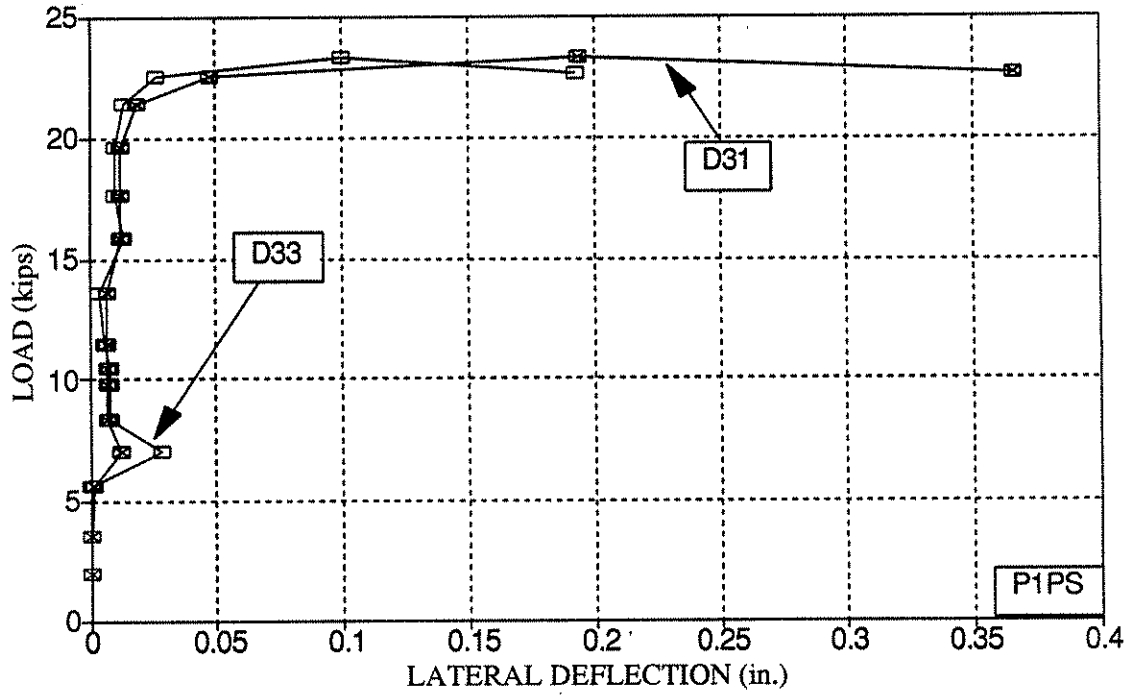

Figure 9-23: Specimen P1PS - Lateral Deflection at Mid-Length

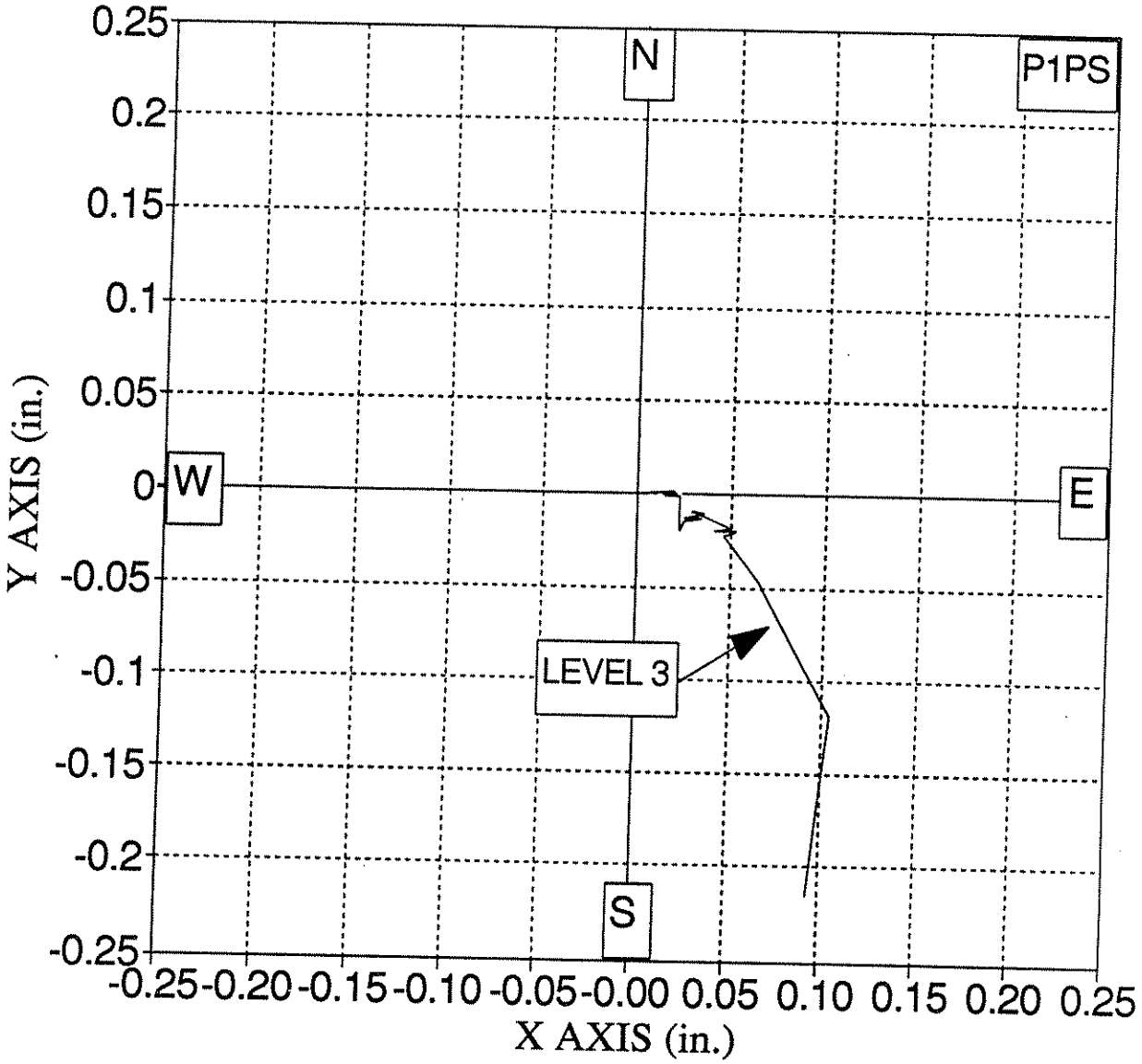

Figure 9-24: Specimen P1PS - Lateral Deflection

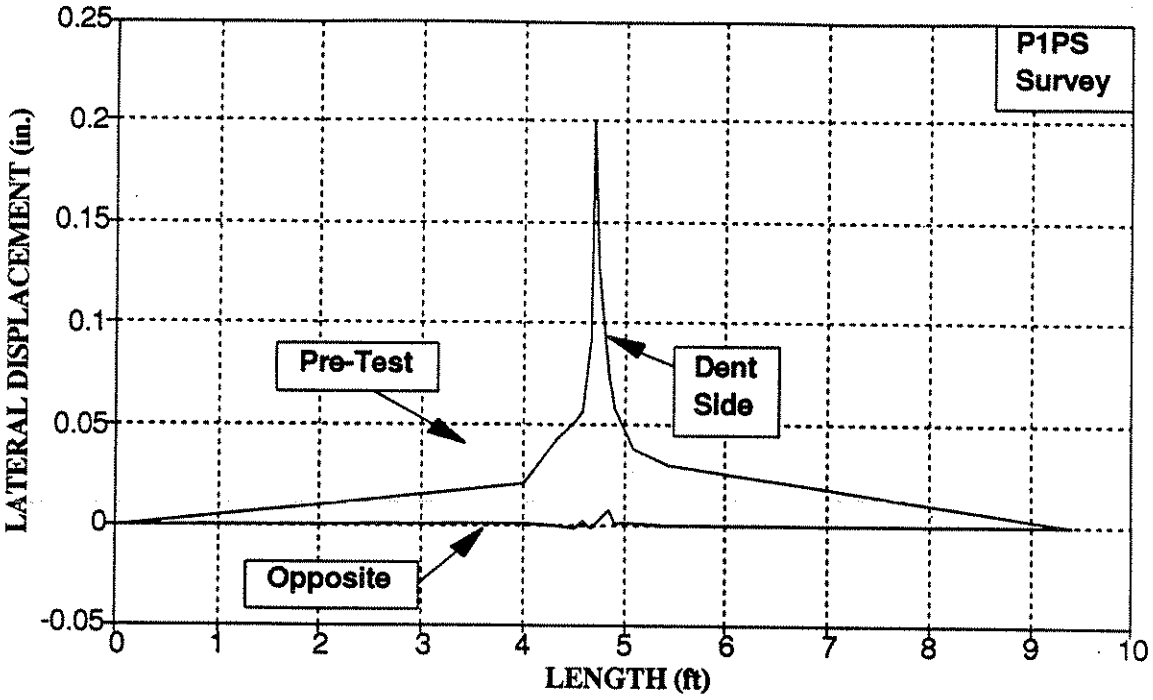

Figure 9-25: Specimen P1PS - Pre-Test Surface Profile

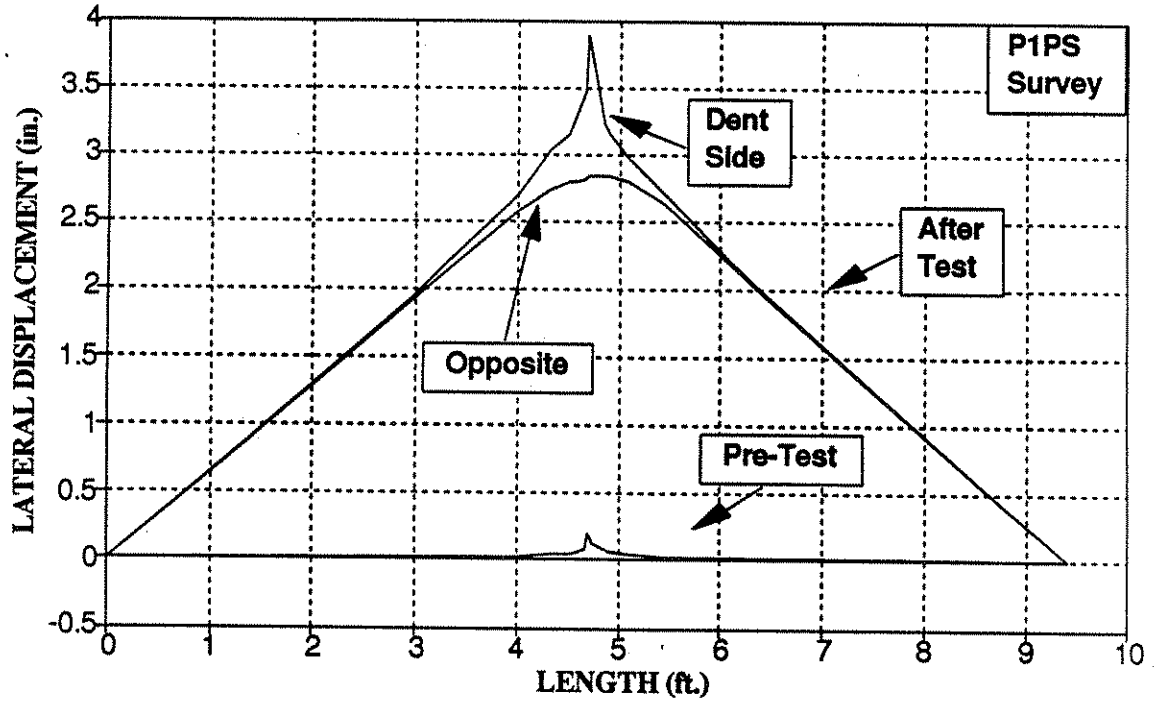

Figure 9-26: Specimen P1PS - Pre- and Post-Test Surface Profiles

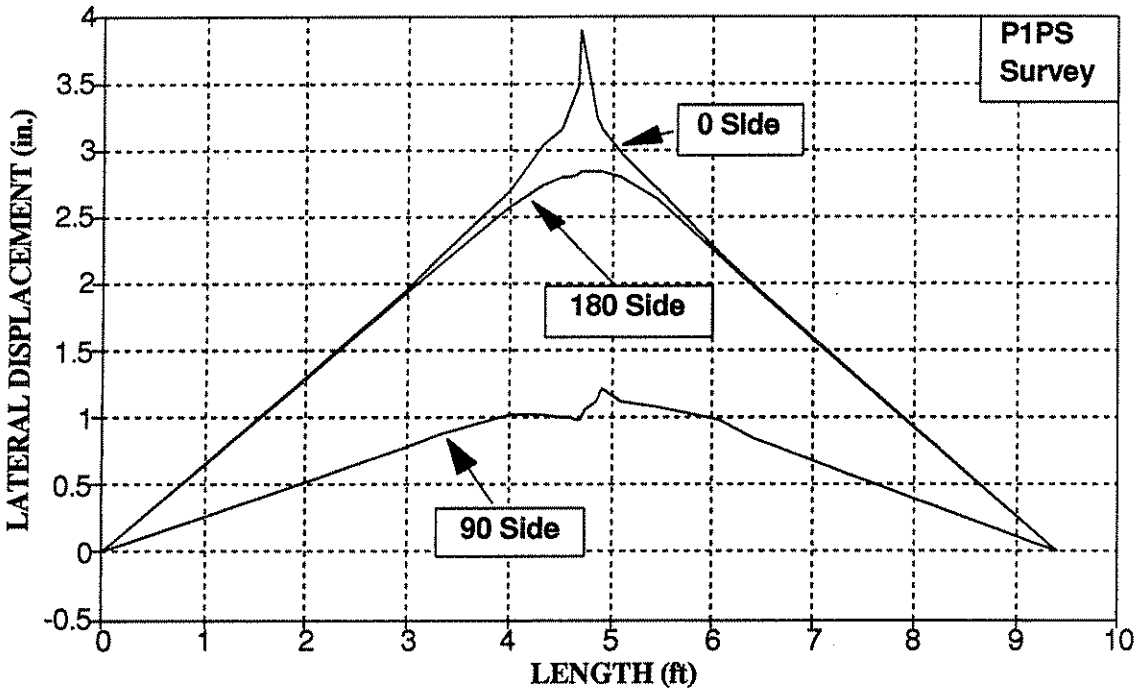

Figure 9-27: Specimen P1PS - Post-Test Surface Profiles of All Sides

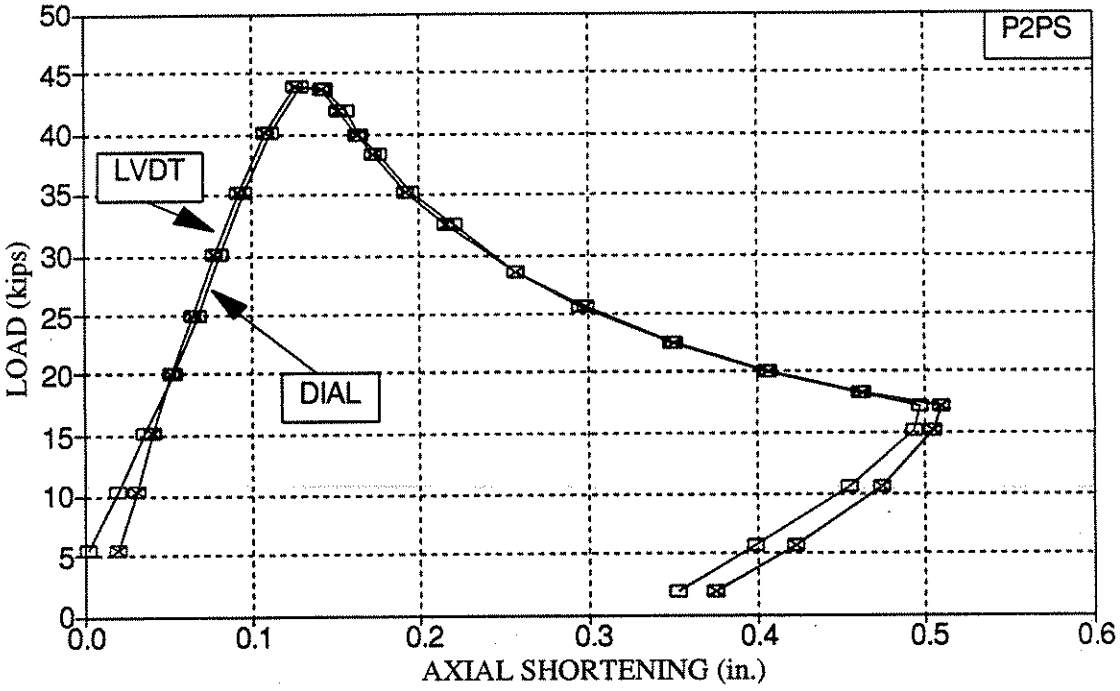

Figure 9-28: Specimen P2PS - Axial Shortening

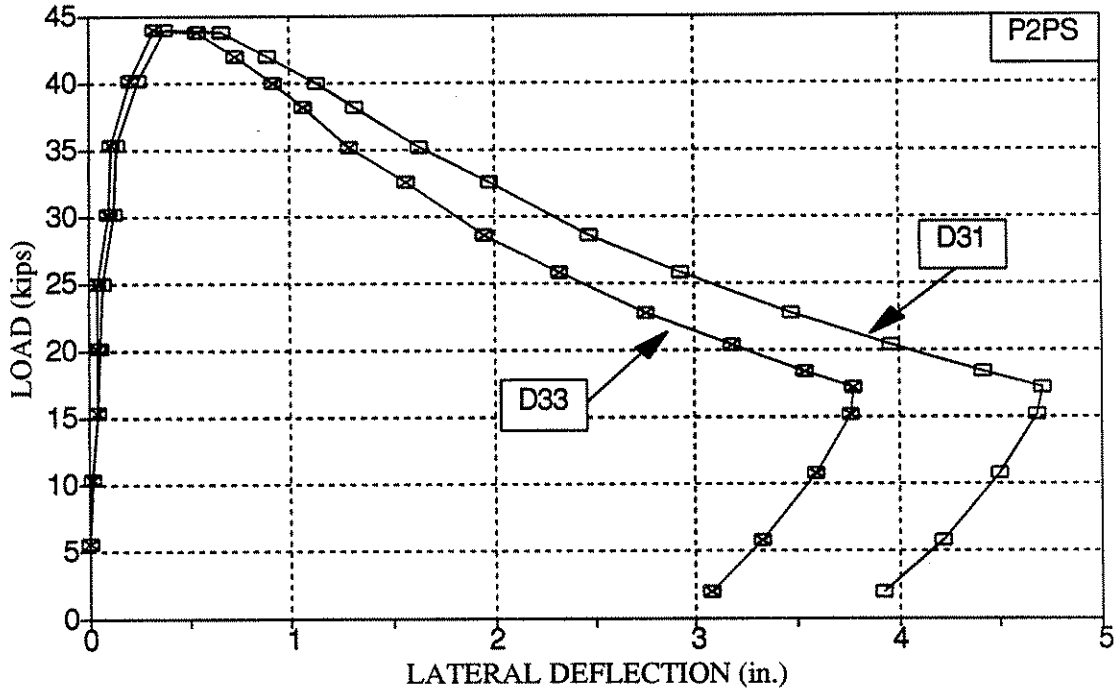

Figure 9-29: Specimen P2PS - Lateral Deflection at Mid-Length

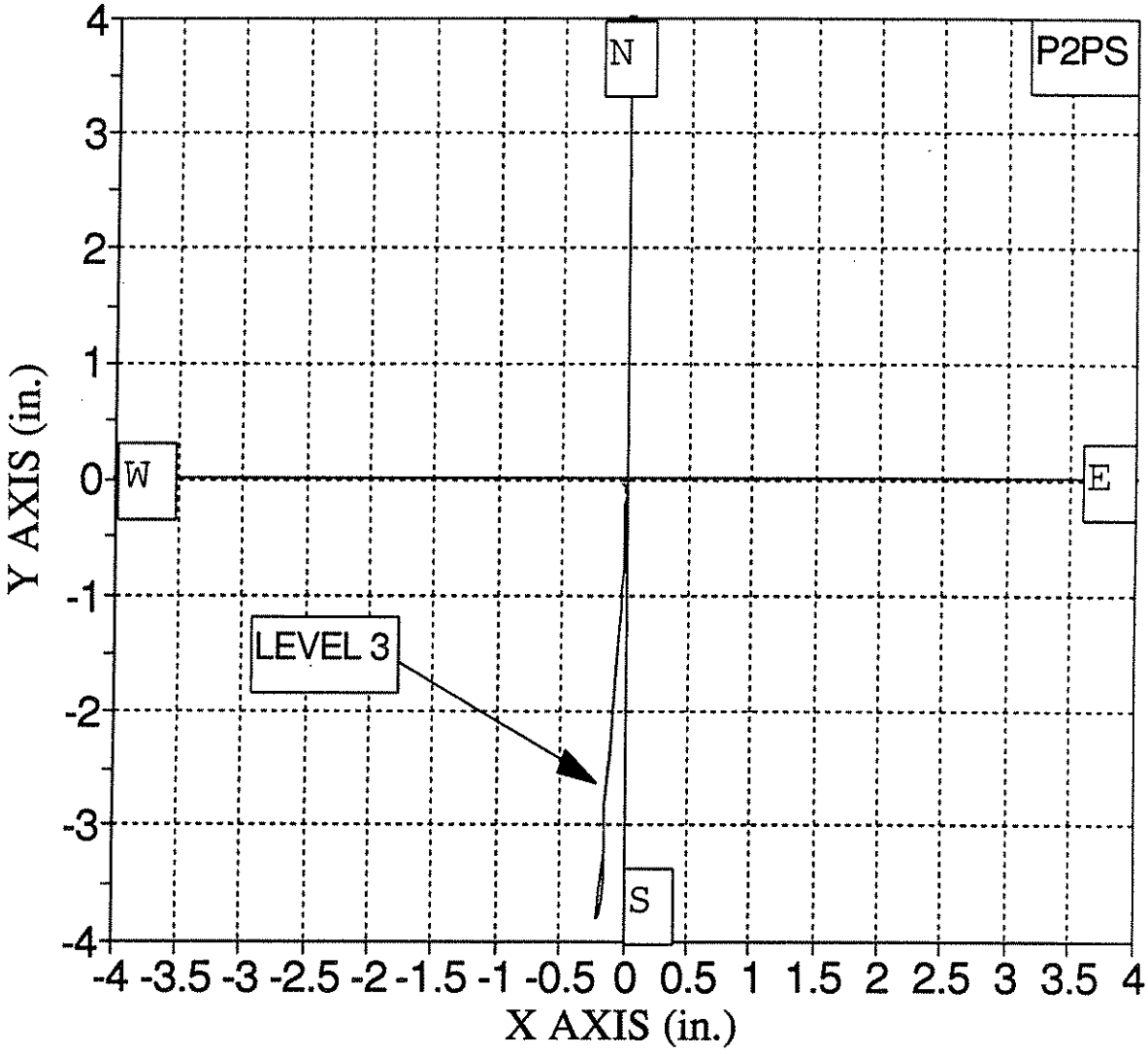

Figure 9-30: Specimen P2PS - Lateral Deflection

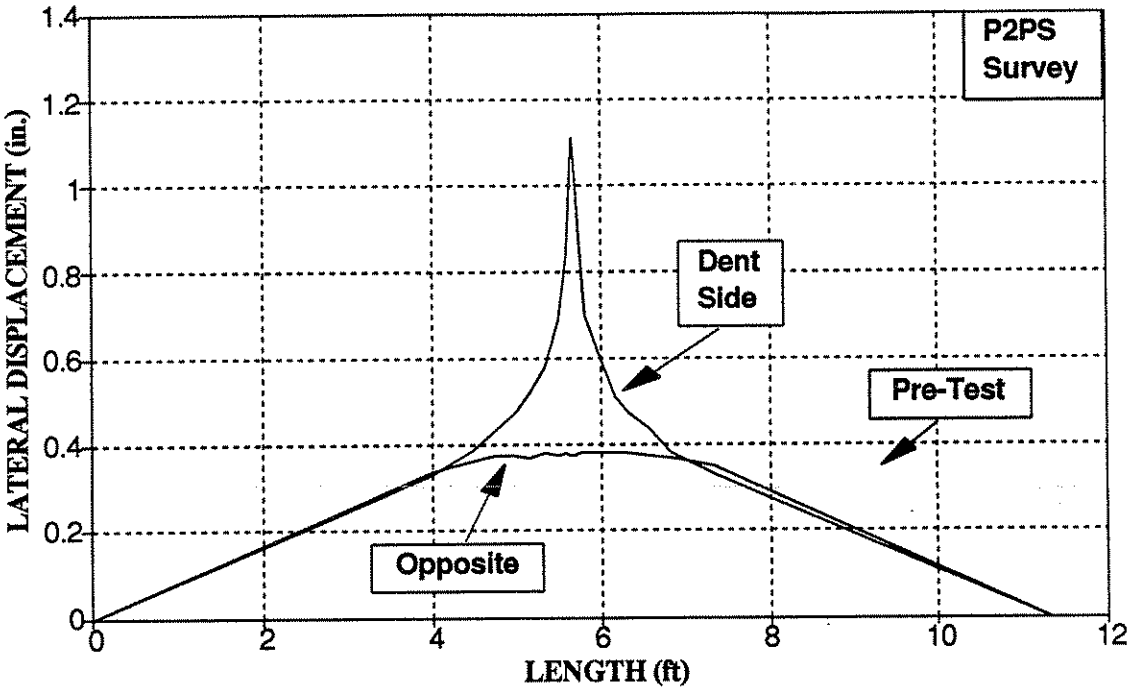

Figure 9-31: Specimen P2PS - Pre-Test Surface Profile

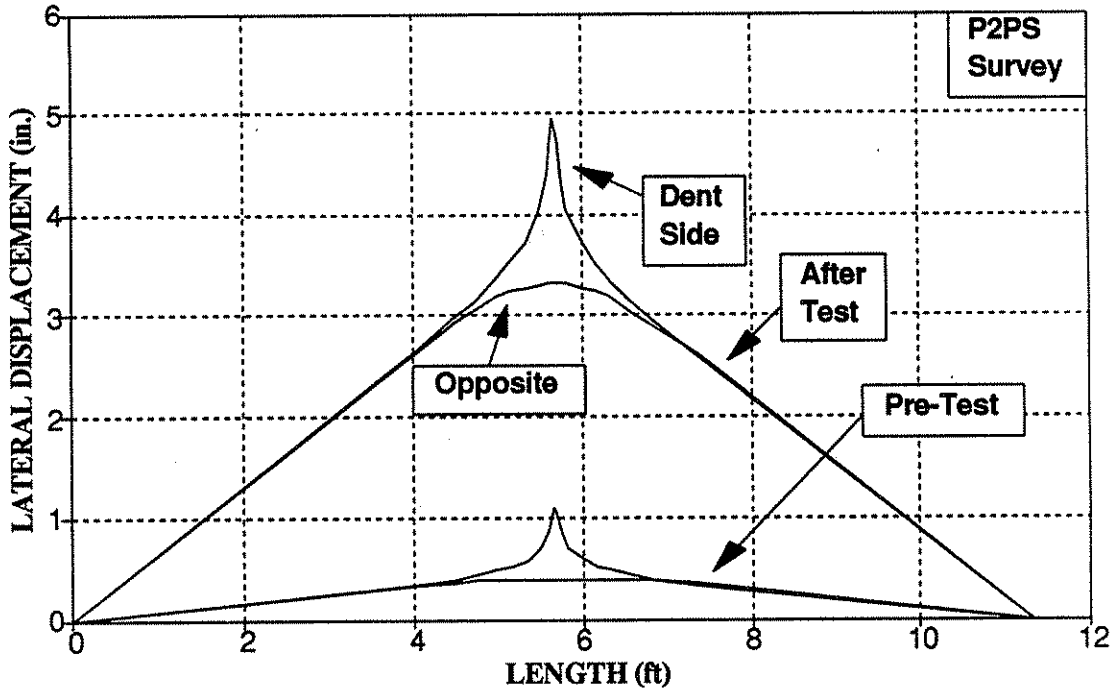

Figure 9-32: Specimen P2PS - Pre- and Post-Test Surface Profiles

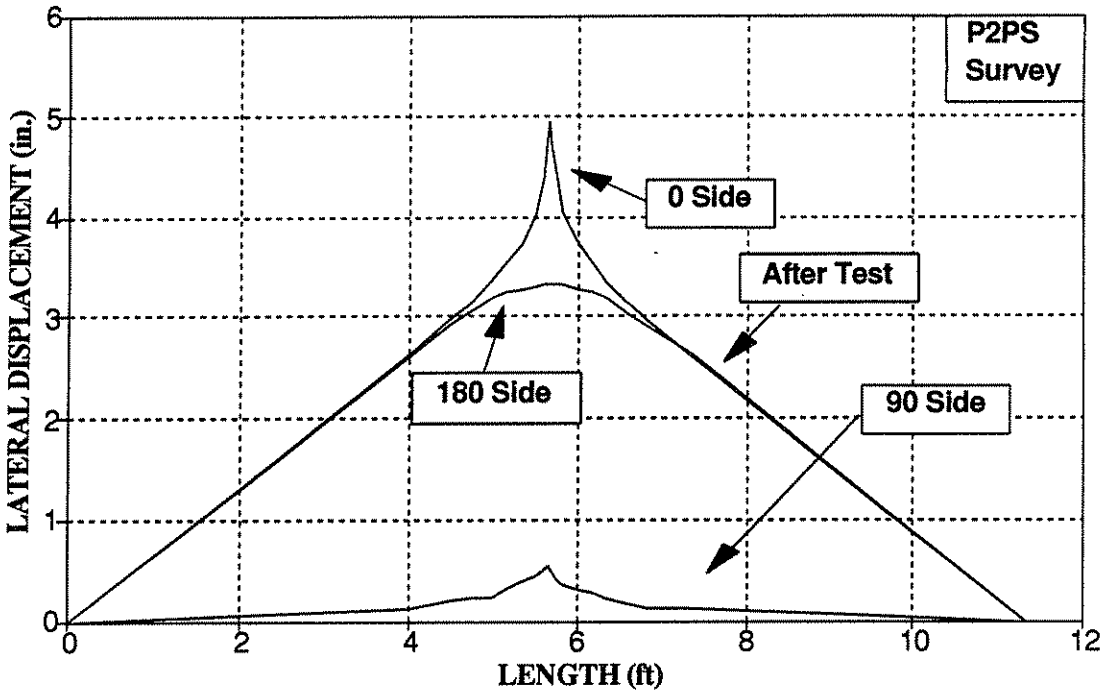

Figure 9-33: Specimen P2PS - Post-Test Surface Profiles of All Sides

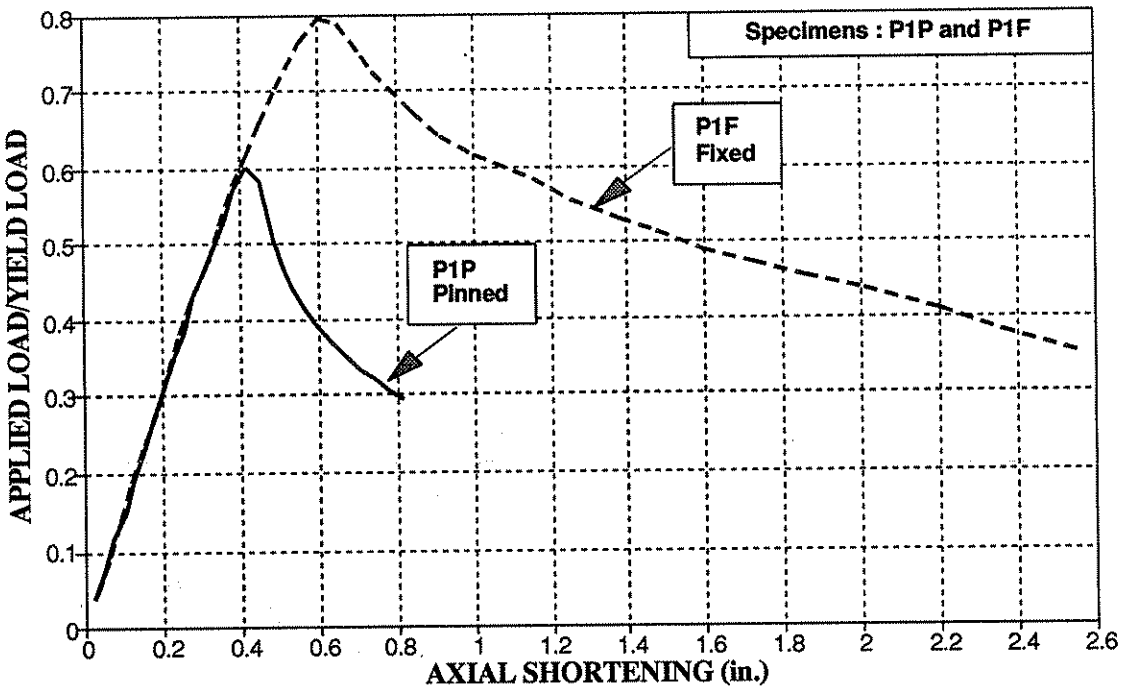

Figure 10-1: Specimens P1F and P1P - Comparison of Behavior of Fixed-Ended and Pin-Ended Specimens

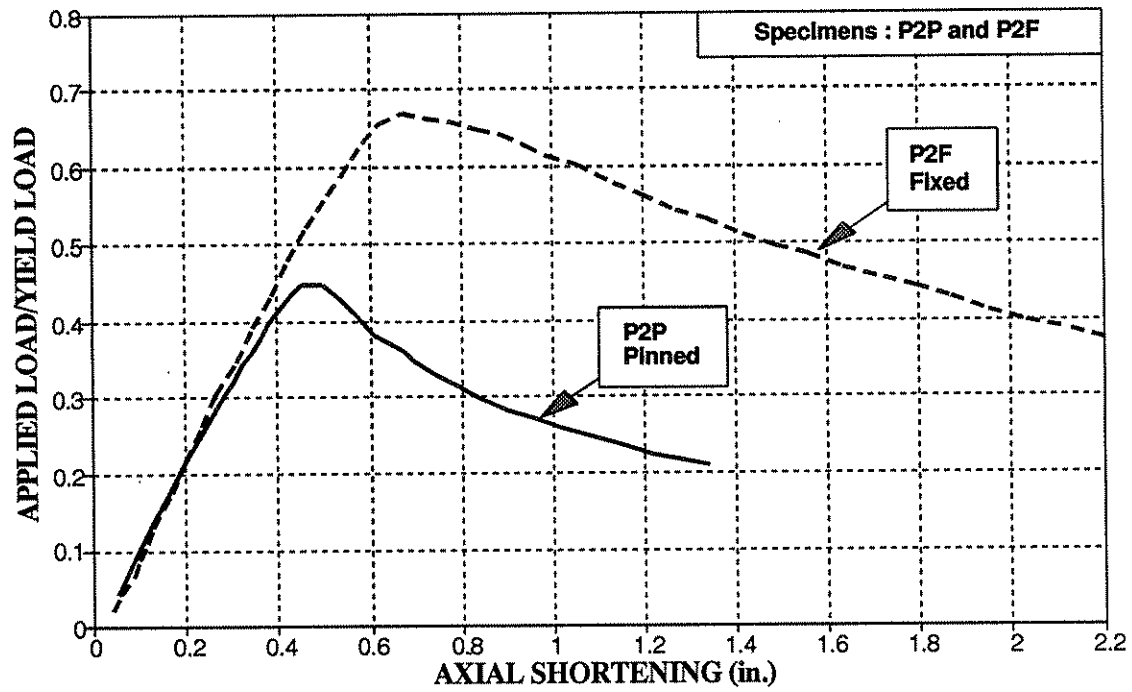

Figure 10-2: Specimens P2F and P2P - Comparison of Behavior of Fixed-Ended and Pin-Ended Specimens

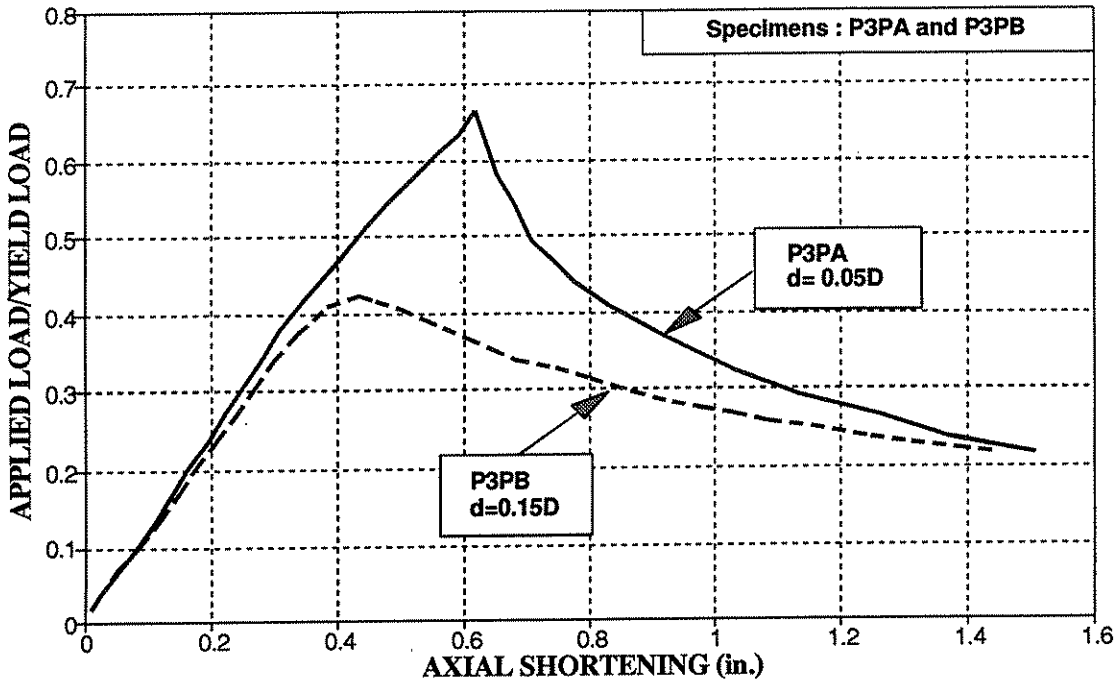

Figure 10-3: Specimens P3PA and P3PB - Comparision of Behavior for Changes of Dent Depth

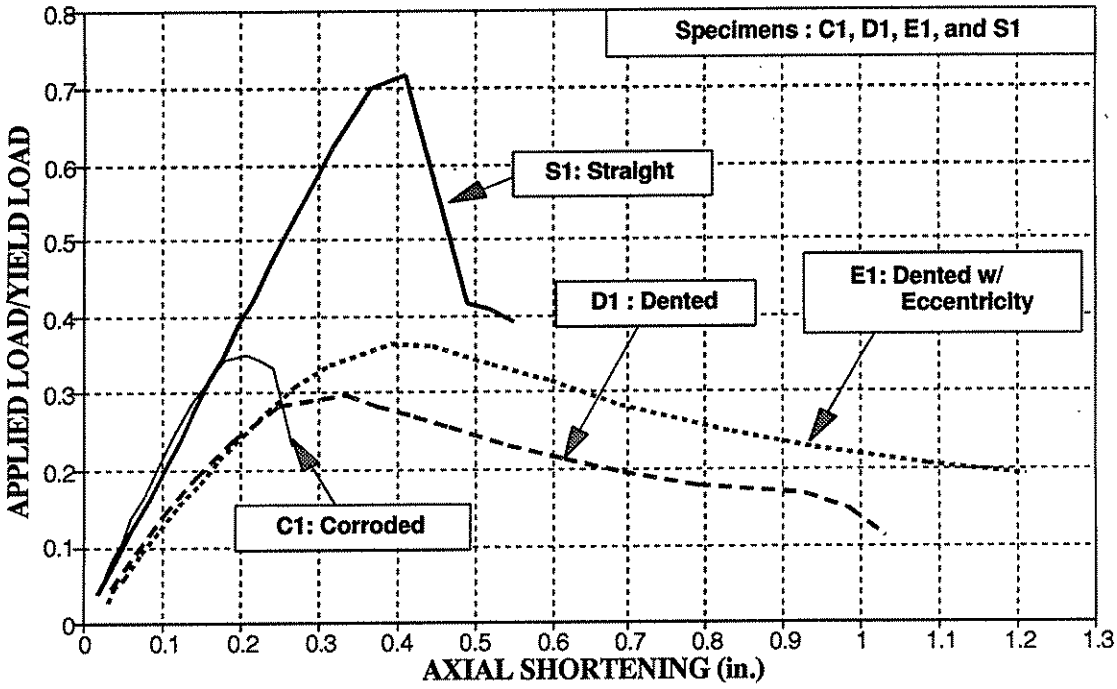

Figure 10-4: Comparison of Series 1 Specimens C1, D1, E1 and S1

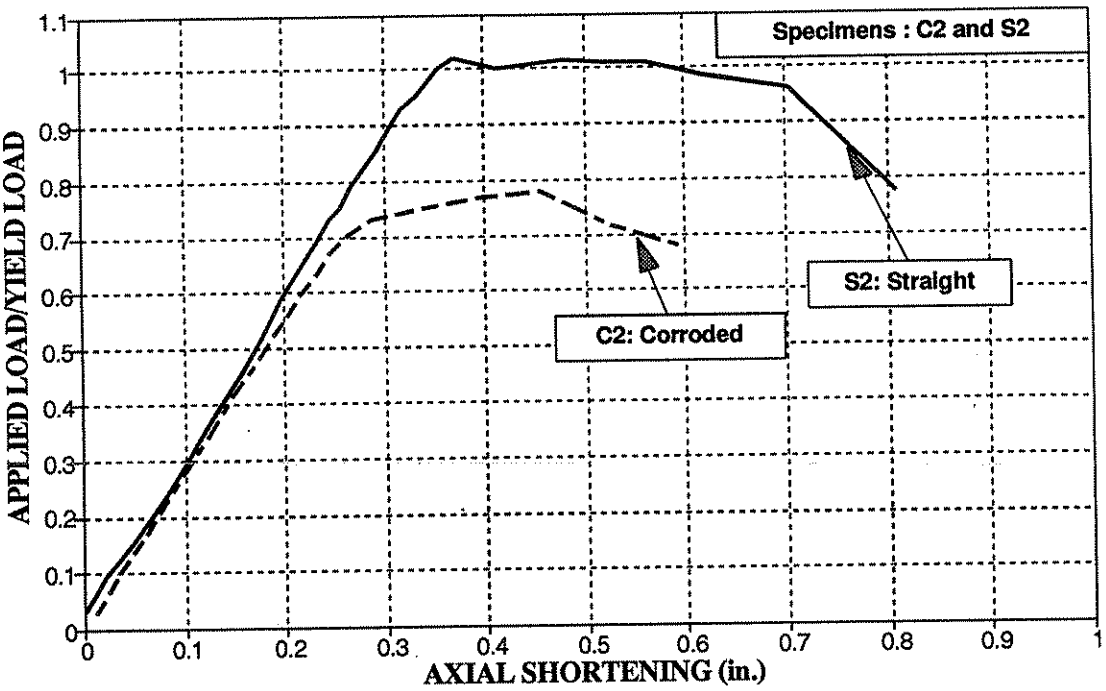

Figure 10-5: Comparision of Series 2 Specimens C2 and S2

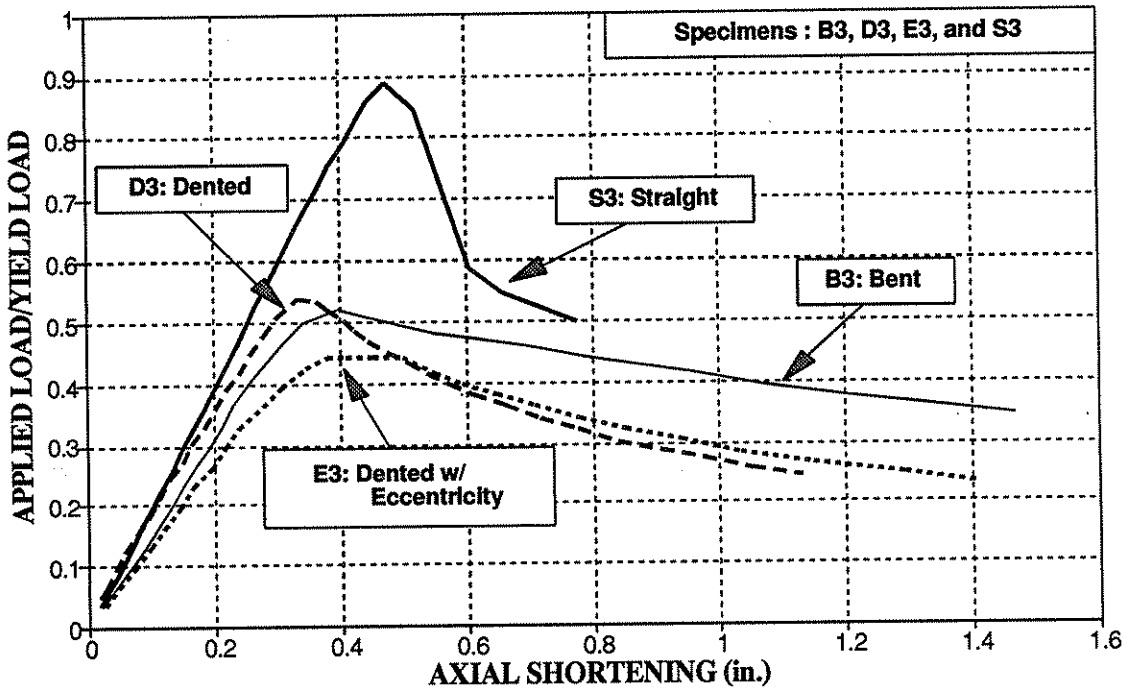

Figure 10-6: Comparision of Series 3 Specimens B3, D3, E3 and S3

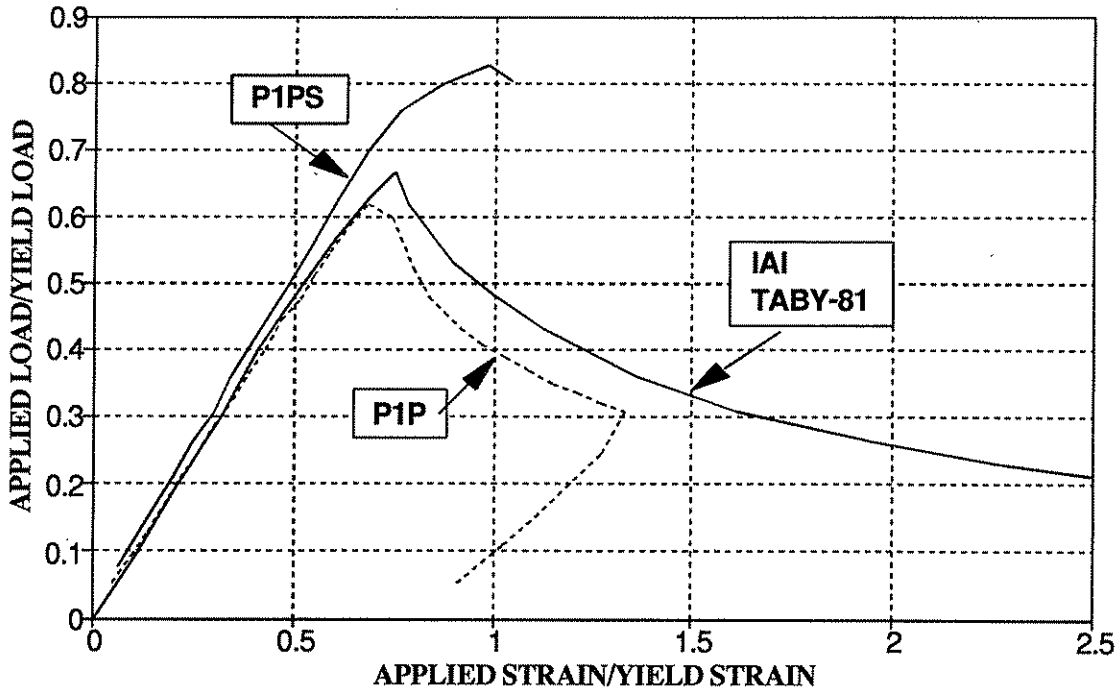

Figure 10-7: Comparison of Specimens P1P, P1PS, and IAI (Taby-81).

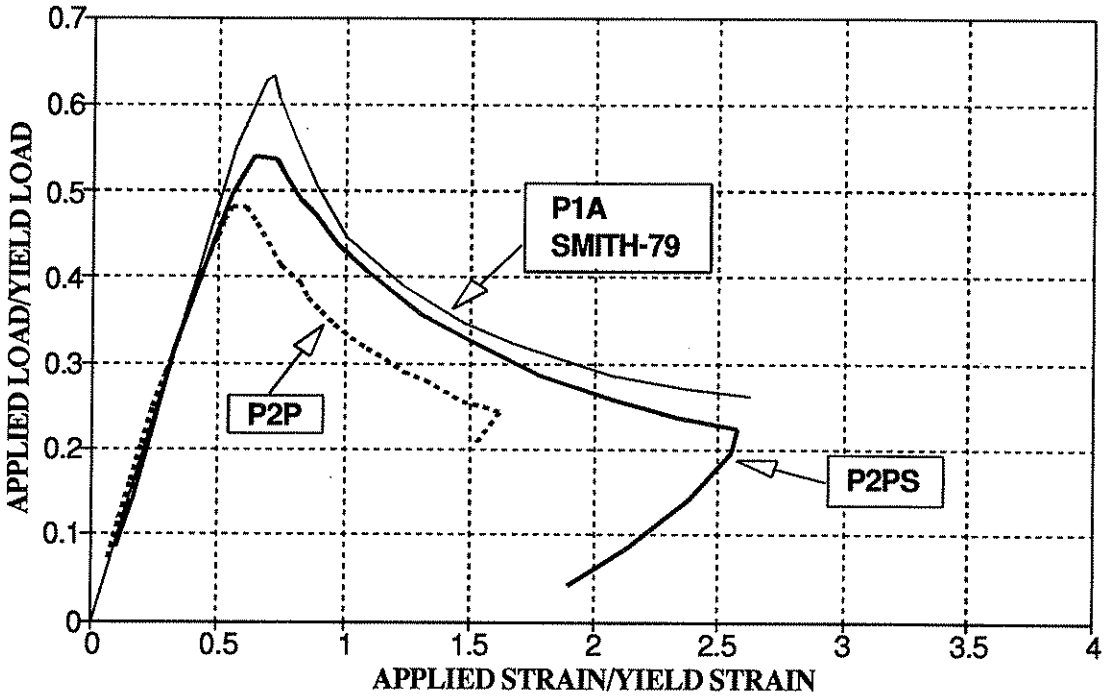

Figure 10-8: Comparison of Specimens P2P, P2PS, and P1A (Smith-79).

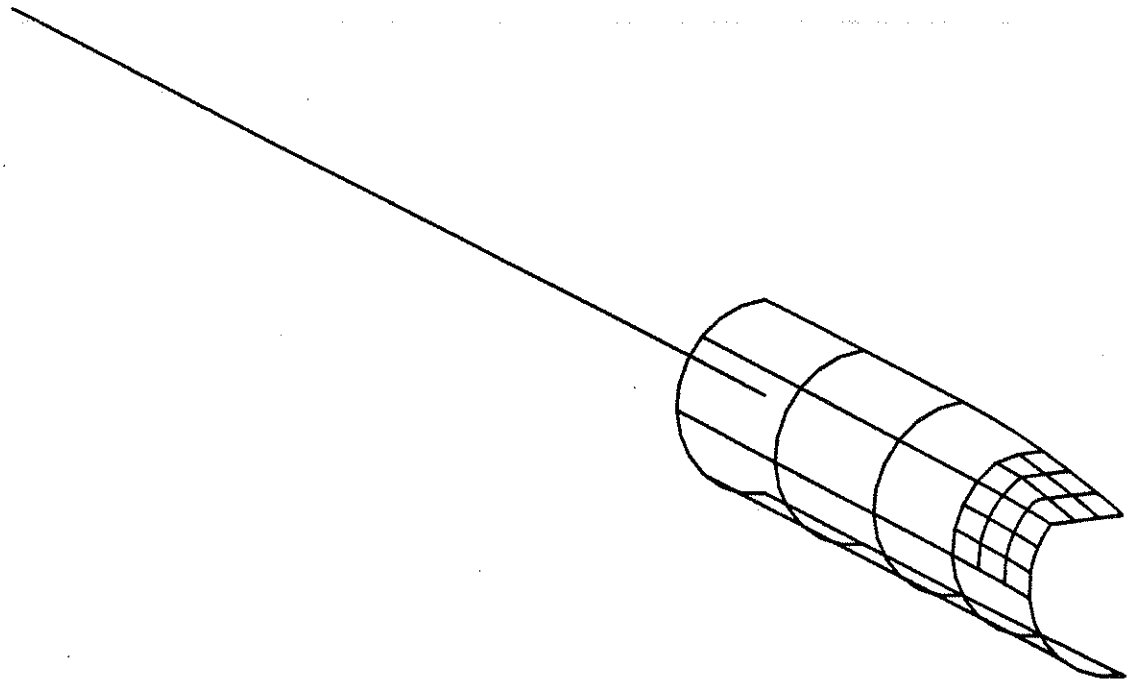

Figure 11-1: A finite element model for a typical specimen.

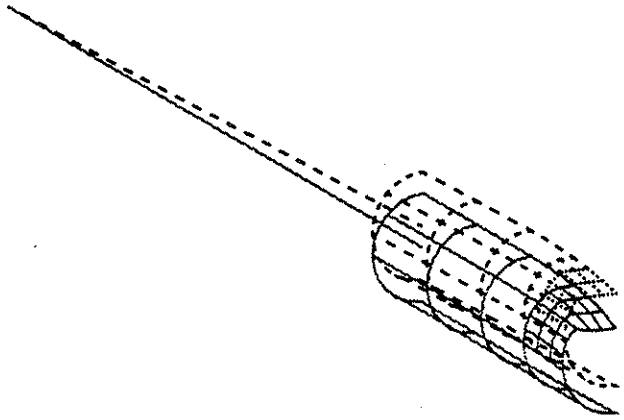

Figure 11-2: Deformations in a typical model in the early post-ultimate range.

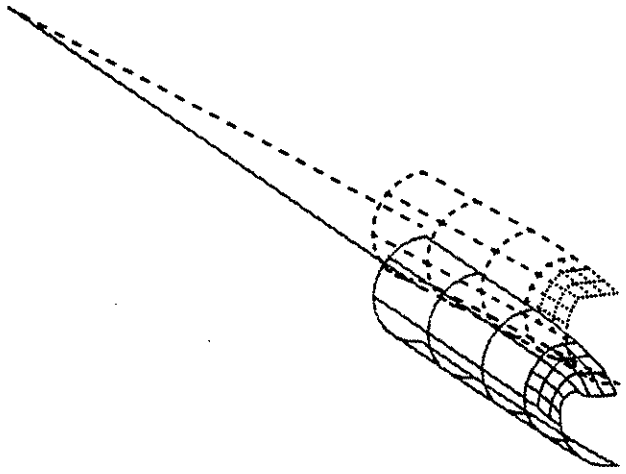

Figure 11-3: Deformations in a typical model in the late post-ultimate range.

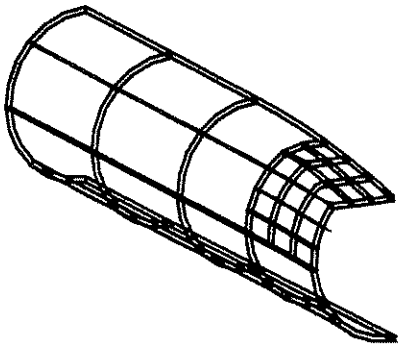

Figure 11-4: Close-up view of the shell elements modeling the damaged portion.

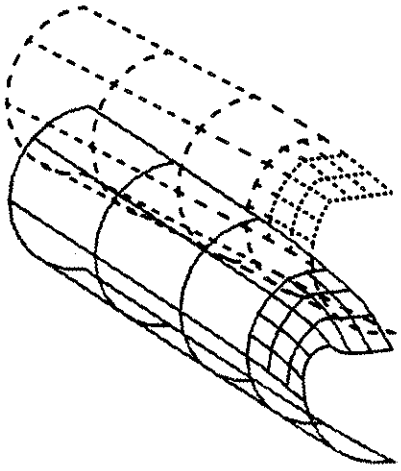

Figure 11-5: Plasticity and distortion modeled by the shell elements.

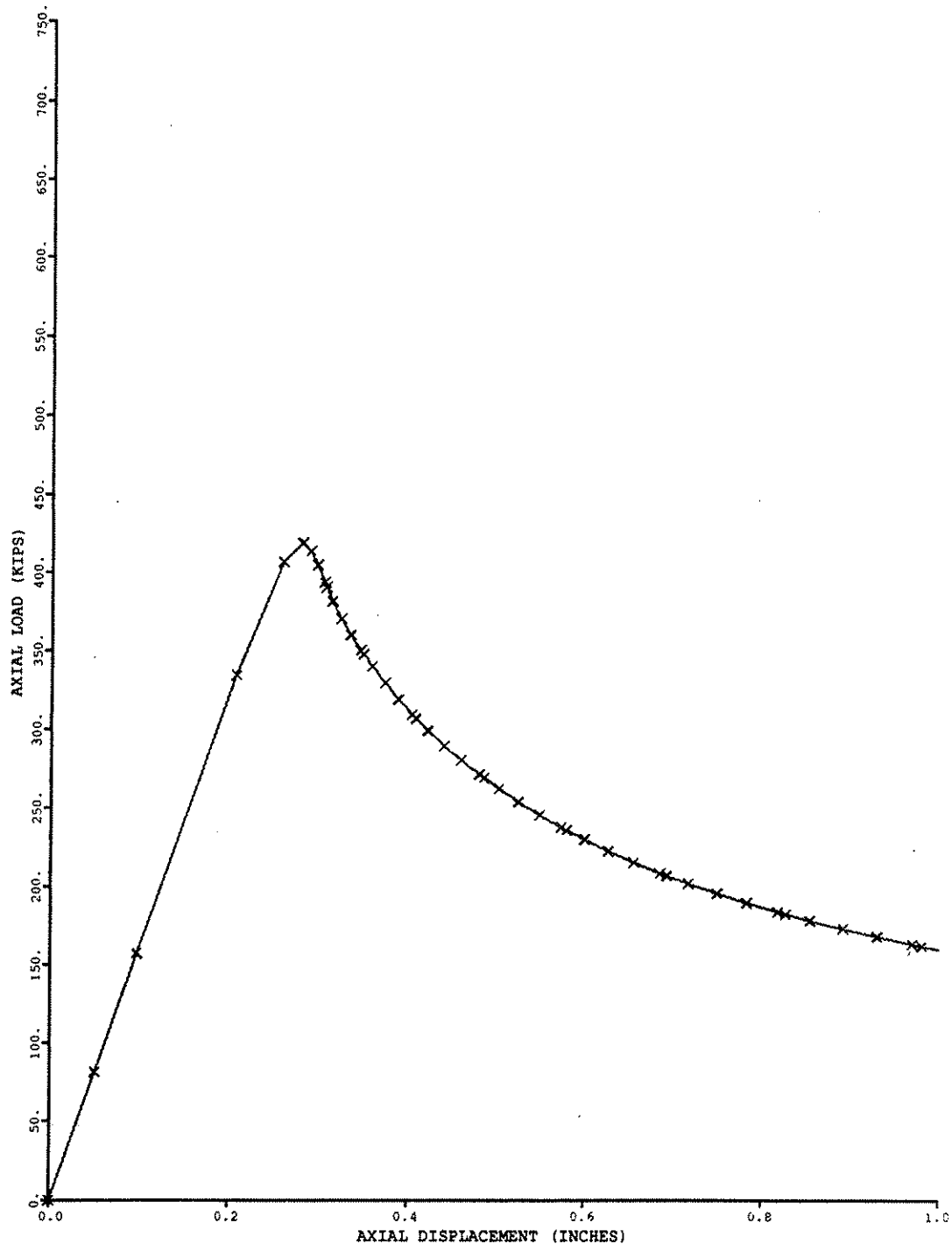

Figure 11-6: A typical load-deformation relationship (Specimen D3).

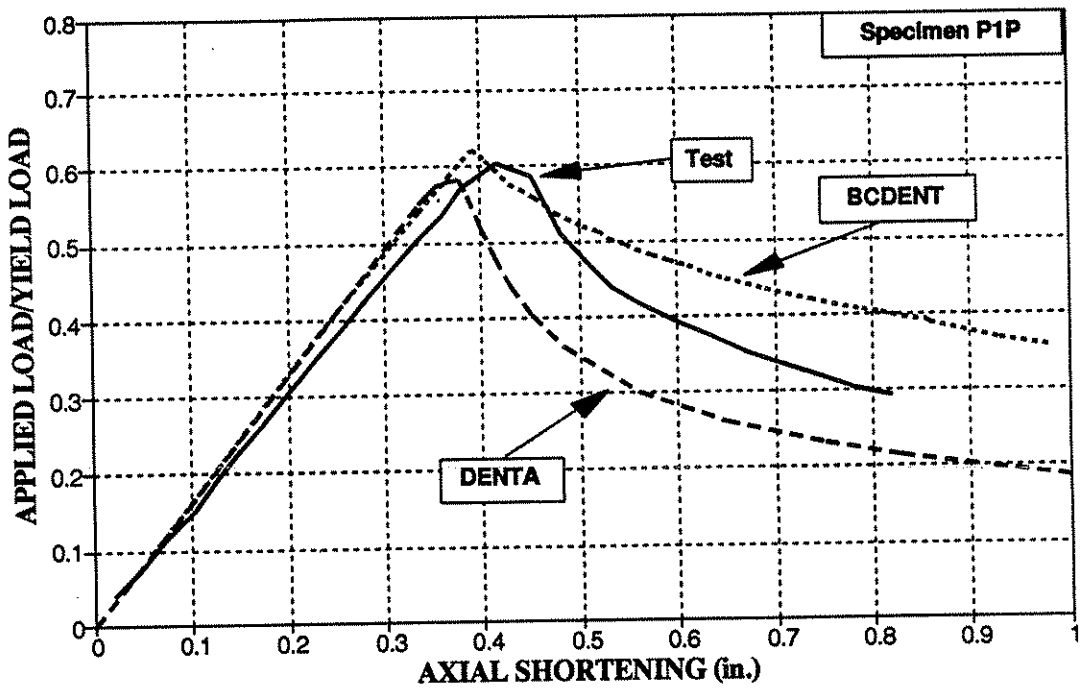

Figure 12-1: Specimen P1P - Comparison of Test, BCDENT, and DENTA

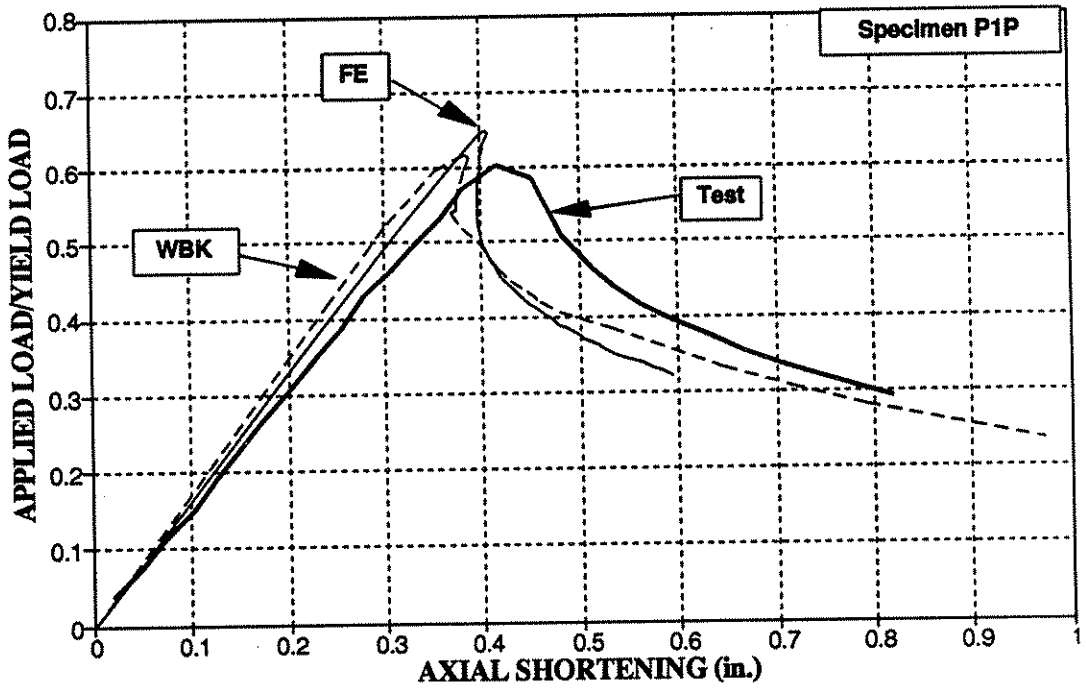

Figure 12-2: Specimen P1P - Comparison of Test, Finite Elements, and WBK

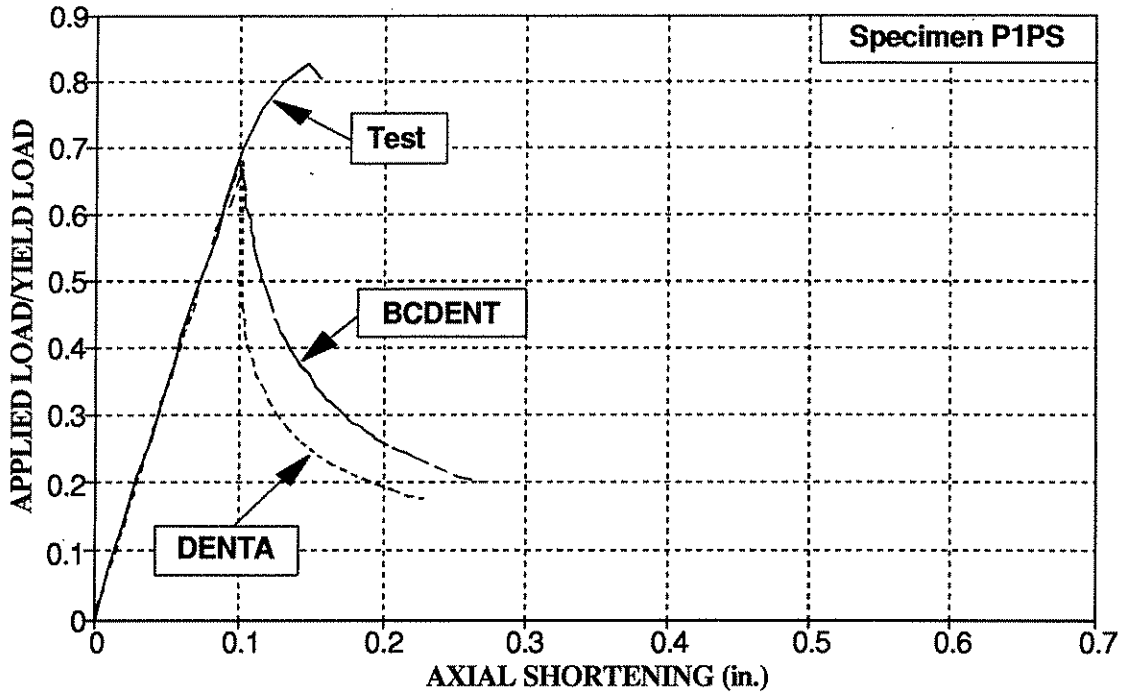

Figure 12-1(a): Specimen P1PS - Comparison of Test, BCDENT, and DENTA.

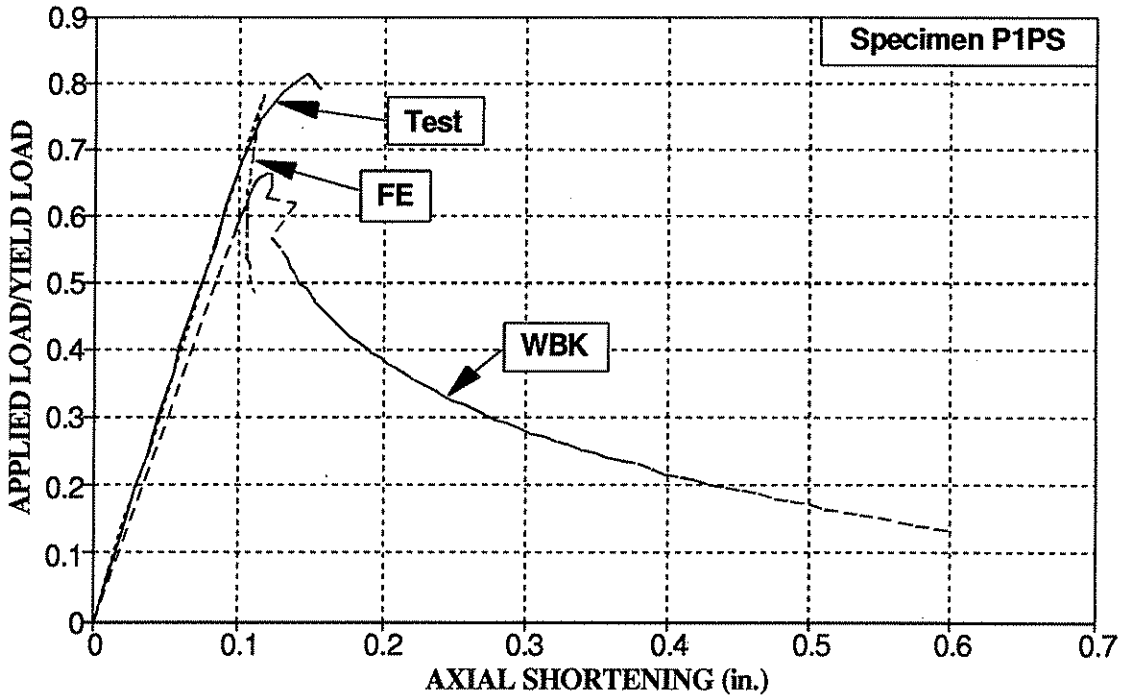

Figure 12-2(a): Specimen P1PS - Comparison of Test, Finite Elements, and WBK.

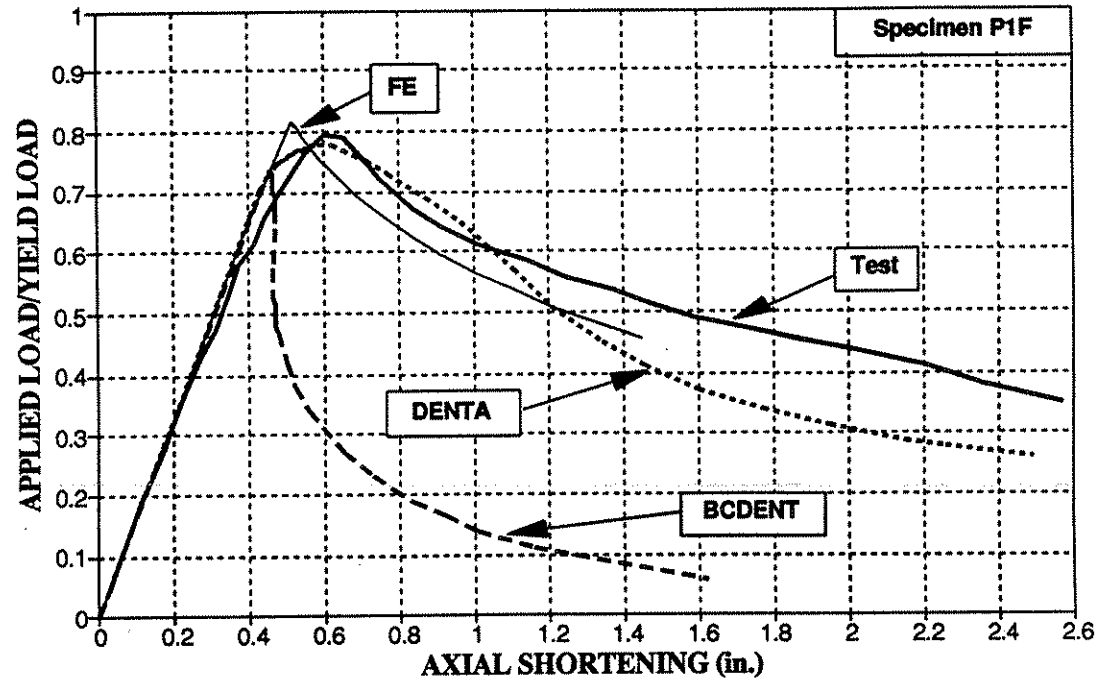

Figure 12-3: Specimen P1F - Comparison of Test, BCDENT, DENTA and Finite Elements

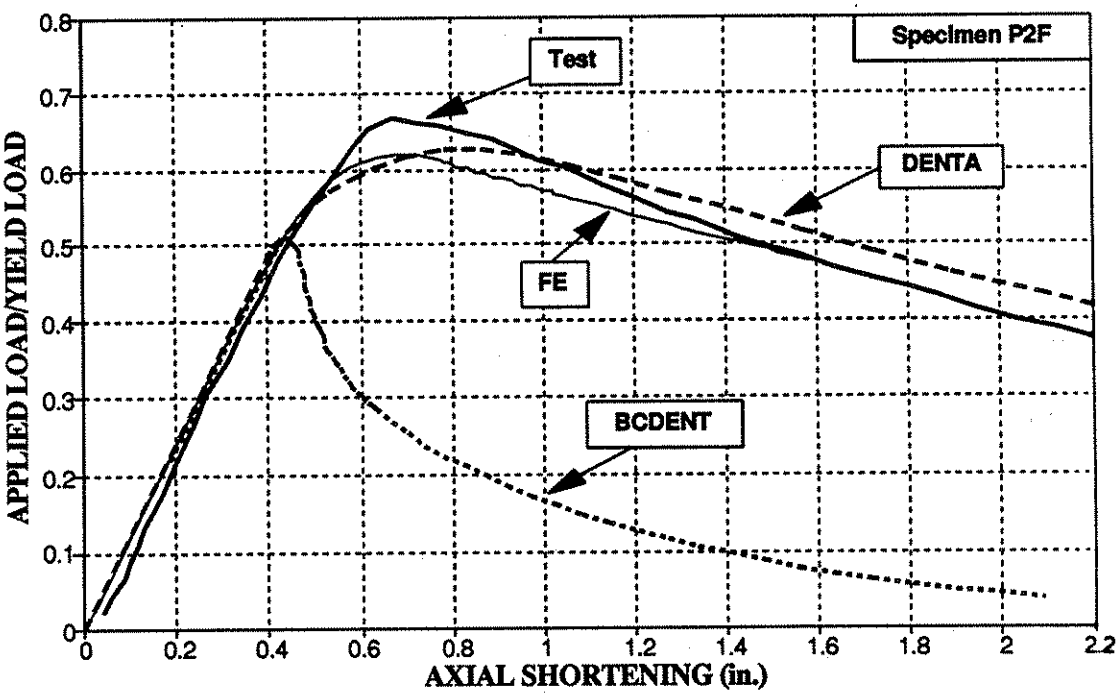

Figure 12-4: Specimen P2F - Comparison of Test, DENTA, BCDENT and Finite Elements

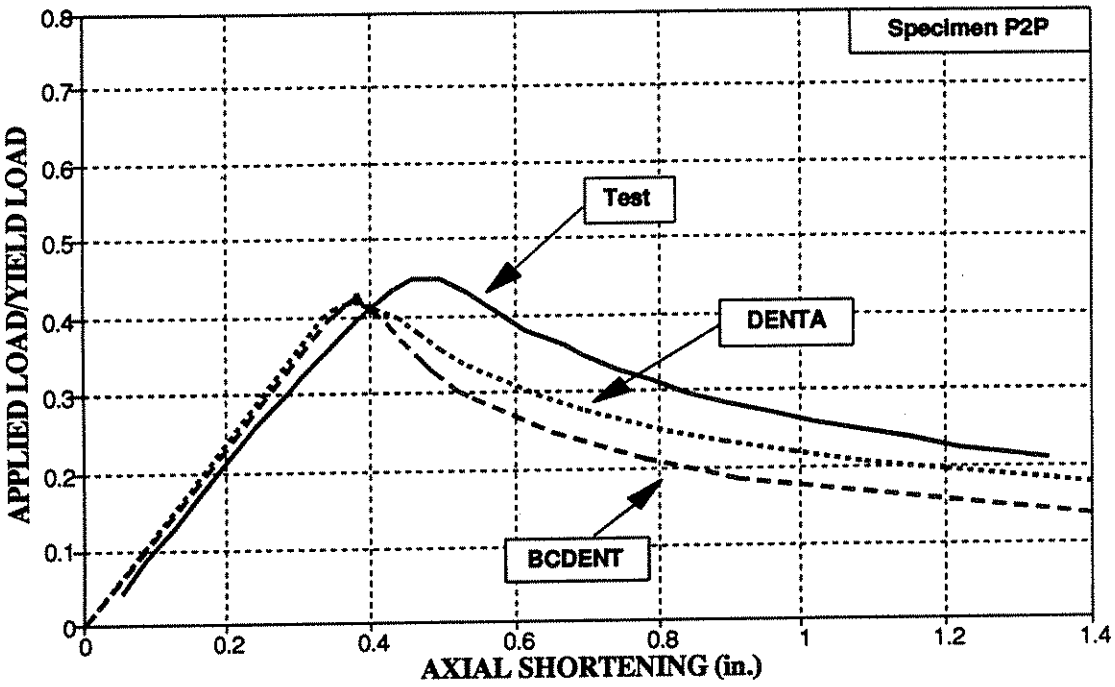

Figure 12-5: Specimen P2P - Comparison of Test, BCDENT, and DENTA

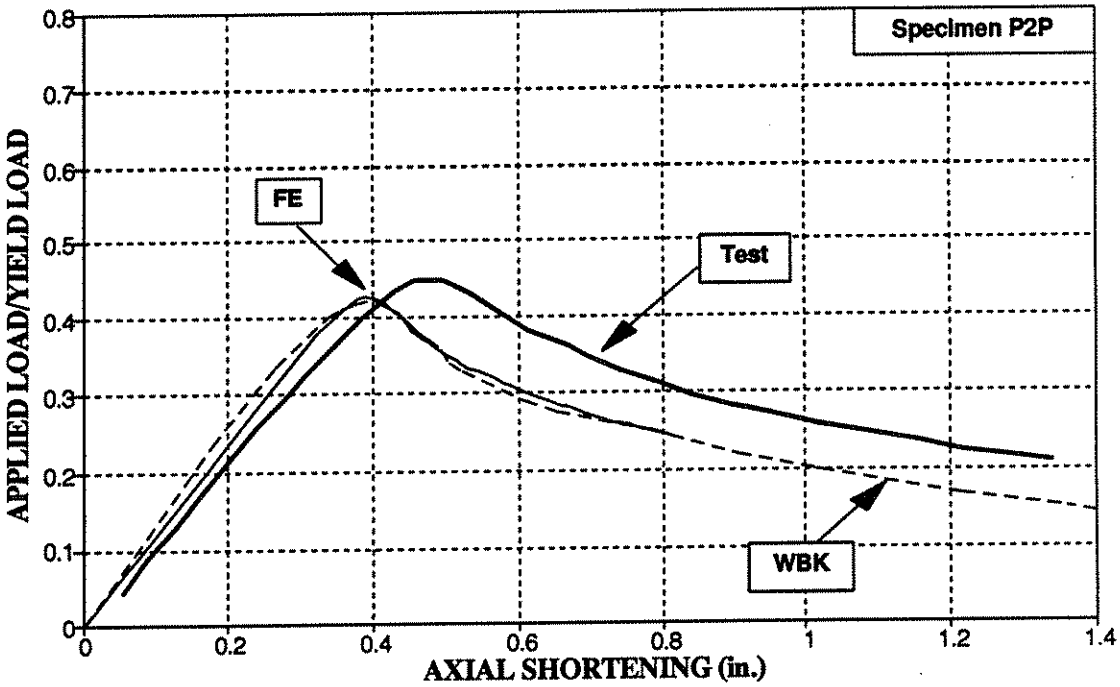

Figure 12-6: Specimen P2P - Comparison of Test, Finite Elements, and WBK

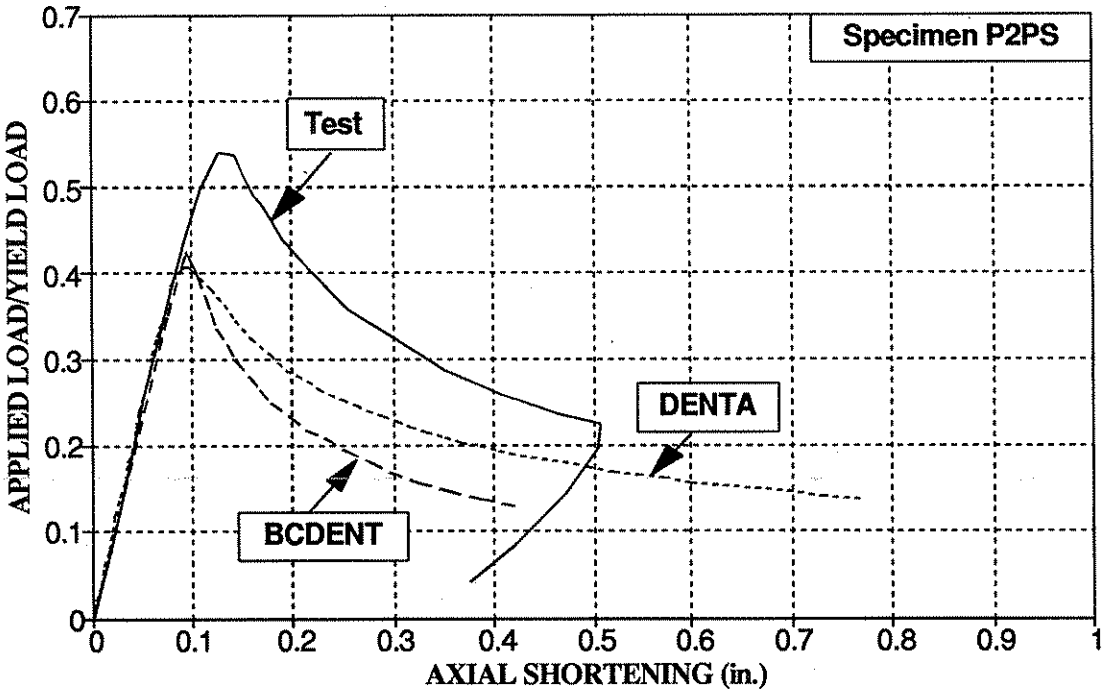

Figure 12-5(a): Specimen P2PS - Comparison of Test, BCDENT, and DENTA.

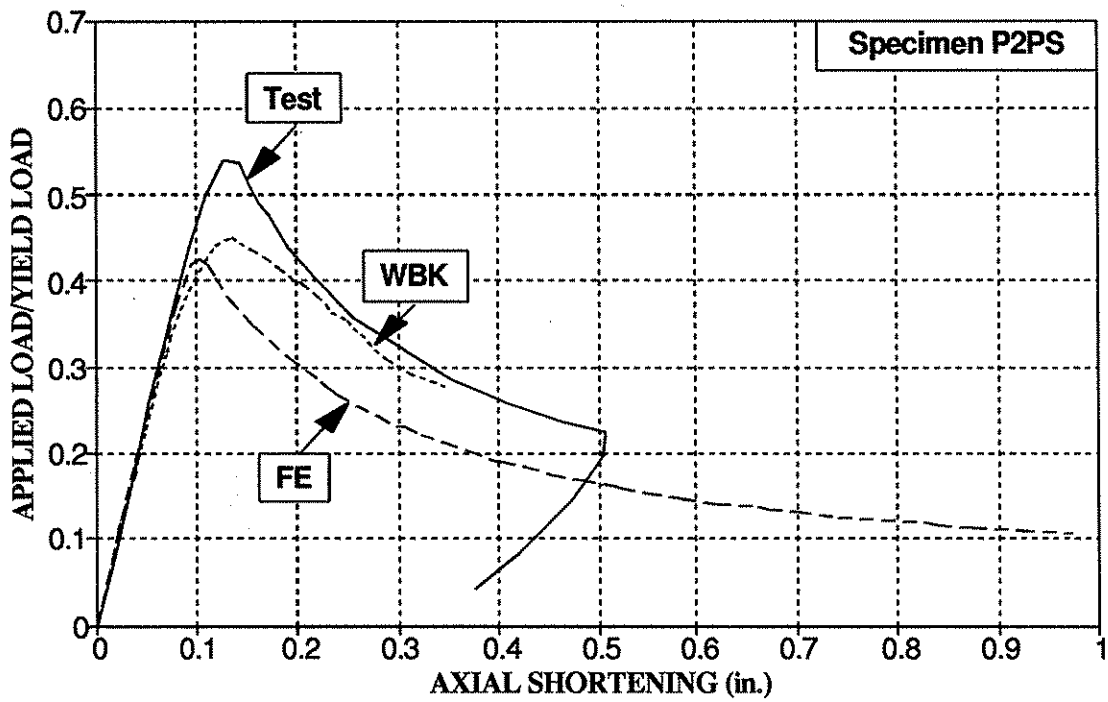

Figure 12-6(a): Specimen P2PS - Comparison of Test, Finite Elements, and WBK.

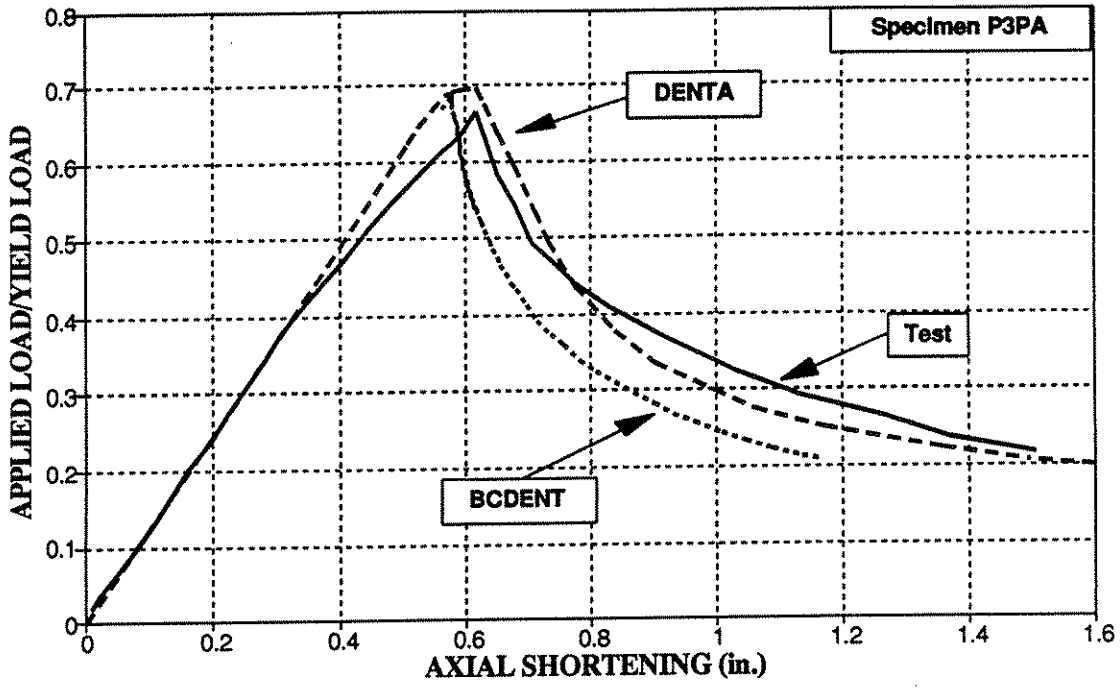

Figure 12-7: Specimen P3PA - Comparison of Test, BCDENT, and DENTA

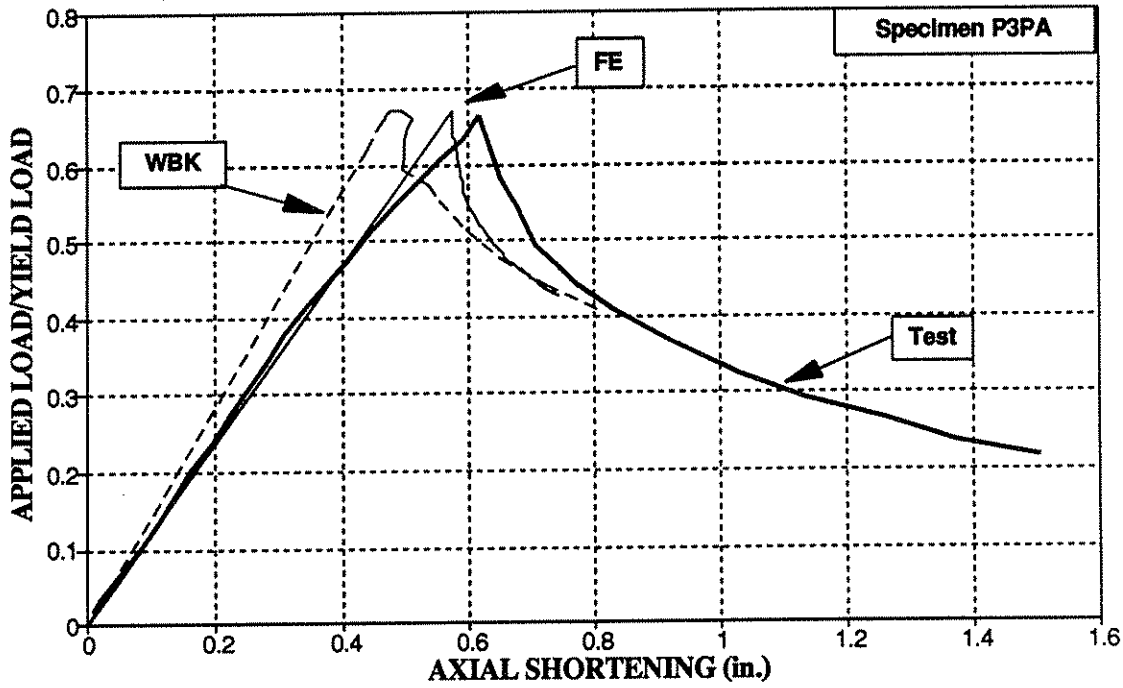

Figure 12-8: Specimen P3PA - Comparison of Test, Finite Elements, and WBK

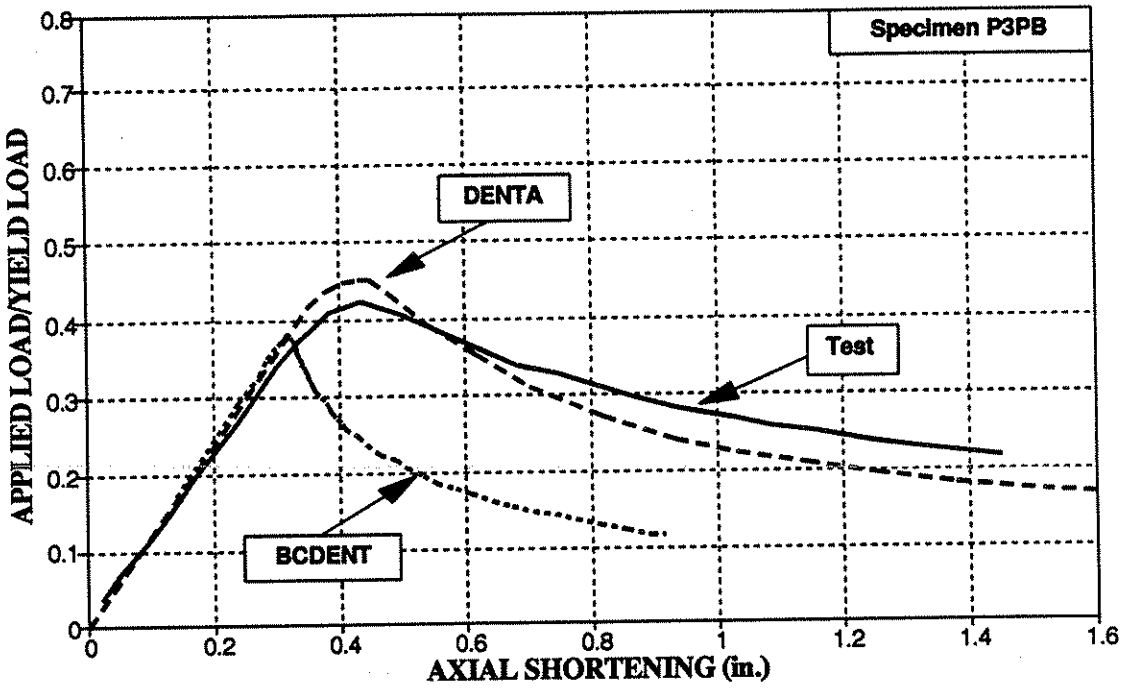

Figure 12-9: Specimen P3PB - Comparison of Test, BCDENT, and DENTA

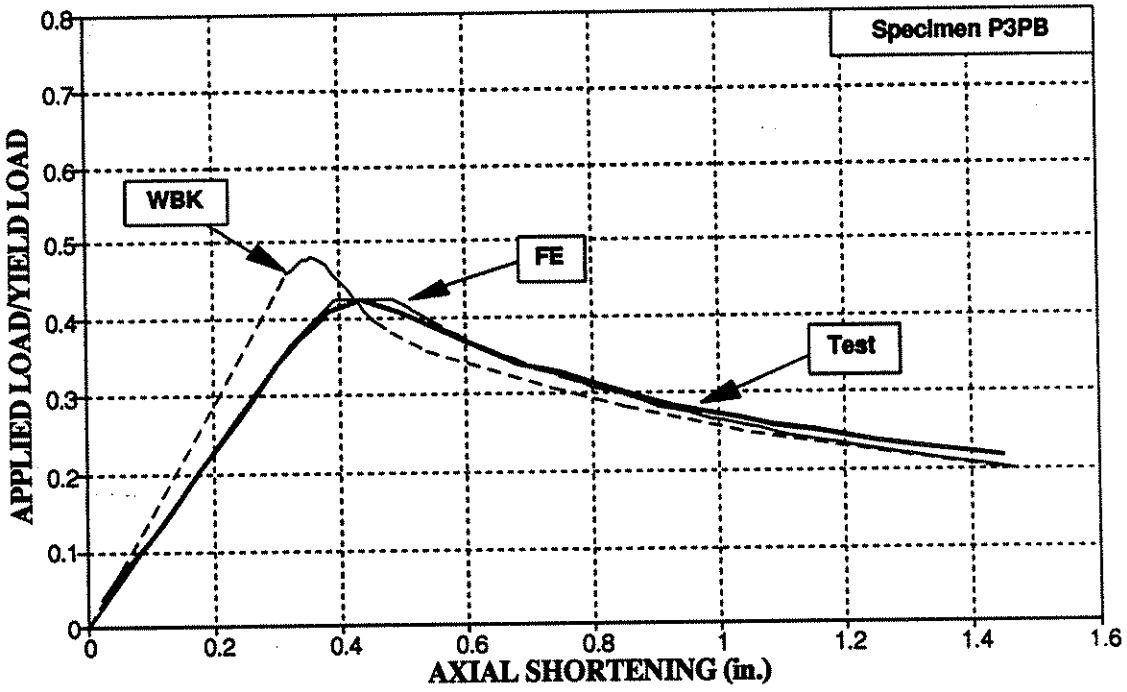

Figure 12-10: Specimen P3PB - Comparison of Test, Finite Elements, and WBK

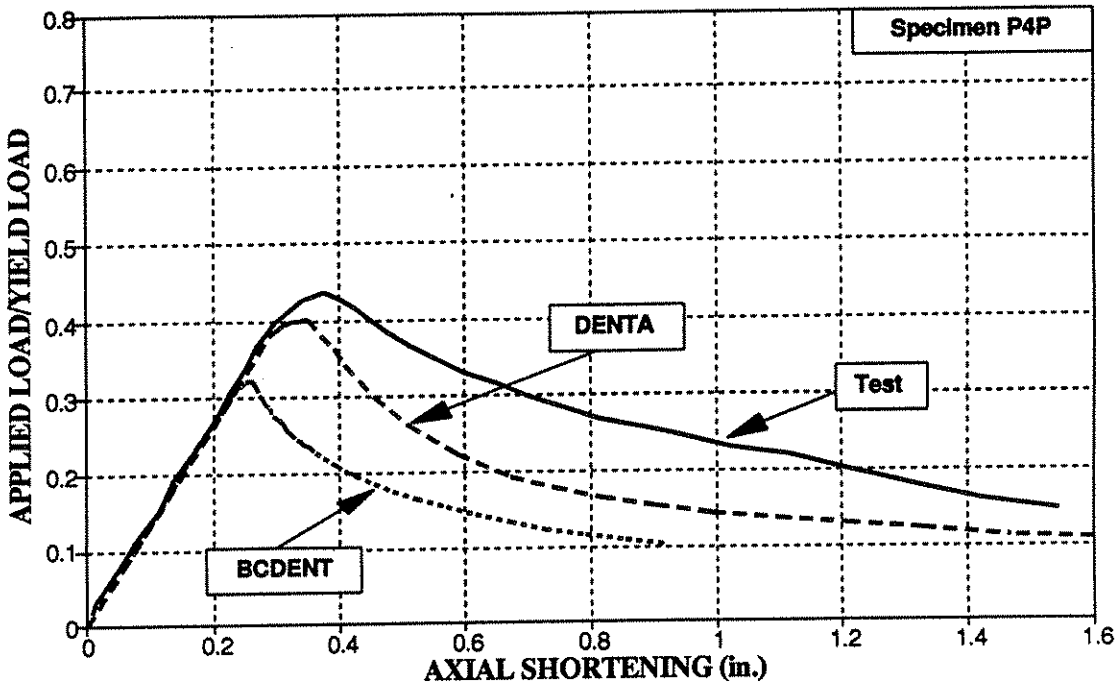

Figure 12-11: Specimen P4P - Comparison of Test, BCDENT, and DENTA

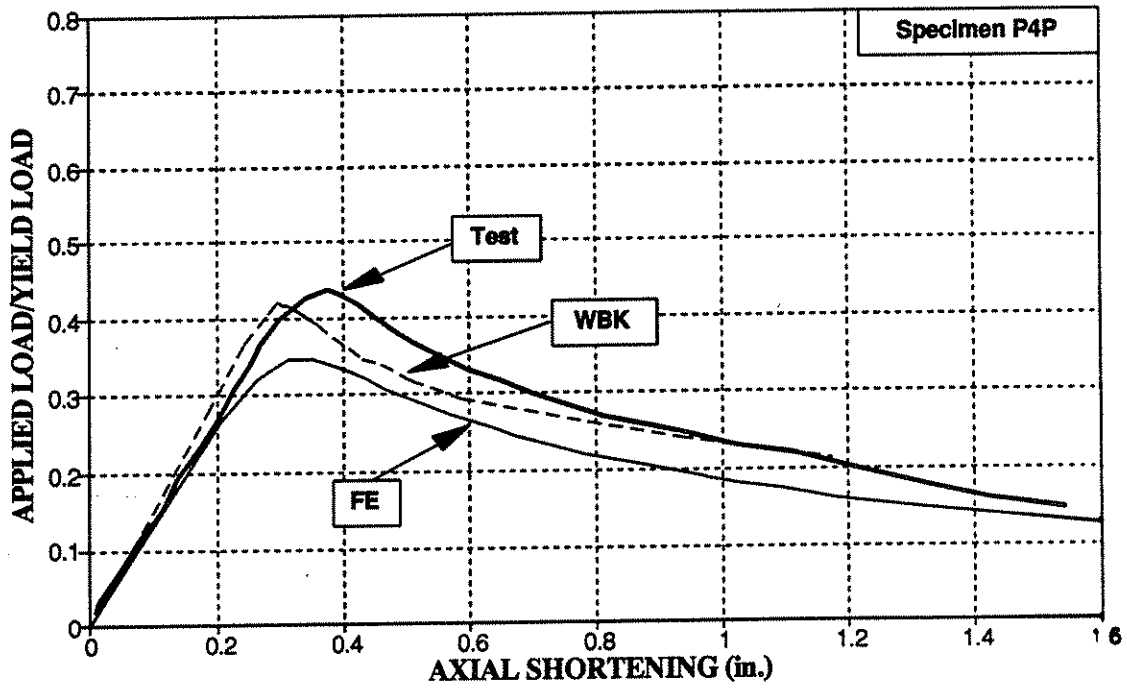

Figure 12-12: Specimen P4P - Comparison of Test, Finite Elements, and WBK

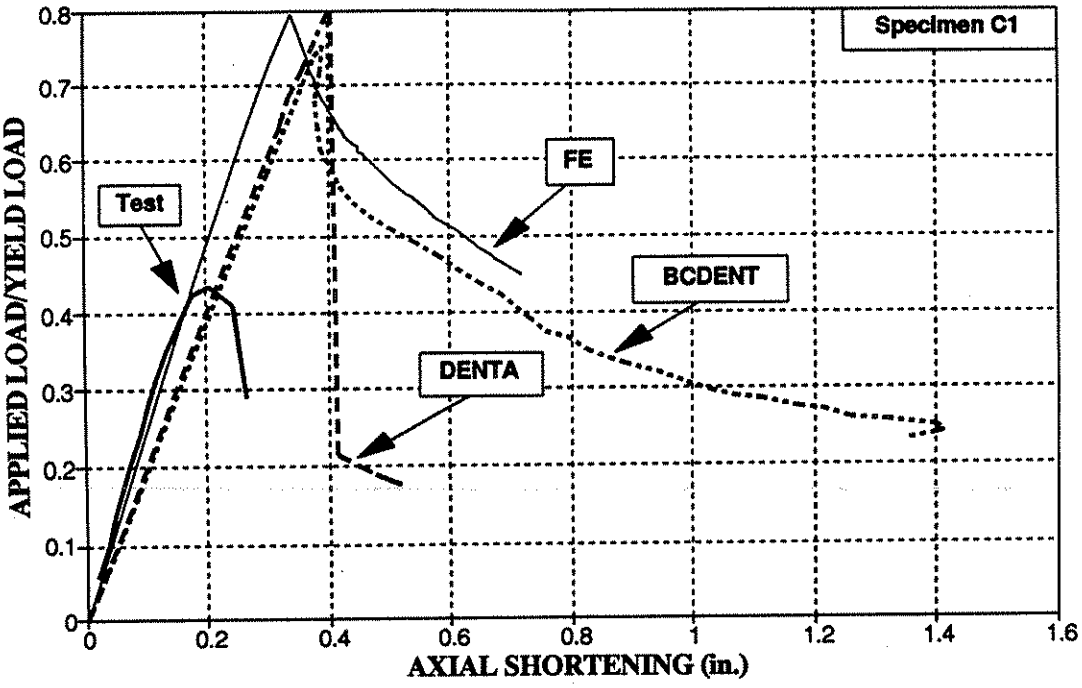

Figure 12-13: Specimen C1 - Comparison of Test, BCDENT, and DENTA

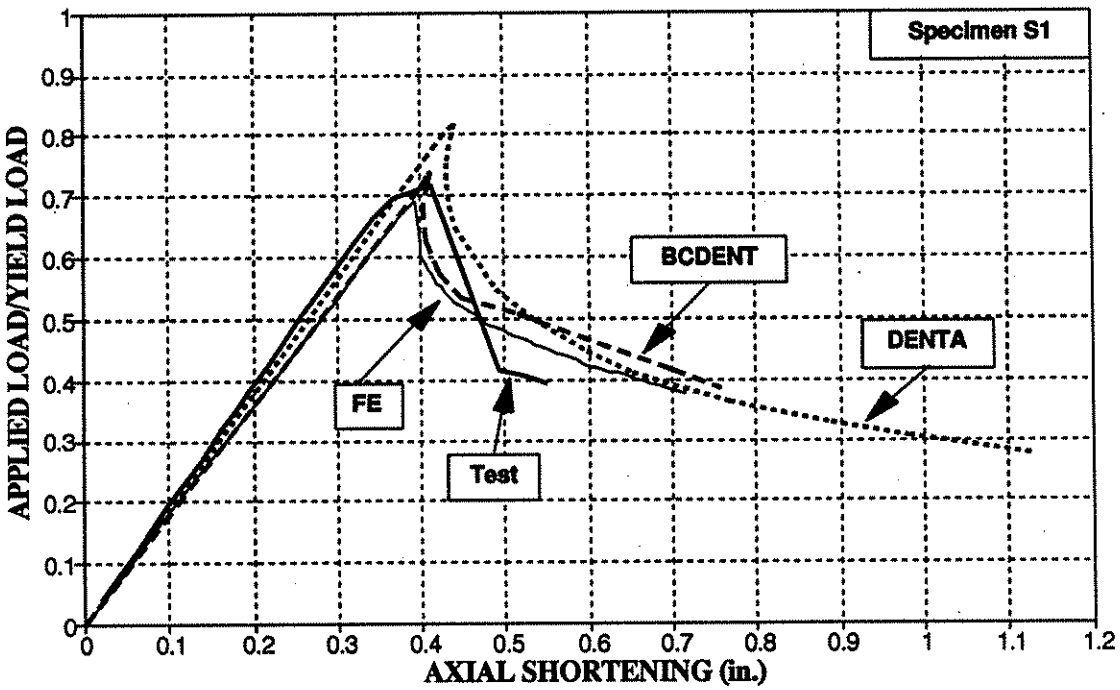

Figure 12-14: Specimen S1 - Comparison of Test, BCDENT, and DENTA

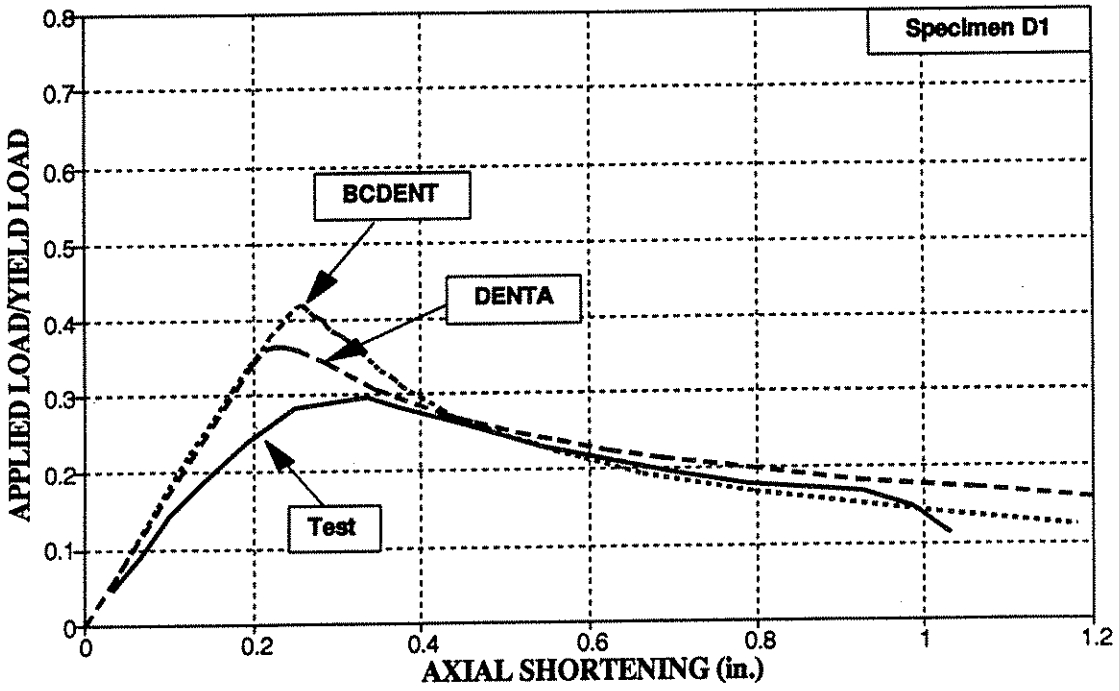

Figure 12-15: Specimen D1 - Comparison of Test, BCDENT, and DENTA

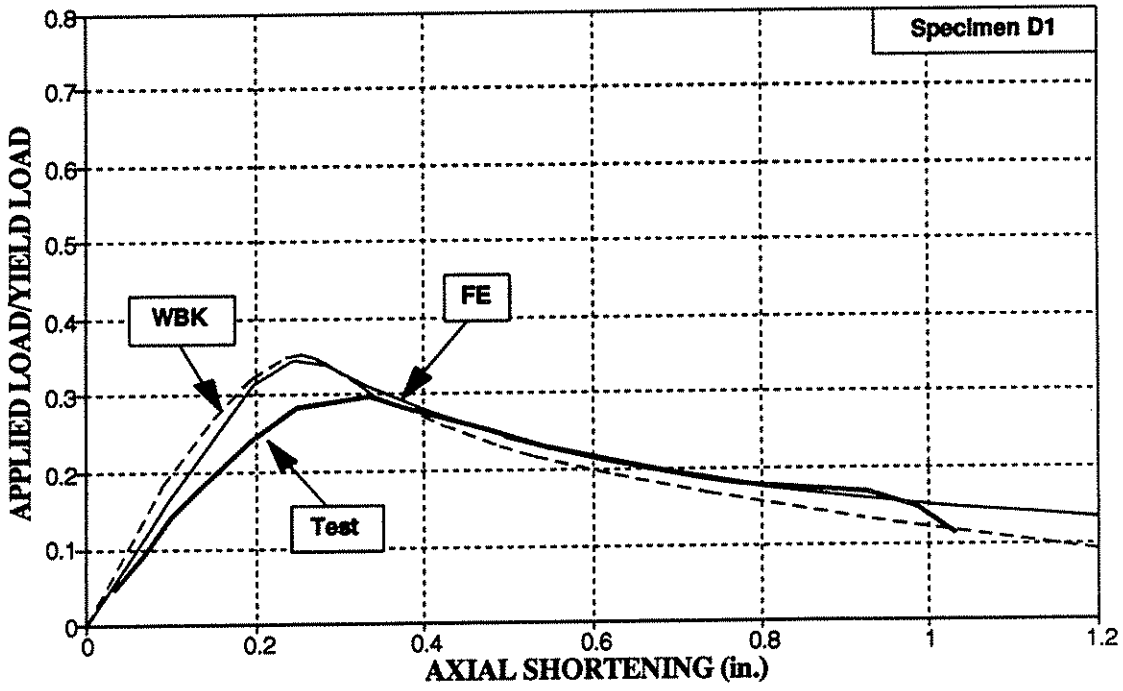

Figure 12-16: Specimen D1 - Comparison of Test, Finite Elements, and WBK

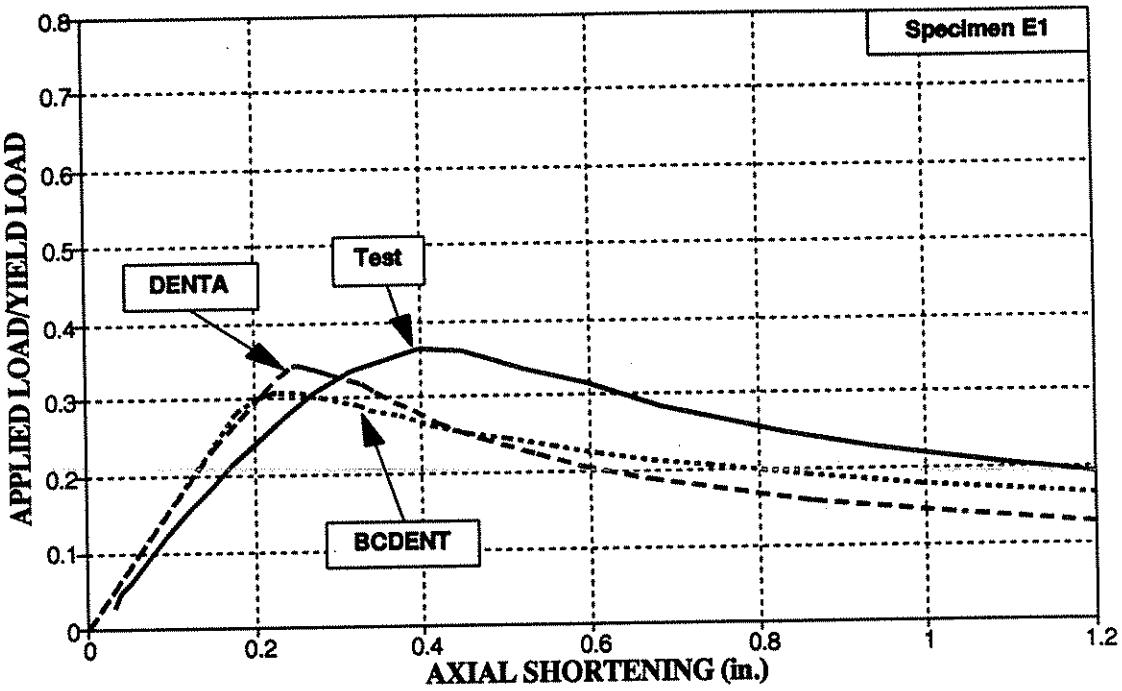

Figure 12-17: Specimen E1 - Comparison of Test, BCDENT, and DENTA

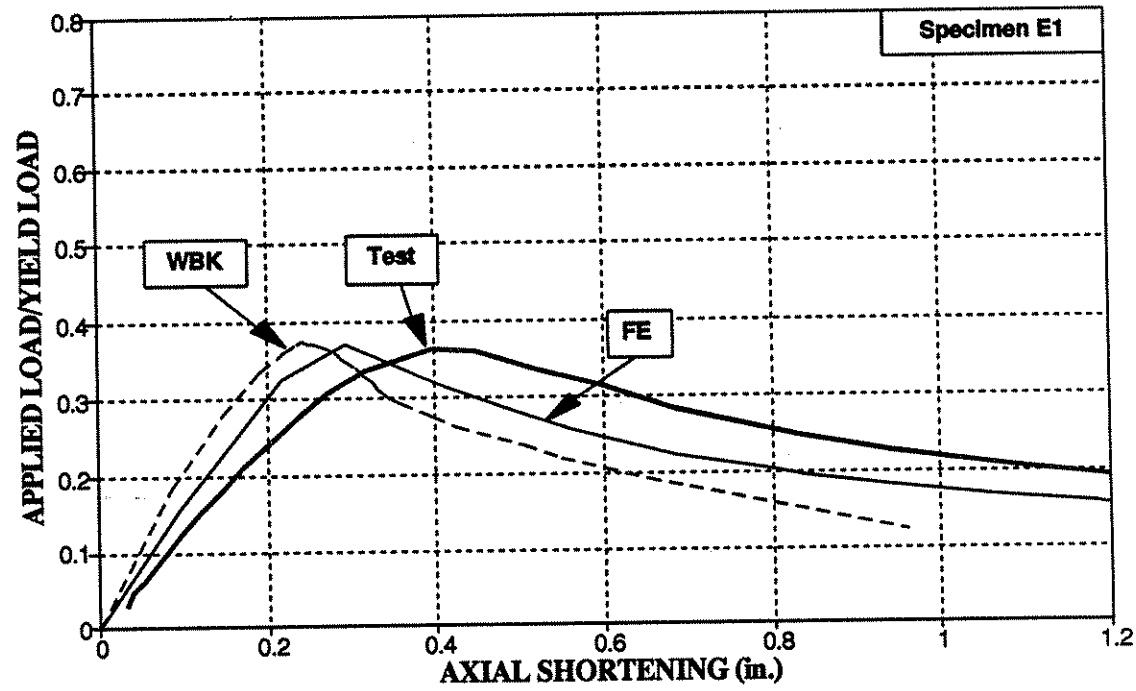

Figure 12-18: Specimen E1 - Comparison of Test, Finite Elements, and WBK

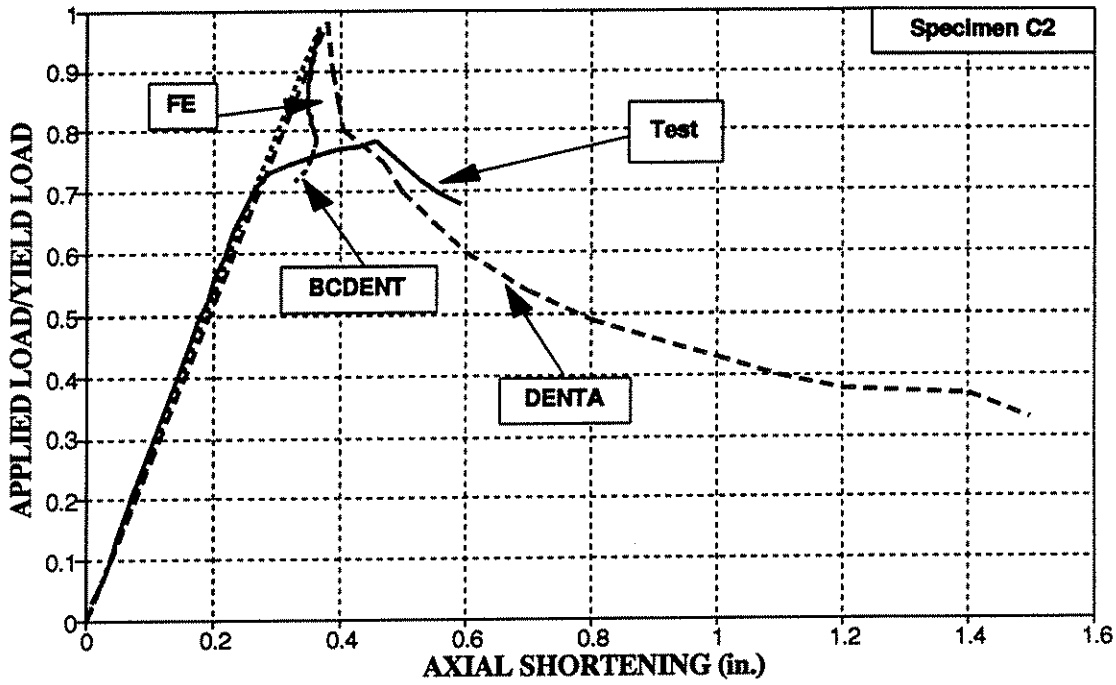

Figure 12-19: Specimen C2 - Comparison of Test, BCDENT, DENTA, and Finite Elements

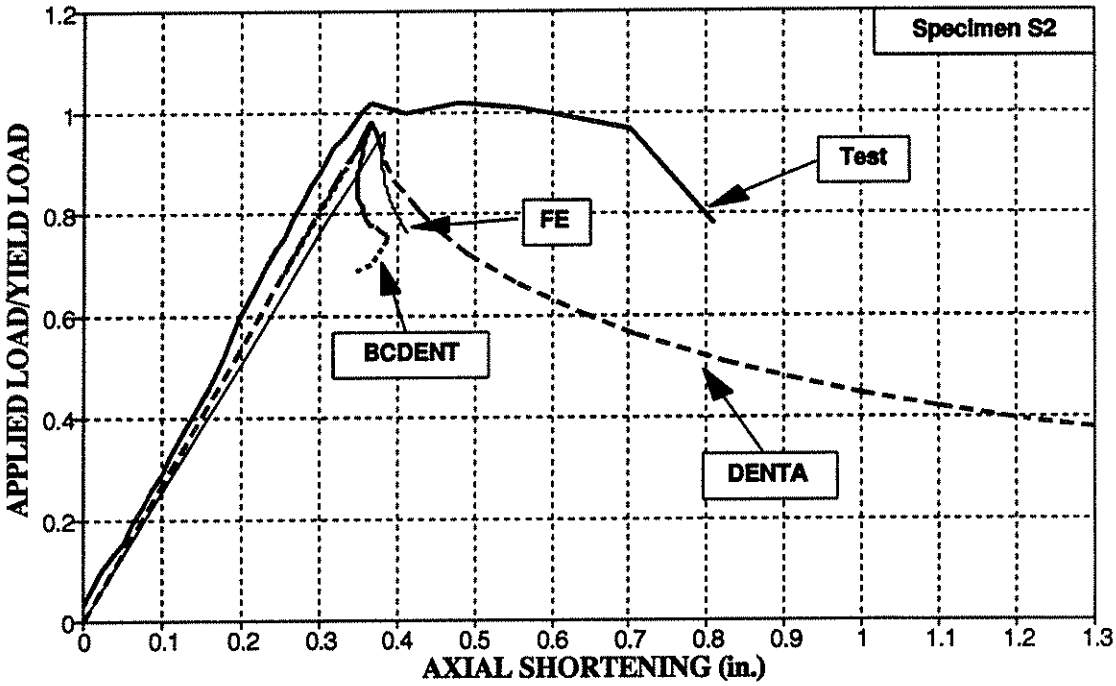

Figure 12-20: Specimen S2 - Comparison of Test, Finite Elements, DENTA, and BCDENT

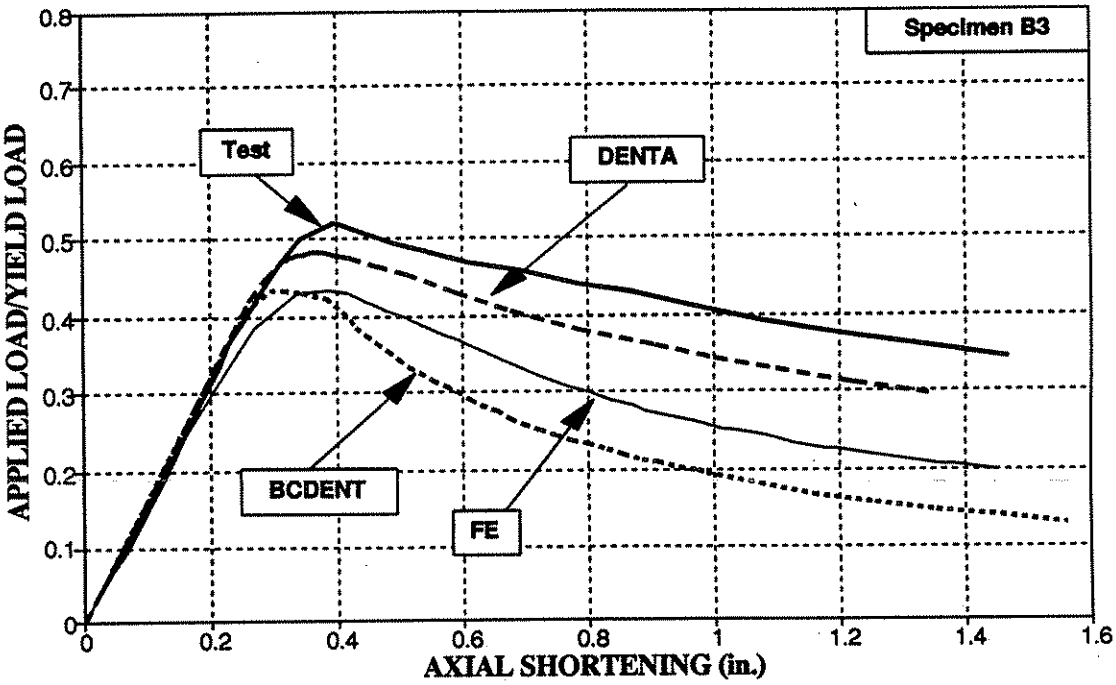

Figure 12-21: Specimen B3 - Comparison of Test, BCDENT, DENTA, and Finite Elements

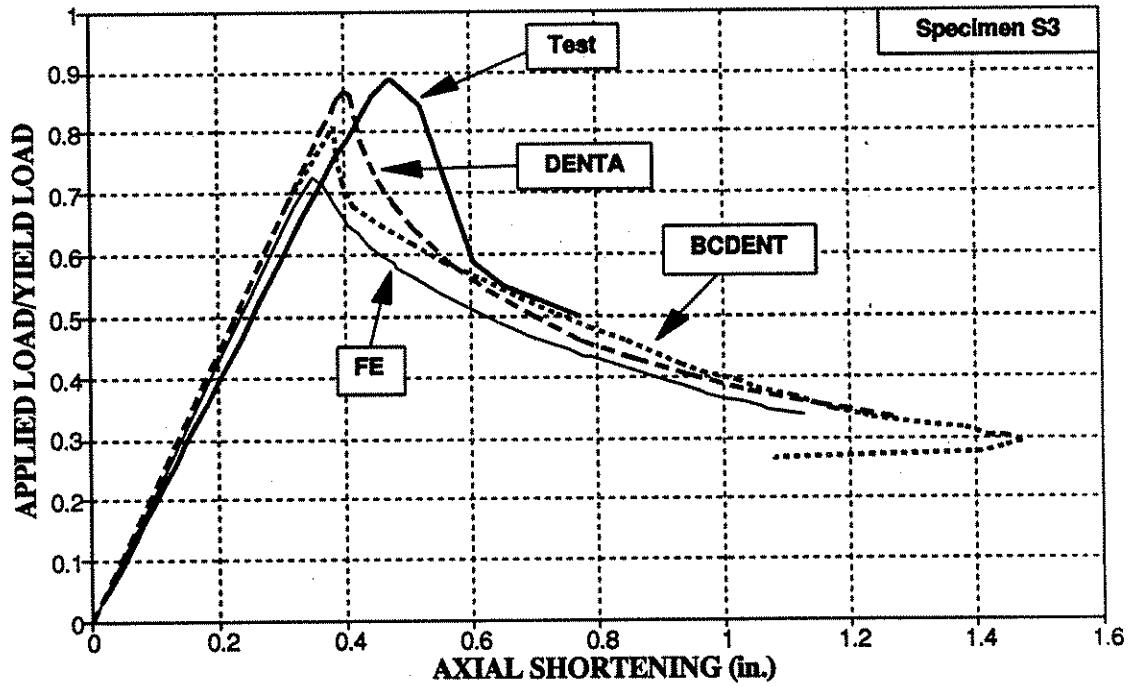

Figure 12-22: Specimen S3 - Comparison of Test, Finite Elements, DENTA, and BCDENT

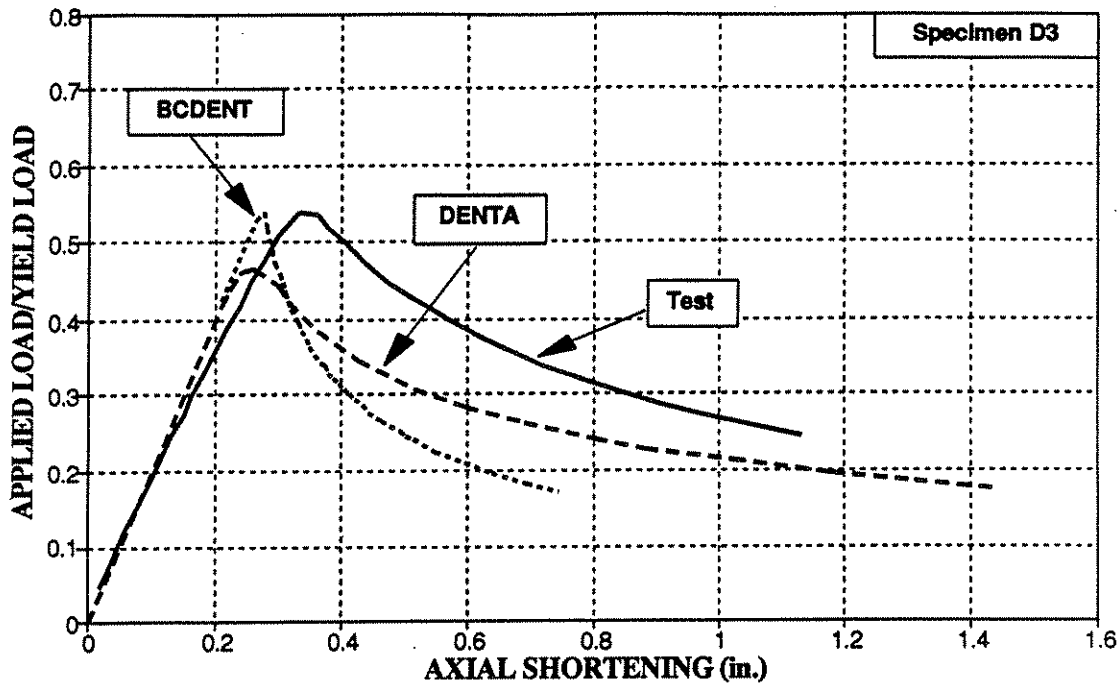

Figure 12-23: Specimen D3 - Comparison of Test, BCDENT, and DENTA

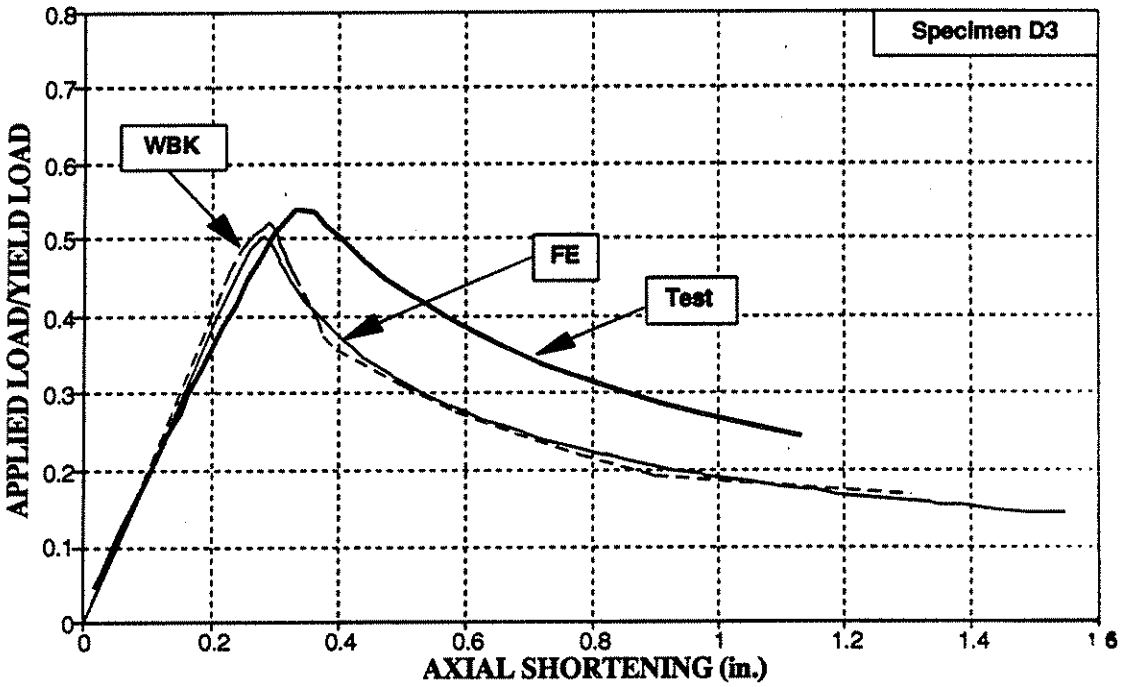

Figure 12-24: Specimen D3 - Comparison of Test, Finite Elements, and WBK

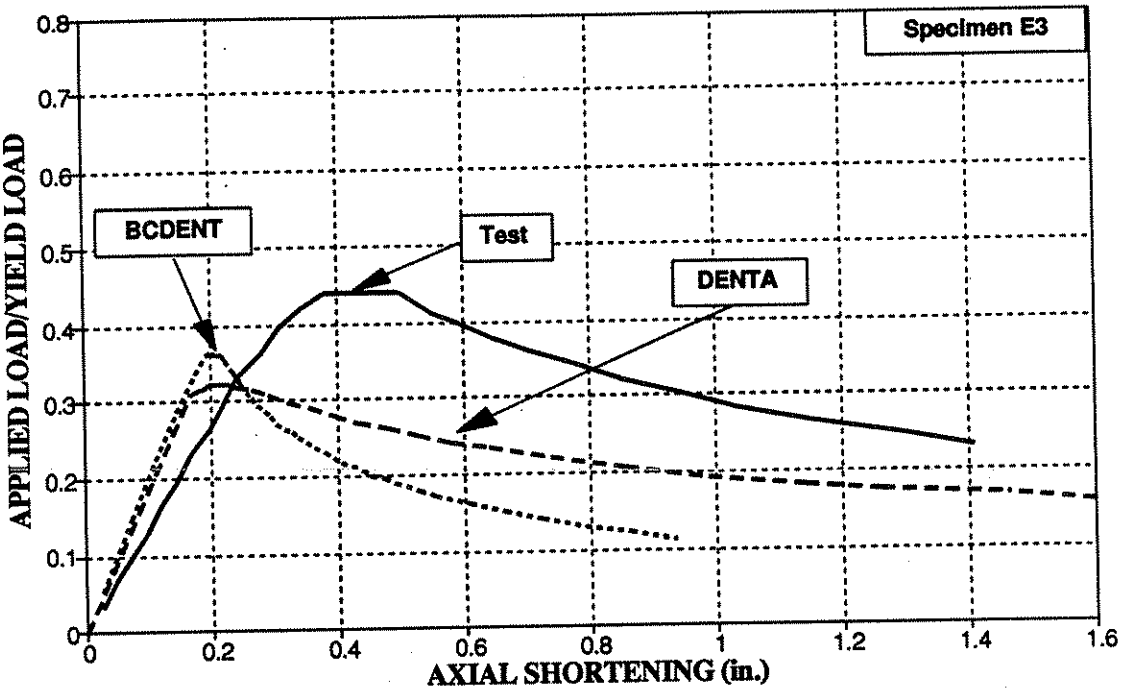

Figure 12-25: Specimen E3 - Comparison of Test, BCDENT, and DENTA

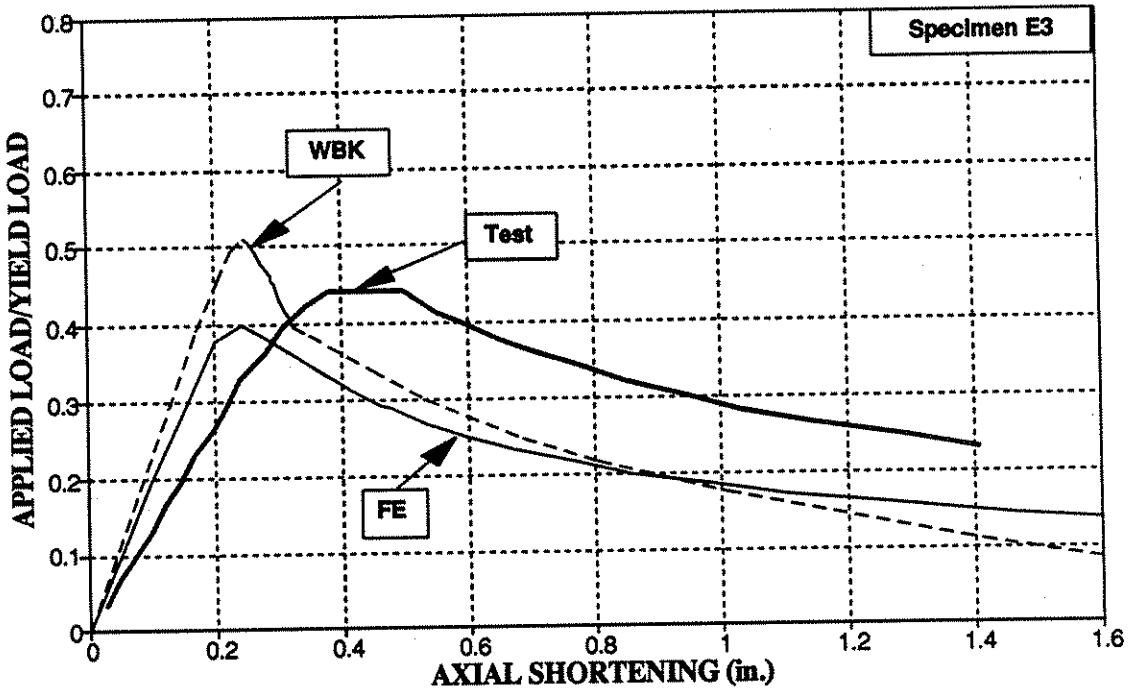

Figure 12-26: Specimen E3 - Comparison of Test, Finite Elements, and WBK

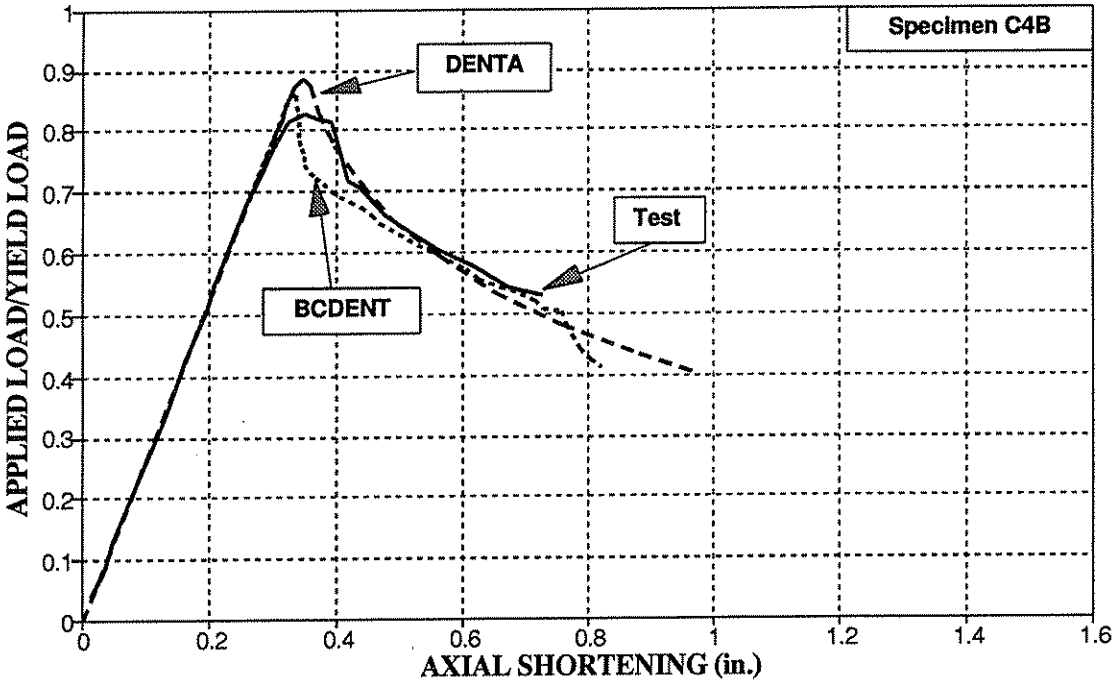

Figure 12-27: Specimen C4B – Comparison of Test, BCDENT and DENTA

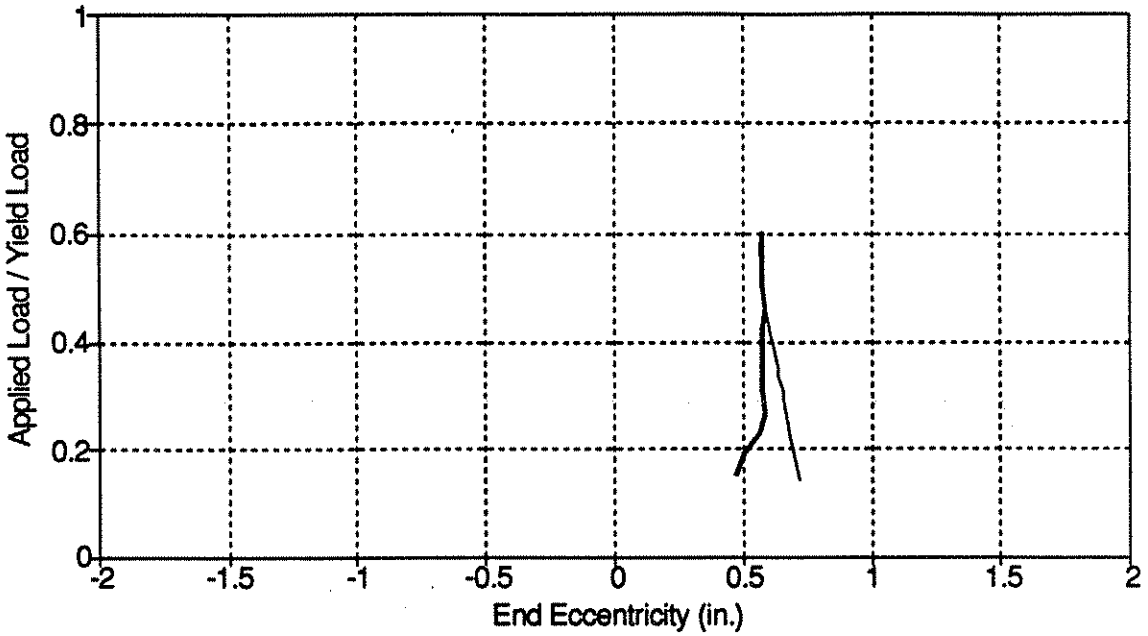

Figure 13-1: Computed End Eccentricity for Specimen P1P

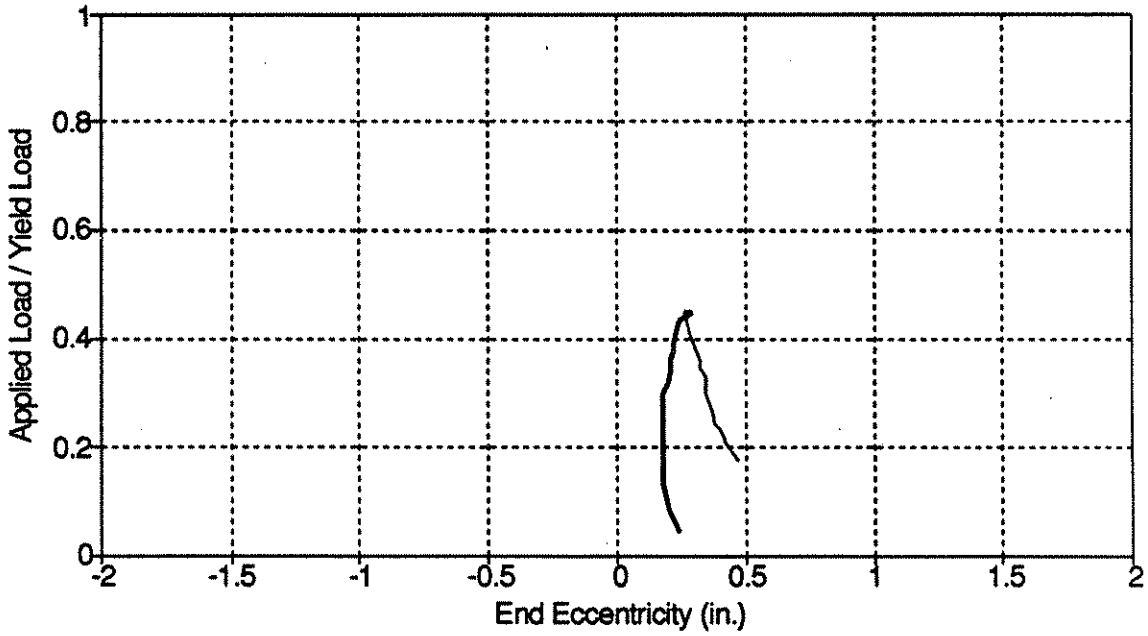

Figure 13-2: Computed End Eccentricity for Specimen P2P

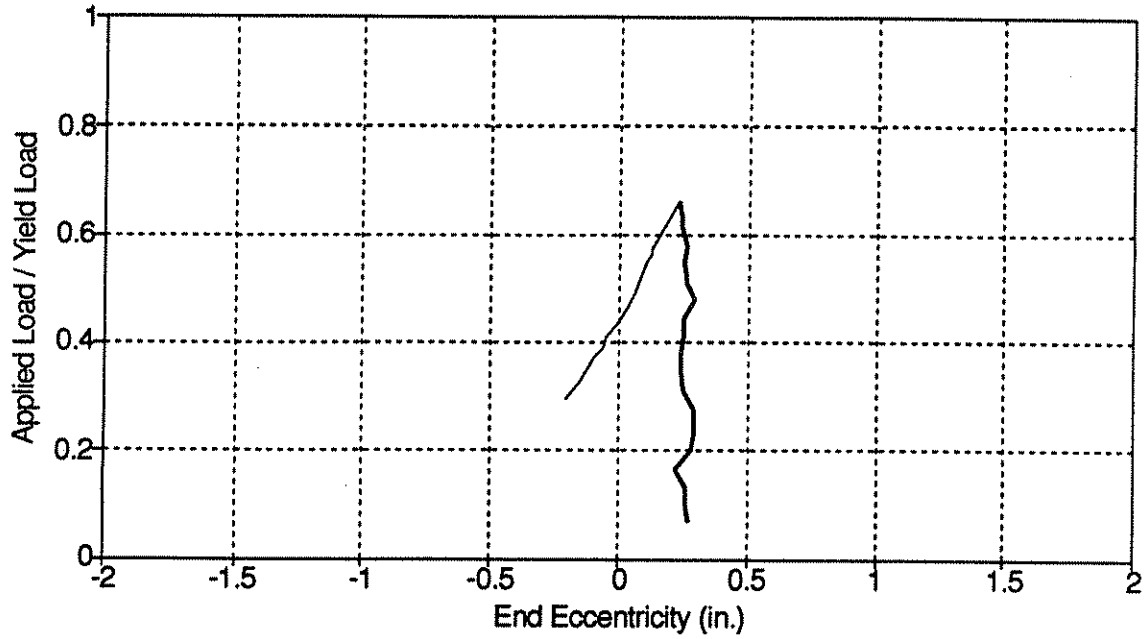

Figure 13-3: Computed End Eccentricity for Specimen P3PA

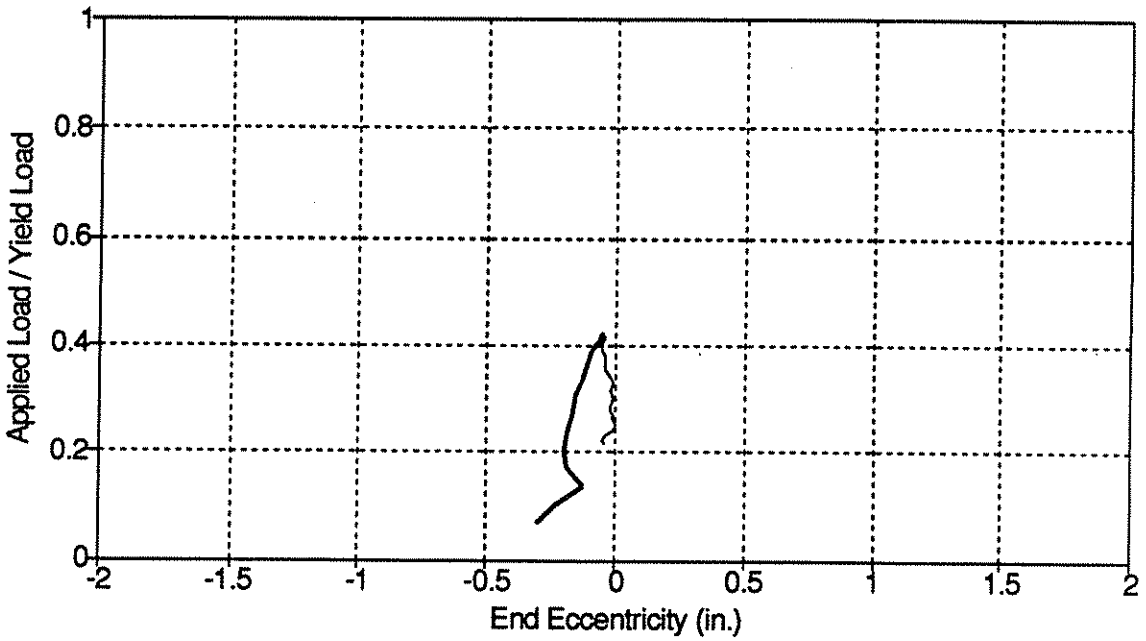

Figure 13-4: Computed End Eccentricity for Specimen P3PB

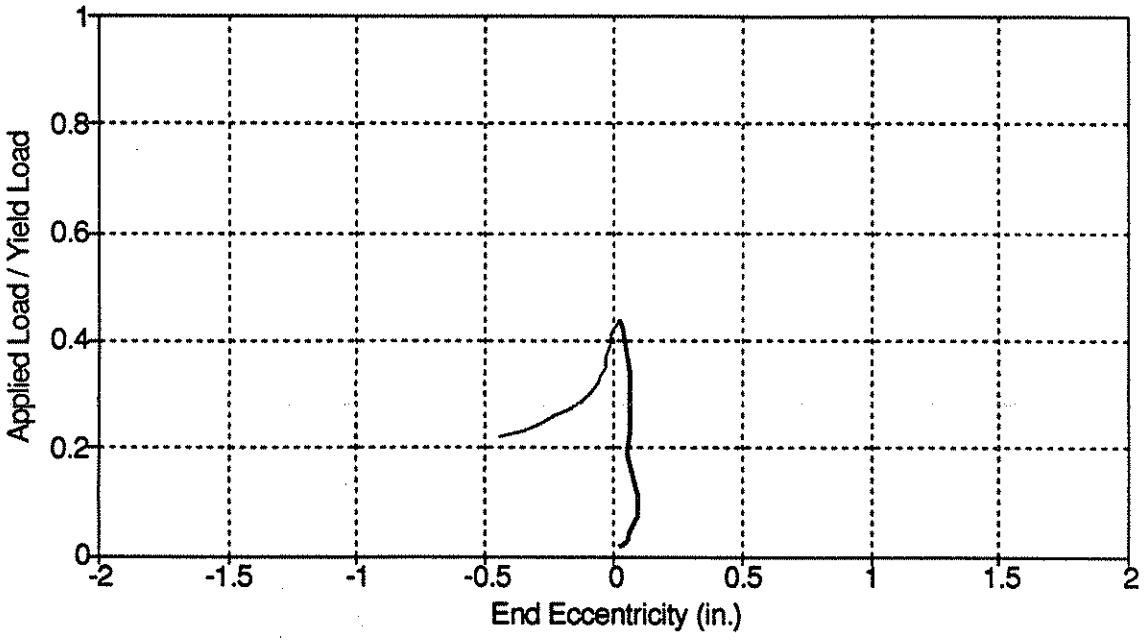

Figure 13-5: Computed End Eccentricity for Specimen P4P

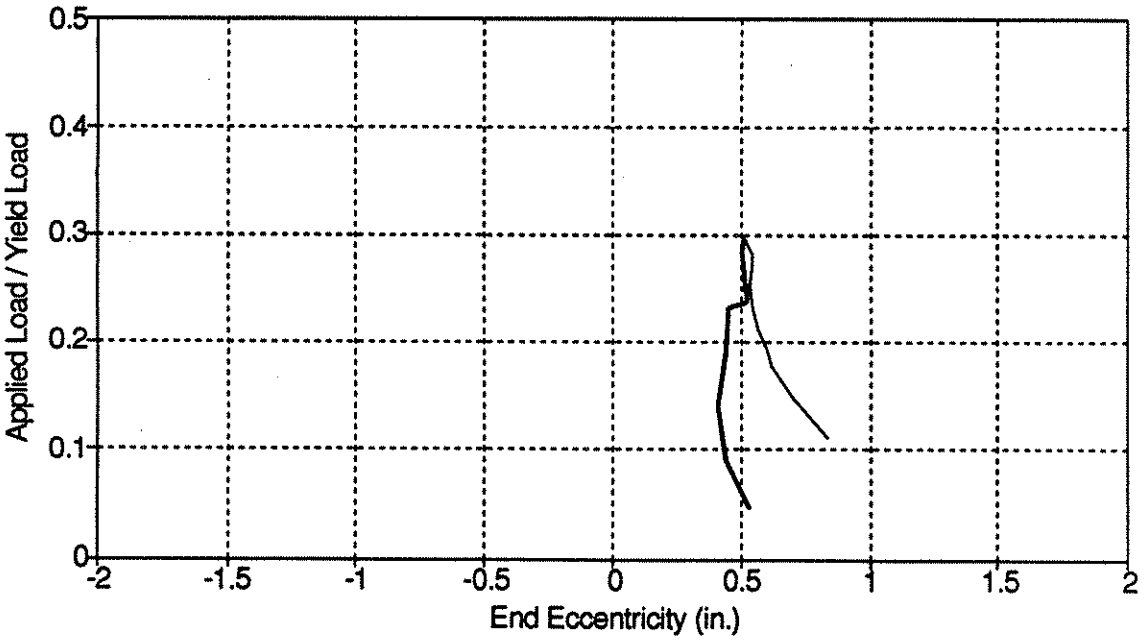

Figure 13-6: Computed End Eccentricity for Specimen D1

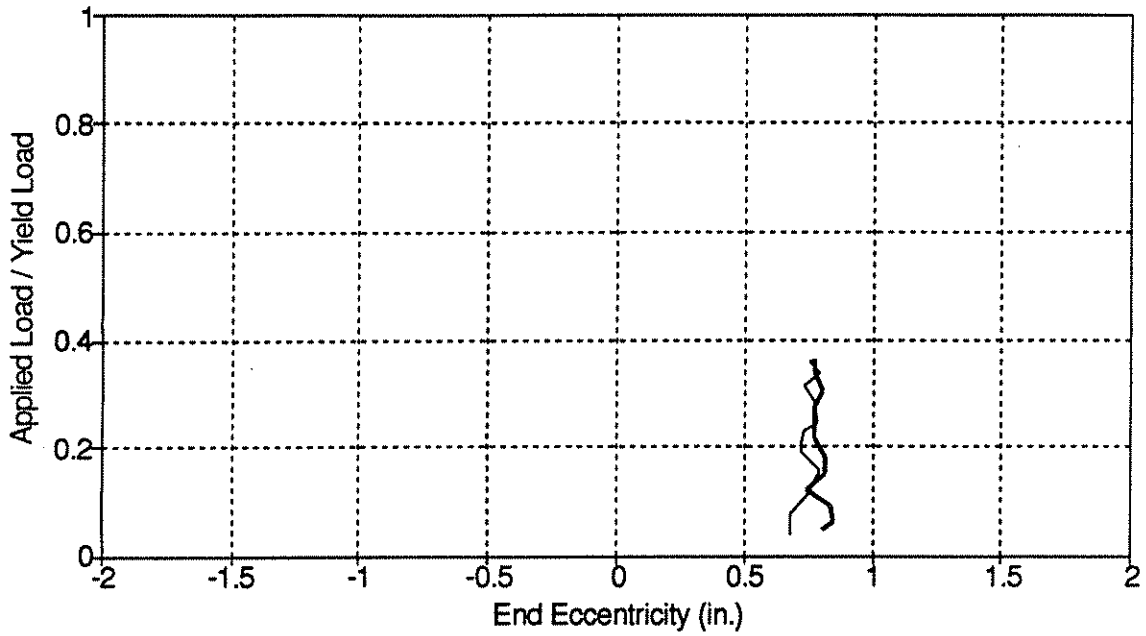

Figure 13-7: Computed End Eccentricity for Specimen E1

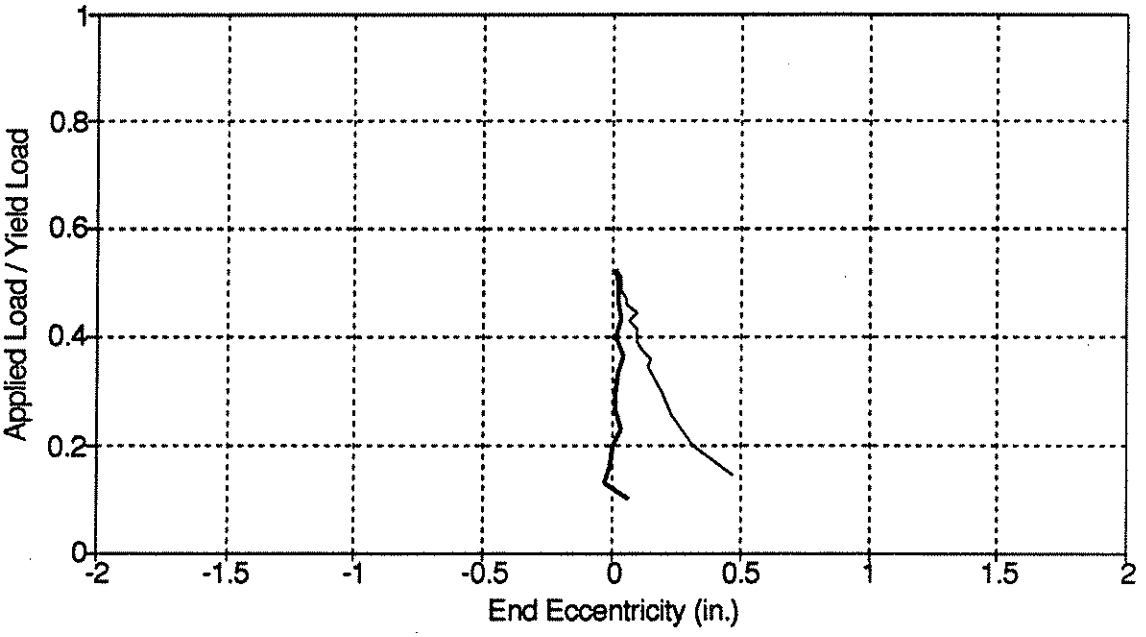

Figure 13-8: Computed End Eccentricity for Specimen B3

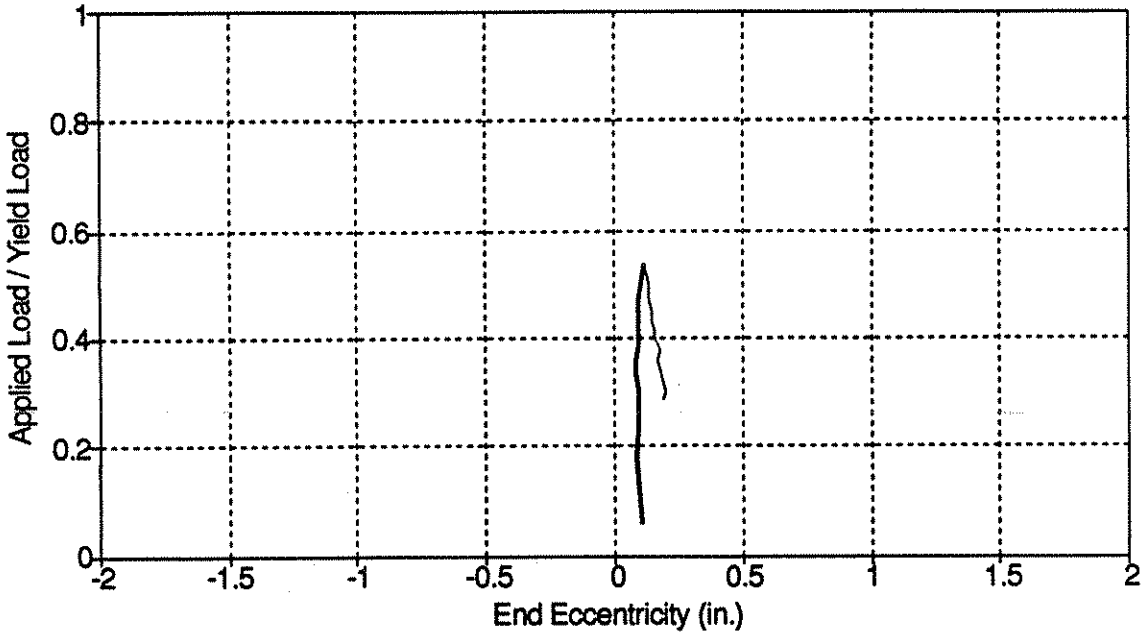

Figure 13-9: Computed End Eccentricity for Specimen D3

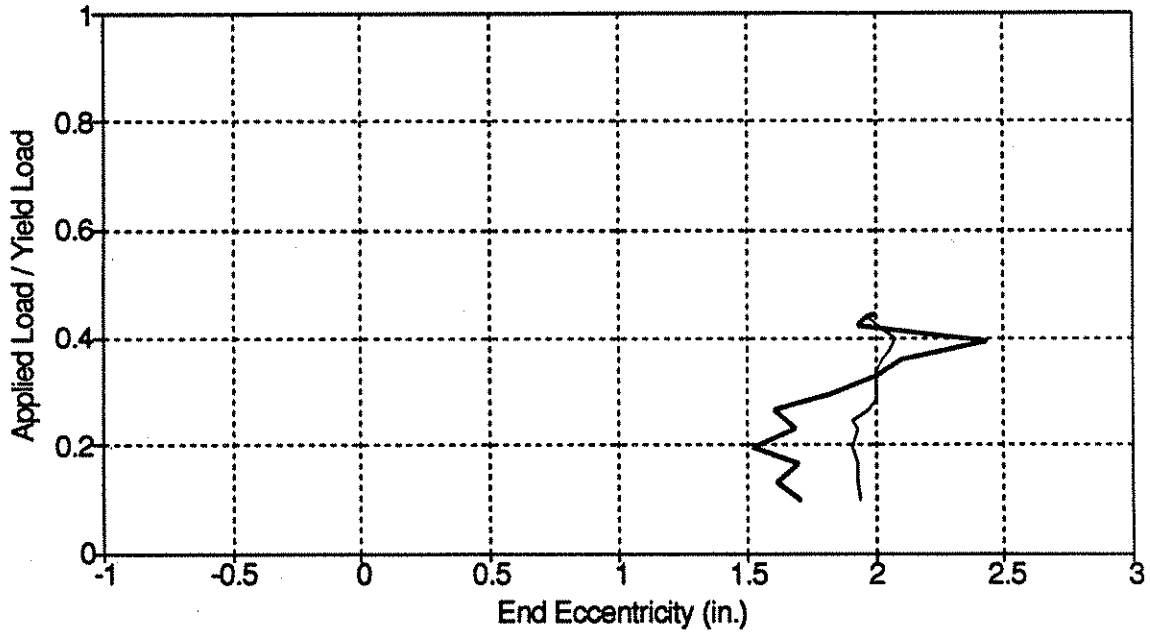

Figure 13-10: Computed End Eccentricity for Specimen E3

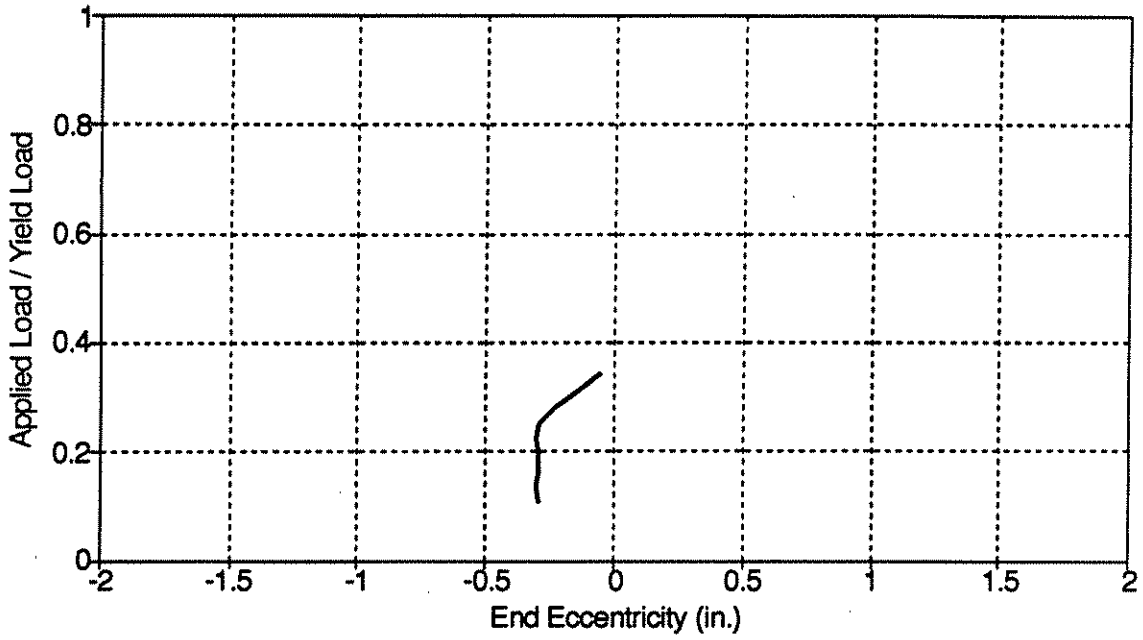

Figure 13-11: Computed End Eccentricity for Specimen C1

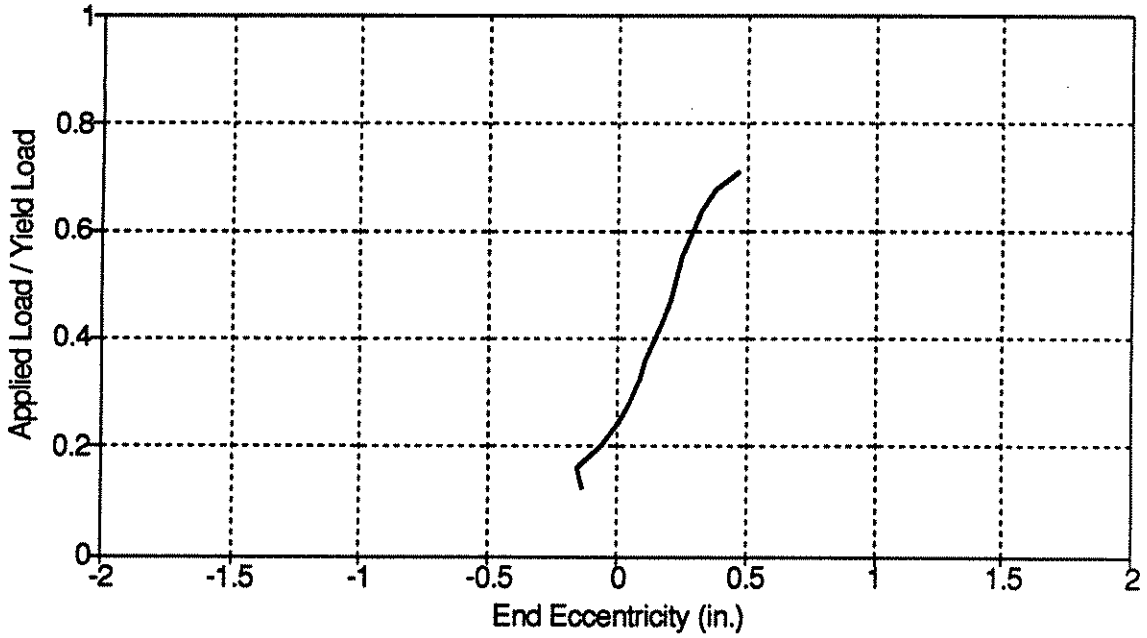

Figure 13-12: Computed End Eccentricity for Specimen S1

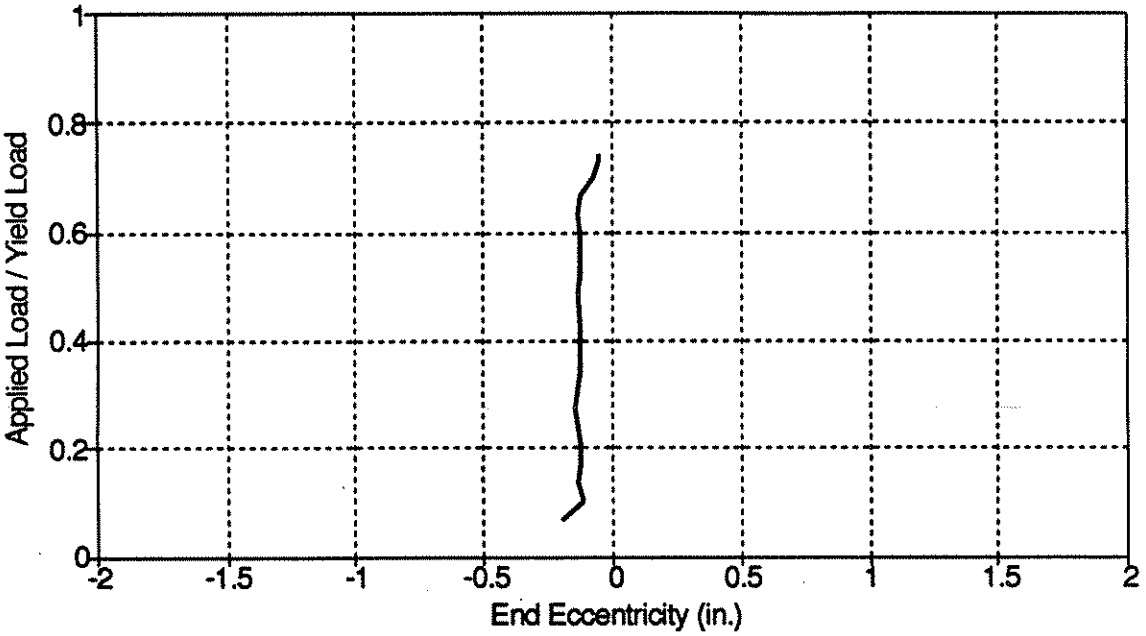

Figure 13-13: Computed End Eccentricity for Specimen C2

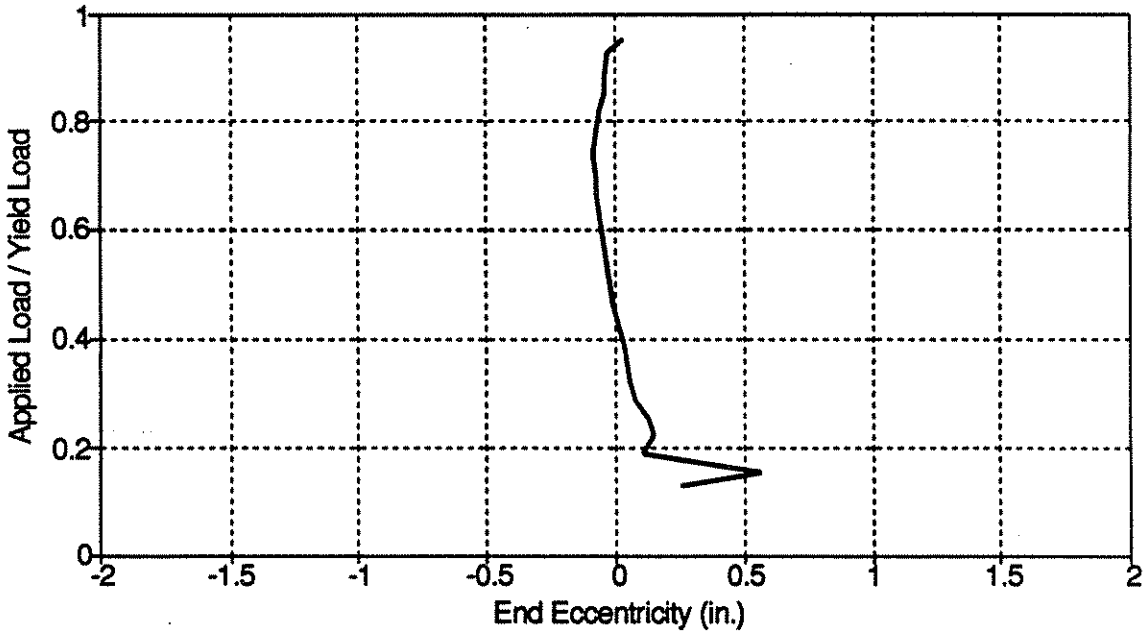

Figure 13-14: Computed End Eccentricity for Specimen S2

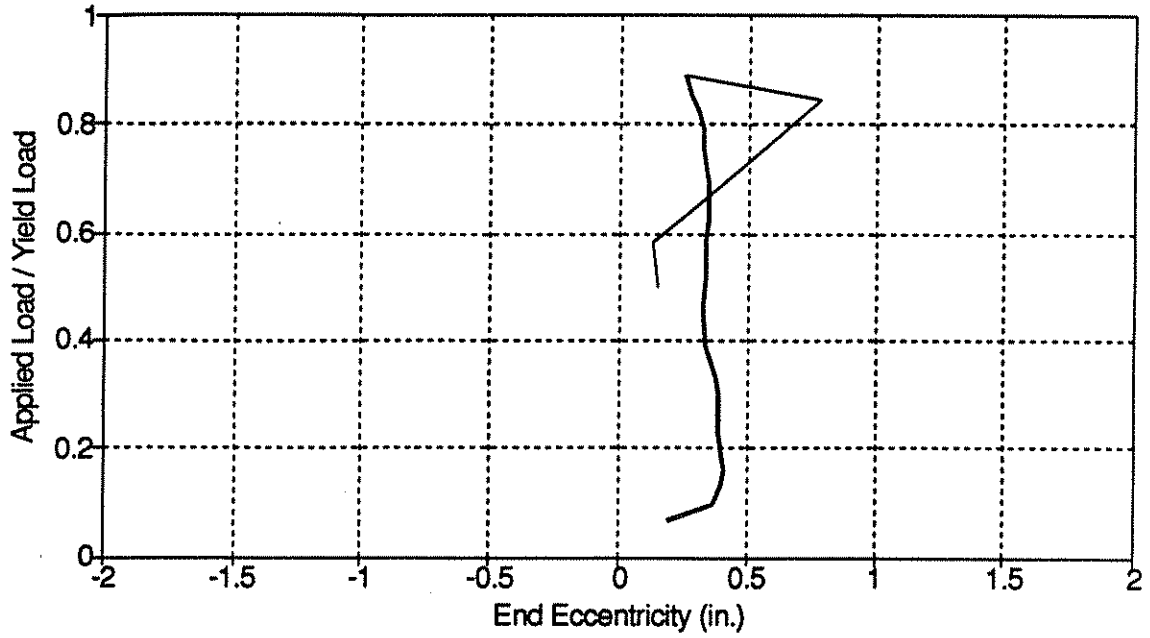

Figure 13-15: Computed End Eccentricity for Specimen S3

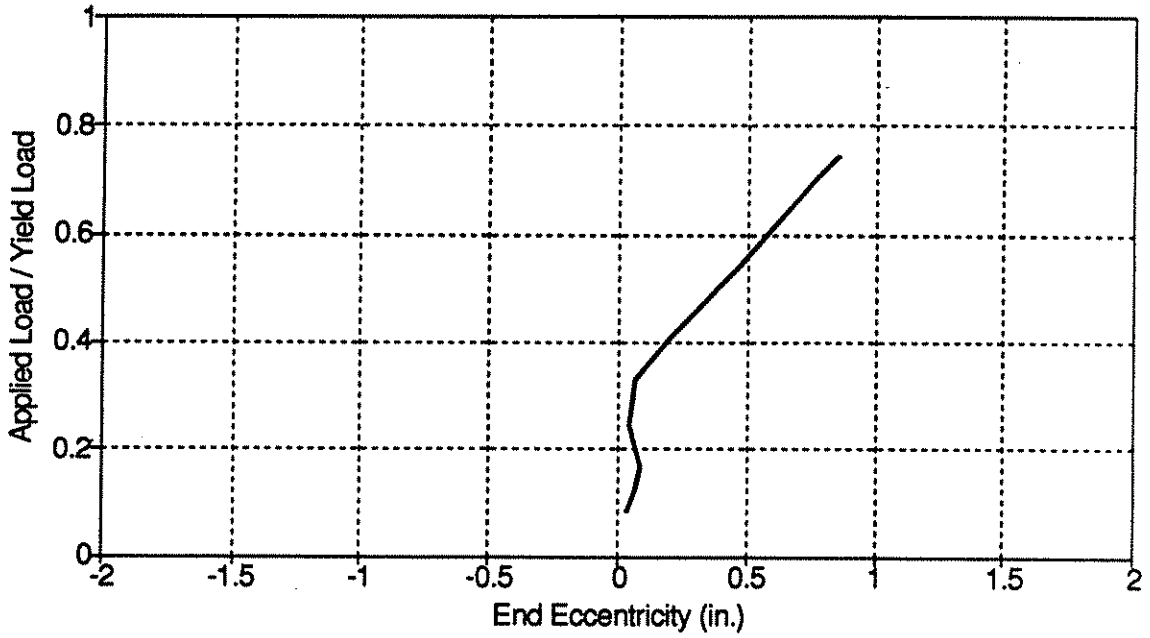

Figure 13-16: Computed End Eccentricity for Specimen C4B

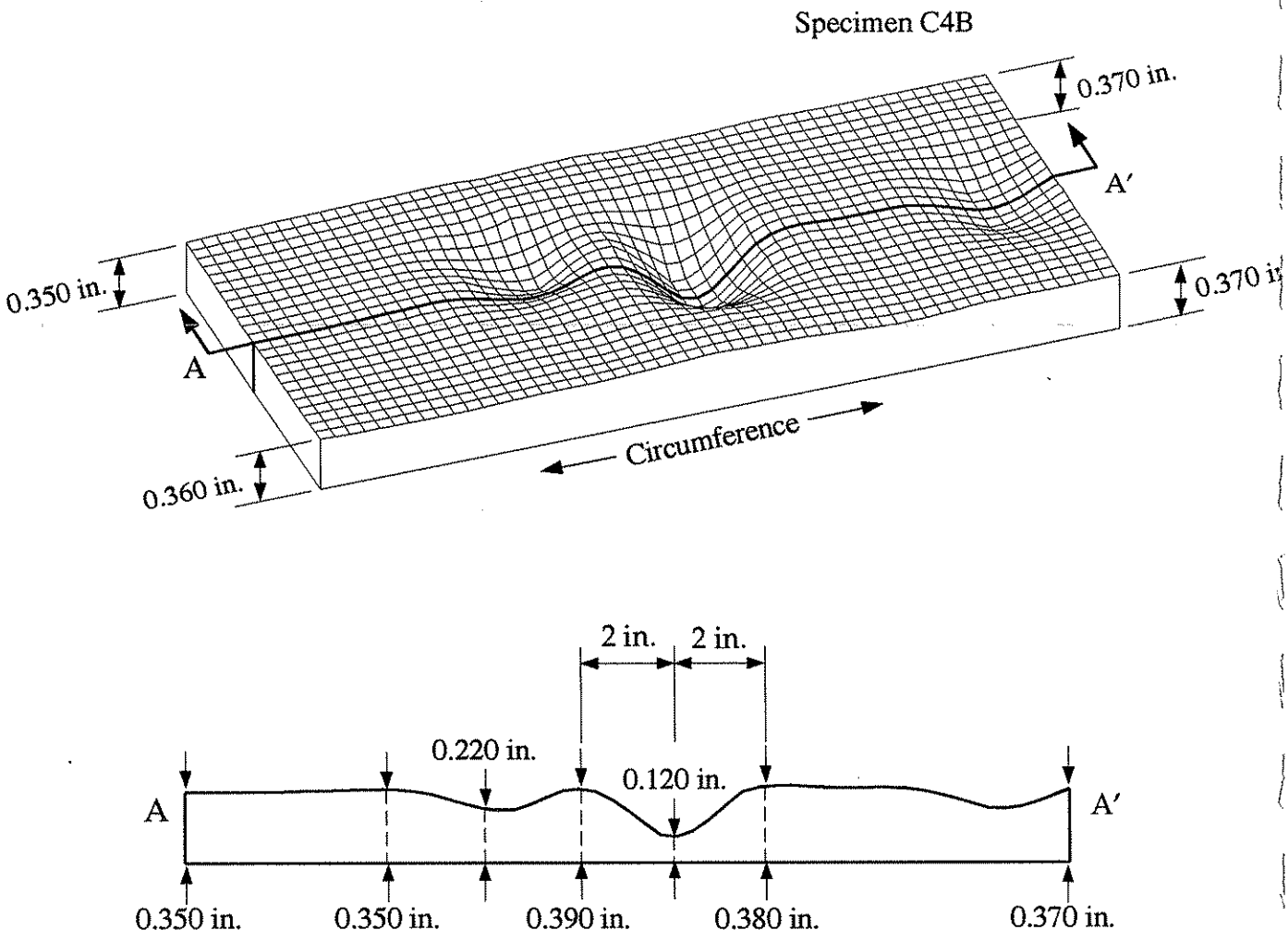

Thickness at Cut A - A'

Figure 14-1: Specimen C4B - Isometric View and Cross Section of Thickness Variation at Location of Local Buckles

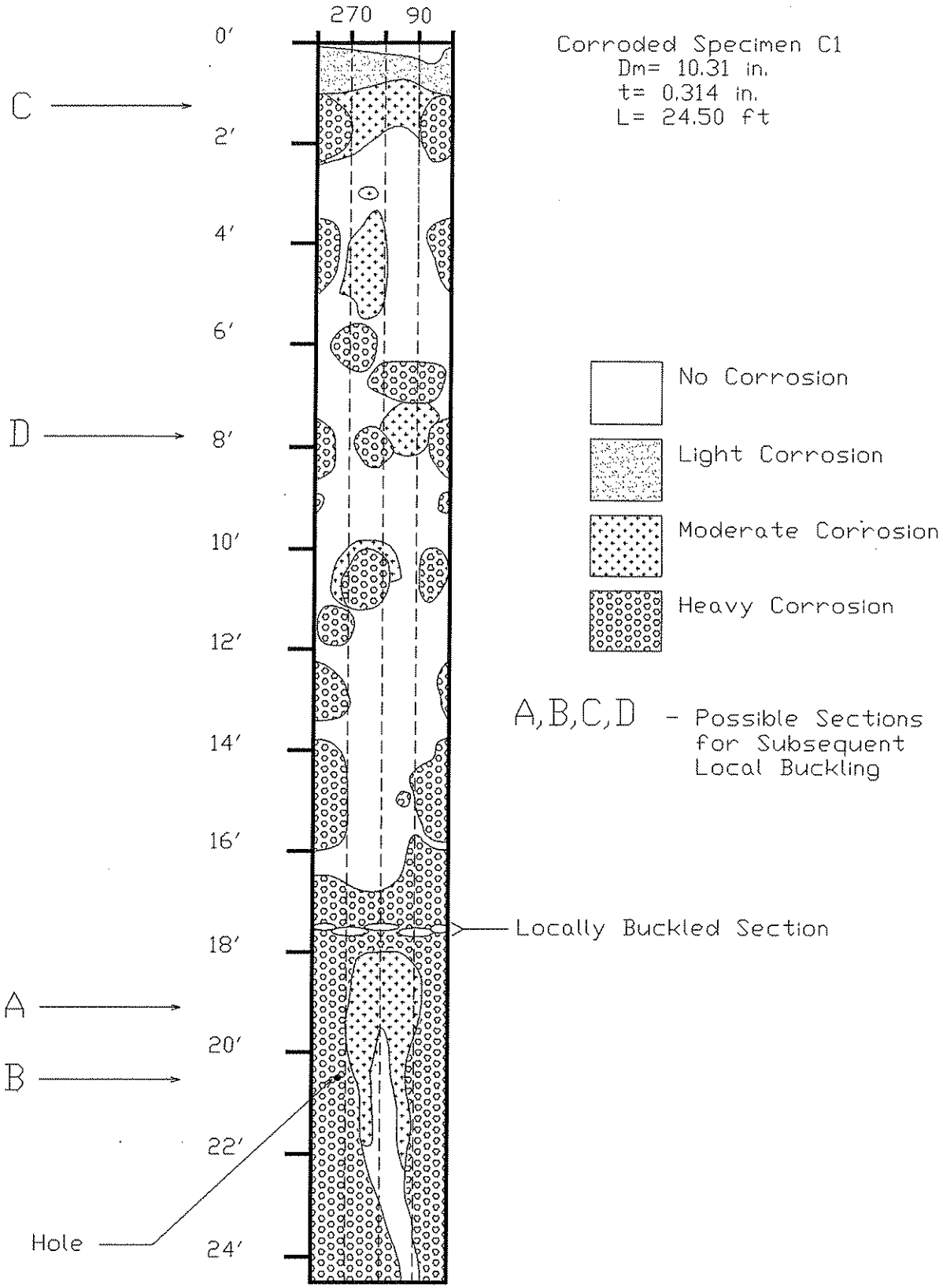

Figure 14-2: Specimen C1 - Map of Corrosion on Unfolded Surface of Tube.

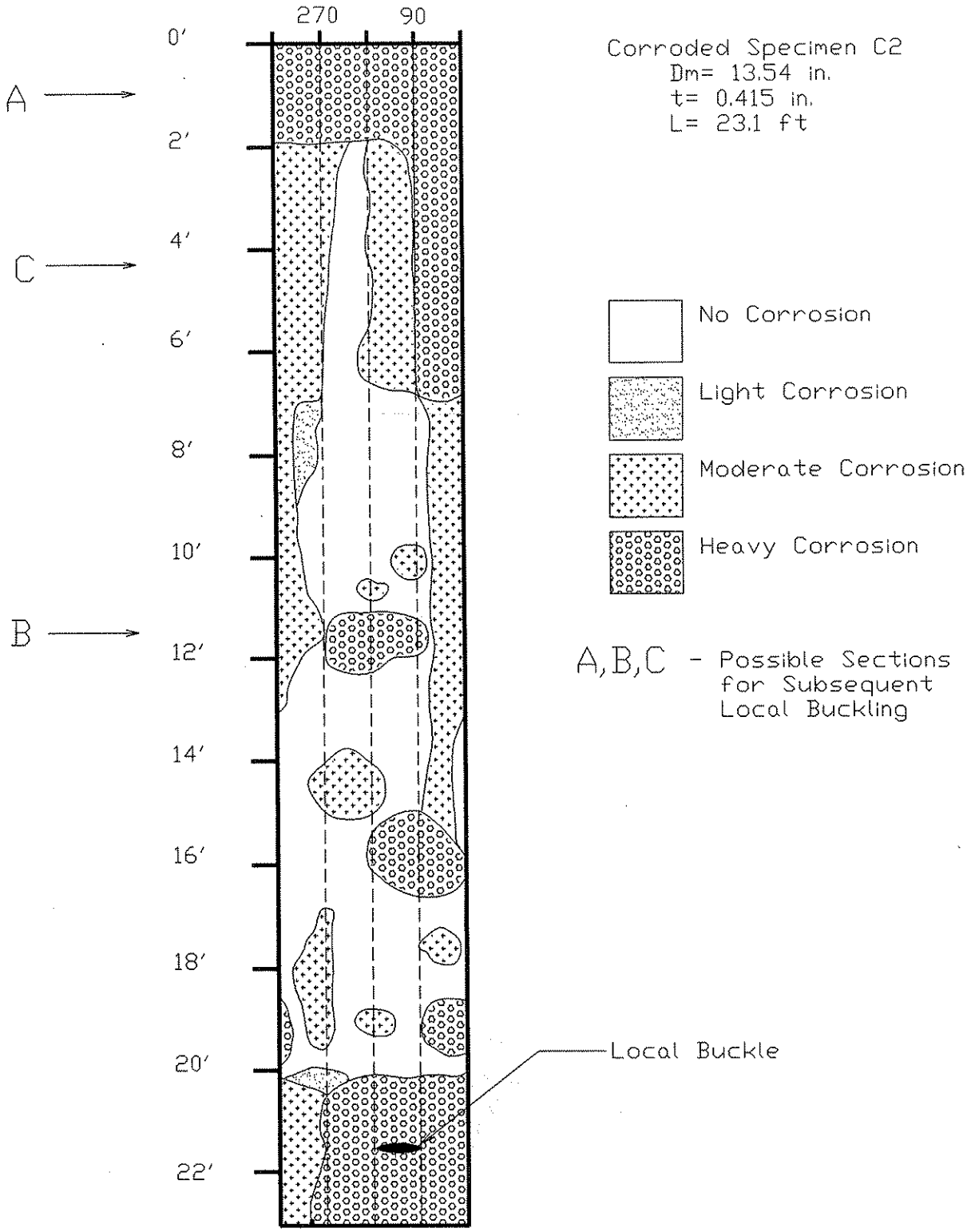

Figure 14-3: Specimen C2 - Map of Corrosion on Unfolded Surface of Tube.

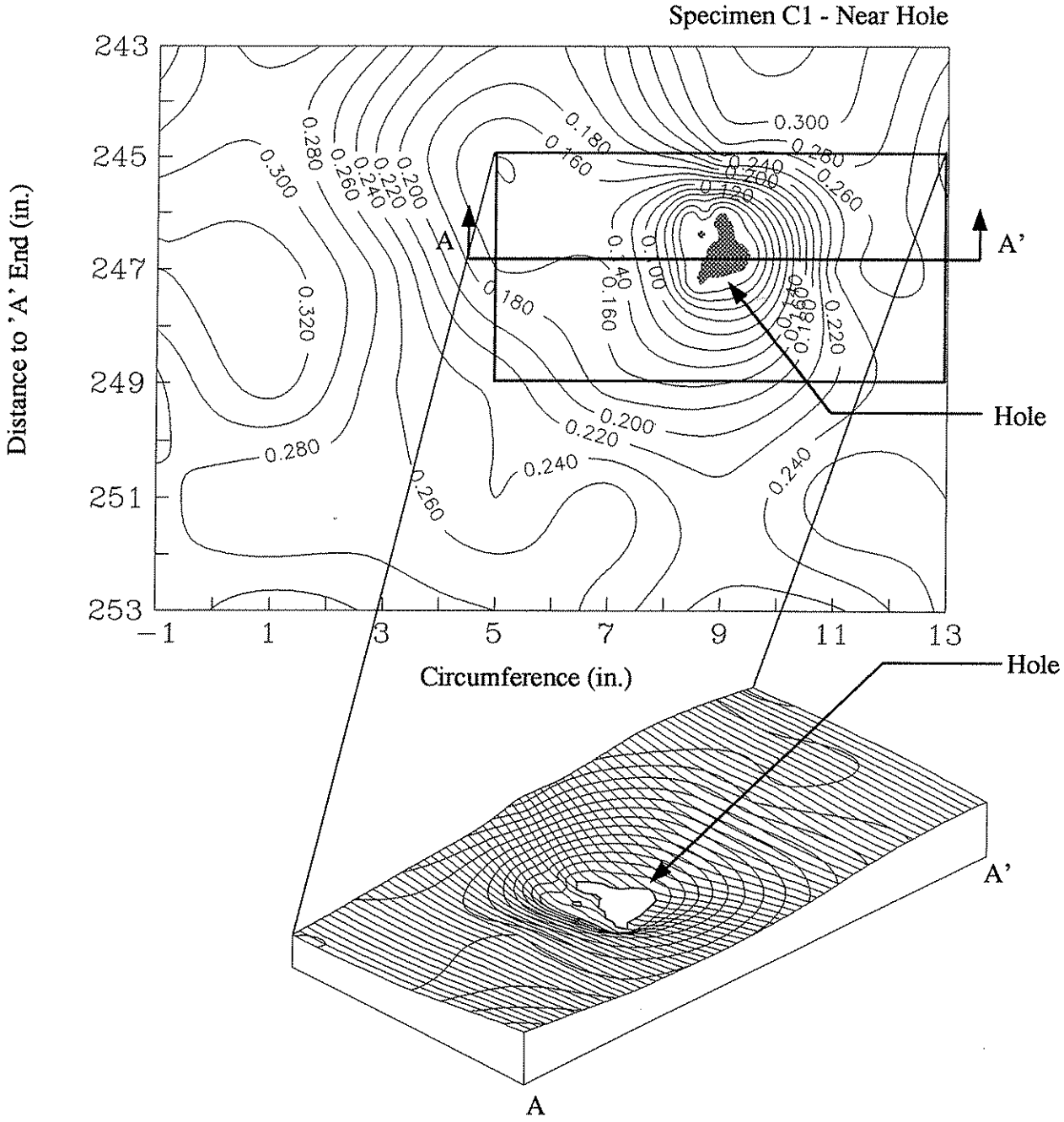

Figure 14-4: Specimen C1 - Contour Plot, Isometric View, and Cross Section of Thickness Variation at Location of Hole

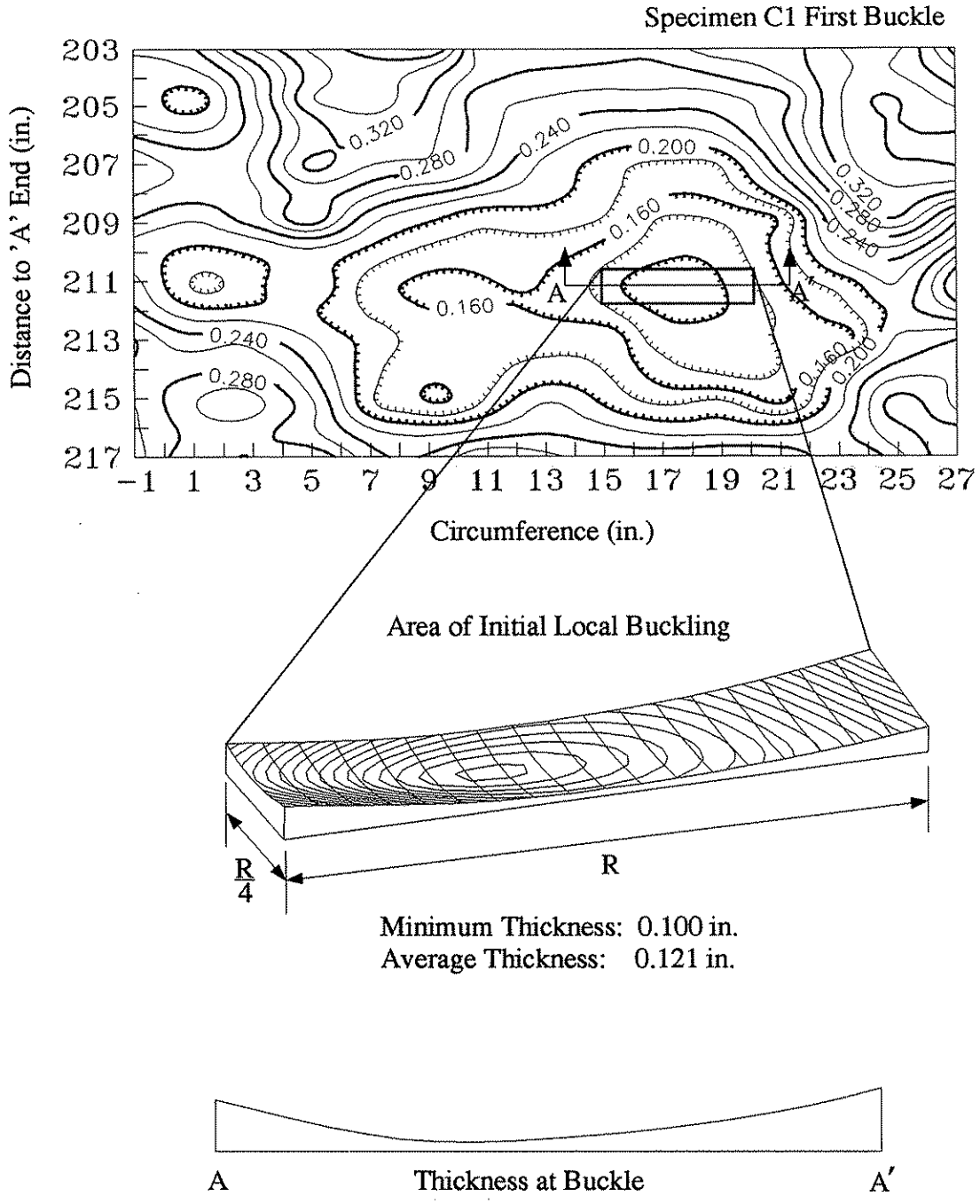

Figure 14-5: Specimen C1 - Contour Plot, Isometric View, and Cross Section of Thickness Variation at Location of Local Buckles

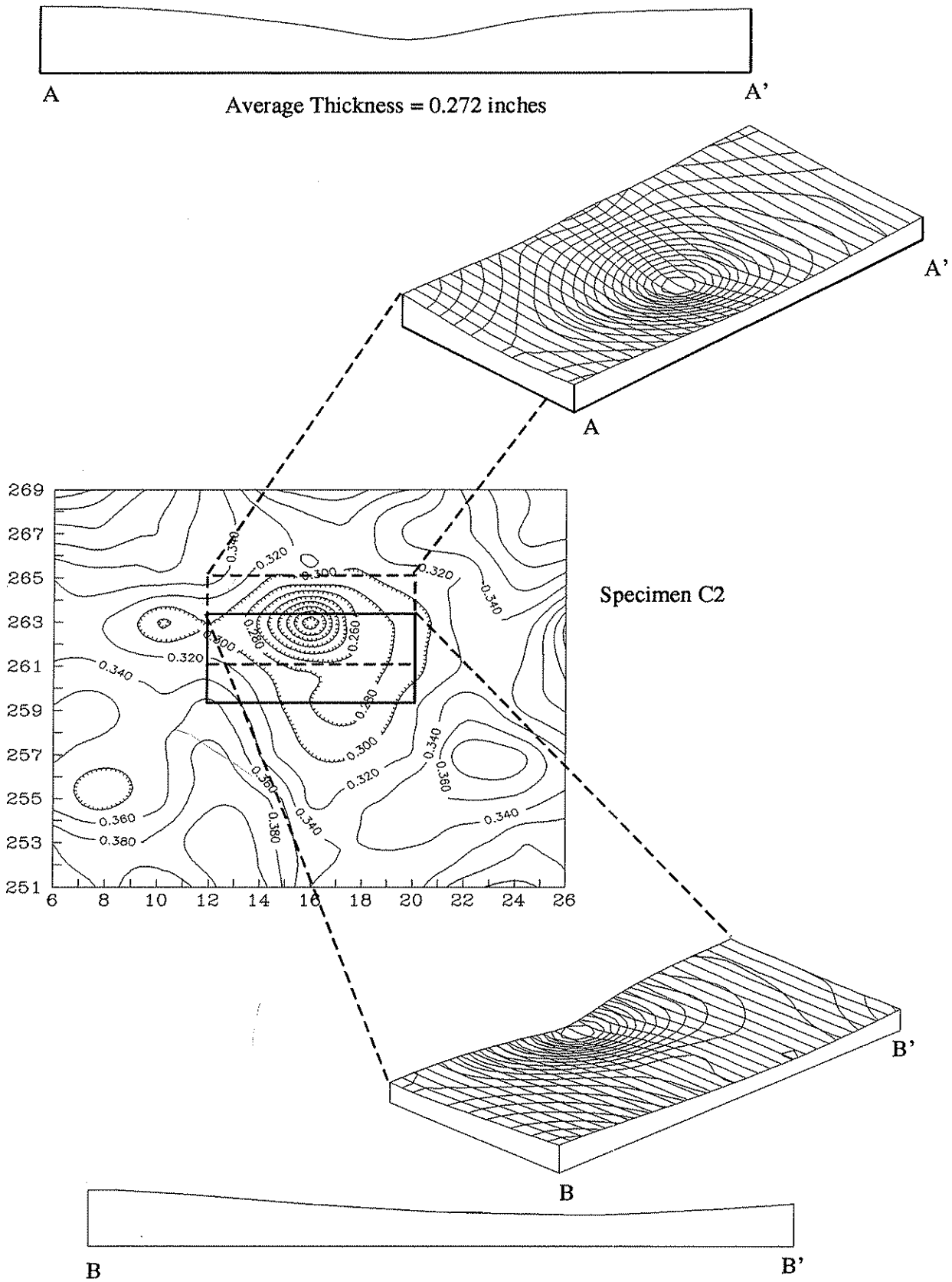

Figure 14-6: Specimen C2 - Contour Plot, Isometric Views, and Cross Sections of Thickness Variation at Location of Local Buckles

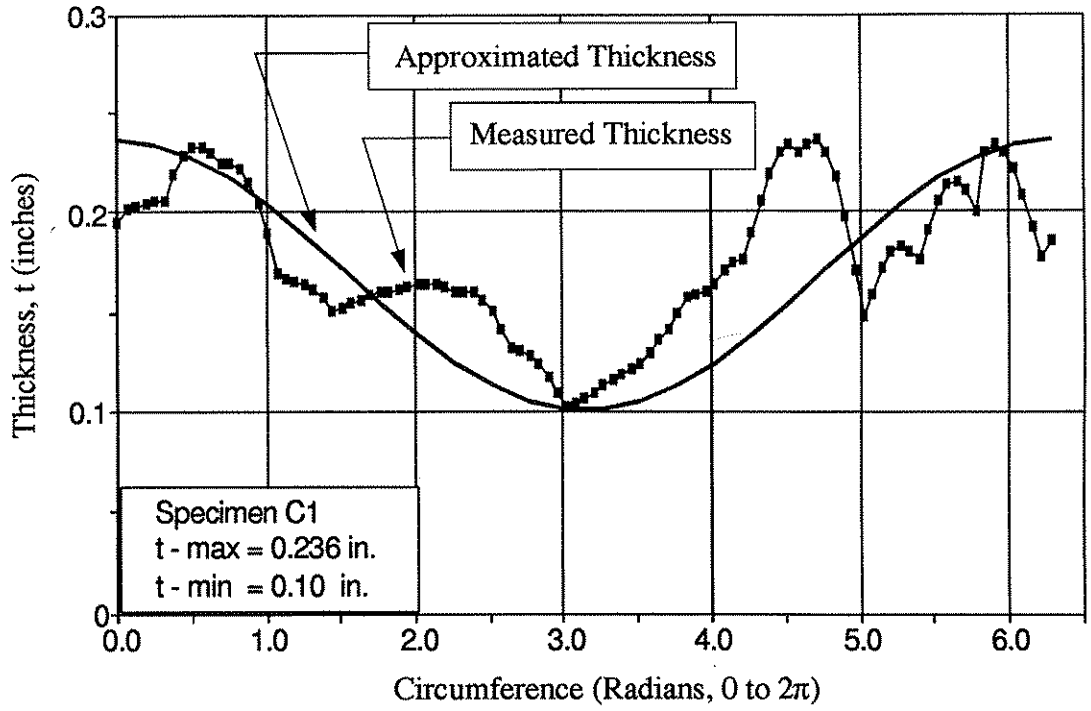

Figure 14-7: Specimen C1 - Thickness Variation from Measured and Approximated Values at Locally Buckled Section.

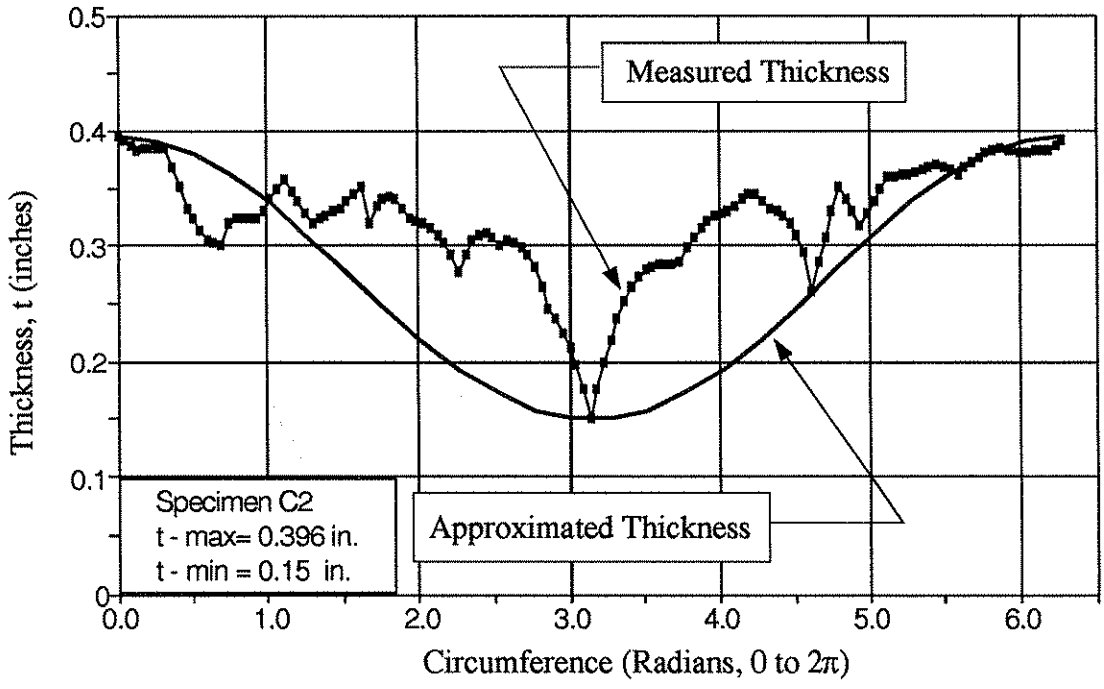

Figure 14-8: Specimen C2 - Thickness Variation from Measured and Approximated Values at Locally Buckled Section.

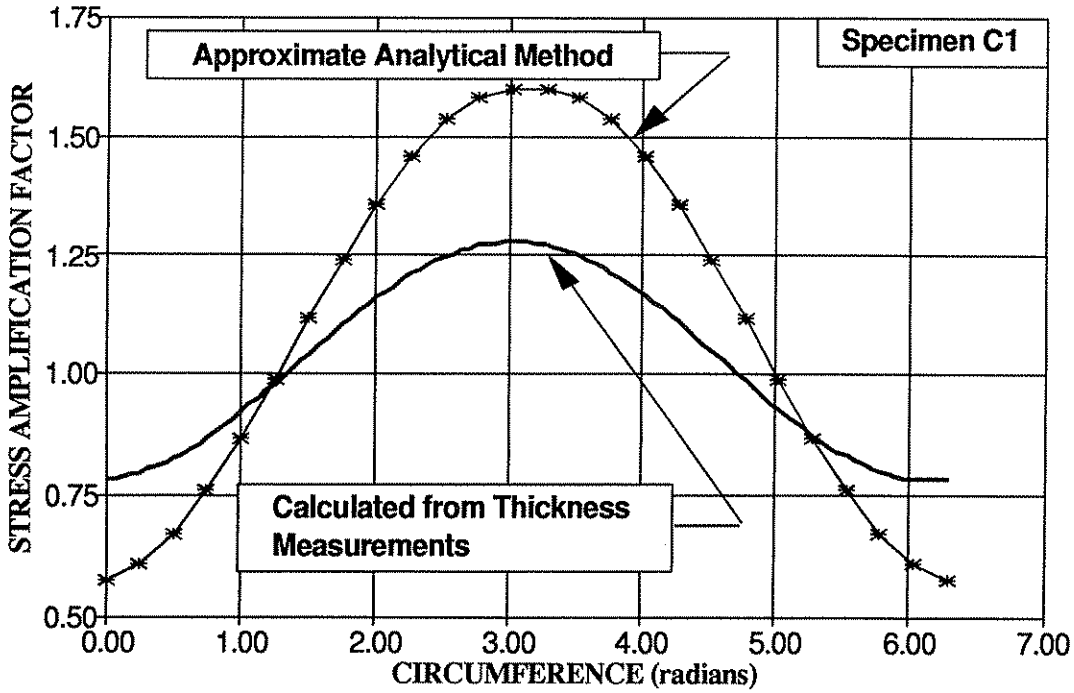

Figure 14-9: Specimen C1 - Stress Distribution around Tube Circumference. (Non-dimensionalized with respect to the stress at the centroid.)

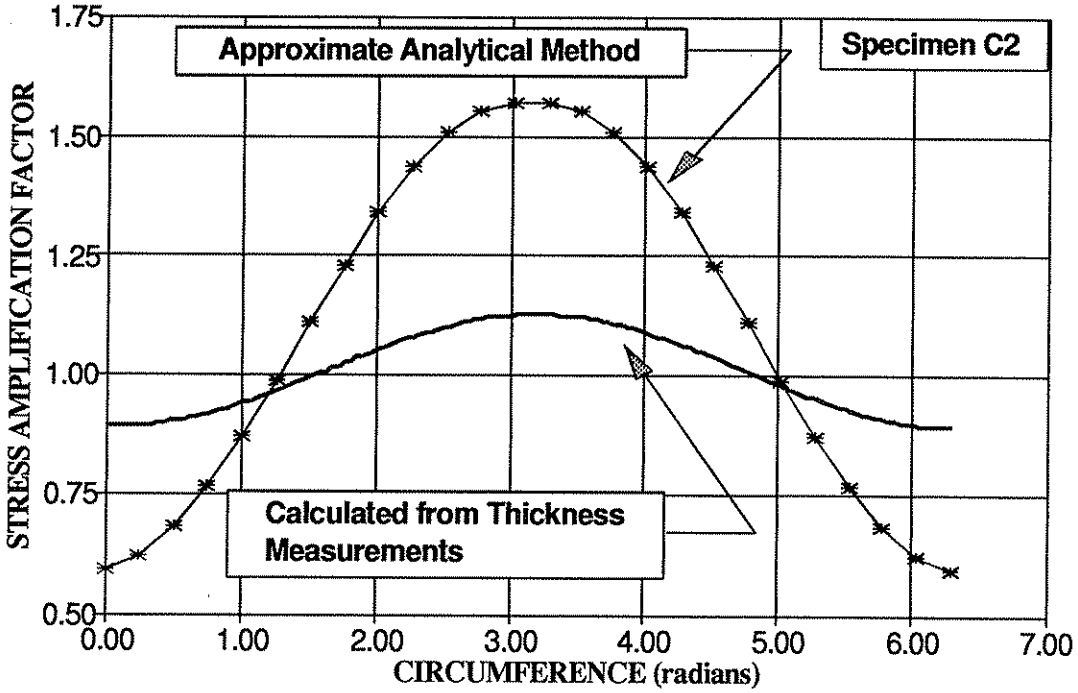

Figure 14-10: Specimen C2 - Stress Distribution around Tube Circumference. (Non-dimensionalized with respect to the stress at the centroid.)

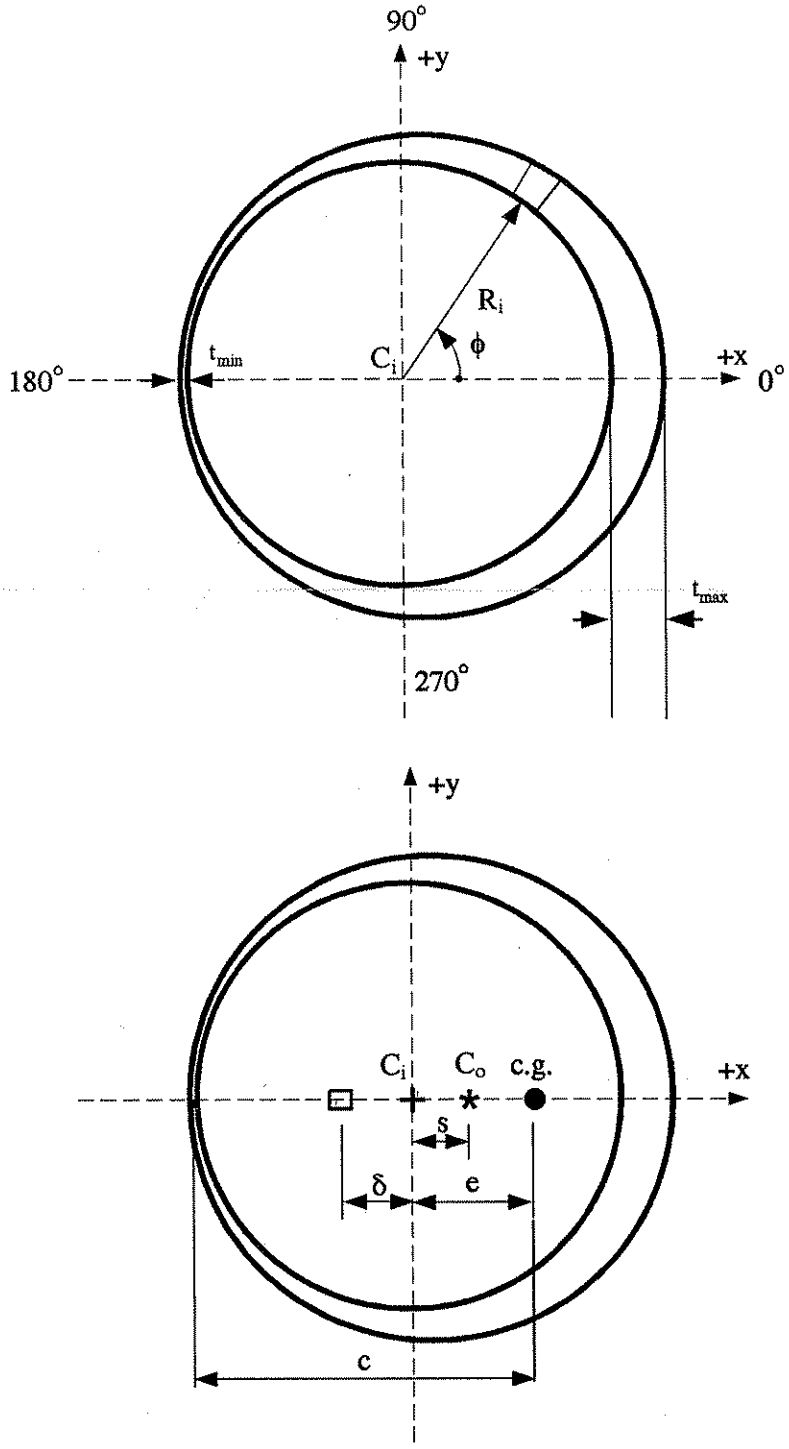

Figure 14-11: Approximate Analytical Model for Corrosion at a Cross Section

PHOTOGRAPHS

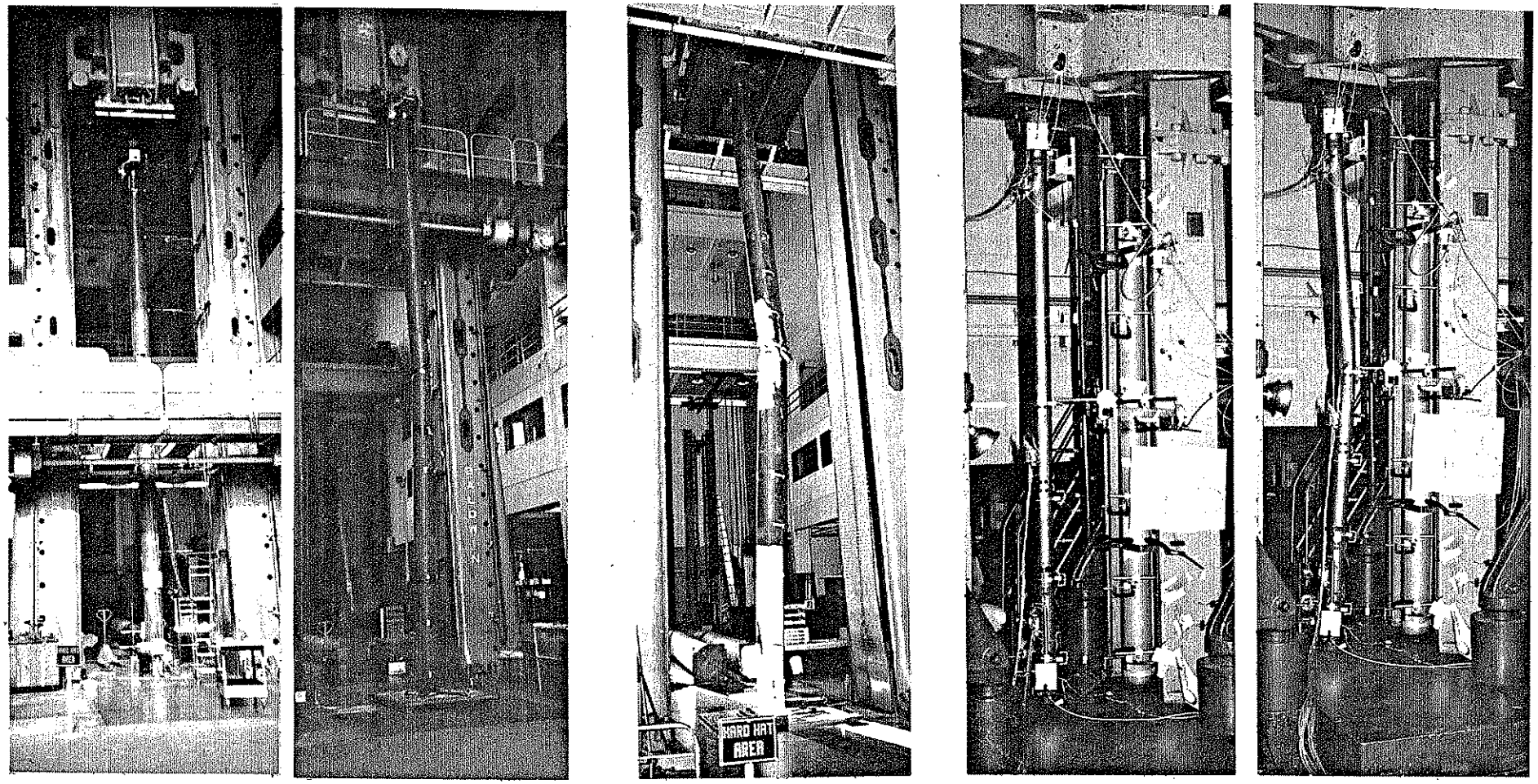

Pre-Test P1P (a)

Post-Test (b)

Post-Test P1F (c)

Pre-Test P1PS (d)

Post-Test (e)

Photo 1-1A: Test Specimens P1P, P1F, and P1PS Before and After Axial Test

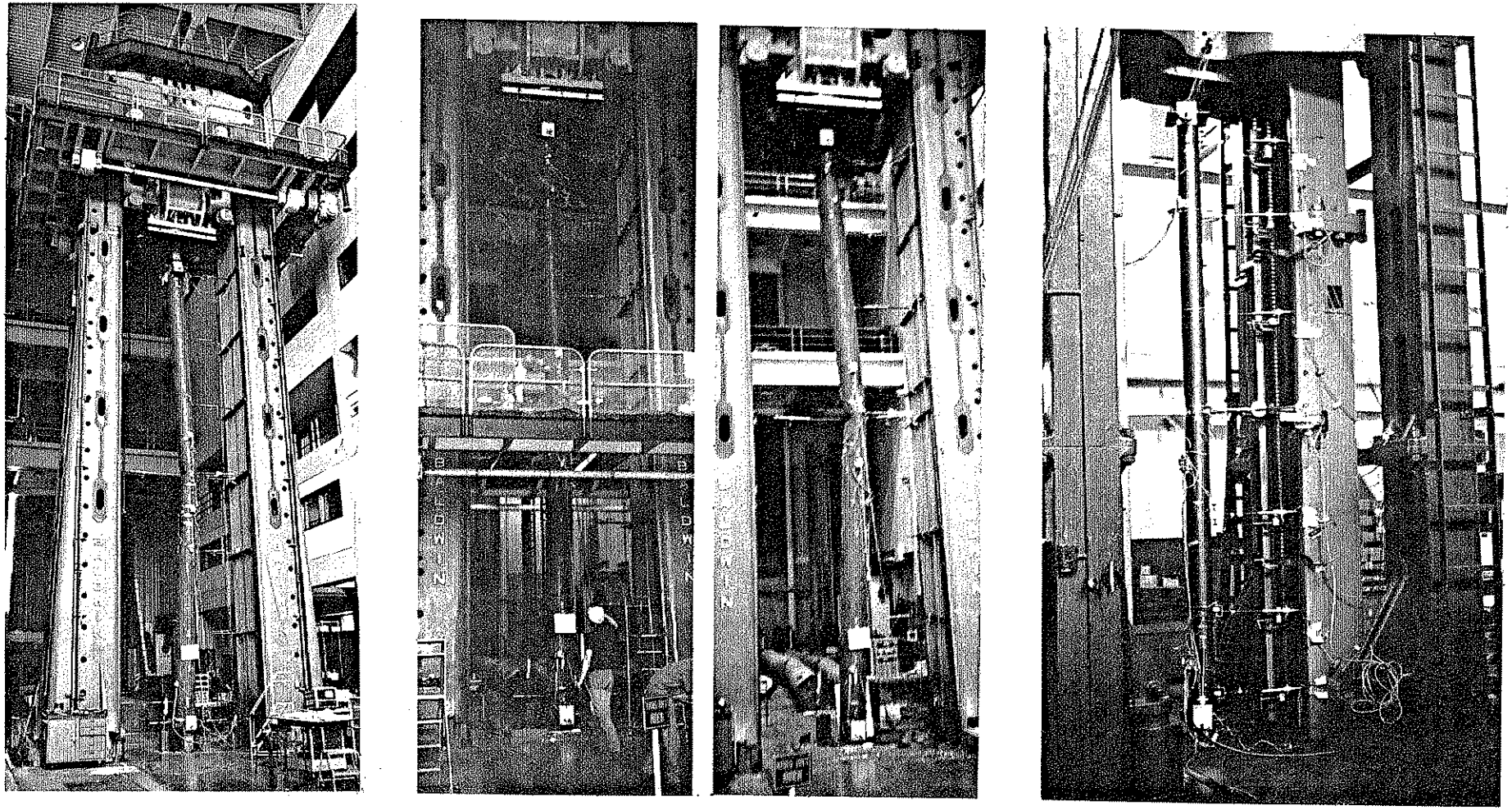

Post-Test
P2P
(a)

Pre-Test
(b)

Post-Test
P2F
(c)

Pre-Test
P2PS
(d)

Photo 1-1B: Test Specimens P2P, P2F, and P2PS Before and After Axial Test

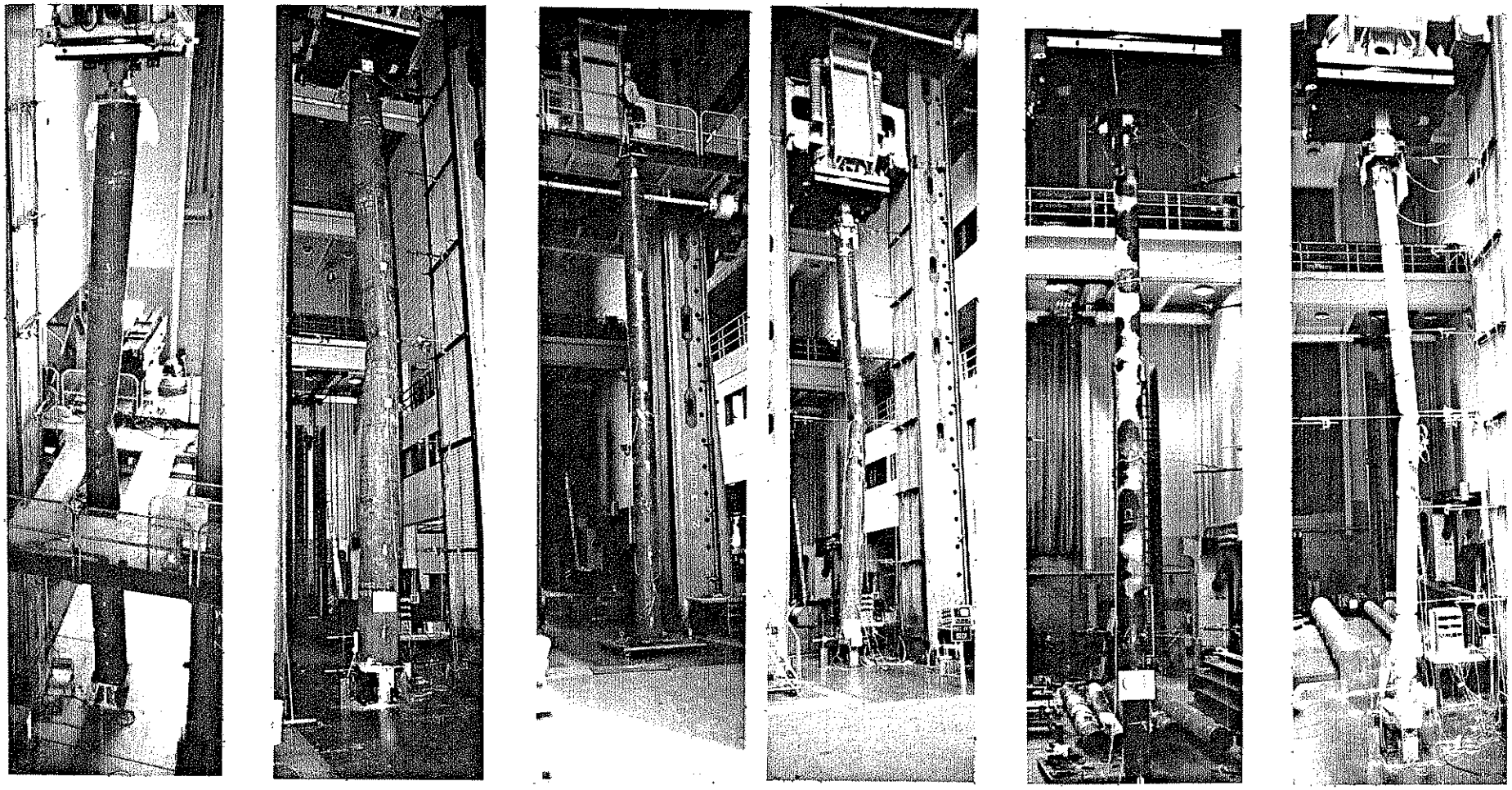

Post-Test P3PA (a)

Post-Test P3PB (b)

Pre-Test (c)

Post-Test P4P (d)

Pre-Test C1 (e)

Post-Test D1 (f)

Photo 1-1C: Test Specimens P3PA, P3PB, P4P, C1, and D1 Before and After Axial Test

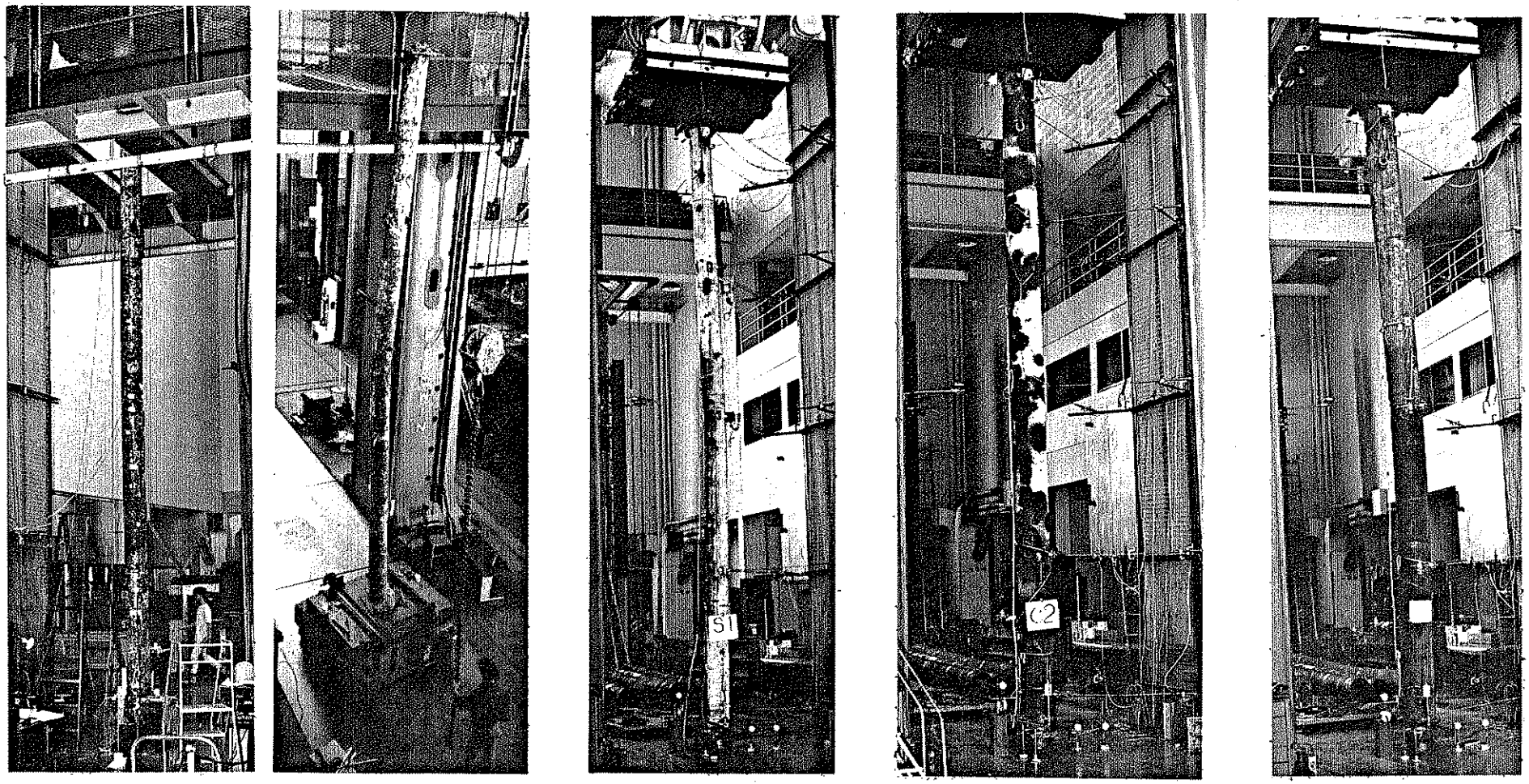

Pre-Test
E1
(a)

Post-Test
(b)

Post-Test
S1
(c)

Pre-Test
C2
(d)

Post-Test
S2
(e)

Photo 1-1D: Test Specimens E1, S1, C2, and S2 Before and After Axial Test

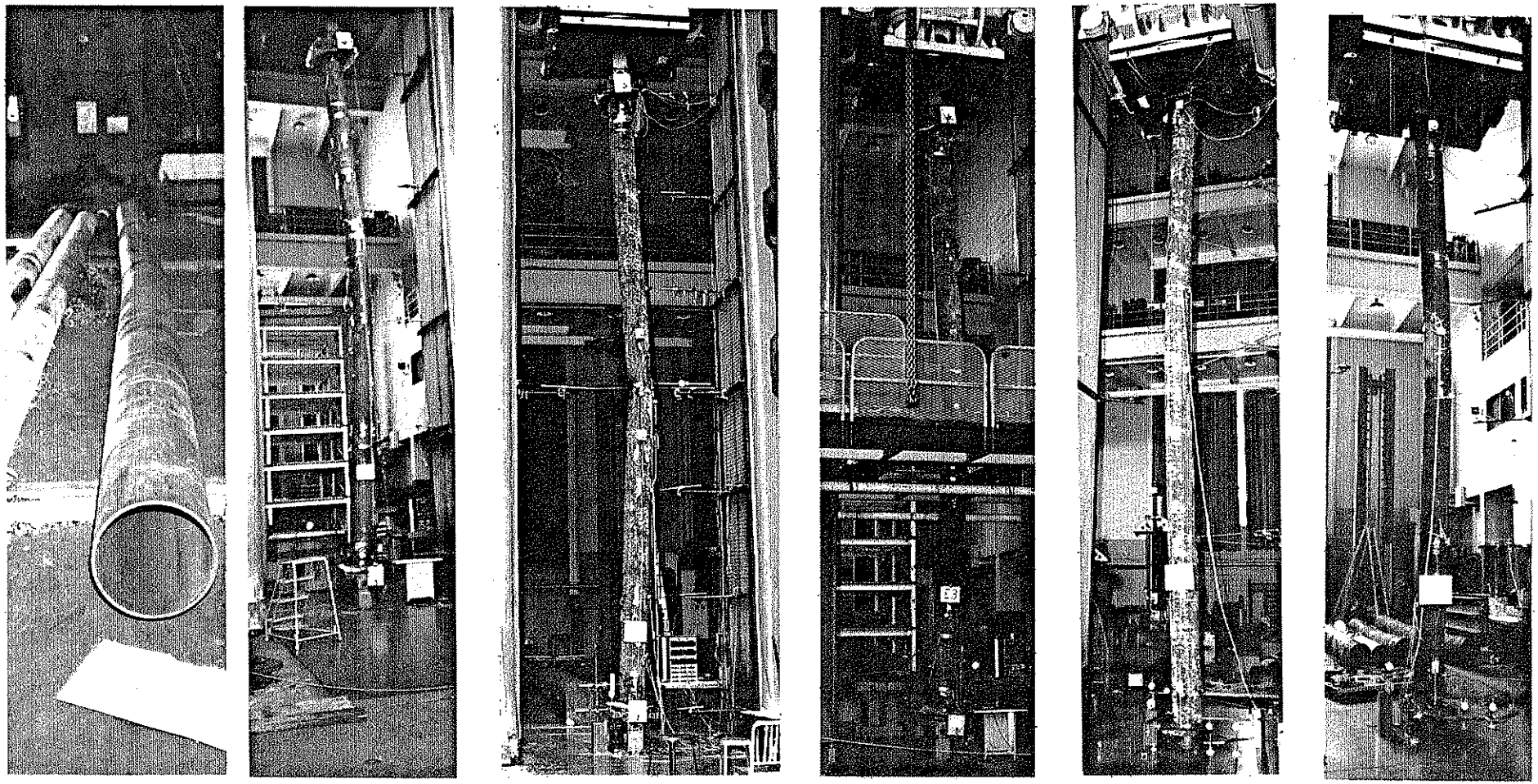

Pre-Test B3 (a)

Post-Test (b)

Post-Test D3 (c)

Post-Test E3 (d)

Post-Test S3 (e)

Post-Test C4B (f)

Photo 1-1E: Test Specimens B3, D3, E3, S3, and C4B Before and After Axial Test

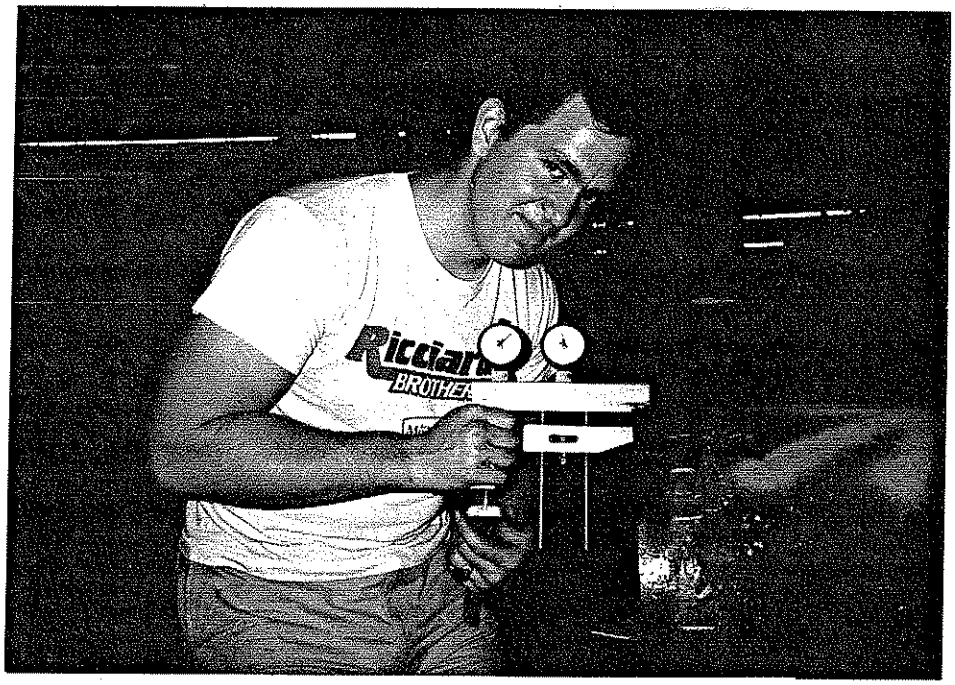

Photo 4-1: Riehle Portable Hardness Tester.

Photo 5-1: Stub-Column P3-SC (Setup and Ring Bulge at Bottom).

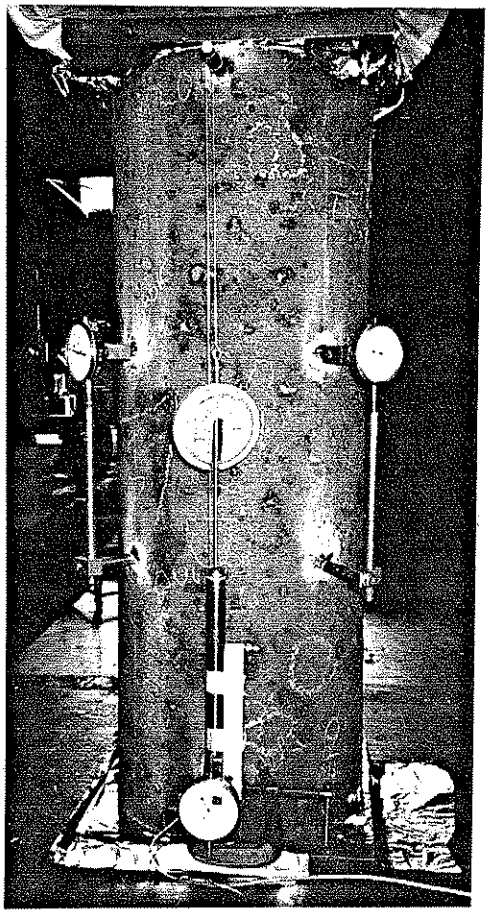

Photo 5-2: Instrumentation and Setup of Stub-Coulmn C4-SC.

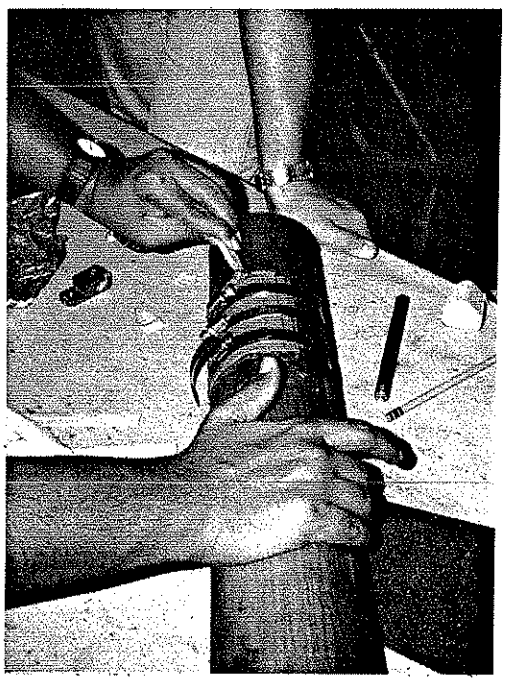

Photo 5-3: Repair of Stub-Coulmn P1S-SC (Small-Scale) by using Epoxied Patch.

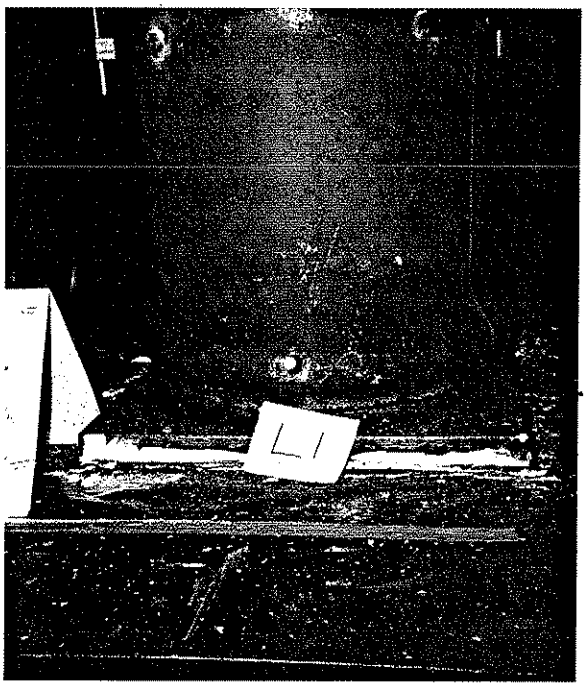

Photo 5-4: Ring Buldge at Bottom of Stub-Column E3-SC.

Photo 5-5: Stub-Column C4B-SC from 'Uniformly' Corroded Specimen C4B.

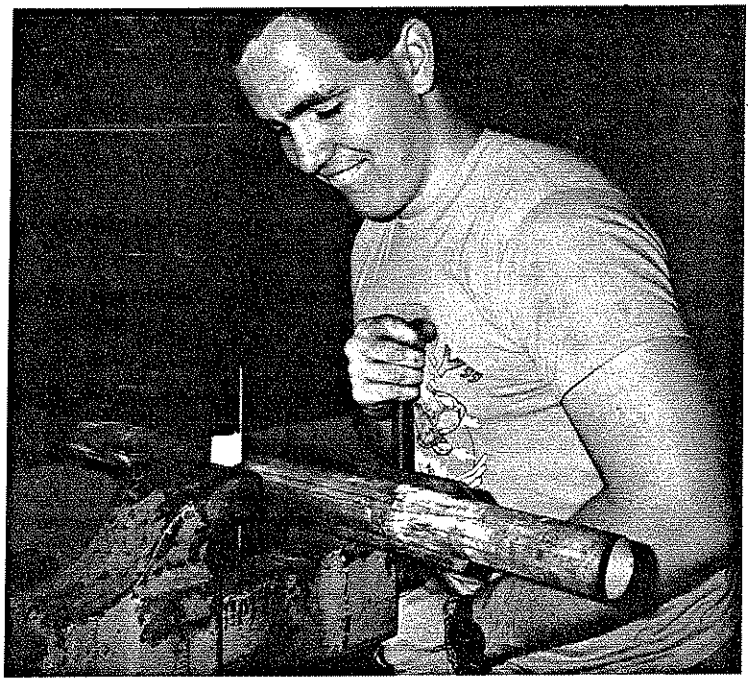

Photo 6-1: Denting of Small-Scale Tubes in Vise.

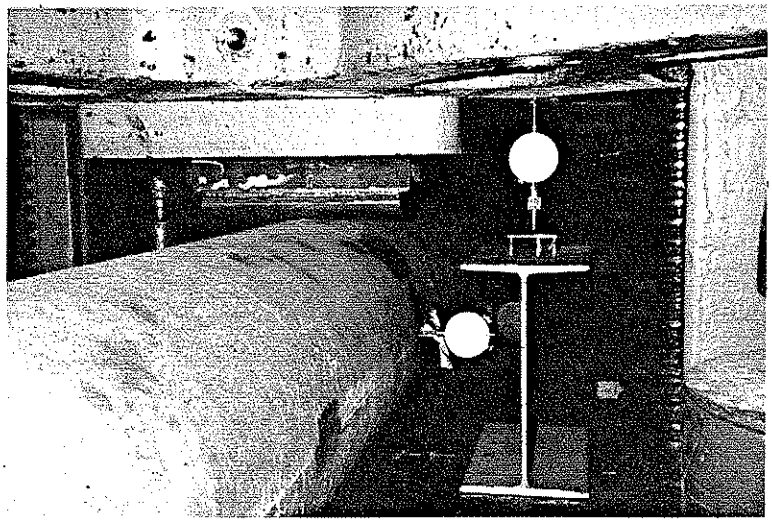

Photo 6-2: Indenter and Instrumentation used for Denting in the 800-kip Machine.

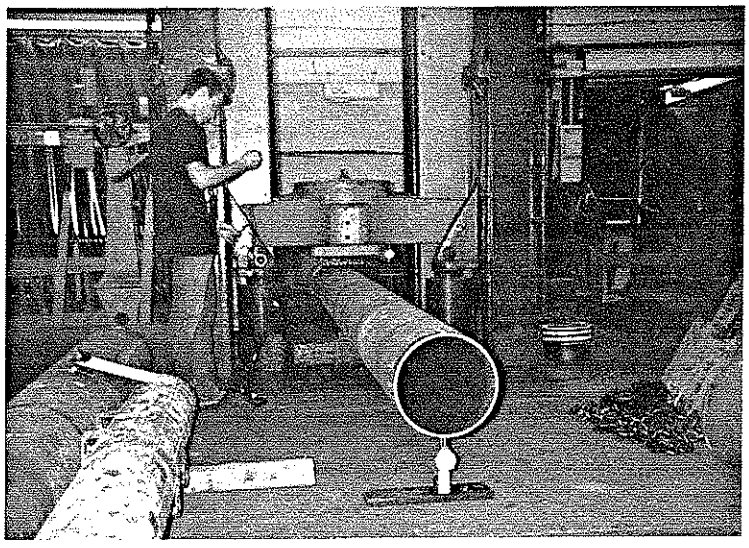

Photo 6-3: Overall View of Denting in the 800-kip Machine.

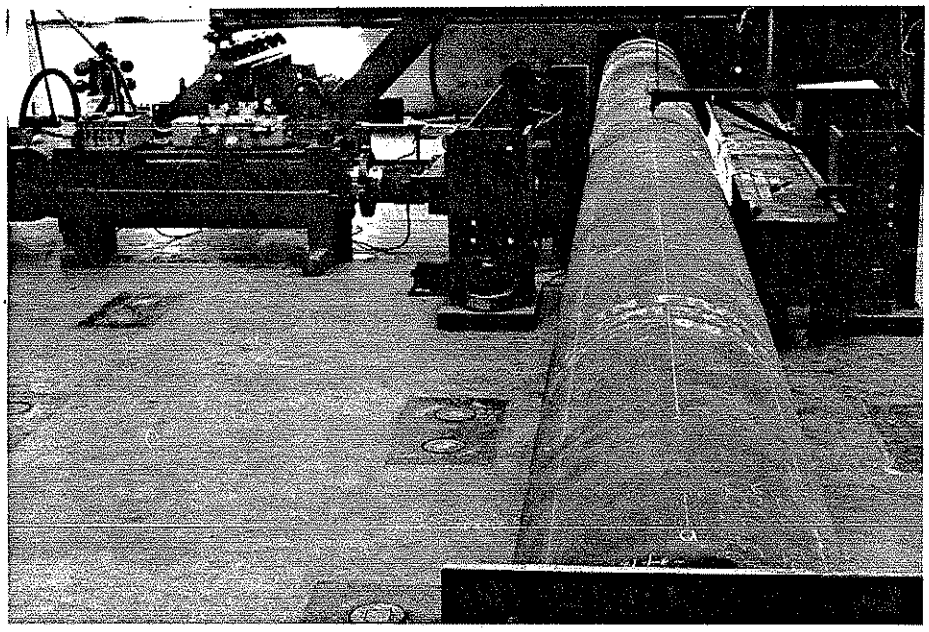

Photo 6-4: Setup for Denting with a Hydraulic Jack.

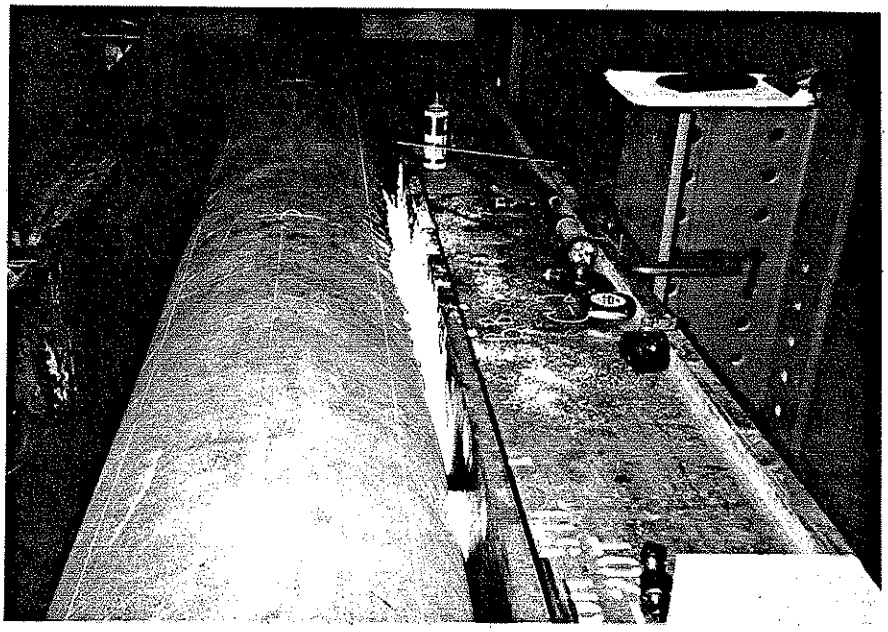

Photo 6-5: Support of the Back of Tube with Hydrostone during Denting with Hydraulic Jack.

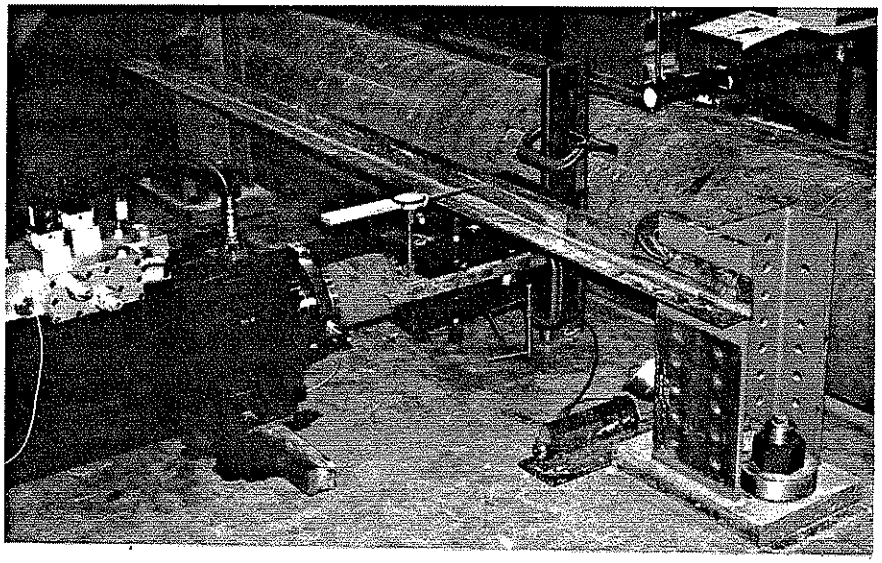

Photo 6-6: Instumentation used for Denting with Hydraulic Jack.

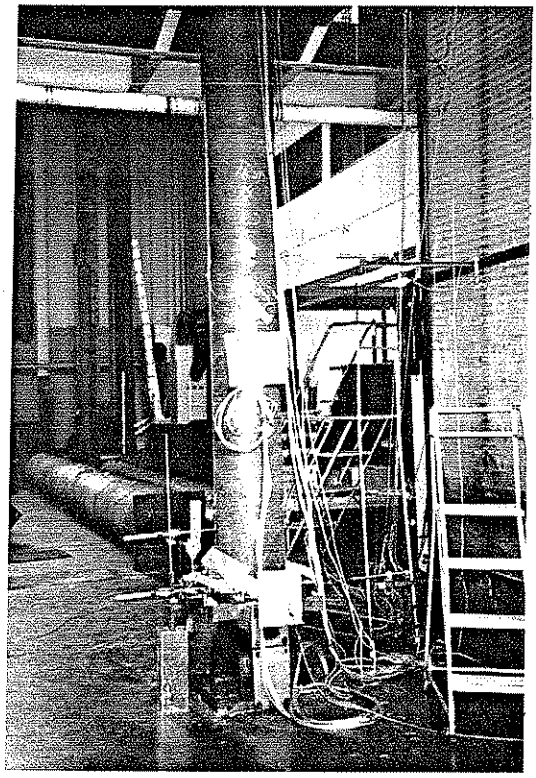

Photo 7-1: Instrumentation - Transverse and Longitudinal LVDTs, and Rotation Gage at End of Tube. (Cylinderical End Fixture)

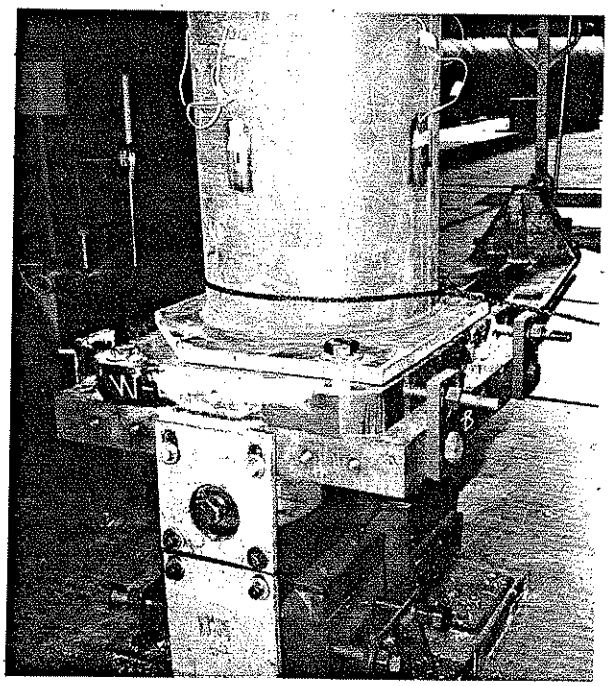

Photo 7-2: Cylindrical Bearing Fixture.

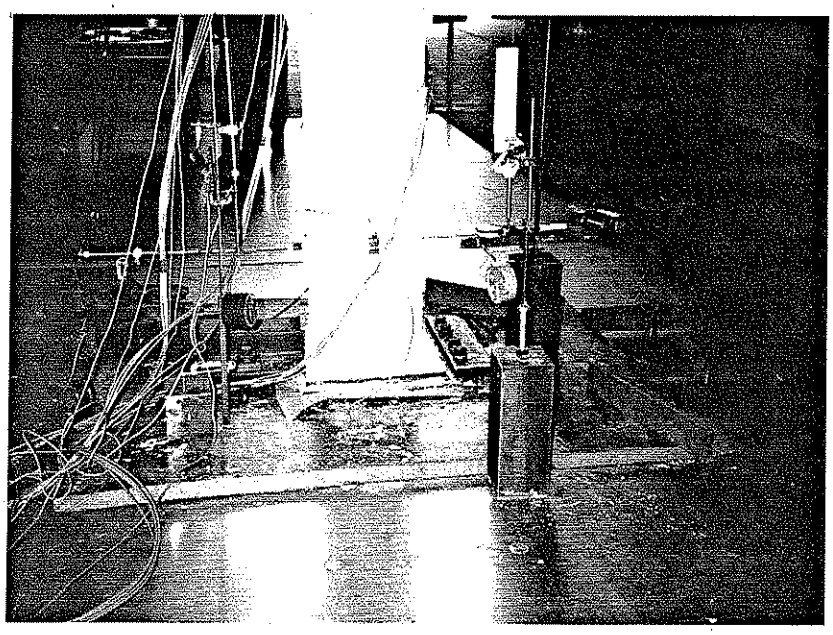

Photo 8-1: Instrumentation - Transverse and Longitudinal LVDTs at End of Tube. (Fixed End Condition)

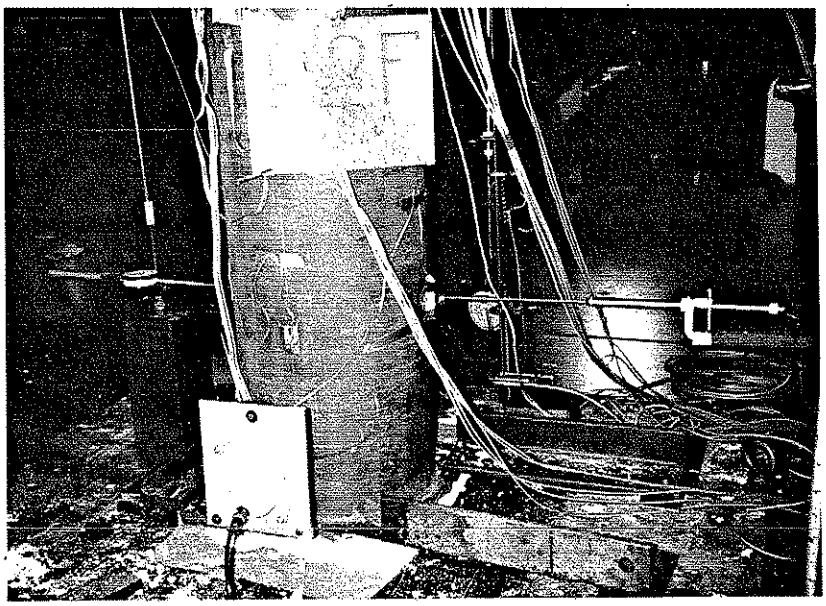

Photo 8-2: Setup of Bottom Fixed End and Rotation Gage for Specimen P2F.

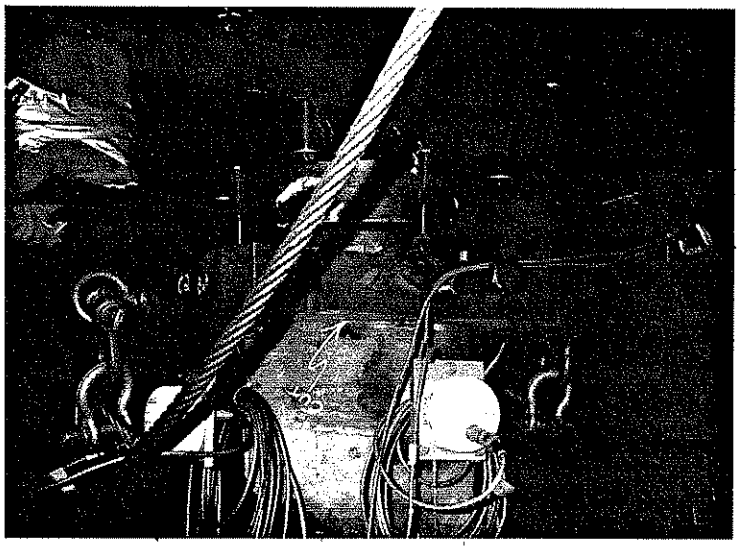

Photo 9-1: Top Spherical Bearing Fixture and Rotation Gages.

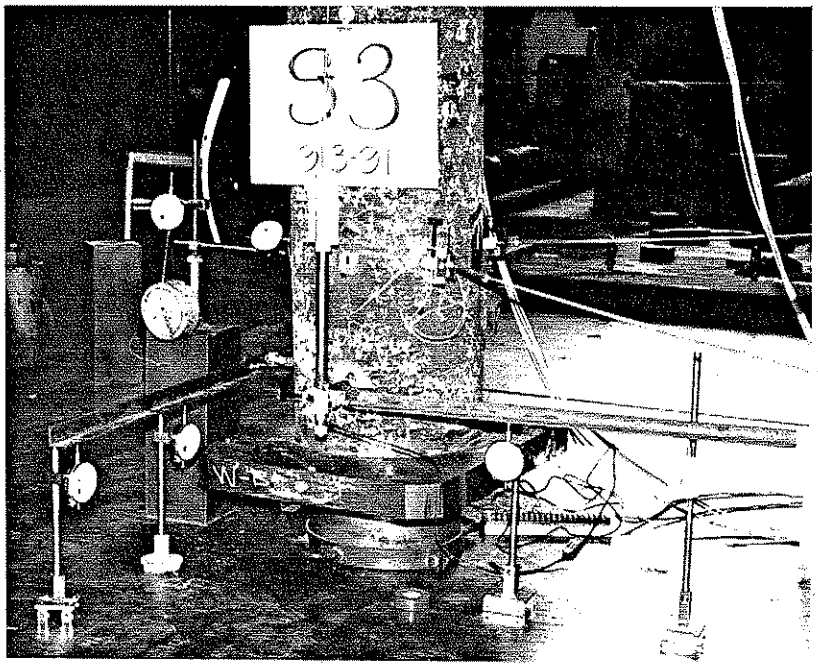

Photo 9-2: Bottom Spherical Bearing Fixture and Arrangement for Measuring End Rotation.

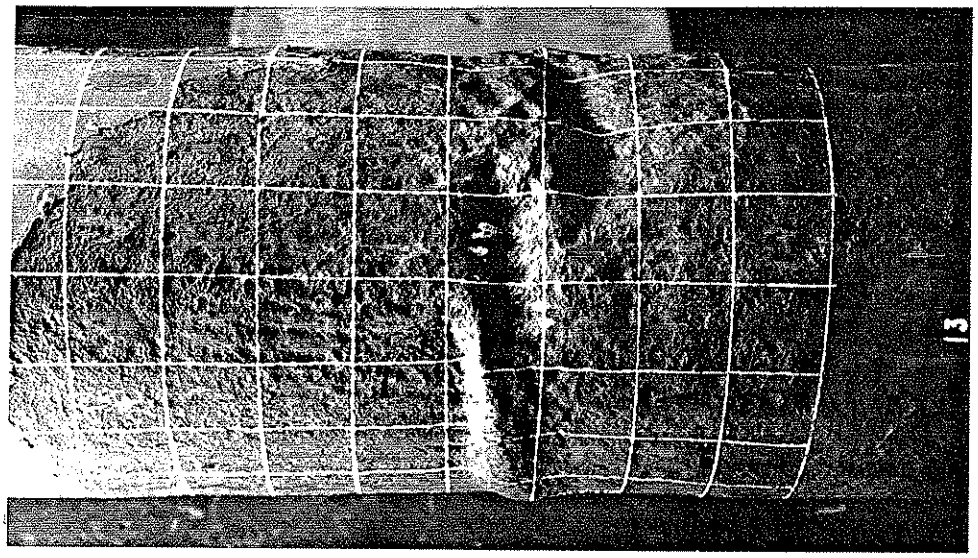

Photo 9-3: Specimen C1 - Local Buckling of Corroded Wall.

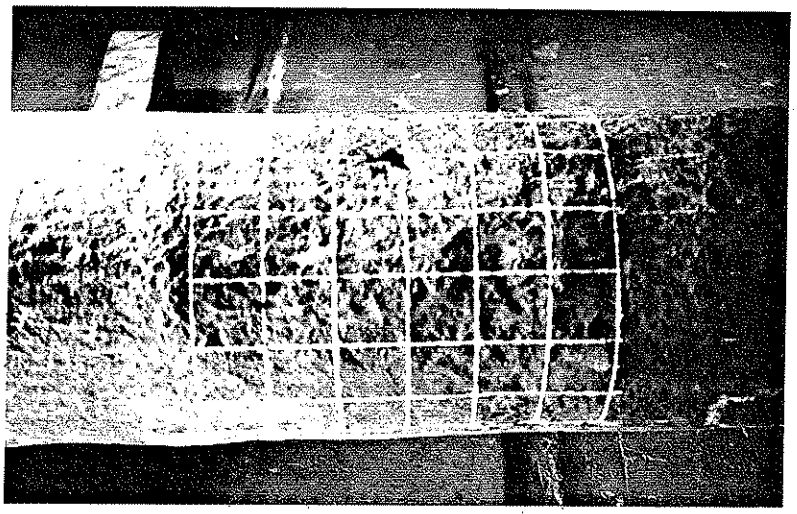

Photo 9-4: Specimen C1 - Hole due to Corrosion, but no Local Buckling.

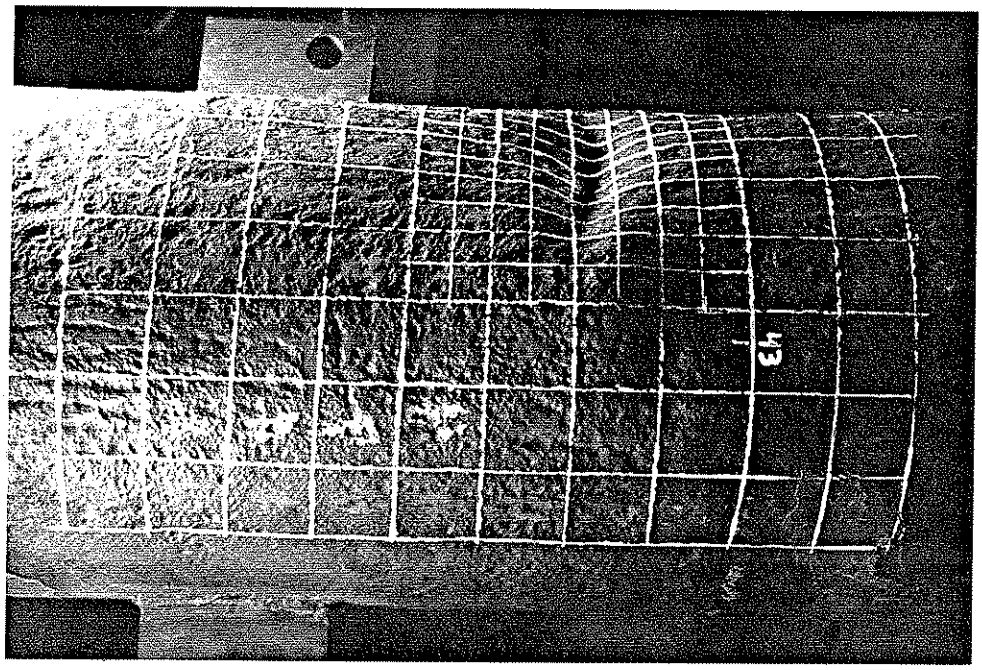

Photo 9-5: Specimen C2 - Local Buckling of Corroded Wall.